GEOCHEMISTRY AND PETROLOGY OF RECENT VOLCANICS OF THE PUYEHUE-CORDON CAULLE AREA, CHILE (40.5°S)

by

David Christian Gerlach

B.A. Trinity University
(1977)

M.A. Rice University
(1980)

Submitted to the Department of
Earth, Atmospheric, and Planetary Sciences
in Partial Fulfillment of the
Requirements of the
Degree of

DOCTOR OF PHILOSOPHY

at the

MASSACHUSETTS INSTITUTE OF TECHNOLOGY

June 1985

© Massachusetts Institute of Technology

Signature of Author_____
Department of Earth, Atmospheric, and Planetary Sciences
April 8, 1985

Certified by_____
Frederick A. Frey
Thesis Supervisor

Accepted by_____
Theodore R. Madden
Chairman
Department Committee on Graduate Students

WITHDRAWN FROM MIT LIBRARIES
MASS. INST. TECH. APR 25 1985
Lindgren

GEOCHEMISTRY AND PETROLOGY OF RECENT VOLCANICS OF THE PUYEHUE-CORDON CAULLE AREA, CHILE (40.5°S)

by

DAVID C. GERLACH

Submitted to the Department of Earth, Atmospheric, and Planetary Sciences on 8 April, 1985, in partial fulfillment of the requirements for the degree of Doctor of Philosophy.

ABSTRACT

The Puyehue-Cordon Caulle area, Chile (40.5°S), is located in the Southern Andes (34°-42°S), one of four active volcanic segments of the Andes of South America. Recent volcanics in this area are subdivided into preglacial and postglacial groups, separated by an erosional hiatus. Puyehue Volcano is a dominantly basaltic stratovolcano which erupted silicic lavas in later stages. Fissural eruptions of rhyodacite and rhyolite comprise the nearby Cordon Caulle group. Cordon Caulle lavas are the youngest historic eruptions (last in 1960) in the area and represent a continuation and locational shift of late-stage activity of Puyehue Volcano. This thesis is a study of geochemical and petrologic variations among lavas of this volcanic center.

Basaltic lavas make up a major portion (70%) of the volume of Puyehue Volcano. The basalts are geochemically heterogeneous and are characterized by variable (> two times) incompatible element abundances, abundance ratios, and $^{87}Sr/^{86}Sr$ (.70381±3 to .70416±3). Two samples of basalt display evidence of selective crustal contamination. Geochemical variability in other basalts may be due to variations in source abundances, source modal mineralogy and variable degrees of partial melting. If sub-arc mantle sources are modified by alkali-enriched, radiogenic (Sr, Pb) components from subducted oceanic crust, basalts derived from sources consisting of variable proportions of this component added to upper mantle might display positive correlations between geochemical parameters identified with this component (e.g., Ba/La vs. $^{87}Sr/^{86}Sr$, Pb/La vs. $^{207}Pb/^{204}Pb$). Puyehue basalts display negative correlations between such parameters (e.g., Ba/Nb vs. $^{87}Sr/^{86}Sr$) and this may be explained by two models: (1) modification of heterogeneous sub-arc mantle by a subduction component, or (2) a two-stage model whereby primary magmas derived from sources consisting of varying mixtures of homogeneous mantle and a subduction component are variably modified by contamination in the upper mantle. Either model may explain a lack of correlation of subduction-linked geochemical parameters observed in many arcs. Positive or negative correlations between such parameters may result from mixing of magmas after separation from geochemically distinct sources. Some Puyehue basalts characterized by abundance ratios (e.g., Ba/Th) similar to estimated mantle values, lower $^{87}Sr/^{86}Sr$ and $^{206}Pb/^{204}Pb$ relative to other basalts, and high $^{207}Pb/^{204}Pb$ relative to MORB and OIB, were derived from a mantle source modified to a lesser degree by a component from subducted crust relative to a mantle source for other basalts. Since these basalts with low Ba/Th and $^{87}Sr/^{86}Sr$ display relatively higher LIL/REE and LIL/HFSE ratios (i.e., Ba/Nb, Sr/Nd), this may suport differentiation on partial melting by a refractory HFSE+REE-bearing phase.

Fractional crystallization, magma mixing, and crustal contamination were mechanisms that produced and modified lavas of Puyehue Volcano. Crystallization occurred at low to moderate pressures (1 Kb to 5 Kb) as indicated by phenocrysts. Compositions of ferromagnesian phenocrysts in silicic lavas of Puyehue Volcano and Cordon Caulle are among the most iron-rich reported for subduction zone-related volcanism. A few basaltic andesites and andesites were produced by magma mixing. On the basis of geochemical evidence, the basaltic andesites resulted from mixing of basaltic and andesitic magmas; their compositions are not consistent with fractional crystallization of basaltic magma. A mixing origin for some andesites is indicated by geochemical compositions and disequilibrium phenocryst assemblages, and mixing endmembers (basalt, dacite, rhyolite) occur within the data set. Other andesites produced by fractional crystallization gave rise to more evolved lavas (dacite to rhyolite) by further fractional crystallization.

Trace element abundance increases and abundance ratios in dacites to rhyolites were partly controlled by the apatite proportion in crystallizing assemblages. Although these lavas form a geochemically coherent group related by fractional crystallization, differences in phenocryst assemblages between samples indicate that crystallization occurred at variable total pressures and P_{H_2O}.

No major geochemical and isotopic differences are observed between preglacial volcanics and postglacial volcanics of the Puyehue-Cordon Caulle area. Among the samples, Sr-isotopic compositions are the most variable while Nd and Pb-isotopic ratios are homogeneous. Basalts dominated the early, main constructional phase of the volcano. Increasingly silicic lavas predominate upsection and basic lavas are rare. Fractional crystallization was the most important petrogenetic process during the evolution of the volcano and operated to a greater extent with time as more evolved lavas were produced in later stages. Lavas produced by magma mixing record increasing compositional contrasts between replenishing magmas and the most evolved magmas present at any stage. The last eruptions of Puyehue Volcano consisted of andesite and dacite produced by fractional crystallization, and mixed andesites. Late-stage lavas of Puyehue Volcano provide indirect evidence of complex magma chamber conditions and geometry, and that the system was continually replenished with geochemically heterogeneous basaltic magmas. Complex processes are suggested for the generation and modification of primary magmas in the sub-arc mantle and high-level processes within the crust have further modified magmas. This implies that detailed studies of single centers or regions are necessary before geographic and temporal magmatic variations may be recognized, and before relative contributions of the subducted oceanic crust, the upper mantle, and the continental crust may be assessed.

Thesis supervisor: Fred A. Frey, Professor of Geology and Geochemistry

Aknowledgements

I am grateful to my thesis supervisor, Fred Frey, for initially suggesting this project and I appreciate his comments and those of Tim Grove which resulted in improvements in the manuscript. I thank Stan Hart for unlimited use of his mass spectrometry laboratory and clean lab facility and Fred Frey for use of his INAA facility. I am also grateful to Mike Rhodes, University of Massachusetts/Amherst for use of his XRF facility. I would also like to thank Don Bankston and Margaret Sulanowska, Woods Hole Oceanographic Institute, for access to the CHN analyzer and assistance in its use. I am also grateful for technical assistance and instruction received from many other people, including Pillalamari Ila, Levent Gulen, Rosemary Hickey, Vincent Salters, Joel Sparks, Doug Chor, B.J. Pegram, Steve Richardson, and Ken Burrhus.

There are many people in Chile I wish to acknowledge:

Leo Lopez-Escobar and Hugo Moreno-Roa, for general logistical assistance and guidance in the project,
the Lopez family of Santiago, the Vargas family of Anticura, and Sr. and Sra. Rolando Escobar of Puerto Montt for their hospitality and for making me feel as a member of their families,
Sr. and Sra. Hector Fredy Vargas, the Vargas brothers (Jose, Carlos, Juan, and Flauvio), and Marcelo Lopez-Lastra for further assistance in the field,
and the park rangers of Parque Nacional Puyehue for their hospitality.

At this end, I am grateful to B.J. Pegram, Rosemary Hickey, Jane Selverstone, Mike Baker, Allen and Reneau Kennedy, Karen Kimball, Vincent Salters, Julie Morris, Chu-Yung Chen, Mike Roden, Howard West, Melinda Darby Dyar, Rosamond Kinzler, Song Yan, Carrie Hengeveld, and Brian Taras for numerous discussions, serious and otherwise, and general moral support.

I am especially grateful to Francis Doughty for patiently typing this tome and for bearing with me the vicissitudes of the revision process. I also must mention the special touch lent by Carolyn Mosher to many of the drafted figures contained herein. This project was funded by NSF grant EAR 8115850 (to F. Frey), the Department Student Research Fund, the Department Thesis Fund, and my personal savings.

To my parents,

Oscar and Mary Gerlach

Table of Contents

List of Tables

List of Figures

1. Introduction and Background Information

1.1. Introduction

It has long been recognized that the volcanic Andes of western South America represent the best example of magmatism associated with the convergence of oceanic crust and continental crust. The distribution of earthquake foci along the margin of western South America indicates that the subducting oceanic Nazca plate is segmented at depth along strike (Stauder, 1973; Barazangi and Isacks, 1976). Individual segments correspond to variations in the apparent dip of the Wadati-Benioff zone (Stauder, 1975; Hanus and Vanek, 1977). Furthermore, this segmentation is expressed in the tectonic characteristics of the overriding lithosphere (Jordan et al., 1983) and has influenced the location of magmatic activity and active volcanism in the recent past and present (Wortel and Vlaar, 1978). Recent and active volcanism is absent in regions located above shallow-dipping (10°) Wadati-Benioff zones (Hanus and Vanek, 1978). Four active volcanic zones of the Andes have been recognized (Casertano, 1962; Gonzalez-Ferran, 1970; Katsui, 1972; Thorpe and Francis, 1979). These include the northern zone (NVZ) in Columbia and Ecuador (5°N-2°S), the central zone (CVZ) of Peru and northern Chile (16°S-28°S), the southern zone, or Southern Andes of central-south Chile (33°-46°S), and the southernmost, or Austral Andes of Chile (49°-55°S).

The NVZ is located on continental crust which is 40-50 km in thickness (cf., Thorpe, 1984, for summary) and volcanos in this region consist mostly of basaltic andesite (Ramirez, 1968; Pichler et al., 1976). The CVZ is located over 70 km thick continental crust as old as PreCambrian (Shackleton et al., 1979). Until recently, Recent volcanics of the CVZ were the focus of the majority of Andean petrological and

geochemical studies (Francis et al., 1974; Pichler and Zeil, 1972; James et al., 1974; Thorpe et al., 1976; Roobol and Francis, 1976; James, 1981, 1982, 1983; Hawkesworth et al., 1979, 1982). The SVZ is located on continental crust averaging 35 km in thickness. Recent volcanics of the SVZ are variable in composition and have been the subject of several recent reconnaissance studies (Drake, 1976; Lopez-Escobar et al., 1977; Dereulle, 1982; Dereulle et al., 1983). The gap in active volcanism located between 46° and 49°S is attributed to the subduction of the Chile Rise spreading ridge (cf. Stern et al., 1984a). Recent volcanics and active volcanos in the Austral Andes are sparsely distributed due to oblique convergence and are the subject of recent preliminary studies (Stern et al., 1976; Stern et al., 1984a).

Within the SVZ, north-south variations in tectonic elements, volcano morphology, and volcanic compositions have been recognized. Active volcanism in this region is bounded by the intersection of the Juan Fernandez ridge with the continental margin at approximately 32°S and the Chile Rise triple junction at approximately 47°S. The Wadati-Benioff zone in this region dips at ~25° and is mostly defined by only shallow earthquakes (Stauder, 1973; Barazangi and Isacks, 1976; Hanus and Vanek, 1978). Crustal thickness in this region decreases from approximately 45 km in the north to 30 km in the south (Lomnitz, 1962; Lowrie and Hey, 1981). Volcanos in the northern part of the SVZ (34°-36°S) are predominantly andesitic strato-volcanos; andesites are rare southward as volcanos become more basaltic to 41°S (Moreno, 1974, 1976; Lopez-Escobar et al., 1977). From 41° to 46°S, volcanic centers may again be predominantly andesitic (Lopez-Escobar, pers. comm., 1984). Results of recent reconnaissance geochemical studies suggest that volcanics of the

northernmost volcanic centers (34°-36°S) are similar to those of the CVZ (Hickey et al., 1984, and in press; Stern et al., 1984a; Lopez-Escobar et al., in press). In addition, results of other recent studies suggest that a significant amount of explosive silicic volcanism occurred in the northern part (34°-36°S) of the SVZ (Grunder, 1983; Hildreth and Drake, 1983; Hildreth et al., 1984; Harrington et al., 1984). Until recently, rhyolites and igimbritic eruptive products were largely unrecognized in the SVZ, aside from the work of Drake (1976), and, within the Andes, were believed to be exclusive to the CVZ of Peru and northern Chile.

Puyehue Volcano is located in the central portion of the SVZ at 40°30'S, and was described by Moreno (1974, 1977) as a predominantly basaltic volcano with minor dacite. The present study reveals that this compositional range is more diverse, but basalts are the dominant eruptive products. Located over relatively thin (30 km) continental crust, Puyehue Volcano therefore represents one extreme in the aforementioned variations within the SVZ, and was chosen for this reason. In addition, the area was mapped by Moreno (1977) and this allowed stratigraphic control in sampling efforts. Detailed study of a single center such as Puyehue Volcano can potentially serve to evaluate the magnitude of local variability in rock types and their geochemical compositions both as a test for true variations between individual centers and of the apparent north-south variations within the SVZ. An additional major objective of this study was to identify shallow level, i.e., crustal processes and their effects on the compositions of magmas, and to distinguish these effects and these processes from those occurring in the sub-arc site of magma generation. Results of this study may also yield insight as to what sub-arc components and processes are involved in magma genesis in the SVZ.

With the above goals in mind, the general approach taken in this study included field observations, detailed sampling within a stratigraphic framework, petrographic studies including analysis of mineral phases, and analysis of bulk composition, including major element contents, Sr, Nd, and Pb isotopic compositions and abundances of trace elements. An attempt was made to integrate all of the above data in constructing a coherent and comprehensive picture of the geochemical character and evolution of Puyehue Volcano and implications for continental arc magma genesis in this region, and in general.

1.2. Regional Geology

The regional geology of the area was mapped by Moreno (1977) and the results of his study are presented in unmodified form in Plate I with locations of samples collected during the present study. Figure 1 is a simplified geologic map of the study area, in which some geologic units recognized by Moreno (1977) are combined for clarity. Figure 2 consists of a geologic map of the SW flank of Puyehue Volcano in which detailed sampling was conducted. Based on sampling, slight modifications were made in the geology of this small area compared to Moreno's (1977) interpretation (Plate I).

Basement rocks in the area of Puyehue Volcano range widely in age. Undifferentiated igneous and metamorphic Paleozoic rocks are exposed to the east and south of the volcano (Fig. 1). Tertiary diorites in the immediate area (Plate I, Fig. 1) may represent the southernmost extension of the Panguipulli batholith (Moreno and Parada, 1976; Herve et al., 1974) which is located to the north, outside of the study area. The diorites locally intrude sediments and metasediments of the Curarrehue

Formation (Plate I), and constitute a significant portion of the Tertiary basement rocks in the study area (Fig. 1).

A thick section of Pliocene to Pleistocene volcanics and volcanogenic sediments unconformably overlies basement in the immediate area. These rocks were subjected to extensive glacial erosion and are exposed in fault scarps and prominent erosional remnants. Moreno (1977) has subdivided these rocks into four units, CCI, CCII, CCIII, and PI (cf. Plate I). Field evidence for these subdivisions was not obvious and in the present study, these rocks will be referred to as the preglacial volcanics (Fig. 1). This preglacial volcanic series includes a wide variety of rock types. Thick sections (up to 200 m in some outcrops) of lapilli, tephra, lahars, minor lenses of tuffaceous sediments, agglomerates, and horizons of basaltic scoria and volcanic bombs are evidence of frequent and explosive activity during this period of volcanism. Small dikes of dacite and rhyodacite and thick (up to 30 m) sills of basalt to basaltic andesite with columnar jointing locally intrude the above. Elongate ridges or cliffs featuring thick sills or flows of basalt have been interpreted by Moreno (1974, 1977) as remnants of an older eroded crater called Cordillera Nevada (Fig. 1 and Plate I), from which most or all of the preglacial volcanics may have issued.

Recent volcanism in the area was renewed after an extensive erosional hiatus and occurs in three areas. Recent to historic eruptions continue in the Cordon Caulle and Carran-Los Venados areas, respectively, in the western and northern portions of the study area (Fig. 1). Puyehue Volcano, exhibiting only minor solfatara activity, is located at the southern end of the area. The Cordon Caulle lavas may be related to late-stage eruptives of Puyehue Volcano. Puyehue Volcano and Cordon

1 Generalized geologic map of the Puyehue-Caulle area (~40°45'S), S. Chile.

2 Geologic sketch map of SW flank of Puyehue Volcano with detailed sample locations in an area of concentrated sampling.

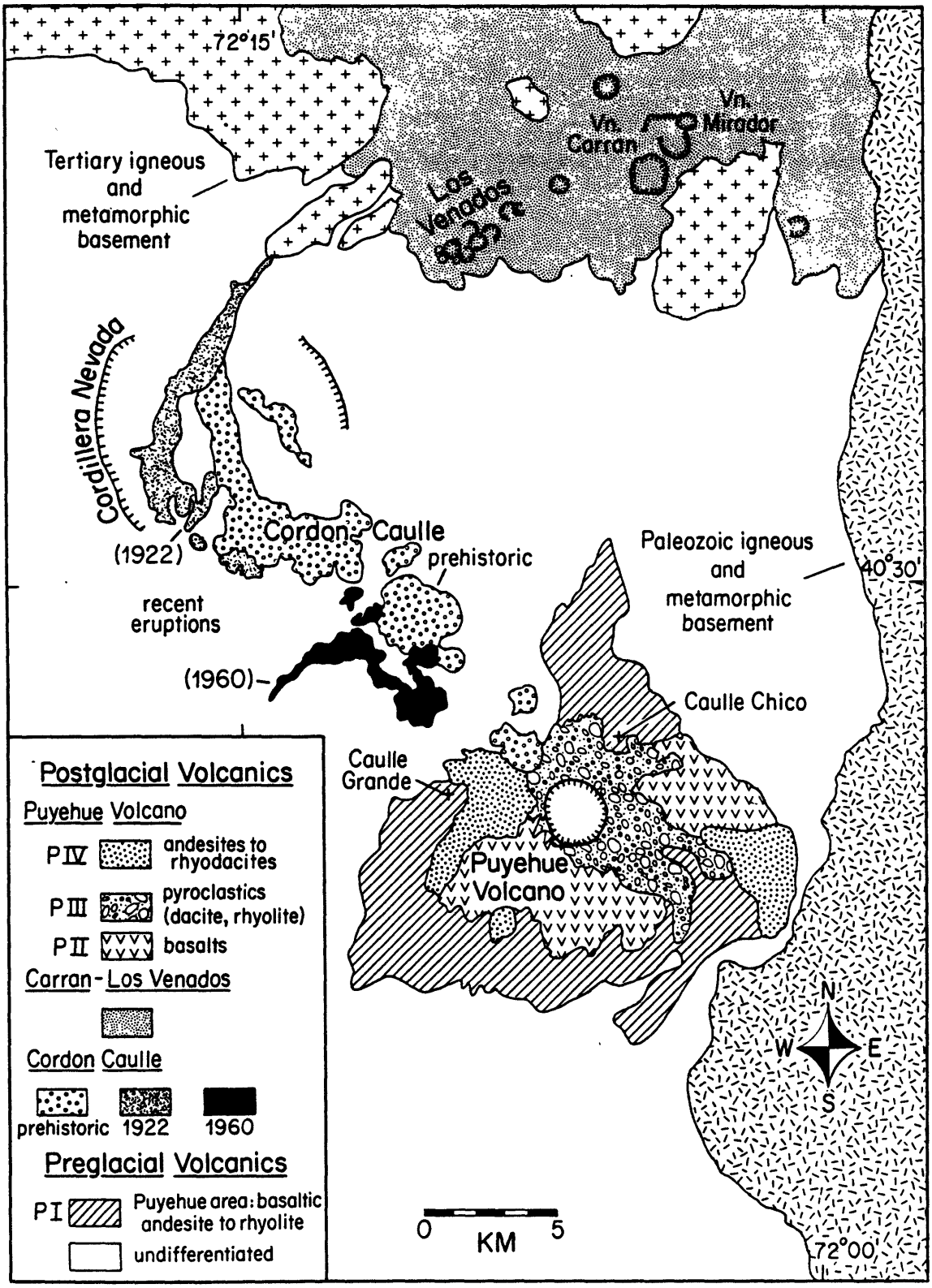
72°15'
Vn. Carran
Vn. Mirador
Los Venados
Tertiary igneous and metamorphic basement
Cordillera Nevada
(1922)
Cordon Caulle
prehistoric
recent eruptions
(1960)
Paleozoic igneous and metamorphic basement
40°30'
Caulle Chico
Caulle Grande
Puyehue Volcano
N
W
E
S
0
KM
5
72°00'
Postglacial Volcanics
Puyehue Volcano
PIV andesites to rhyodacites
PIII pyroclastics (dacite, rhyolite)
PII basalts
Carran-Los Venados
Cordon Caulle
prehistoric
1922
1960
Preglacial Volcanics
PI Puyehue area: basaltic andesite to rhyolite
undifferentiated

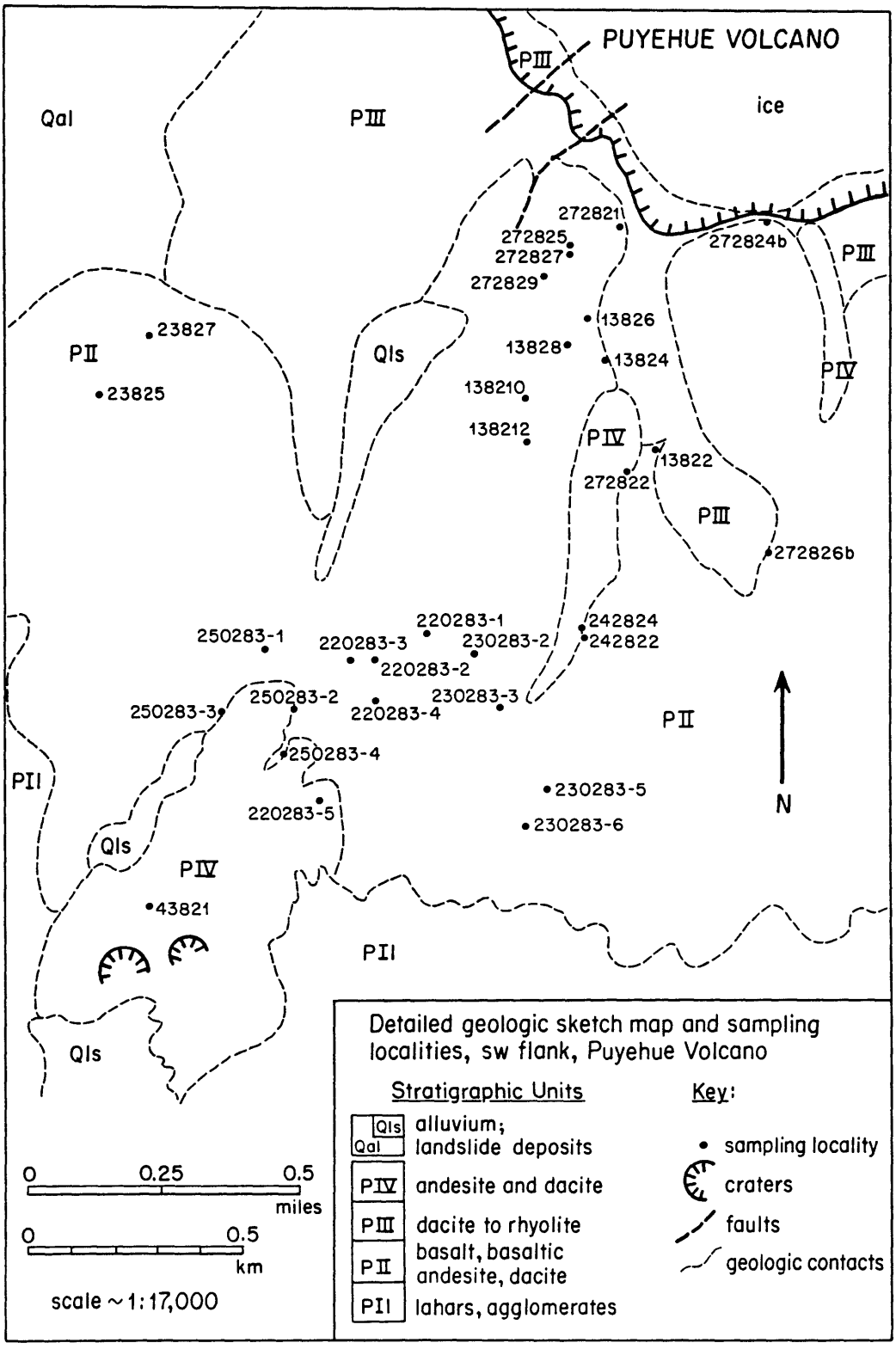
PUYEHUE VOLCANO
PIII
Qal
PIII
ice
272821
272825
272827
272829
272824b
PIII
23827
PII
23825
Qls
13826
13828
13824
PIV
138210
138212
PIV
13822
272822
PIII
272826b
220283-1
242824
250283-1
220283-3
230283-2
242822
220283-2
250283-3
250283-2
220283-4
230283-3
PII
250283-4
PII
230283-5
220283-5
230283-6
N
Qls
PIV
43821
PII
Qls
0 0.25 0.5
miles
0 0.5
km
scale ~1:17,000
Detailed geologic sketch map and sampling localities, sw flank, Puyehue Volcano
Stratigraphic Units
Qls Qal alluvium; landslide deposits
PIV andesite and dacite
PIII dacite to rhyolite
PII basalt, basaltic andesite, dacite
PII lahars, agglomerates
Key:
sampling locality
craters
faults
geologic contacts

Caulle are the topic of the present study. The Carran-Los Venados volcanics are minor in volume, are geochemically distinct, are probably unrelated to Puyehue Volcano and Cordon Caulle, and will be described in detail elsewhere.

1.3 Puyehue Volcano: Stratigraphy

Puyehue Volcano rises to 2236 m in elevation and is built on a plateau (approximately 1300 m in elevation) of eroded preglacial volcanics and lahars as described above. The volcano is flat-topped in profile due to a large 2.5 km diameter summit caldera. The northern, western, and southern flanks of the volcano are almost entirely covered by pumice from a 1960 eruption of the Cordon Caulle to the northwest. Exposures are best developed in eroded stream valleys on the lower flanks of the volcano or in minor fault scarps and collapse features at higher elevations.

Puyehue Volcano may have been constructed over an older edifice similar in age to the Cordillera Nevada, as represented by prominent erosional remnants, Caulle Chico and Caulle Grande, on the northern and western flanks (Figure 1 and Plate 1). These preglacial volcanics were designated as unit PI by Moreno (1977). They include thick sections of weathered yellow tephra intruded by massive dikes and sills of basaltic andesite, andesite, and dacite, and are essentially indistinguishable from the preglacial volcanics in other portions of the study area.

Following a period of extensive glacial erosion, the major portion of Puyehue Volcano was constructed by frequent eruptions of basalt flows with rare flows and dikes of basaltic andesite and dacite as represented by rocks of unit PII (Moreno, 1977). Basalt is by far the dominant

constituent of unit PII and in fact comprises at least 70% of the volume of the volcano. Basalt flows range up to 20 m in thickness with massive interiors and vesicular, oxidized flow tops. In rare exposures of contacts between flows, intervening soil horizons were not observed and in some cases, the overlying flow in its lower portion incorporated angular blocks from the surface of the lower flow, thus attesting to the relatively brief intervals between eruptions.

With time, the style of eruptions became more explosive as represented by the pyroclastics of unit PIII mainly exposed at higher elevations near the crater rim and on the eastern and northeastern flanks of the volcano (Fig. 1). Unit PIII consists of moderately thick (up to 100 m) sections of tephra that weathers to a distinctive yellow, pink, and red variegated color. Most of the tephra contains abundant inclusions of vesicular to scoriaceous basalt, which, though highly altered, contain numerous fresh phenocrysts of olivine and plagioclase. Higher up in the section thin flows and horizons of pumice bombs ranging in composition from dacite to rhyolite are predominant. These more silicic eruptions were followed shortly thereafter by caldera collapse resulting in the present morphology of the volcano.

The last eruptive activity of Puyehue Volcano produced the dacite and andesites of unit PIV (Moreno, 1977). Dacites were erupted from vents near the crater rim and flowed down the west flank of the volcano (Fig. 1). Andesite flows occur on the south and east flanks and display pahoehoe to scoriaceous texture. A large pyroclastic cone of andesite was erupted low on the south flank (Fig. 2). Fumarolic activity on the northwest crater rim may be related to recent eruptions of the Cordon Caulle to the northwest.

Cordon Caulle volcanics volcanics are among the most silicic lavas studied, and form three stratigraphic units, produced during three major eruptions. The earliest, CCIV, is the most widespread but no exact date is available for this eruption. Lavas and pyroclastics of the CCV and CCVI units were erupted in 1921-1922 and in 1960, respectively. All three units are geochemically similar to late-stage silicic lavas and pyroclastics of Puyehue Volcano and may be genetically related to the latter. If so, the apparent shift in vent loci may have been induced by structural controls (Moreno, 1977).

2. Sampling

Samples were collected from all stratigraphic units of the volcano. Continuous stratigraphic sections are not well exposed due to the blanket of pumice and samples were mostly obtained from isolated outcrops. The distribution of samples and detailed locations are provided in Figure 2 and Plate I. Aerial photos aided in determining the best localities for sample collecting. An attempt was made to cover a lot of ground, though many areas were inaccessible. Nevertheless, the sampling is believed to be a thorough and reasonable representation of the total spectrum of rock types present and of their total exposed volumes, especially for postglacial volcanics. A total of 170 samples were collected from 120 localities (Plate I), with up to five samples collected in some localities. For petrographic studies and chemical analysis, twenty samples of preglacial volcanics were chosen in addition to 26 samples from unit PII, six from unit PIII, and six from unit PIV of Puyehue Volcano. Of the various Cordon Caulle eruptive units, five samples from unit CCIV, four from unit CCV, and eight from unit CCVI were selected for detailed study.

Estimated volumes of rock types comprising each stratigraphic unit of Puyehue Volcano are given in Table 1. Basalts may be under-represented: the 70% volume estimate of post-glacial basaltic volcanics comprising the volcano is based on field observation of their areal distribution. Although the later PIII and PIV units consisting of andesites to rhyolites are widespread, their significantly lower volume is estimated on their observed thicknesses exposed in stream valleys near the crater rim. From Table 1, it is evident that eruptions became more silicic with time.

3. Petrography

In subsequent discussion of the origin and petrogenesis of the various volcanics, distinctions or subdivisions are made on the basis of rock types rather than stratigraphic unit. Each stratigraphic unit includes more than one rock type, i.e., each unit is not characterized by compositional uniformity, even though a broad trend towards more evolved compositions may be indicated for the evolution of the volcano. This may only be related to the physical evolution of the volcano, in that relatively more silicic lavas were more frequently and more easily erupted in later stages. It can not be presumed that magma not represented by the compositions of erupted lavas did not exist at depth at any given time throughout the evolution of the volcano. In later discussions of geochemical characteristics and evidence for various petrogenetic processes, it is more direct to relate the discussion to rock types rather than to stratigraphic units. This is also justified on the basis that no distinct compositions variations in a given rock type with time were observed.

Table 1

Estimated relative volumes of stratigraphic units and rock types of Puyehue Volcano

stratigraphic unit	rock type	estimated proportion of unit	estimated proportion of total volcano volume
PI	basaltic andesite andesite, dacite, rhyodacite	-	-
PII	basalt basaltic andesite dacite	90% 5% 5%	70% 10-15%
PIII	basalt + basaltic andesite dacite to rhyodacite rhyolite	tr. 80-90% 10-20% (?)	10-15%
PIV	andesite dacite	50% 50%	≤ 5%

The nomenclature of rock types that is used in this study is that of Peccerillo and Taylor (1975), which is based primarily on SiO_2 content. The term basalt refers to those rocks with up to 52% SiO_2, basaltic andesites range from 52% to 56% SiO_2, andesites from 56% to 63% SiO_2, dacites from 63% to 70% SiO_2 (rhyodacites refer to higher SiO_2 dacites), and rhyolites contain over 70% SiO_2.

Modal analyses of representative samples are presented in Table 2. Compositions of phenocrysts and groundmass minerals were obtained by electron microprobe analysis and results are presented in Figures 3 to 5, and selected representative analyses are listed in Table 3.

3.1 Basalts:

Basalts predominate unit PII and are generally porphyritic, containing up to 25% phenocrysts dominantly of plagioclase and olivine with trace amounts of clinopyroxene and spinel (Table 2). Groundmass textures are varied and may be subophitic, intergranular, or trachytic, with the groundmass grain size and vesicularity depending upon sample location within flows or dikes. Subophitic to intersertal textures with subequal proportions of plagioclase and pyroxene, with minor olivine, glass, and spinel, are typical of more mafic basalts such as sample 13828. Intergranular textures are characteristic of basalts such as 272825, and trachytic textures with plagioclase dominating the groundmass mineralogy are observed in samples such as 138212, which are closer to basaltic andesites in composition. The latter are also generally nearly aphyric.

Plagioclase is the dominant phenocryst mineral except in samples which may have accumulated olivine (242822a). Plagioclase phenocrysts

Table 2

Modal analyses (1000-1500 pts) of representative samples of post-glacial basalts, basaltic andesites, and andesites from Puyehue volcano

	basalts							
Sample	13828	272829	13826	272825	272824b	272821	138210	13824
groundmass %	81.0	78.0	86.7	89.3	81.8	82.8	75.3	75.0
phenocrysts %								
plagioclase	11.2	12.5	12.8	9.9	13.3	10.2	23.0	24.0
olivine	7.8	7.5	0.5	0.8	4.4	2.9	1.5	1.0
clinopyroxene	-	-	-	-	0.6	0.5	-	-
spinel	-	2.0	-	-	-	3.5	0.2	-

	basalts					
Sample	13822	242822a	220283-2	220283-4	220283-1	230283-2
groundmass %	85.7	73.7	85.1	75.5	79.7	88.6
phenocrysts %						
plagioclase	8.4	2.7	11.0	22.2	13.6	7.8
olivine	5.8	23.4	3.9	2.3	6.6	3.5
clinopyroxene	-	-	-	-	-	tr.
spinel	-	0.2	-	-	tr.	-

	basalts		basaltic andesites			andesites	
Sample	230283-5	250283-2	272827	220283-3	272826b	220283-5	272822
groundmass %	88.9	88.0	94.6	96.3	97.0	96.2	82.0
phenocrysts %							
plagioclase	7.0	10.7	3.4	2.0	2.1	2.1	11.4
olivine	4.0	1.3	0.9	1.7	0.9	0.9	5.1
clinopyroxene	-	-	-	-	-	0.3	0.3
spinel	-	-	1.1	-	-	0.5	1.1

Table 3

Representative analyses of phases in Puyehue Volcano lavas

	13828					272825						
	plagioclase		olivine	spinel		plagioclase		olivine		clinopyroxene		spinel
	core of large phenocryst	small groundmass phenocryst	core of phenocryst	phenocryst core	phenocryst rim	core of large phenocryst	small groundmass phenocryst	core of large phenocryst	small groundmass phenocryst	small groundmass microphenocrysts augite	small groundmass microphenocrysts pigeonite	inclusion in olivine
SiO_2	46.03	48.81	39.82	0.73	0.60	46.59	51.81	38.77	36.53	50.59	53.54	0.21
Al_2O_3	34.04	33.04	-	4.99	2.68	33.45	29.71	-	0.30	2.85	1.52	27.06
TiO_2			-	4.39	9.88			-	0.05	0.72	0.21	1.73
FeO	0.31	0.50	18.85	26.29	33.64	0.60	1.07	16.55	27.64	11.76	17.07	17.50
MgO	0.06	0.11	41.68	5.59	3.79	0.14	0.29	44.00	34.27	16.03	21.92	12.62
CaO	17.33	15.64	0.20	-	-	17.52	13.13	0.18	0.36	16.99	5.17	-
Na_2O	1.40	2.23				1.49	3.92			0.30	0.17	
K_2O	0.08	0.13				0.05	0.15			0.04	0.03	
MnO			0.06	-	-			0.26	0.63	0.38	0.64	0.52
Cr_2O_3			-	13.98	4.25			-	0.02	0.18	0.01	24.68
Fe_2O_3				42.26	43.38							15.39
Totals:	99.26	100.46	100.60	98.23	98.22	99.84	100.09	99.76	99.81	99.85	100.28	99.71

	272826a					138212			272824b								
	plagioclase		olivine	spinel	glass	plagioclase		olivine	plagioclase		olivine		pyroxene			spinel	
													small groundmasss microphenocrysts				
	phenocryst core	phenocryst rim	core of phenocryst	inclusion in olivine	inclusion in olivine	core of phenocryst	groundmass micro-phenocryst	small phenocryst	core of large phenocryst	small groundmass phenocryst	core of large phenocryst	small resorbed phenocryst	augite	ortho-pyroxene	pigeonite	small ground-mass pheno-cryst	inclu-sion in olivine
SiO_2	47.86	51.22	39.11	0.09	49.85	48.09	54.76	37.40	47.20	53.86	38.29	37.35	51.04	53.66	53.60	1.05	0.20
Al_2O_3	32.98	30.44	0.04	26.75	18.07	31.83	27.47	0.04	34.05	27.50	0.01	0.05	1.93	1.96	0.82	2.04	6.29
TiO_2			-	0.52	0.63			0.01			0.05	0.04	0.64	0.42	0.23	12.28	3.85
FeO	0.52	0.57	15.59	16.45	9.33	0.82	1.39	27.22	0.84	1.36	20.65	26.98	11.17	16.78	17.81	35.43	27.51
MgO	0.19	0.23	44.98	12.73	7.46	0.09	0.16	35.06	0.13	0.25	41.13	35.42	16.19	23.61	23.23	3.38	4.93
CaO	16.71	14.51	0.22		11.32	16.55	11.51	0.21	16.53	11.84	0.16	0.20	18.54	2.40	4.02	0.19	0.02
Na_2O	1.85	3.03			2.41	2.39	4.75		1.79	4.31			0.25	0.09	0.07		
K_2O	0.09	0.11			0.37	0.07	0.35		0.14	0.48			0.05	0.04	-		
MnO			0.20	0.66	0.15			0.59			0.40	0.53	0.43	0.68	0.59	0.54	0.70
Cr_2O_3			-	34.43	0.02		-				0.02	-	0.02	0.02	0.02	0.30	20.85
Fe_2O_3				8.58												44.15	36.21
Totals:	100.20	100.10	100.13	100.21	99.62	99.84	100.41	100.53	100.67	99.61	100.71	100.57	100.27	99.65	100.39	99.36	100.60

Table 3 (continued)

Representative analyses of phases in Puyehue Volcano lavas

	272822									212826				
	plagioclase		olivine	augite		pigeonite		spinel	ilmenite	plagioc-clase	augite	ortho-pyroxene	spinel	ilmenite
	core of large phenocryst	phenocryst in cluster	core of large phenocryst	core of phenocryst	core of phenocryst	large phenocryst: core	phenocryst: rim	phenocryst in cluster	phenocryst in cluster	core of phenocryst	small phenocryst	small phenocryst	small phenocryst	small phenocryst
SiO_2	48.02	57.43	39.20	52.28	51.52	50.46	50.55	0.24	0.13	57.22	51.00	51.51	0.29	0.45
Al_2O_3	32.26	25.76	-	1.57	3.40	0.53	0.53	2.54	0.39	26.51	1.58	0.77	2.33	0.35
TiO_2				0.48	0.55	0.35	0.39	16.13	45.50		0.67	0.30	18.33	47.56
FeO	0.65	0.49	16.17	13.46	9.07	24.71	26.10	41.19	33.32	0.49	13.74	23.67	44.42	38.55
MgO	0.18	0.04	44.11	13.43	16.55	15.91	16.67	2.77	3.86	0.05	13.88	20.46	1.94	1.59
CaO	16.76	9.26	0.20	18.29	18.49	6.33	3.97	0.10	-	9.13	17.79	1.99	-	-
Na_2O	1.94	6.16	0.29	0.22	0.01	-			6.14	0.26				
K_2O	0.06	0.38		-	0.02	0.03	0.01			0.27	0.05	0.01		
MnO			0.32	0.40	0.22	1.01	1.10	0.58	0.55		0.73	1.07	0.71	0.83
Cr_2O_3			-	-	0.06	0.06	0.04	-	-		0.06	0.05	-	-
Fe_2O_3								36.31	15.37				31.87	9.43
Totals:	99.87	99.52	100.00	100.21	100.08	99.40	99.37	99.86	99.12	99.79	99.76	99.83	99.89	98.76

	242824										
	plagioclase				olivine		clinopyroxene		spinel		ilmenite
	core of large resorbed phenocryst	core of large phenocryst	small phenocryst	small phenocryst	core of phenocryst	phenocryst in cluster	phenocryst core	phenocryst rim	in basalt inclusion	phenocryst in cluster	lamellae in spinel phenocryst
SiO_2	47.41	59.98	52.62	60.70	39.50	31.09	50.08	50.56	0.43	0.20	0.16
Al_2O_3	33.30	25.19	29.70	24.23	0.02	0.07	0.97	0.62	24.06	1.51	0.51
TiO_2					-	0.17	0.40	0.26	0.89	22.91	40.98
FeO	0.62		0.86	0.29	16.28	56.69	20.05	24.87	18.08	47.92	30.75
MgO	0.16	0.04	0.25	0.03	44.15	9.89	9.62	9.96	11.24	2.34	2.85
CaO	16.57	7.20	13.01	6.39	0.22	0.33	17.50	12.88	-	-	0.09
Na_2O	2.04	7.41	3.90	7.93			0.25	0.10			
K_2O	0.07	0.42	0.17	0.51			0.02	-			
MnO					0.19	1.92	0.94	1.17	0.67	0.71	0.68
Cr_2O_3					-	0.12	-	0.03	32.78	-	-
Fe_2O_3									11.70	23.98	22.98
Totals:	100.18	100.59	100.50	100.07	100.36	100.28	99.84	100.45	99.85	99.57	99.00

Table 3 (continued)

Representative analyses of phases in Puyehue Volcano lavas

	202825								
	plagioclase			clinopyroxene					spinel
	large phenocryst: core	rim	phenocryst in xenolith	small phenocryst	phenocryst in xenolith	pigeonite phen. core	rim	small phenocryst	small phenocryst
SiO_2	60.64	59.68	54.62	50.86	51.30	50.02	50.97	50.30	0.91
Al_2O_3	24.39	24.67	27.76	0.87	2.34	1.07	0.97	0.42	2.10
TiO_2				0.29	0.81	0.37	0.37	0.17	14.73
FeO	0.35	0.49	0.74	19.46	9.68	24.44	17.01	29.18	41.38
MgO	-	0.04	0.10	11.56	15.34	11.67	10.64	13.57	0.98
CaO	6.59	7.31	11.12	15.57	19.85	10.89	18.22	3.96	-
Na_2O	7.53	7.02	4.97	0.19	0.26	0.17	0.31	0.06	
K_2O	0.41	0.35	0.19	0.04	0.03	0.03	0.03	0.04	
MnO				1.15	0.44	1.45	1.07	1.91	0.94
Cr_2O_3				0.07	0.02	0.07	0.01	0.03	0.02
Fe_2O_3									38.43
Totals:	99.90	99.56	99.50	100.07	100.05	100.18	99.71	99.64	99.49

Table 3b

Representative analyses of phases in Cordon Caulle lavas

	72822 (CCV)							42824a (CCCVI)						
	plagioclase			augite	orthopyroxene	spinel	ilmenite	plagioclase			augite	orthopyroxene	spinel	ilmenite
	large phenocryst		small micro-phenocryst	phenocryst	phenocryst			large phenocryst		small micro-phenocryst	phenocryst	phenocryst		
	core	rim						core	rim					
SiO_2	59.77	57.70	59.03	50.53	50.82	0.14	0.13	54.82	58.12	61.09	50.86	50.92	0.22	0.26
Al_2O_3	24.23	25.57	24.85	1.31	0.41	2.11	0.39	28.15	25.43	23.42	1.03	0.52	1.89	0.24
TiO_2	-	-	-	0.41	0.24	17.47	45.80	-	-	-	0.44	0.18	18.41	47.82
FeO	0.41	0.49	0.50	13.12	25.87	43.29	33.57	0.60	0.49	0.60	15.53	27.19	44.99	38.41
MgO	0.01	0.06	0.03	13.94	19.16	2.13	3.68	0.07	0.04	0.00	12.44	17.90	1.53	1.90
CaO	7.36	8.73	7.49	19.08	1.74	0.00	0.08	10.85	8.01	6.06	18.45	1.70	0.00	0.00
Na_2O	7.25	6.29	6.94	0.37	0.00	-	-	5.60	6.89	7.29	0.41	0.02	-	-
K_2O	0.42	0.39	0.40	0.00	0.01	-	-	0.23	0.39	0.74	0.00	0.00	-	-
MnO	-	-	-	0.64	1.16	0.67	0.79	-	-	-	0.81	1.22	0.76	0.88
Cr_2O_3	-	-	-	-	-	0.04	0.16	-	-	-	0.02	0.00	0.00	0.00
Fe_2O_3	-	-	-	-	-	33.36	15.49	-	-	-	-	-	31.81	10.43
Totals:	99.46	99.22	99.24	99.40	99.40	99.21	100.08	100.31	99.38	99.20	99.98	99.65	99.62	99.95

	(212821 (CCVI)								182821b (CCIV)					
	plagioclase				augite	orthopyroxene	spinel	ilmenite	plagioclase		olivine	augite	pigeonite	spinel
	large phenocryst		small phenocryst											
	core	rim	core	rim	phenocryst	phenocryst			core	rim	phenocryst	phenocryst	phenocryst	
SiO_2	55.54	59.04	60.48	59.29	51.46	51.07	0.18	0.13	59.57	60.74	30.78	50.10	50.06	0.41
Al_2O_3	27.75	25.30	24.52	25.33	1.01	0.49	1.74	0.15	24.81	23.92	0.08	0.65	0.46	1.72
TiO_2	-	-	-	-	0.34	0.17	18.00	48.65	-	-	0.12	0.30	0.19	18.53
FeO	0.38	0.46	0.28	0.42	15.05	26.04	43.68	38.26	0.38	0.40	56.50	20.73	31.61	45.64
MgO	0.01	0.00	0.00	0.00	12.75	19.24	2.23	2.56	0.02	0.03	9.57	8.48	11.02	0.85
CaO	10.33	7.69	6.70	7.43	18.58	1.75	0.00	0.00	6.46	5.95	0.31	18.62	5.27	0.00
Na_2O	5.49	7.09	7.30	6.55	0.31	0.00	-	-	8.12	8.27	-	0.16	0.07	-
K_2O	0.19	0.34	0.35	0.32	0.00	0.00	-	-	0.48	0.49	-	0.03	0.02	-
MnO	-	-	-	-	0.75	1.21	0.63	0.76	-	-	2.29	1.09	1.77	0.89
Cr_2O_3	-	-	-	-	0.00	0.05	0.21	0.00	-	-	0.06	0.07	0.11	0.03
Fe_2O_3	-	-	-	-	-	-	32.91	9.41	-	-	-	-	-	31.21
Totals:	99.69	99.91	99.63	99.34	100.25	100.02	99.58	99.92	99.82	99.81	99.70	100.24	100.58	99.28

3(a) Results of microprobe analysis of plagioclase in Puyehue lavas. Each symbol represents one point analysis. Open symbols refer to analyses of phenocryst cores or interiors, closed symbols refer to analyses of groundmass microphenocrysts or phenocryst rims.

(b) Microprobe analyses of plagioclase in Cordon Caulle rhyodacites and rhyolites, symbols as above.

4 Results of microprobe analysis of olivines in Puyehue lavas, with symbols as explained in Figure 3.

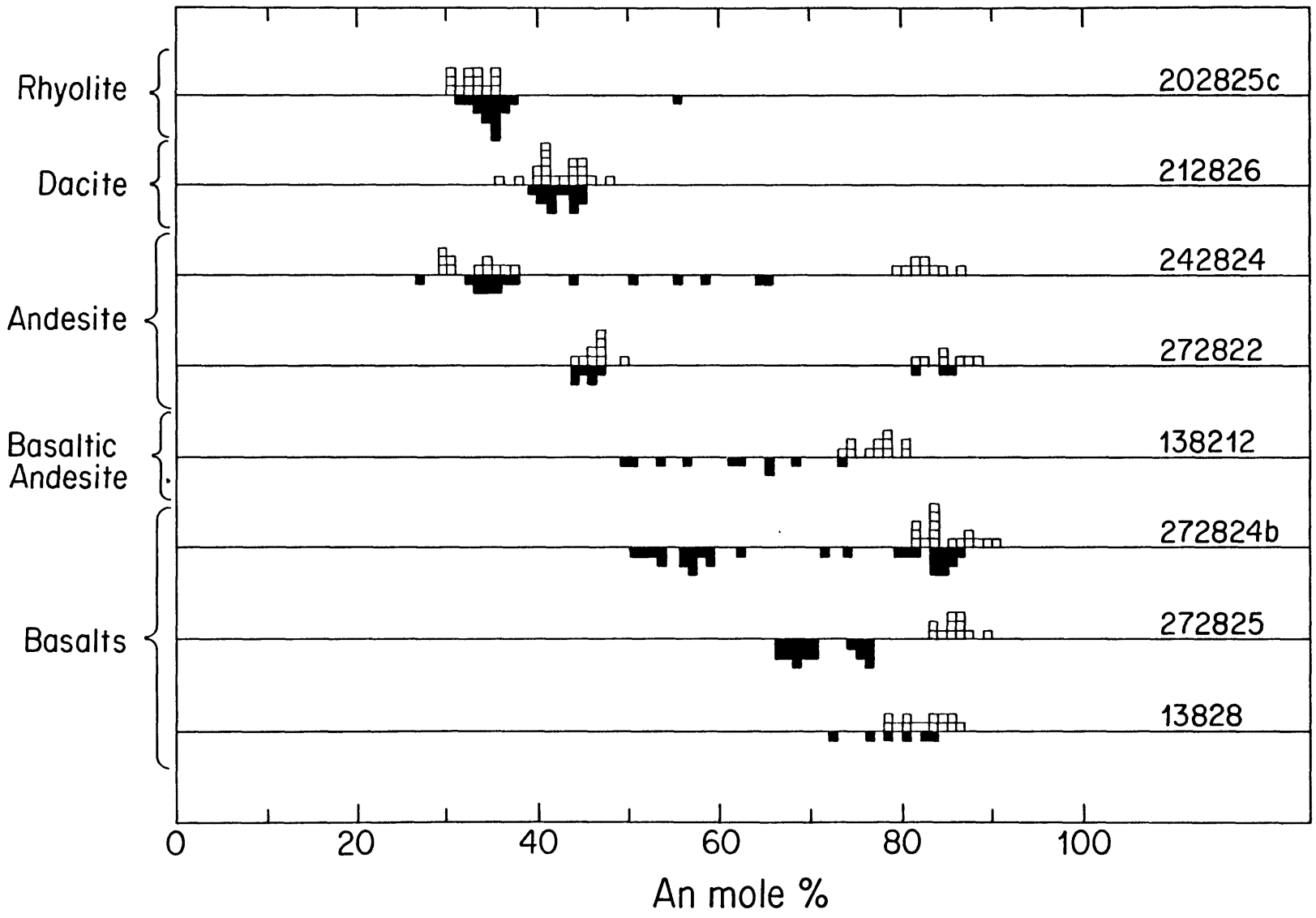
Rhyolite
Dacite
Andesite
Basaltic Andesite
Basalts
202825c
212826
242824
272822
138212
272824b
272825
13828
0
20
40
60
80
100
An mole %

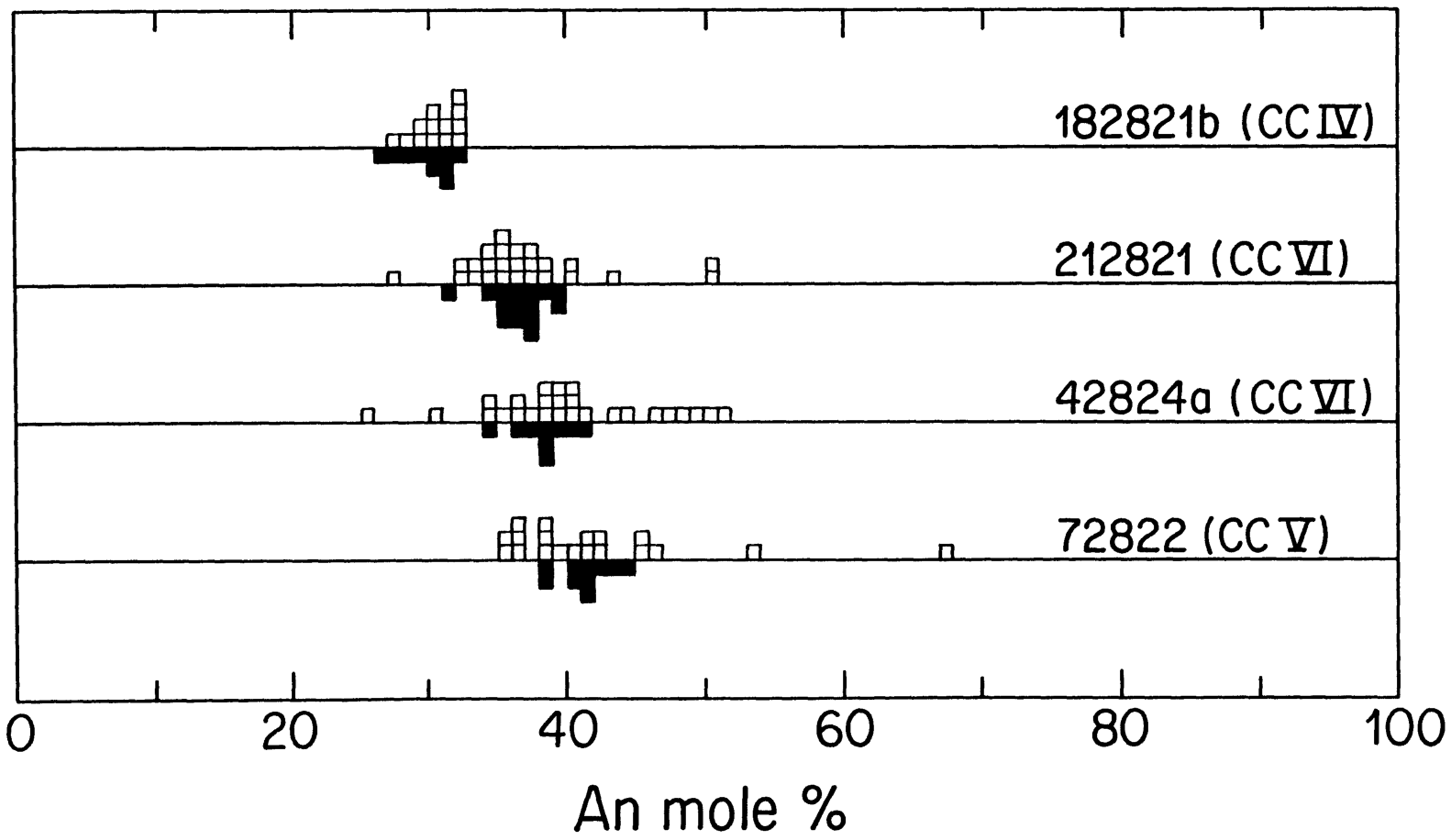
182821b (CC IV)
212821 (CC VI)
42824a (CC VI)
72822 (CC V)
0
20
40
60
80
100
An mole %

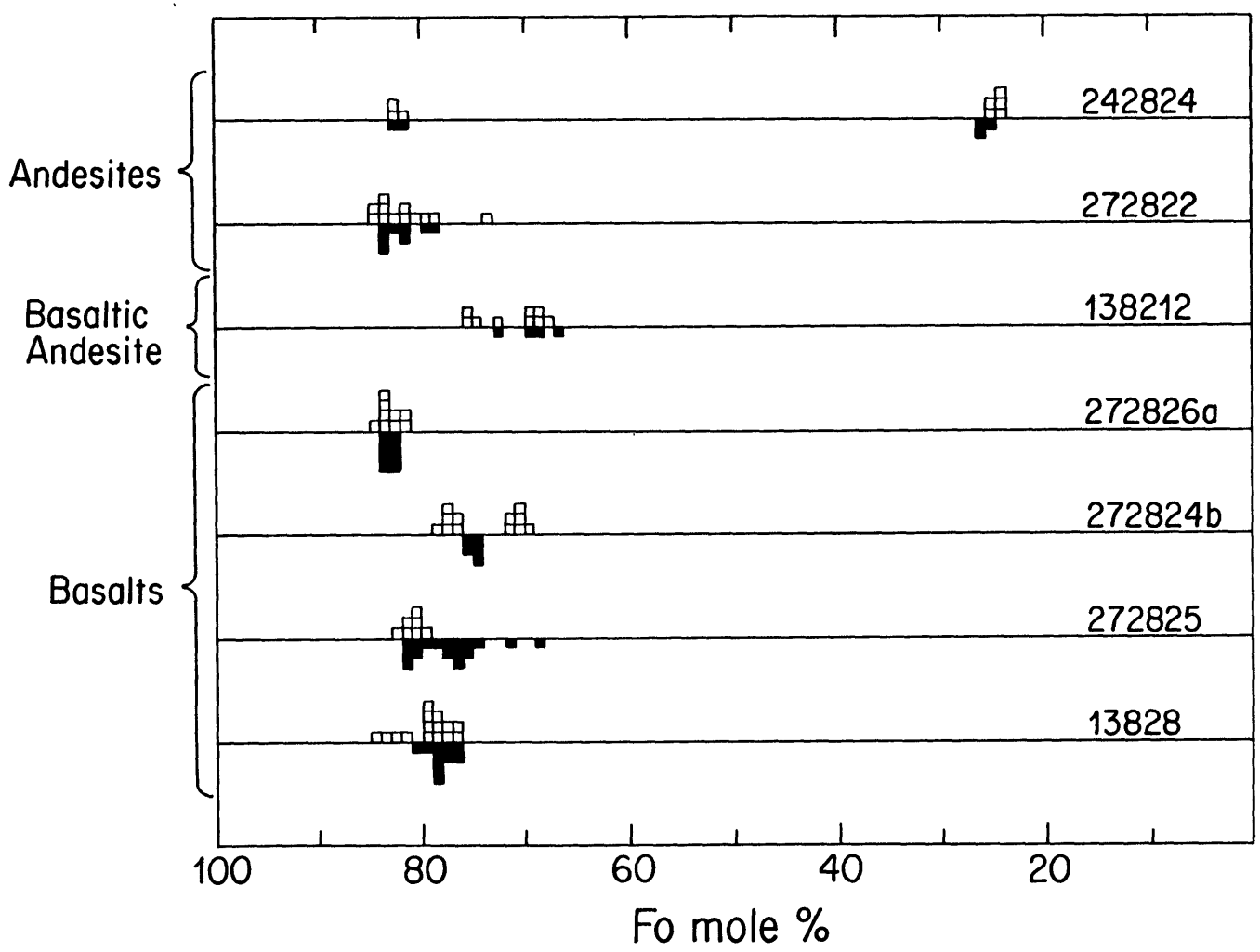
Andesites
Basaltic Andesite
Basalts
242824
272822
138212
272826a
272824b
272825
13828
100
80
60
40
20
Fo mole %

5 Pyroxene compositions in Puyehue lavas and compiled from literature sources for comparison.

(a) compositions of groundmass pyroxenes in representative basalts, phenocrysts in mixed andesites, and pyroxene phenocrysts in dacite and rhyolite from Puyehue Volcano.

(b) analyses of pyroxene and iron-rich olivine phenocrysts from Hakone Volcano, Japan (Nakamura and Kushiro, 1970), Asio, Japan (Kuno, 1969), Marianas Arc (Dixon and Batiza, 1979), and Bishop Tuff (Hildreth, 1979).

(c) compositions of pyroxene phenocrysts in Cordon Caulle lavas.

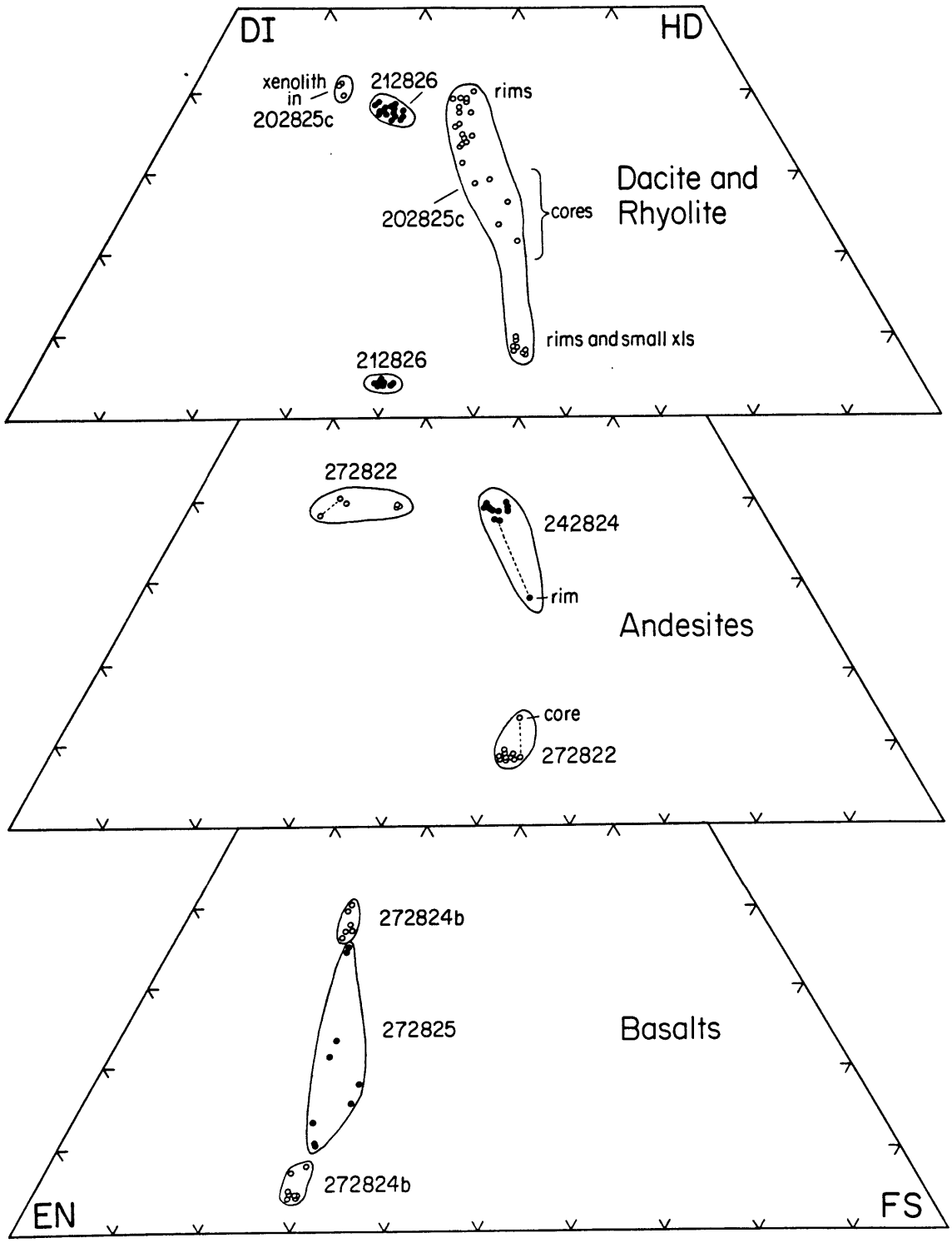
DI
HD
xenolith in 202825c
212826
rims
202825c
cores
Dacite and Rhyolite
rims and small xls
212826
272822
242824
rim
Andesites
core
272822
272824b
272825
Basalts
272824b
EN
FS

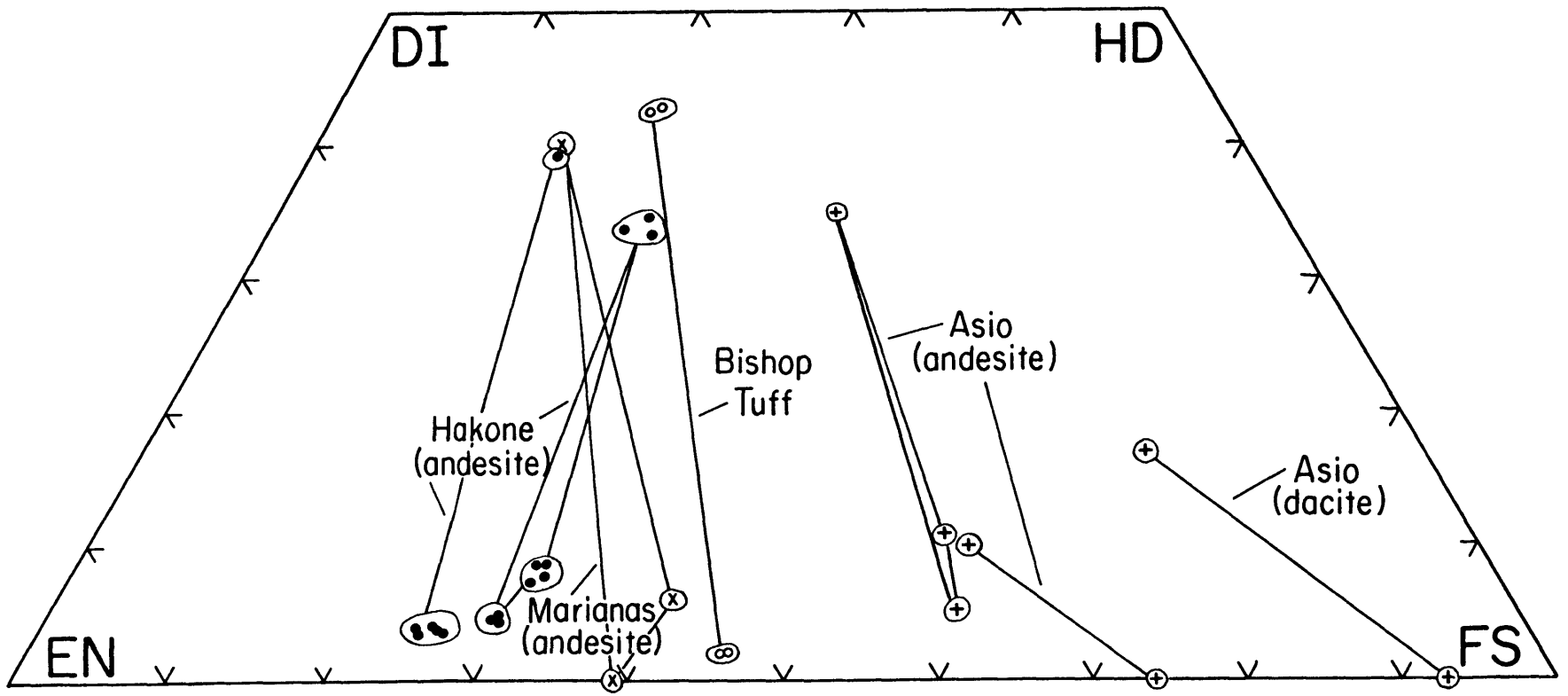
DI
HD
EN
FS
Bishop
Tuff
Hakone
(andesite)
Marianas
(andesite)
Asio
(andesite)
Asio
(dacite)

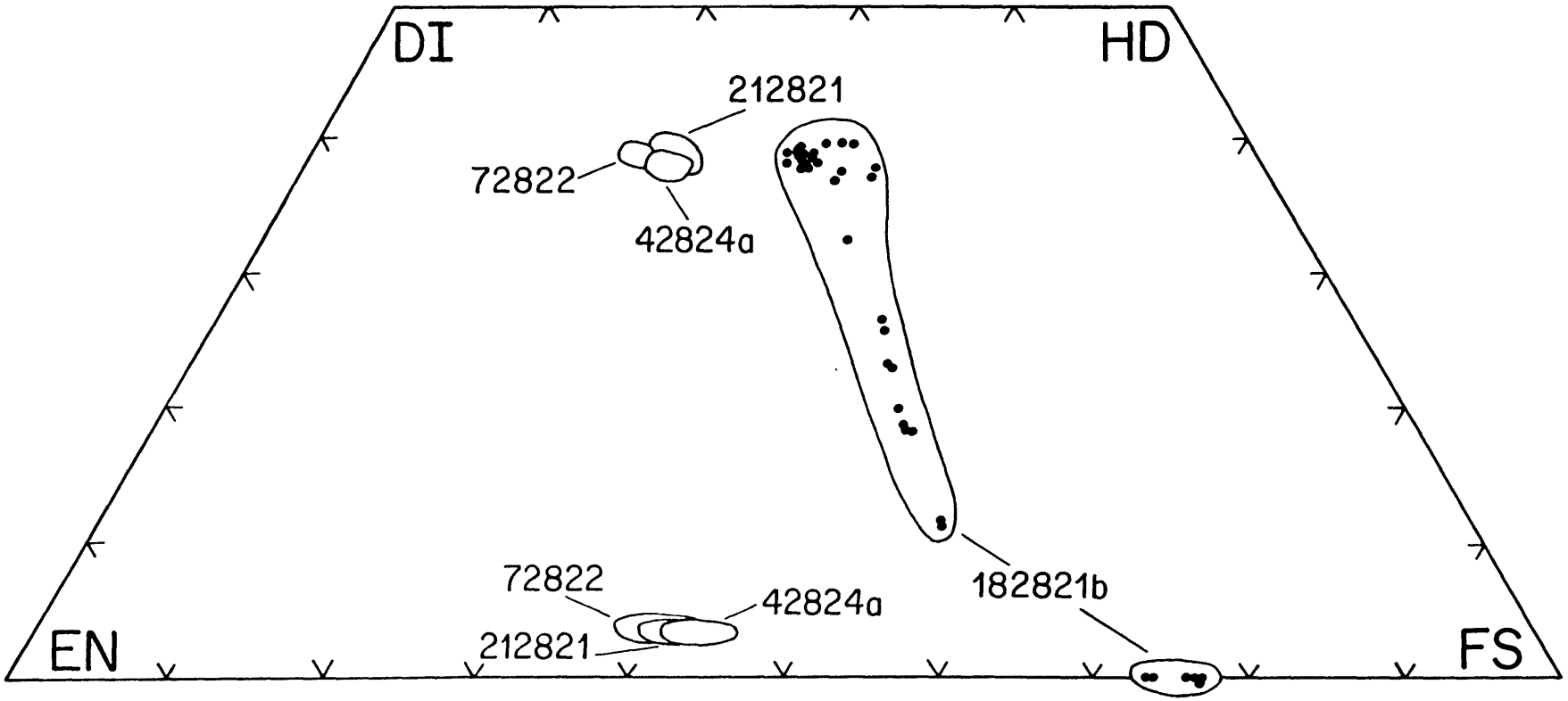
DI
HD
212821
72822
42824a
182821b
72822
42824a
212821
EN
FS

may be large (2-3 mm) and occur in intergrown clusters up to 5 mm in size, or may be small, grading in size to that of microphenocrysts in the groundmass. Plagioclase phenocryst cores range in composition from An_{90} to An_{78} and may display subdued normal zoning up to 5% An content (Fig. 3a, Table 3a). Most phenocrysts contain a few inclusions of glass or crystallized glass; in some samples, the inclusions are numerous, resulting in a sieve-like texture. Some plagioclase phenocrysts in sample 272824b display one or more zones riddled with inclusions alternating with inclusion-free zones and a clear outer rim or overgrowth. The alternating zones (those with and without inclusions) in these phenocrysts rarely differ in composition by more than 5% An and the clear zones and outer rims correspond to more calcic compositions. In all basalts, groundmass plagioclase microphenocryst compositions span a compositional range of An_{83} to An_{50} (Fig. 3a). Borderline basaltic andesites such as 138212 contain small, rare phenocrysts of An_{81} to An_{73} composition, while rim and groundmass miocrophenocryst compositions range from An_{73} to An_{50}.

Olivine phenocrysts vary in abundance (Table 2) and size, from microphenocrysts to larger (up to 3 mm in diameter) rounded or subhedral grains. Cores of large phenocrysts are Fo_{84} to Fo_{77} in composition and display very little, if any, compositional zoning within this range (Fig. 4). Groundmass olivines in 272825 and small olivine phenocrysts in 272824b and 138212 are more iron-rich, ranging from Fo_{78} to Fo_{68} in composition. Large olivine phenocrysts (Fo_{84} to Fo_{80}) in basalt 272825 display thin iron-rich rims (Fo_{70}). Olivine phenocrysts in 272824b are bimodal in their textural and compositional characteristics. Larger olivine phenocrysts (1-2 mm in diam.) in this sample average Fo_{78} in

composition while smaller phenocrysts averaging Fo_{71} display distinctive largely opaque reaction rims, presumably consisting of spinel and glass.

Pyroxenes occur only as groundmass phases in the basalts. In samples 272825 and 272824b these include subcalcic augite ($Wo_{35}En_{46}Fs_{19}$ to $Wo_{41}En_{43}Fs_{16}$), pigeonite ($Wo_9En_{65}Fs_{26}$ to $Wo_{24}En_{53}Fs_{23}$), and orthopyroxene with an average composition of $Wo_{4.5}En_{67.5}Fs_{28}$ (Fig. 5a and Table 3a). Chrome-rich magnetites occur as discrete, zoned phencorysts in some basalts (sample 13828, Table 3a) and titaniferous magnetites occur in the groundmass of most others (272824b, Table 3a). Chromian spinels are common as inclusions in olivine phenocrysts (samples 272825, 272824b, and 272826b, Table 3a).

3.2 Basaltic andesites

All basaltic andesites studied are nearly aphyric, with very fine-grained pilotaxitic, intergranular, or trachytic groundmass textures. The groundmass mineralogy is dominated by microlites of plagioclase and spinel, and spinel is relatively more abundant as a groundmass phase in samples with higher TiO_2 content (next section). Flows and dikes of basaltic andesite were usually coarsely vesicular. Of the rare phenocrysts observed, plagioclase was predominant as small lath-shaped euhedra with sieve-textured interiors in some samples. Olivine phenocrysts are rare and small in size (<0.5 mm in diam.). Clinopyroxene phenocrysts are absent.

With the exception of sample 272826b, all other basaltic andesites sampled belong to stratigraphic unit PI (Table 1) and are of preglacial age. Sample 272826b is from a sill intruding deposits of tephra and basaltic scoria in the lowermost PIII strata. This sample is somewhat

altered in that rare olivine microphenocrysts are partly replaced by iddingsite and chlorite, and interstitial groundmass glass has been partly altered to chlorite.

3.3 Andesites

Andesites of unit PI are extremely fine grained, nearly aphyric, and distinguished from basaltic andesites only by the appearance of spinel and rare orthopyroxene phenocrysts. Small (<1 mm in length) plagioclase phenocrysts are the most common phenocryst phase, and small rare olivine phenocrysts are commonly embayed. As in the basaltic andesites described earlier, spinel microlites are present in significant amounts in the groundmass. Groundmass mineral proportions are locally variable in the PI andesites, resulting in a mottled or flow-banded appearance.

PIV andesites contrast greatly with PI andesites. The PIV andesites are subordinate in volume to all other rock types (Table 1) and are typically vesicular and porphyritic with glassy to intergranular groundmass textures. Microphenocrysts of plagioclase and spinel in the groundmass tend to be blocky in shape. Andesites (samples 43821 and 220283-5) from the PIV cinder cone on the south flank of the volcano (Fig. 1) are vesicular and aphyric, almost glassy.

Two samples studied in detail (242824 and 272822) contain disequilibrium phenocryst assemblages. Sample 272822 was collected from an aa flow near the top of the crater on the south face of Puyehue Volcano. Plagioclase phenocrysts in this sample are bimodal in composition (Fig. 3a). Large calcic plagioclase phenocrysts (An_{82} to An_{88}) display extensive sieve-like resorption or reaction textures and are less abundant than phenocrysts of An_{44} to An_{49} composition which

occur as clear euhedra ranging in size from microphenocrysts to phenocrysts 2 mm or more in length. Olivine phenocrysts ranging in composition from Fo_{85} to Fo_{74} reach 5 mm in diameter (Fig. 4). Small, rare augite phenocrysts ($Wo_{38}En_{47}Fs_{15}$ to $Wo_{39}En_{38}Fs_{23}$) occur in sample 272822 (Fig. 5a). These augite phenocrysts may be in equilibrium with the resulting mixed groundmass composition of the andesite, but are not in equilibrium with the bulk composition, since the latter is affected by olivine phenocrysts possibly retained from a presumed basaltic mixing endmember. Pigeonite phenocrysts are zoned from cores of composition $Wo_{13}En_{39}Fs_{48}$ to rims averaging $Wo_{8.5}En_{42.5}Fs_{49}$. The pigeonite phenocrysts are not in equilibrium with the bulk composition of andesite 272822 nor the augite phenocrysts, based on experimental exchange K_D's, and may have crystallized out of a rhyodacitic magma. Ilmenite, titanomagnetite, and pigeonite may be in clusters with the more sodic plagioclase phenocrysts. Olivine, augite, and calcic plagioclase phenocrysts occur as discrete phenocrysts mixed with the above, or in dark, highly vesicular domains displaying diffuse contacts with the groundmass. The latter are interpreted as partially assimilated inclusions of scoriaceous basaltic material.

Sample 242824 was collected from a pahoehoe flow also on the south flank of Puyehue at a lower elevation relative to the locality of 272822 (Fig. 2). The fine-grained intergranular groundmass of 242824 is similar to that of 272822, but contains small but significant amounts of pyroxene and olivine microphenocrysts and is more vesicular. Plagioclase phenocrysts again display a strong bimodal compositional distribution (Fig. 3a). Calcic plagioclase phenocrysts (An_{80} to An_{87}) in 242824 contain fewer inclusions than those in 272822, and these may be arranged

in concentric zones as in the plagioclase phenocrysts described earlier in basalt 272824b. The sodic (An_{29} to An_{37}) phenocrysts in 242824 are larger in size (up to 2 mm length) and relatively more sodic than their counterparts in 272822. Plagioclase phenocryst rim, overgrowth, and groundmass microphenocryst compositions in 242824 span a wide compositional range of An_{27} to An_{66} (Fig. 3a). Large (up to 3 mm) olivine phenocrysts of composition Fo_{83} containing Cr-spinel inclusions occur in dark, diffuse basaltic inclusions as in 272822. Iron-rich olivine phenocrysts (ferrohortonolite) averaging Fo_{24} in composition occur in clusters with ferroaugite, titanomagnetite, and sodic plagioclase, and may display very slight reverse zoning (Fig. 4). A few phenocrysts of ferroaugite typically averaging $Wo_{39}En_{28}Fs_{33}$ in composition (Fig. 5a) are zoned to rims of subcalcic ferroaugite ($Wo_{28}En_{30}Fs_{42}$).

Iron-rich phenocrysts such as the pigeonites in 272822, and the ferrohortonolites (olivine) and subcalcic ferroaugites in 242824 are rarely encountered in calc-alkaline rocks. Instead, pyroxene compositions comparable to these are more characteristic of pyroxene groundmass phases in many calc-alkaline volcanics (Nakamura and Kushiro, 1969; Ewart, 1976; Sakuyama, 1981). Olivine phenocrysts as iron rich as Fo_{46} have been analyzed in andesites from Boqueron Volcano, El Salvador (Fairbrothers et al., 1978). Ferroaugite ($Wo_{35}En_{29}Fs_{36}$), ferropigeonite ($Wo_{10}En_{34}Fs_{56}$), ferrohypersthene ($Wo_{5}En_{36}Fs_{59}$), and ferrohortonolite (Fo_{26}) were described in andesite dikes near Asio, Japan, by Kuno (1969). In the same locality, a dacite dike was found to contain ferropigeonite ($Wo_{17}En_{18}Fs_{65}$) and fayalite (Fig. 5b).

3.4 Dacites, rhyodacites, and rhyolites

Dacites occur in the preglacial unit PI or as rare flows intercalated with PII basalts. The dacites are typically porphyritic (10-15% phenocrysts) with pilotaxitic to hyalopilitic groundmass textures. Plagioclase phenocrysts are most abundant, euhedral, and small in size (<1 mm in length). Spinel phenocrysts are next in abundance and a few may be found in clusters with plagioclase and rare phenocrysts of clinopyroxene and orthopyroxene. Olivine phenocrysts (to 2 mm in diameter) mantled by small plagioclase phenocrysts occur in sample 23825.

Rhyodacites are common as relatively later eruptive products in unit PIII of Puyehue Volcano. Rhyodacite lavas are also porphyritic (5-15% phenocrysts) with similar groundmass textures as observed in the dacites. Samples 1428210 and 212824 are exceptional in that they were taken from the fresh interiors of large, glassy, vesicular pumice bombs up to 60 cm in diameter. The major distinguishing feature between dacites and rhyodacites is the complete absence of olivine phenocrysts and the relatively greater abundance of clinopyroxene and orthopyroxene phenocrysts in the rhyodacites. Plagioclase phenocrysts may be large (up to 3 mm length), frequently display slight normal or oscillatory zoning, and in sample 212826 range in composition from An_{36} to An_{48}, overlapping with groundmass microphenocryst compositions (Fig. 3a). Both augite phenocrysts (average: $Wo_{38}En_{40}Fs_{22}$) and orthopyroxene phenocrysts (average: $Wo_{4}En_{57}Fs_{39}$) in 212826 are apparently in equilibrium and display little compositional zoning and occur in clusters with plagioclase, titanomagnetite, and ilmenite phenocrysts (Fig. 5a).

Rhyolite samples analyzed in this study were found in the uppermost PIII strata. Rhyolites are glassy, vesicular lavas with minor flowbanding expressed by concentrations of crystallites and contain few phenocrysts (3-5% total). Plagioclase phenocrysts in sample 202825c vary little in composition (An_{31} to An_{36}); a small phenocryst of An_{56} composition in this sample (Fig. 3a) occurs in a small xenolith, possibly of andesitic composition. Small groundmass augite in this xenolith is similar in composition to augite in some of the basalts (Fig. 5a). Small clinopyroxene phenocrysts in 202825c are consistently zoned from cores of subcalcic ferroaugite ($Wo_{22}En_{34}Fs_{44}$ to $Wo_{29}En_{33}Fs_{38}$) to rims of either borderline ferroaugite ($Wo_{31}En_{35}Fs_{34}$ to $Wo_{40}En_{30}Fs_{30}$) or pigeonite (average $Wo_9En_{40}Fs_{51}$). This is similar to the zoning observed in the pigeonite phenocrysts in andesite 272822 but is the reverse of that observed in the ferroaugite phenocrysts in 242824 (Fig. 5a). The augite and pigeonite compositions analyzed in 202825c are similar in composition to the augite phenocrysts in 242824 and the pigeonite phenocrysts in 272822, respectively.

3.5 Cordon Caulle rhyodacites and rhyolites

Rhyodacites and rhyolites of this unit are typically glassy to hyalopilitic in texture, and sparsely porphyritic, containing about 5% phenocrysts on the average and up to 10% locally in some samples. Flowbanding is expressed by variations in the concentrations of microphenocrysts and microlites. Microphenocrysts and microlites of feldspar are usually aligned parallel to flowbands. In some samples, the lava was apparently quite viscous such that differential flowage on a scale of mm to cm created shear stresses that caused fracturing of

phenocrysts. Fragments of single phenocrysts occur in elongated 'trains.' Plagioclase phenocrysts are most abundant, and augite, orthopyroxene, pigeonite, and magnetite occur in subequal proportions. Ilmenite phenocrysts, when present, are subordinate in volume to magnetite phenocrysts. Representative analyses of phenocrystic phases are presented in Table 3b.

Sample 72822 is a rhyodacite from the CCV unit, produced in the 1921-1922 eruption. Plagioclase phenocrysts in this sample are mostly clear and euhedral, and the range in compositions from An_{35} to An_{46} (Fig. 3b) is due to normal, reverse, and oscillatory zoning observed in many phenocrysts. More calcic compositions (An_{53} to An_{67}) correspond to rare, slightly resorbed phenocrysts displaying reverse zoning or relatively more sodic (An_{40}) overgrowths. Augite phenocrysts average $Wo_{39}En_{40}Fs_{21}$ (Fig. 5c) and a few appear to display slight reverse zoning (1-2%) with respect to En and Fs components. Orthopyroxene phenocrysts average $Wo_4En_{57}Fs_{39}$ in composition and likewise may display subdued reverse zoning.

Rhyodacites of the CCVI unit erupted in 1960 as represented by samples 42824a and 212821 are very similar to CCV rhyodacites such as sample 72822 but are geochemically more evolved as discussed in later sections. Plagioclase phenocrysts in 42824a and 212821 are also variable in composition (An_{25} to An_{52}) but include more sodic compositions compared to those in 72822 (Fig. 3b). The variability in plagioclase phenocrysts is also related to normal, reverse, and oscillatory zoning. Relatively more calcic compositions (up to An_{52}) are observed in a few rare phenocrysts but these lack any evidence of resorption. Augite phenocrysts in both samples average $Wo_{38}En_{38}Fs_{24}$ in composition (Fig. 5c)

and also display suggestions of reverse compositional zoning, as do some orthopyroxene phenocrysts, which average $Wo_3En_{54}Es_{43}$ in composition. In rhyodacites from both the CCV and CCVI units, phenocrysts may occur in clusters of attached, touching, or intergrown crystals. Many such clusters consist of all phenocrysts minerals present, including plagioclase, augite, orthopyroxene, magnetite, and ilmenite, or subsets thereof.

Rhyolites of the relatively earlier CCIV unit are generally more glassy in texture than the rhyodacites, and phenocrysts in the rhyolites are smaller (< 1 mm) in size compared to those in the rhyodacites. Plagioclase phenocrysts in the rhyolites display little or no significant compositional zoning (Table 3b) and are restricted in composition (An_{26} to An_{32}) as in sample 182821b (Fig. 3b). Phenocrysts of ferroaugite average $Wo_{39}En_{28}Fs_{33}$ in composition, are slightly more Fe-rich than those in PIII rhyolite 202825c (Fig. 5a), and are identical to those in the PIV mixed andesite 242824. A few phenocrysts of ferroaugite appear to be zoned to ferropigeonite compositions. A preliminary SEM inspection revealed that pigeonite compositions occur as patchy intergrowths (T. Grove, pers. comm.) and this may be due to a sudden change in the physical conditions of crystallization. Ferropigeonite phenocrysts in the CCIV rhyolite 182821b are variable in composition ($Wo_{27}En_{30}Fs_{43}$ to $Wo_{11}En_{34}Fs_{55}$) and compositional zoning relationships are unclear, if these are zoning relationships. This range in pigeonite compositions in 182821b is similar to that observed in sample 202825c, although those in the latter are zoned to relatively lower Ca contents (to Wo_8). Fe-rich olivine phenocrysts in 182821b are slightly variable in composition (Fo_{23} to Fo_{27}) and are similar to those analyzed in the andesite 242824 (cf.,

Figs. 4 and 5c). Ilmenite phenocrysts were not observed in sample 182821b. As in the rhyodacites, clusters of phenocrysts are common in CCIV rhyolites. As exemplified in sample 182821b, phenocryst clusters may consist of some or all phenocryst minerals, including plagioclase, ferroaugite, ferropigeonite, olivine, and magnetite.

4. Geochemistry

Analytical methods are discussed in Appendix I, and results are presented in Tables 4 and 5. A total of 74 samples from Puyehue Volcano and Cordon Caulle were analyzed for major-element compositions. Abundances of Nb, Zr, Zn, Ni, Cr, V, Ba, and Sr were measured in 69 samples and those of Rb, Sr, Y, Pb, and Ga were measured in 53 samples by XRF. Abundances of REE, Sc, Cr, Co, Hf, Ta, and Th were measured in 48 samples by INAA. Abundances of K, Rb, Sr, Cs, and Ba were measured by isotope dilution methods in 32 samples, and abundances of Sm and Nd by this method in 27 samples. Sr-isotopic compositions were determined in 32 samples, 29 samples were analyzed for Nd-isotopic composition, and 8 samples for Pb-isotopic composition.

4.1 Alteration

Most samples analyzed in this study display little or no petrographic evidence of alteration, as also indicated by very low H_2O contents typically <0.2 wt.% (Table 4). Three PII samples (272826b, 13822, and 138210) are the most altered and have up to 0.5 wt.% H_2O. In these samples, olivine phenocrysts are partly or entirely replaced by chlorite, plagioclase phenocrysts may be cloudy, and the groundmass is partly altered to chlorite and displays iron-staining. In fine-grained,

Table 4

Major-element and trace element analyses of lavas from Puyehue Volcano

Preglacial Volcanics

PI

Sample number	162826	82825	222825a	1428212	162828a	172829c	82821
[1]SiO_2	51.61	53.73	54.32	54.31	54.73	55.02	56.46
Al_2O_3	17.65	14.79	16.16	16.28	15.66	15.20	14.85
TiO_2	1.29	2.56	1.26	1.26	1.66	1.57	1.73
Fe_2O_3	10.26	12.14	10.39	10.48	10.52	10.78	11.22
MgO	5.23	3.47	4.18	4.20	4.26	4.31	3.26
CaO	9.87	7.30	8.66	8.65	8.48	8.16	6.81
Na_2O	2.89	3.84	3.34	3.60	3.40	3.44	3.89
K_2O	0.62	1.04	0.83	0.77	0.89	1.16	1.30
MnO	0.18	0.20	0.18	0.17	0.18	0.18	0.20
P_2O_5	0.24	0.54	0.27	0.26	0.21	0.27	0.37
total	99.84	99.61	99.59	99.98	99.99	100.09	100.09
[2]CO_2	0.08	0.02	0.17	0.04	0.06	0.07	0.05
H_2O^+	0.35	0.15	0.39	0.07	0.43	0.47	0.12
[3]Sc	37.1	38.8		36.0	39.7	38.4	35.1
V	289	305	283	280	326	300	334
Cr	122	1	31	33.4	51.4	57	1
Co	30.4	26.9		26.6	25.5	27.5	25.6
Ni	46	9	11	19	24	27	13
Zn	90	27	103	101	103	111	126
Ga		19.1	18.7	19.2	19.0	18.9	19.9
K		8503		6389	7412		10917
Rb		23.2	18.7	17.25	20.6	27.6	33.9
Sr	426	423.3	396.1	401.0	391.7	385.6	347.6
Cs		1.68		0.75	1.63		2.54
Ba	229	340.7	245	257.2	277.3	349	380.9
Y		36.2	24.8	25.7	20.1	27.1	35.0
Zr	94.3	154	106	102	130	155	173
Nb	2.8	5.0	2.4	2.9	4.7	5.7	5.1
Hf	2.63	3.57		2.62	3.19	3.77	4.26
Ta	0.14	0.27		0.19	0.20	0.30	0.32
Pb	-	11	6	10	10	9	13
Th	2.16	3.22	2.4	1.99	1.41	3.58	4.19
La	10.5	17.6		10.8	7.65	13.4	16.6
Ce	27.5	41.3		26.3	19.4	31.0	39.4
Nd	17.0	24.7		16.0	11.5	17.7	21.8
Sm	4.22	6.29		3.98	2.90	4.47	5.77
Eu	1.35	2.03		1.34	1.25	1.48	1.73
Tb	0.69	0.96		0.50	0.52	0.74	0.94
Yb	2.41	3.55		2.56	2.25	2.95	3.75
Lu	0.35	0.53		0.40	0.35	0.46	0.55

Table 4

Major-element and trace element analyses of lavas from Puyehue Volcano

Preglacial Volcanics (continued)

Sample number	52824b	82826b	182828c	92822	82824	142824	222821b
[1]SiO_2	56.59	56.59	56.80	56.82	59.56	59.75	60.51
Al_2O_3	15.62	15.11	16.06	15.68	15.64	15.50	15.85
TiO_2	1.36	1.73	1.15	1.60	1.38	1.26	1.24
Fe_2O_3	9.84	10.52	8.77	9.76	8.36	8.75	8.58
MgO	3.40	3.09	3.65	3.12	2.41	2.29	2.12
CaO	7.10	6.92	7.73	6.81	5.68	5.64	5.40
Na_2O	4.15	4.14	3.61	4.09	4.53	4.36	4.41
K_2O	1.43	1.18	1.15	1.21	1.73	1.64	1.64
MnO	0.19	0.20	0.16	0.19	0.19	0.18	0.17
P_2O_5	0.34	0.48	0.26	0.53	0.55	0.41	0.41
total	100.02	99.96	99.34	99.81	100.03	99.78	100.41
[2]CO_2	0.60	0.20	0.07	0.05	-	0.03	0.09
H_2O^+	0.73	0.24	0.21	0.12	0.18	0.32	0.21
[3]Sc		34.1				24.5	23.3
V	247	250	206	183	125	115	107
Cr	26	2	29	15	12	4.5	1
Co		21.2				15.2	14.3
Ni	17	12	11	11	15	11	9
Zn	106	118	93	115	106	100	112
Ga		19.5	17.6	19.1		18.7	19.0
K		10022					13605
Rb		27.8	24.5	27.7		42.7	40.9
Sr	358	394.3	386.6	405.9	361	338.5	353.7
Cs		2.00					1.89
Ba	389	333.1	358	362	525	479	479.1
Y		36.5	26.7	37.6		42.3	50.0
Zr	180	167	168	172	223	230	220
Nb	4.7	5.4	4.3	5.2	7.1	7.0	6.3
Hf		4.09				5.30	5.25
Ta		0.27				0.34	0.35
Pb		12	12	12		14	14
Th		3.40	3	4		4.89	5.17
La		18.0				22.2	25.1
Ce		44.0				50.9	62.7
Nd		25.2				29.1	36.5
Sm		6.19				6.77	8.32
Eu		1.93				1.83	2.01
Tb		0.94				1.07	1.18
Yb		3.77				4.41	5.13
Lu		0.56				0.66	0.74

Table 4

Major-element and trace element analyses of lavas from Puyehue Volcano

Preglacial Volcanics (continued)

Sample number	72821	72825a	23825	182823a	162821	202822b
[1]SiO_2	63.56	64.05	64.57	64.65	68.94	71.65
Al_2O_3	14.95	15.65	14.58	14.79	14.21	13.92
TiO_2	1.15	0.92	1.04	0.94	0.53	0.36
Fe_2O_3	7.20	6.57	7.20	6.90	5.22	4.09
MgO	1.44	1.34	1.37	1.54	0.23	0.04
CaO	4.13	4.03	3.82	4.08	2.28	1.71
Na_2O	4.84	4.91	4.68	4.41	5.16	5.25
K_2O	2.20	2.19	2.33	2.64	2.59	2.85
MnO	0.18	0.15	0.15	0.13	0.14	0.13
P_2O_5	0.41	0.30	0.32	0.25	0.12	0.05
total	100.06	100.11	100.06	100.33	99.42	100.05
[2]CO_2	-	-	0.06	0.02	0.14	0.19
H_2O^+	0.27	0.19	0.27	0.22	0.16	0.15
[3]Sc		19.1	20.4	19.3		
V	35	38.3	31	91	2	2
Cr	1	3	16.8	15	1	1
Co		7.49	8.86	11.9		
Ni	7	9	13	15	2	2
Zn	124	102	100	93	116	116
Ga		18.5	18.7	17.3	18.5	19.0
K						
Rb		58.1	63.2	79.8	64.3	73.0
Sr	338	288.8	267.4	244.7	200.8	141.9
Cs						
Ba	563	623	601	643	765	749
Y		46.7	57.5	47.4	28.7	58.9
Zr	294	293	287	322	333	383
Nb	8.7	8.6	6.6	8.3	8.7	10.5
Hf		6.75	7.01	7.25		
Ta		0.46	0.45	0.49		
Pb		18	20	22	26	23
Th		6.80	7.88	9.69	9	8
La		28.3	34.5	28.5		
Ce		71.4	69.8	69.1		
Nd		38.2	43.2	35.6		
Sm		8.14	9.42	7.78		
Eu		2.02	2.03	1.68		
Tb		1.30	1.48	1.20		
Yb		5.08	5.73	5.12		
Lu		0.76	0.91	0.77		

Table 4

Major-element and trace element analyses of lavas from Puyehue Volcano

PII

Sample number	242822a	272825	13826	13824	220283-2	230283-2	13828
[1]SiO_2	48.39	50.30	50.45	50.69	50.82	50.90	50.91
Al_2O_3	14.64	18.88	18.94	18.81	18.01	17.88	16.49
TiO_2	0.70	0.85	0.83	0.92	0.90	0.90	0.65
Fe_2O_3	10.78	9.56	9.48	9.25	9.23	9.21	9.02
MgO	14.32	5.91	5.91	5.17	6.88	6.92	9.52
CaO	8.55	10.59	10.53	10.59	10.01	9.95	10.36
Na_2O	2.19	2.95	2.90±.04	3.27	3.09	2.85	2.46
K_2O	0.31	0.44	0.42	0.46	0.55	0.56	0.49
MnO	0.17	0.15	0.14	0.17	0.17	0.17	0.13
P_2O_5	0.13	0.14	0.13	0.14	0.20	0.19	0.11
total	99.87	99.77	99.73	99.47	99.86	99.53	100.14
[2]CO_2	0.12	0.00	0.04	-	0.08	0.04	0.05
H_2O^+	0.17	0.16	0.06	0.26	0.29	0.21	0.10
[3]Sc	26.4	31.7	32.3±.4			29.9	31.8
V	163	219	205	233	206	201	193
Cr	640.	112.	118.3±2.8	114	113	117	426.
Co	64.5	33.5	34.2±.35			35.0	41.8
Ni	302	50	50	39	58	65	147
Zn	78	80	78	82	81	82	73
Ga	14.9	17.4	18.0				16.4
K		3567	3570			4709	4031
Rb	6.0	7.75	7.52			10.8	7.49
Sr	352.4	436.6	434.5	446	472	455.2	496.3
Cs		0.58	0.51			0.65	0.60
Ba	133	146.4	142.8	172	210	209.0	138.7
Y	13.6	16.4	16.6				12.1
Zr	46	59	58	64	81	80	43
Nb	1.7	2.0	2.1	1.6	2.8	2.7	1.4
Hf	1.21	1.44	1.50±.05			1.83	1.12
Ta	0.09	0.13	0.09±.02			0.10	0.06
Pb	2	5	5				5
Th	0.81	0.88	0.87±.08			1.43	1.72
La	5.43	6.09	6.00±.19			9.76	6.36
Ce	13.6	15.3	15.3±.8			24.6	15.4
Nd	8.4	9.3	9.32±42			13.9	8.7
Sm	2.17	2.36	2.55±15			3.34	2.08
Eu	0.78	0.92	0.93±.01			1.06	0.77
Tb	0.39	0.42	0.47±.04			0.45	0.34
Yb	1.33	1.60	1.66±.09			1.85	1.26
Lu	0.20	0.26	0.26±.01			0.27	0.20

Table 4

Major-element and trace element analyses of lavas from Puyehue Volcano

PII (continued)

Sample number	220283-1	250283-1	272829	250283-2	220283-4	272821	250283-4
[1]SiO_2	50.94	50.97	51.22	51.23	51.39	51.58	51.69
Al_2O_3	18.12	18.17	16.57	18.32	20.30	18.36	18.16
TiO_2	0.94	0.90	0.66	0.98	0.70	0.89	0.94
Fe_2O_3	9.19	9.39	8.93	8.97	7.69	9.24	9.06
MgO	6.78	6.59	9.40	5.89	4.74	5.97	5.62
CaO	10.08	10.13	10.34	9.94	11.14	10.06	10.06
Na_2O	2.86	3.11	2.38	2.82	2.70	2.69	3.10
K_2O	0.55	0.48	0.49	0.58	0.47	0.67	0.56
MnO	0.15	0.17	0.15	0.18	0.14	0.15	0.19
P_2O_5	0.21	0.19	0.12	0.17	0.13	0.19	0.21
total	99.82	100.10	100.26	99.08	99.40	99.80	99.59
[2]CO_2	-	-	0.04	-	0.04	0.04	-
H_2O^+	0.20	0.17	0.17	0.44	0.18	0.08	0.24
[3]Sc	30.3		32.4	30.2	28.9		
V	202		193	212	178	214	
Cr	120		441.	158	88	96	
Co	34.5		41.5	32.2	26.0		
Ni	65		141	62	22	46	
Zn	80		72	83	68	84	
Ga			16.5			17.9	
K	4627		4129	4870	-	-	
Rb	10.3		7.49	12.7	-	15.8	
Sr	462.2		494.8	435.0	456	476.7	
Cs	0.63		0.58	0.94	-	-	
Ba	209.6		140.1	195.4	155	198	
Y			12.0			17.4	
Zr	79		41	77	56	81	
Nb	3.3		1.3	2.7	1.7	2.3	
Hf	1.93		1.18	2.04	1.56		
Ta	0.15		0.06	0.16	0.08		
Pb			5.5			6.7	
Th	1.29		1.74	1.73	1.13	2.5	
La	9.45		6.33	8.36	6.60		
Ce	23.8		16.2	22.6	16.9		
Nd	13.8		9.8	13.1	10.1		
Sm	3.29		2.27	3.14	2.69		
Eu	1.06		0.83	1.02	0.89		
Tb	0.41		0.33	0.50	0.53		
Yb	1.74		1.21	1.98	1.57		
Lu	0.26		0.17	0.29	0.26		

Table 4

Major-element and trace element analyses of lavas from Puyehue Volcano

PII (continued)

Sample number	272824b	230283-5	138210	138212	220283-3	272827
[1]SiO_2	51.83	51.84	52.14	52.19	52.44	52.84
Al_2O_3	18.29	18.13	20.95	16.29	16.41	16.40
TiO_2	0.89	0.96	0.67	1.30	1.34	1.32
Fe_2O_3	9.19	8.65	7.59	10.69	10.72	10.73
MgO	6.00	5.80	4.48	5.52	5.63	5.49
CaO	10.03	10.05	11.67	8.97	8.97	8.97
Na_2O	3.02	2.95	2.30	3.19	3.08	3.12
K_2O	0.65	0.59	0.33	0.84	0.85	0.86
MnO	0.16	0.16	0.12	0.18	0.17	0.18
P_2O_5	0.20	0.17	0.15	0.26	0.29	0.29
total	100.26	99.30	100.40	99.43	99.90	100.20
[2]CO_2	0.00	-	0.26	0.06	-	0.16
H_2O^+	0.14	0.37	0.40	0.13	0.26	0.31
[3]Sc	31.1	31.9		35.2	35.8	34.6
V	216	214	170	273	286	274
Cr	100.	119	77	108.	108	105.
Co	32.7	30.3		33.2	32.9	32.4
Ni	51	49	34	52	47	54
Zn	88	79	69	104	100	98
Ga	17.8		17.7	18.5		18.0
K	5547	4962		6961	7136	7159
Rb	15.8	11.3	5.6	18.3	18.5	20.2
Sr	476.3	463.0	452.8	397.2	398.0	396.6
Cs	0.90	0.68		1.46	1.45	1.46
Ba	188.1	218.1	151	271.3	273.5	269.7
Y	17.4		14.3	27.4		28.1
Zr	80	83	59	123	118	120
Nb	3.0	3.3	2.7	3.8	2.6	3.2
Hf	1.94	2.09		2.88	2.98	2.85
Ta	0.11	0.16		0.31	0.26	0.17
Pb	5		6	12		11
Th	1.04	1.37	1.4	2.24	2.14	2.13
La	8.76	8.35		12.9	12.9	12.9
Ce	20.9	21.5		30.2	34.3	31.4
Nd	12.1	11.8		18.1	20.2	19.5
Sm	3.15	2.98		4.46	4.84	4.55
Eu	1.13	1.02		1.40	1.41	1.40
Tb	0.49	0.43		0.72	0.73	0.77
Yb	1.75	1.68		2.79	2.80	2.80
Lu	0.29	0.26		0.42	0.42	0.42

Table 4

Major-element and trace element analyses of lavas from Puyehue Volcano

PII (continued)

Sample number	13822	272826b	250283-3	23827	230283-3	230283-6
[1]SiO_2	52.99	54.19	55.24	63.84	64.25	66.51
Al_2O_3	18.24	17.29	17.32	14.85	15.07	14.41
TiO_2	0.94	0.70	0.97	1.01	0.63	0.63
Fe_2O_3	8.53	8.17	8.65	7.22	6.18	5.80
MgO	5.81	5.94	4.76	1.59	1.68	1.04
CaO	10.19	9.40	8.17	4.19	4.17	3.24
Na_2O	2.61	2.92	3.65	4.30	4.66	4.70
K_2O	0.58	0.83	0.85	2.23	2.28	2.59
MnO	0.17	0.14	0.18	0.14	0.6	0.13
P_2O_5	0.20	0.13	0.06	0.30	0.13	0.13
total	100.26	99.71	99.85	99.67	99.21	99.18
[2]CO_2	0.09	0.09	-	0.06	0.04	-
H_2O^+	0.49	0.49	0.22	0.16	0.25	0.22
[3]Sc		28.0				17.8
V	209	152		24	53	28
Cr	119	126.		20	22	13
Co		29.5				5.94
Ni	52	64		9	10	11
Zn	83	77		96	100	98
Ga	17.2	16.6		18.5		
K		6796				
Rb	11.7	19.9		58.5		
Sr	460.6	349.6		297.1	268	222
Cs		1.20				
Ba	226	270.6		540	613	667
Y	16.5	21.6		54.2		
Zr	85	122		271	305	342
Nb	3.3	3.7		7.1	8.3	9.0
Hf		2.77				8.40
Ta		0.20				0.50
Pb	5	8		15		
Th	1.5	2.75		7.9		8.51
La		11.7				31.1
Ce		27.8				78.7
Nd		15.3				40.5
Sm		3.49				9.75
Eu		1.02				1.93
Tb		0.64				1.39
Yb		2.28				5.72
Lu		0.38				0.85

Table 4

Major-element and trace element analyses of lavas from Puyehue Volcano

PIII

Sample number	212822	172822b	1428210	212824	202825a	202825c
[1]SiO_2	67.82	67.90	68.45	68.77	70.16	70.46
Al_2O_3	14.33	14.53	14.64	14.43	14.14	13.92
TiO_2	0.63	0.65	0.75	0.75	0.68	0.41
Fe_2O_3	5.71	5.84	4.97	4.92	4.47	4.73
MgO	0.46	0.45	0.89	0.66	0.44	0.28
CaO	2.56	2.62	2.85	2.57	2.12	2.02
Na_2O	5.17	5.16	5.05	5.12	5.09	5.27
K_2O	2.54	2.50	2.51	2.58	2.75	2.75
MnO	0.15	0.16	0.13	0.12	0.12	0.13
P_2O_5	0.15	0.16	0.17	0.17	0.12	0.10
total	99.52	99.97	100.41	100.09	100.09	100.07
[2]CO_2	0.09	0.05	0.06	0.04	0.03	0.09
H_2O^+	0.18	0.64	0.21	0.30	0.14	0.12
[3]Sc		17.4	14.4	14.0		14.9
V	4	3	22	19	10	4
Cr	1	0.9	10.5	4.8	1	0.9
Co		2.12	5.89	4.79		1.70
Ni	4	8	12	8	2	8
Zn	104	102	91	95	86	116
Ga	19.7	18.9	17.4	17.7	17.3	19.2
K				21442		22538
Rb	66.9	65.0	65.3	66.5	72.2	68.3
Sr	226.9	233.9	194.8	182.6	163.4	161.2
Cs				4.70		5.20
Ba	674	684	676	667.5	688	779.7
Y	53.6	52.6	51.2	52.1	53.6	58.6
Zr	334	332	333	343	355	370
Nb	9.0	9.3	9.2	9.7	9.4	10.1
Hf		7.55	7.79	7.88		8.20
Ta		0.51	0.48	0.51		0.55
Pb	21	21	22.9	21	23	22
Th	8.5	7.32	7.76	7.77	9	8.25
La		29.5	28.4	28.9		33.4
Ce		69.4	66.4	70.9		84.0
Nd		35.9	33.6	37.0		43.8
Sm		8.35	8.02	8.02		8.90
Eu		2.00	1.67	1.67		1.84
Tb		1.23	1.20	1.12		1.32
Yb		5.69	5.62	5.55		6.41
Lu		0.85	0.85	0.86		0.96

Table 4

Major-element and trace element analyses of lavas from Puyehue Volcano

PIV

Sample number	220283-5	43821	272822	242824	23823a	212826
[1]SiO_2	57.86	58.11	58.71	62.80	66.13	66.69
Al_2O_3	15.33	15.46	15.71	15.57	14.36	14.42
TiO_2	1.44	1.57	0.85	0.68	0.96	0.98
Fe_2O_3	9.21	9.69	7.83	6.74	6.14	6.21
MgO	2.79	2.56	4.31	2.20	0.91	0.97
CaO	5.98	5.94	6.81	5.10	3.22	3.26
Na_2O	4.15	4.24	3.74	4.37	5.22	5.27
K_2O	1.45	1.45	1.53	2.12	2.29	2.25
MnO	0.22	0.20	0.15	0.13	0.14	0.16
P_2O_5	0.62	0.68	0.22	0.13	0.28	0.29
total	99.05	99.90	99.86	99.84	99.65	100.50
[2]CO_2	-	0.08	0.02	0.03	0.12	0.02
H_2O^+	0.20	0.16	0.19	0.18	0.12	0.11
[3]Sc	28.0	27.6	24.5	20.7	18.8	19.3
V	80	61	111	75	29	31
Cr	19	10.	158.	35.2	0.6	1.1
Co	14.5	13.2	20.5	12.6	6.11	6.37
Ni	8	12	55	19	8	9
Zn	121	123	91	95	113	106
Ga		18.5	17.6	17.4	18.6	18.8
K	12284		12711	17109	-	18582
Rb	35.1	35.1	38.9	54.0	57.5	56.5
Sr	377.8	381.3	374.7	289.6	230.7	230.4
Cs	2.50		2.94	3.62	-	3.96
Ba	445.9	443	408.2	549.9	628	633.6
Y		46.7	33.2	42.7	51.9	52.3
Zr	192	194	191	279	308	301
Nb	5.6	6.8	4.8	7.1	9.0	9.0
Hf	4.87	4.50	4.48	6.32	6.62	6.78
Ta	0.40	0.38	0.29	0.43	0.48	0.43
Pb		18	14	17	20	20
Th	4.56	4.35	5.18	6.06	6.66	6.60
La	22.5	23.7	18.1	24.9	29.0	29.4
Ce	61.3	59.2	46.5	56.4	71.8	70.7
Nd	35.6	35.0	24.6	29.2	37.7	37.2
Sm	8.07	7.80	5.49	7.05	8.42	8.26
Eu	2.26	2.39	1.45	1.67	2.04	2.02
Tb	1.15	1.16	0.86	1.04	1.26	1.30
Yb	4.07	4.30	3.40	4.60	5.62	5.74
Lu	0.61	0.64	0.51	0.68	0.83	0.85

Table 4 (continued) Cordon Caulle Lavas

Sample number	CCIV 182821b	301821b	172826a	428210	142821
[1]SiO_2	71.33	71.06	71.41	70.97	70.13
Al_2O_3	13.96	13.81	13.96	13.82	13.91
TiO_2	0.36	0.36	0.38	0.37	0.38
Fe_2O_3	4.32	4.42	4.26	4.48	4.36
MgO	0.14	0.15	0.15	0.15	0.33
CaO	1.74	1.77	1.75	1.80	1.88
Na_2O	5.06	5.09	5.12	5.04	5.48
K_2O	2.82	2.81	2.84	2.82	2.73
MnO	0.14	0.15	0.13	0.14	0.15
P_2O_5	0.07	0.08	0.07	0.07	0.09
total	99.94	99.70	100.07	99.66	99.44
[2]CO_2	0.04	0.11	0.15	0.11	-
H_2O^+	0.19	0.18	0.13	0.21	0.29
[3]Sc	14.1	14.1	12.4		
V	10	3	2	4	2
Cr	1	2	1	1	1
Co	1.2	1.2	1.4		
Ni	8	7	7	7	2
Zn	120	121	117	118	116
Ga	18.4	18.5	19.1	18.9	
K	23432	23016			
Rb	71.2	70.4	74.1	73.1	
Sr	141.6	143.1	147.4	146.5	
Cs	5.10	5.65			
Ba	774.7	784.0	760	740	724
Y	60.3	59.3	60.5	59.9	
Zr	385	388	391	373	365
Nb	10.2	10.6	10.2	9.9	9.7
Hf	8.68	8.44	8.83		
Ta	0.58	0.55	0.53		
Pb	23.2	24.3	24.3	23.9	
Th	8.87	8.84	8.29	9	
La	34.9	34.7	33.8		
Ce	84.2	87.5	77.8		
Nd	40.8	44.6	38.2		
Sm	9.28	9.12	9.14		
Eu	1.80	1.82	1.79		
Tb	1.43	1.50	1.40		
Yb	6.66	6.62	6.63		
Lu	0.99	1.00	0.98		

Table 4 (continued) Cordon Caulle Lavas

Sample number	CCV (1921-1922) 428210	72822	42823b	42826
[1]SiO_2	68.55	68.96	69.30	68.71
Al_2O_3	14.32	14.34	14.48	14.26
TiO_2	0.79	0.79	0.77	0.73
[3]Fe_2O_3	4.90	4.92	4.80	4.69
MgO	0.62	0.60	0.57	0.70
CaO	2.52	2.55	2.43	2.40
Na_2O	4.95	5.15	5.06	5.26
K_2O	2.59	2.62	2.62	2.61
MnO	0.12	0.11	0.13	0.14
P_2O_5	0.17	0.17	0.15	0.16
total	99.53	100.21	100.31	99.66
[2]CO_2	0.01	0.02	0.07	—
H_2O^+	0.14	0.13	0.15	0.22
[3]Sc	14.3	15.1		
V	17	13	13	14
Cr	0.4	0.8	<1	5
Co	4.24	4.40		
Ni	1	7	7	4
Zn	97	93	91	94
Ga	18.2	18.0	17.2	
K	21503	21331		
Rb	65.2	65.2	68.4	
Sr	185.9	188.0	183.2	183
Cs	4.78	4.77		
Ba	687.4	690.9	674	685
Y	52.9	54.4	51.4	
Zr	338	341	338	341
Nb	9.7	9.5	9.2	9.5
Hf	7.77	7.65		
Ta	0.51	0.51		
Pb	22.1	21.5	20.5	
Th	8.31	7.99	8.3	
La	29.1	30.9		
Ce	71.2	71.9		
Nd	36.7	36.8		
Sm	8.40	8.41		
Eu	1.73	1.83		
Tb	1.16	1.34		
Yb	5.57	5.84		
Lu	0.85	0.87		

Table 4 (continued) Cordon Caulle Lavas

Sample number	CCVI (1960) 42824a	2818226bh	212823a	52821	52826	212821	142825a
[1]SiO_2	69.73	69.92	69.52	69.83	70.01	69.62	69.00
Al_2O_3	14.18	14.11	14.18	14.20	14.06	14.13	14.07
TiO_2	0.70	0.68	0.68	0.70	0.65	0.67	0.69
Fe_2O_3	4.59	4.48	4.46	4.53	4.34	4.43	4.50
MgO	0.50	0.48	0.46	0.46	0.43	0.45	0.64
CaO	2.24	2.15	2.19	2.23	2.05	2.15	2.25
Na_2O	5.01	5.13±20	5.50	5.09	4.99	5.05	5.40
K_2O	2.73	2.75	2.77	2.72	2.80	2.75	2.68
MnO	0.10	0.11	0.09	0.12	0.11	0.11	0.14
P_2O_5	0.14	0.14	0.14	0.14	0.12	0.14	0.16
total	99.92	99.95	99.99	100.02	99.56	99.50	99.54
[2]CO_2	0.05	0.08	0.04	0.00	0.03	0.03	0.03
H_2O^+	0.13	0.12	0.14	0.21	0.11	0.11	0.21
[3]Sc	14.0	13.3±4	13.8	14.1	12.7		
V	10	10	10	11	13		9
Cr	1	0.9±4	1.5	0.6	0.7		1
Co	3.91	3.58±7	3.71	3.74	3.32		
Ni	8	8	8	8	5		8
Zn	87	85	87	86	87		84
Ga	17.9	17.2	17.7	17.6	17.1	17.5	
K	22408	22634	22578				
Rb	68.2	70.5	69.7	70.9	72.9	71.4	
Sr	168.9	160.9	162.8	168.9	1 56.7	162.5	172
Cs	5.00	5.15	5.00				
Ba	722.9	735.1	765.5	702	704		687
Y	52.9	52.7	53.6	52.9	54.0	52.9	
Zr	357	362	360	359	366		352
Nb	9.7	9.5	9.6	9.5	9.9		9.8
Hf	7.85	8.33±17	8.03	8.26	8.52		
Ta	0.59	0.54±3	0.56	0.54	0.52		
Pb	23.8	22.7	24.3	22.1	22.7	22.4	
Th	8.35	8.29±24	8.55	8.61	9.04	8.7	
La	31.2	30.4±8	31.7	31.4	30.2		
Ce	77.4	73.6±4.0	77.1	75.7	74.3		
Nd	37.1	36.7±2.0	37.0	38.5	38.4		
Sm	8.44	8.22±18	8.44	8.16	8.49		
Eu	1.76	1.68±4	1.74	1.77	1.63		
Tb	1.28	1.25±6	1.33	1.41	1.23		
Yb	5.95	5.86±16	6.22	5.84	5.82		
Lu	0.91	0.89±3	0.92	0.91	0.92		

Footnotes to Table 4

[1]Major elements by XRF analysis except Na_2O from INAA. Total iron as Fe_2O_3.

[2]CO_2 and H_2O^+ analyses performed on different powder splits than those used in XRF major-element analyses.

[3]Sc,Cr, Co, Hf, Ta, Th, and REE abundances determined by INAA. Cr and Th abundances for samples not analyzed by INAA were determined by XRF analysis. V, Ni, Zn, Ga, Rb, Sr, Ba, Y, Zr, Nb, and Pb abundances by XRF analysis. K, Rb, Sr, Ba, and Cs abundances were determined in selected samples by isotope dilution. Two samples (basalt 13826h and rhyodacite 281822bh) were analyzed by INAA several times (See Appendix) and uncertainties expressed for these two samples in Table 4 refer to one standard deviation about the mean.

nearly aphyric PI basaltic andesites with elevated H_2O contents (to ~.5 wt.%), iron staining along cracks is the only petrographic indication of alteration. Sample 272826a is a sample of mixed basaltic and silicic tephra from unit PIII. Olivine and plagioclase phenocrysts in inclusions of basaltic scoria in this sample are fresh (Fig. 4), however the scoria groundmass is highly oxidized (iron-stained). The host tephra in this sample is devitrified, iron-stained, and contains veins of silica and zeolites.

Abundances of Cs, Rb, K, and possibly Ba in volcanic rocks may be affected by subaerial alteration (Noble, 1965; Wood et al., 1976; Feigenson et al., 1983). Ratios of these elements do not correlate with H_2O contents in any of the samples in this study. For example, Rb/Cs ratios in fresh samples of basalt and basaltic andesite range from 12.5 to 17.6, whereas samples containing 0.4 to 0.5 wt.% H_2O, which may or may not appear altered in thin section as described above, range in Rb/Cs ratios from 12.6 to 23. Evidence of alteration may be manifest as co-variations of H_2O contents with ratios of alkalies to less mobile trace elements. In general, samples with high H_2O contents were not analyzed for most trace elements. A subset of basalts and basaltic andesites, including samples with high (up to 0.5 wt.%) and low H_2O contents, are characterized by relatively restricted ranges of Cs/La (0.10-0.11), Rb/La (1.52-1.70), and Rb/Cs (13.6-16.6) ratios. An apparently fresh (H_2O = 0.07 wt.%) sample of basaltic andesite (sample 1428212, unit PI) has low Cs (Cs/La = 0.07, Rb/Cs = 23), while another visibly altered sample (sample 162828a, H_2O = 0.43 wt.%) may have gained in Cs and Rb (Cs/La = 0.21, Rb/La = 2.69, Rb/Cs = 12.6), or at least suffered no loss in alkali abundances. Thus, relationships involving H_2O

contents and abundances of alkalies and relatively immobile trace elements are not straightforward, and it is impossible with the available data to assess the relative degrees of mobility of Rb, Cs, K, and Ba or to identify the mechanisms of alteration. The most likely agents of alteration in a volcanic setting include meteoric water and volcanogenic hydrothermal fluids, the effects of which range from minor deuteric alteration in lava flows, to extensive hydration and alteration associated with hot springs solfataras, and fumaroles. Subsequent interpretations involving Cs, Rb, Ba, and K abundances in clearly altered samples (numbers 272826b, 13822, 138210, 172829c, 162828a, 162826, and 222825a) will proceed with caution.

4.2 Major elements

Samples from Puyehue Volcano and Cordon Caulle range in SiO_2 from 48 to 72 wt.% (Table 4). On a plot of K_2O vs. SiO_2 (Fig. 6a) after Peccerillo and Taylor (1975), all but two samples fall in the intermediate-K_2O series of calcalkaline rocks. Basaltic andesites and andesites ranging in SiO_2 from 54 to 63 wt.% SiO_2 seem to be more common in the older preglacial PI unit and are not as well represented among the relatively younger volcanics (units PII, PIII, and PIV) of the main volcano (Fig. 6a). On a total alkali (Na_2O+K_2O) vs. SiO_2 plot used by Kuno (1966) to classify basalts as tholeiitic, high-alumina, or alkalic, all samples from Puyehue Volcano fall into the high-alumina basalt field.

A plot of FeO*/MgO vs. SiO_2 was used by Miyashiro (1975) to classify volcanic rocks as calcalkaline or tholeiitic. In Figure 6b, relatively younger basalts and basaltic andesites ranging in SiO_2 48-54 wt.% largely

'straddle' the boundary between the tholeiitic and calcalkaline fields. Without exception, preglacial basaltic andesites and andesites ranging from 54-65 wt.% SiO_2 are characterized by relatively higher FeO*/MgO, while relatively younger post-glacical volcanics in this same range, though sparsely represented, fall above and below the boundary. Two andesites with particularly low FeO*/MgO correspond to the two PIV andesites described earlier which display dramatic disequilibrium phenocryst assemblages. However, since the majority of evolved lavas display high FeO*/MgO ratios and plot in the upper field, Puyehue Volcano may be classified as a tholeiitic volcano.

The basalts (48-52 wt.% SiO_2) as a group are diverse in their major-element compositions. Alumina contents vary from approximately 16 to 21 wt.% (Table 4) but are not simply correlated with CaO content in that CaO/Al_2O_3 ratios range from 0.54 to 0.63. Many basalts with similar major-element compositions have variable K_2O and TiO_2 contents (Fig. 6a, Fig. 8a). Basalts with relatively higher Na_2O/K_2O ratios (5.5 to 7.1) are generally also higher in Al_2O_3 and CaO. This may be due to plagioclase accumulation and will be addressed further in a later section, in addition to possible olivine accumulation in some basalts with MgO contents up to 14.3 wt.%.

Abundances of Al_2O_3, Fe_2O_3, MgO and CaO decrease and Na_2O and K_2O increase (Fig. 7) with increasing SiO_2 content in all of the samples as is typical of most calcalkaline suites (Gill, 1981). Abundances of TiO_2 and P_2O_5 first increase dramatically with increasing SiO_2 from low values to values among the highest observed in the island arcs and continental arcs (see Thorpe, 1982). After maximum values in basaltic andesites and andesites, TiO_2 and P_2O_5 contents decrease with increasing SiO_2 (Fig. 8).

6(a) K_2O vs. SiO_2 classification diagram after Peccerillo and Taylor (1975). Most Puyehue lavas plot as medium-K volcanic suite.

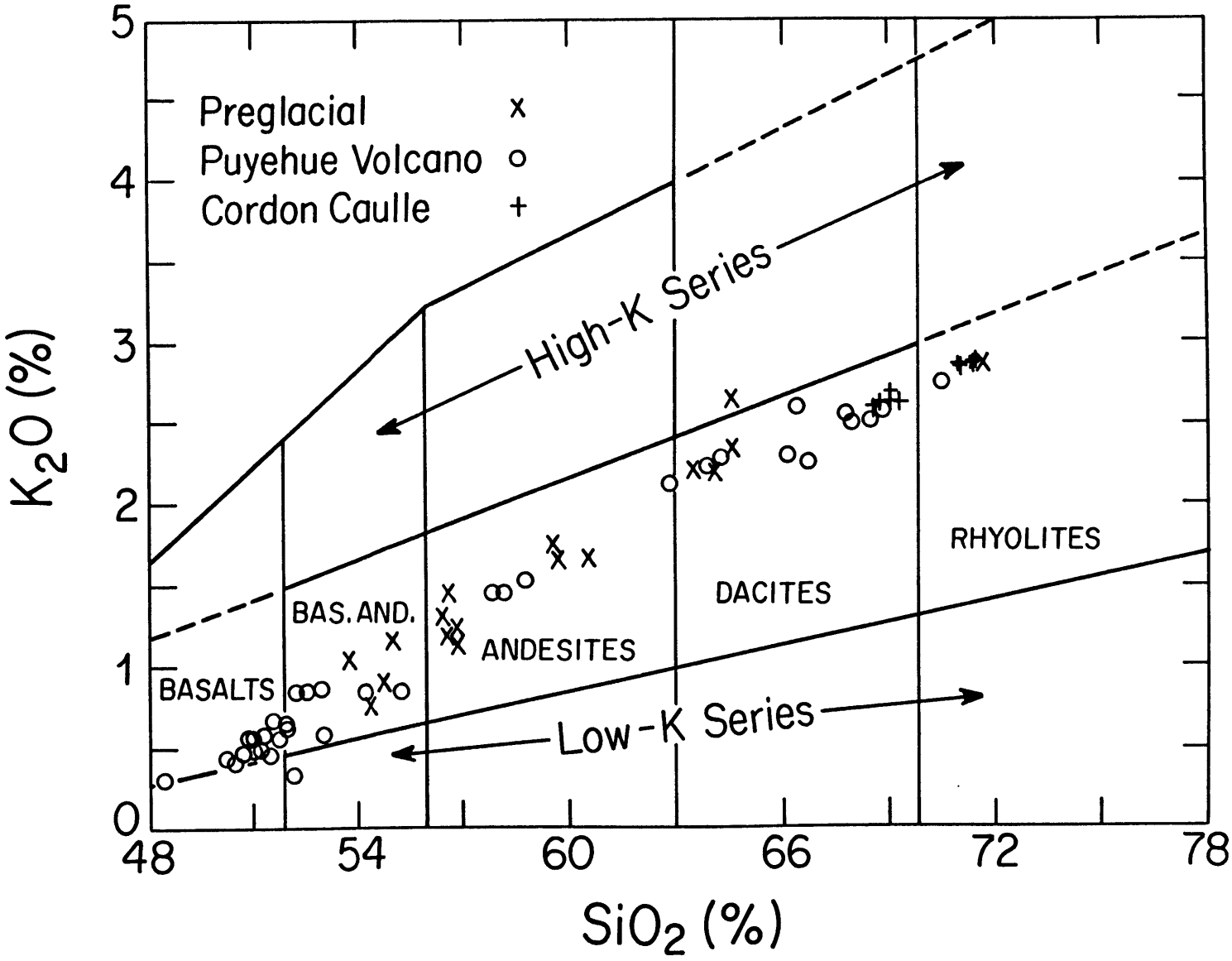
Preglacial
Puyehue Volcano
Cordon Caulle
High-K Series
Low-K Series
BASALTS
BAS. AND.
ANDESITES
DACITES
RHYOLITES
K_2O (%)
SiO_2 (%)
0
1
2
3
4
5
48
54
60
66
72
78

6(b) FeO*/MgO vs. SiO_2 plot (with total iron as FeO) adapted from Miyashiro (1975) with boundary between tholeiitic and calcalkaline series lavas.

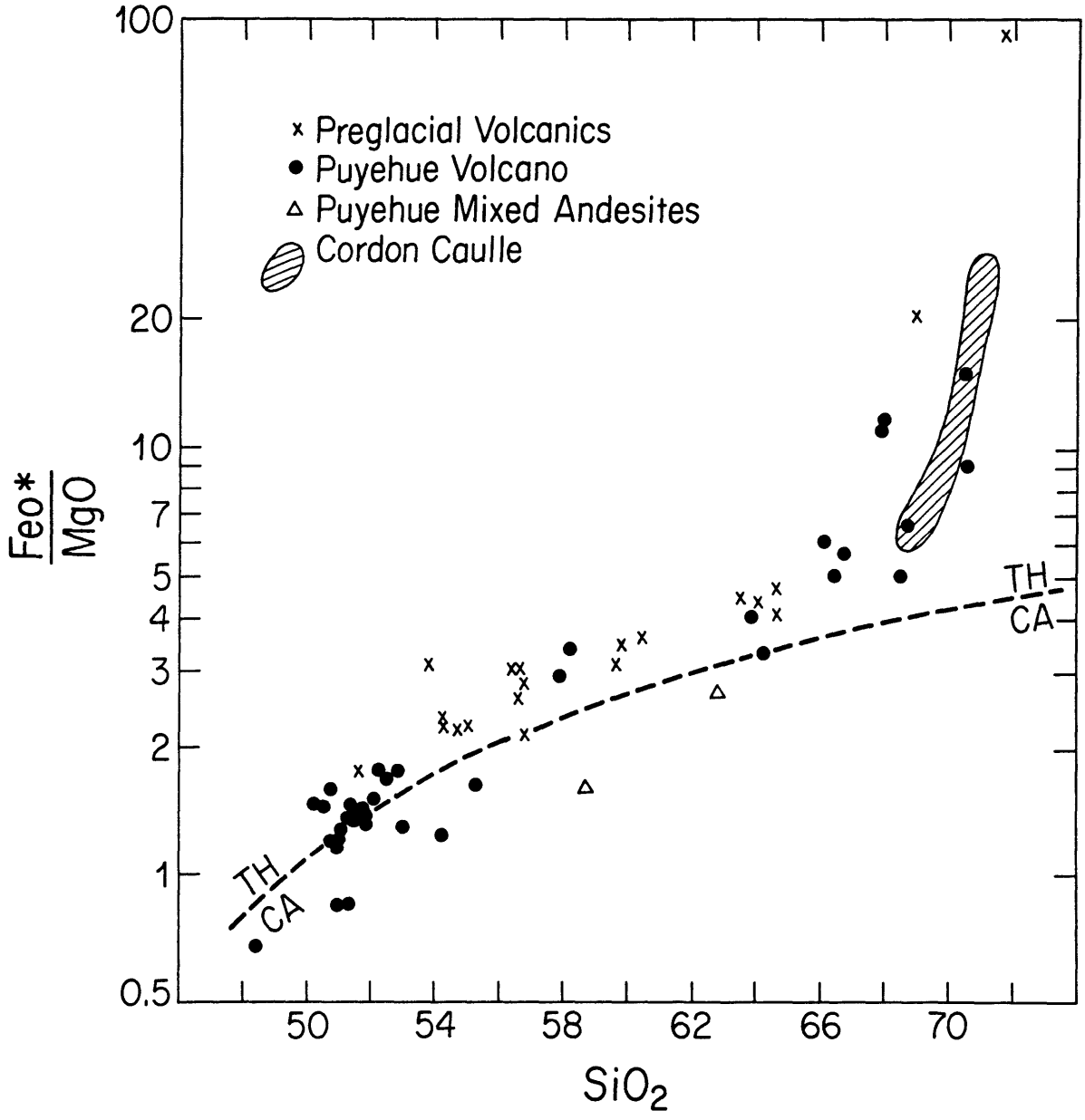
100
20
10
7
5
4
3
2
1
0.5
50
54
58
62
66
70
SiO_2
$\frac{FeO^*}{MgO}$
× Preglacial Volcanics
● Puyehue Volcano
△ Puyehue Mixed Andesites
Cordon Caulle
TH
CA
TH
CA

7 Major-element Harker variations diagrams for lavas from Puyehue Volcano and Cordon Caulle. Symbols for preglacial volcanics are crosses (X), for Puyehue Volcano are open circles (o), and Cordon Caulle are plus signs (+).

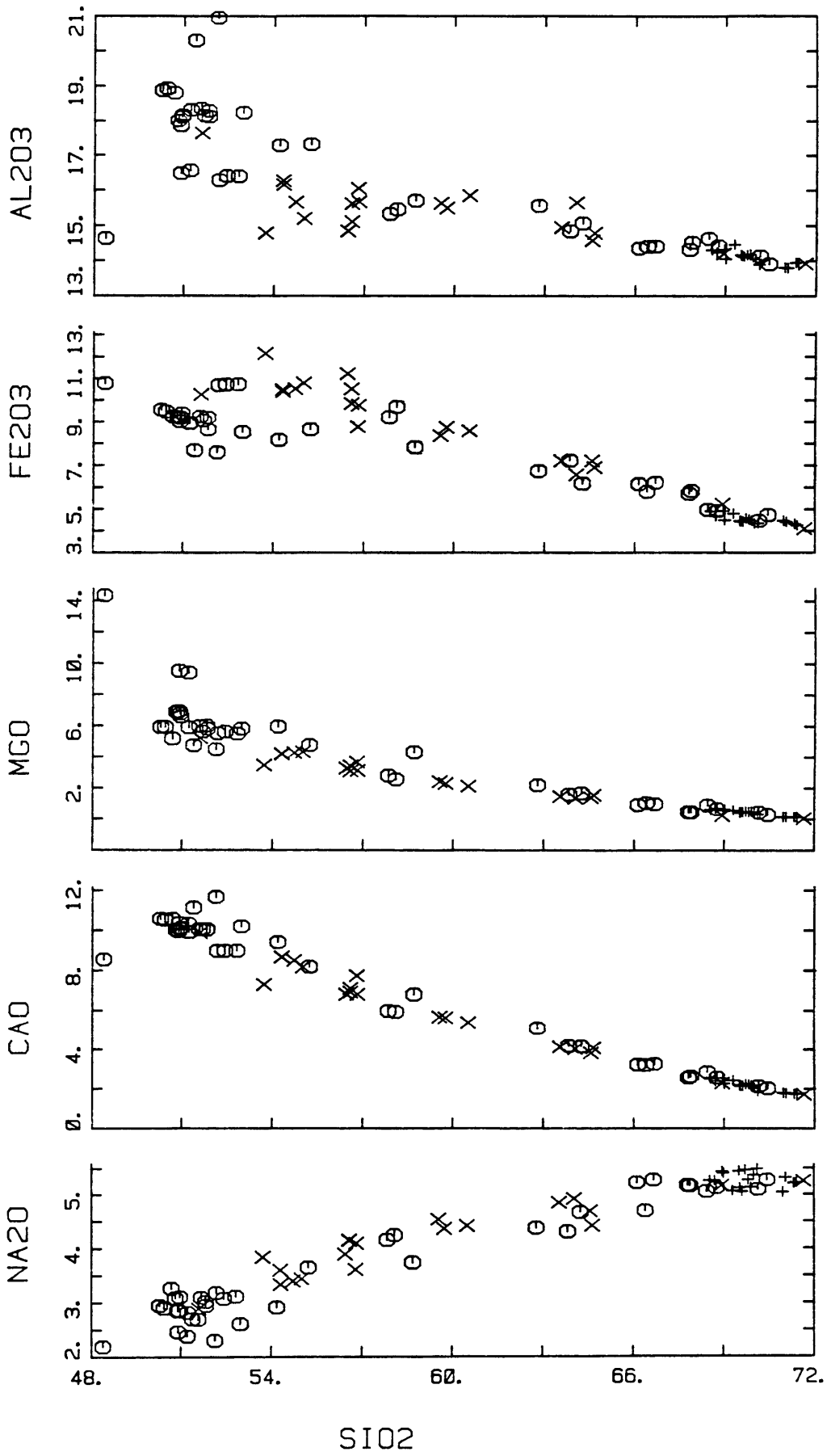
AL203
13. 15. 17. 19. 21.
FE203
3. 5. 7. 9. 11. 13.
MGO
2. 6. 10. 14.
CAO
0. 4. 8. 12.
NA20
2. 3. 4. 5.
48. 54. 60. 66. 72.
SIO2

8 Minor-element variation diagrams for lavas from Puyehue Volcano and Cordon Caulle. Symbols as in Figure 7.

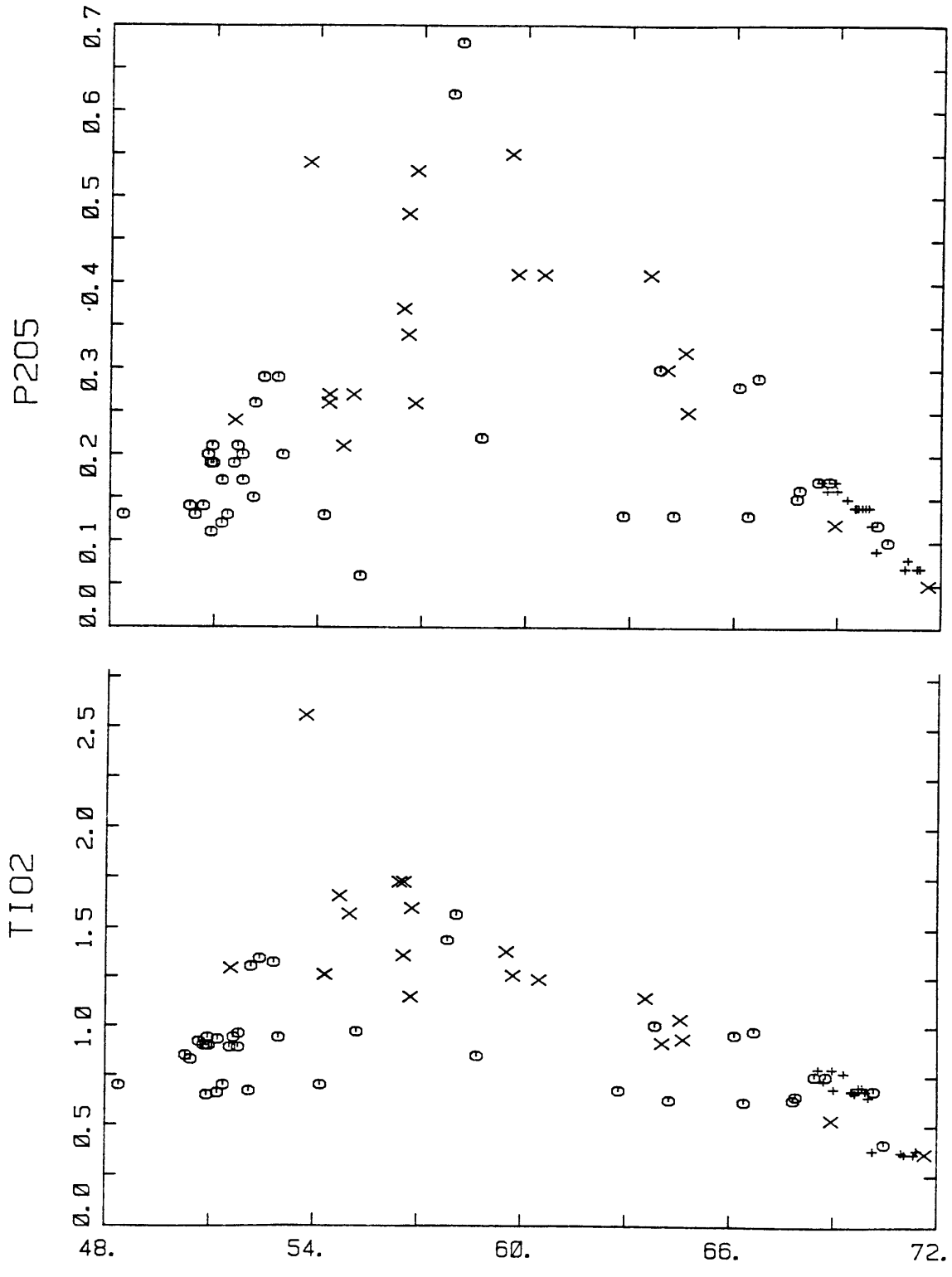
P2O5
0.0
0.1
0.2
0.3
0.4
0.5
0.6
0.7
TIO2
0.0
0.5
1.0
1.5
2.0
2.5
48.
54.
60.
66.
72.
SIO2

TiO_2 contents are relatively higher (to 2.5 wt.%) in several preglacial basaltic andesites compared to post-glacial basaltic andesites (Fig. 8a). P_2O_5 contents peak at higher values (to 0.68 wt.%) in postglacial andesites relative to preglacial andesites (Fig. 8b).

4.3. Trace elements

Abundances of Co, Ni, Cr, and Sr decrease, and Ba, Cs, Rb, Zr, Nb, Ta, Hf, Th, Y, Zn, and Pb abundances increase, with increasing SiO_2 content (Fig. 9, Table 4). Both Sc and V abundances increase from basalts to basaltic andesites and decrease thereafter (Fig. 9). In the entire sample suite, increases on the order of a factor of 10 are observed in Cs, Rb, and Th abundances, with only a 4- to 6-fold increase in Ba, K, Hf, Zr, Y, and REE abundances.

The light REE (LREE) are not greatly enriched relative to the heavy REE (HREE) with increasing SiO_2 content (Fig. 10). The total range in La/Yb ratios (3.4-6.0) in Puyehue samples is lower and more restricted than La/Yb ratios of 9.0-16.0 in basalts to rhyolites from the Laguna del Maule volcanic complex at 36°N (Frey *et al.*, 1984). A few basalts display slight positive Eu anomalies; throughout the remainder of the suite, increasingly negative Eu anomalies are correlated with increasing SiO_2 content.

Postglacial PII basalts of Puyehue volcano are diverse in their trace element abundances. This is most apparent in basalts containing 6-7% MgO, which range nearly two-fold in Th, Ba, La, Rb, Cs, and Hf abundances (Fig. 11, Table 4). Abundance ratios in the basalts of similarly incompatible elements such as Ba/Th (80-181), Ba/Nb (62-108), Ba/Rb (11.9-19.4), K/Rb (350-550), and Zr/Sm (18-28) vary widely, while

9 Variation of selected trace element abundances with SiO_2 in lavas from Puyehue Volcano and Cordon Caulle. Symbols as in Figure 7. In these diagrams and all others henceforth, crosses refer to maximum estimated analytical uncertainty based on replicate analyses (See Appendix).

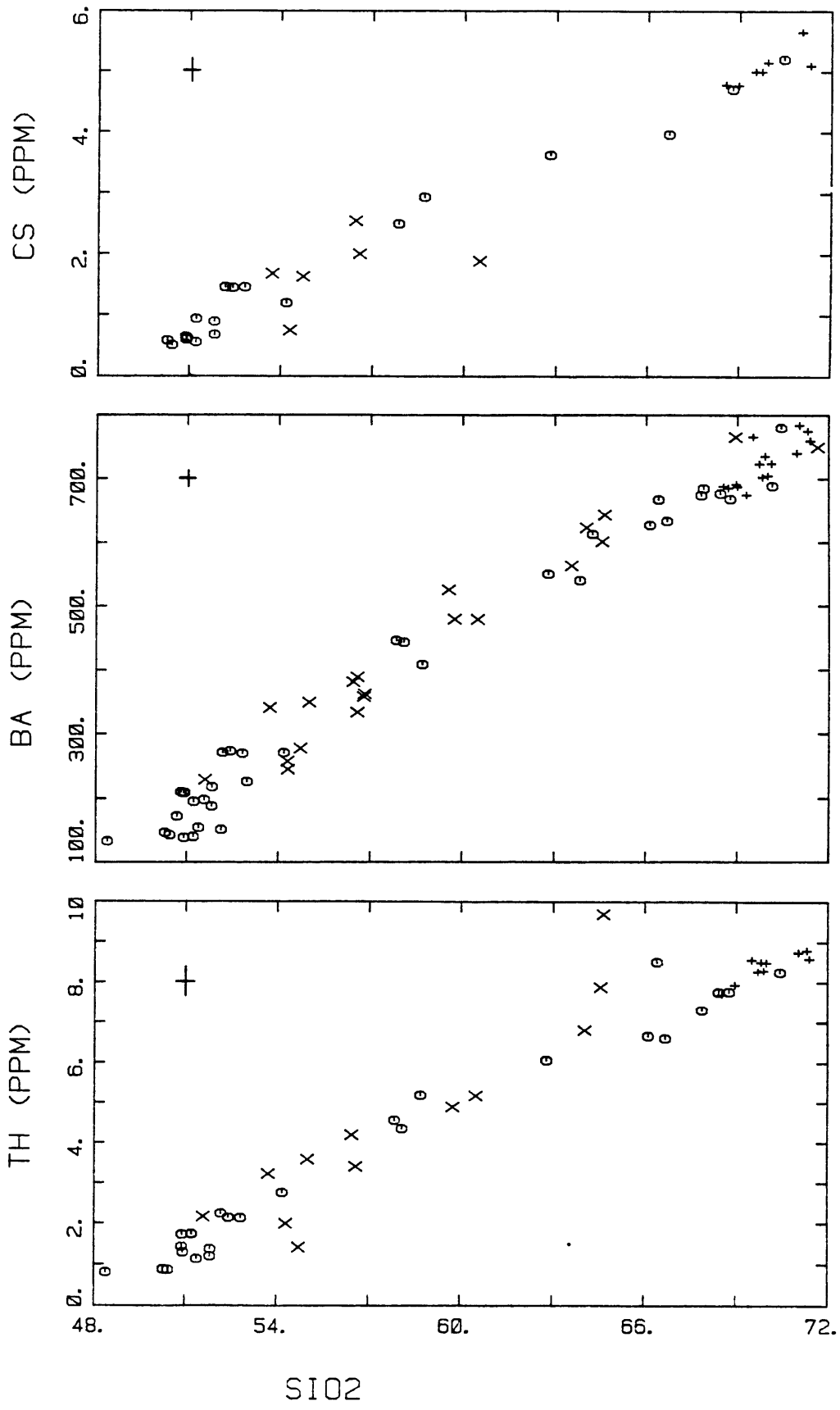
CS (PPM)
0.
2.
4.
6.
BA (PPM)
100.
300.
500.
700.
TH (PPM)
0.
2.
4.
6.
8.
10
48.
54.
60.
66.
72.
SIO2

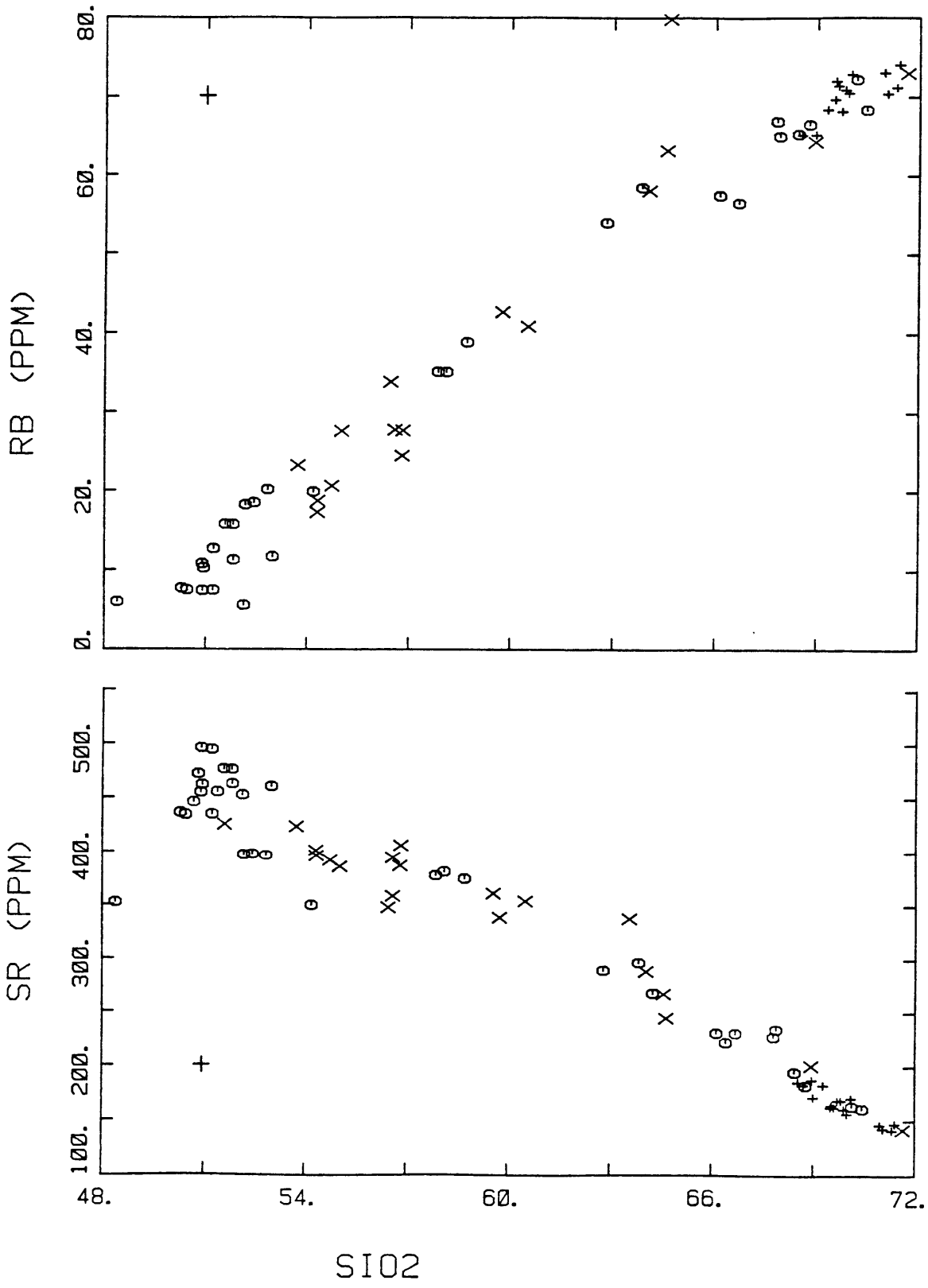
RB (PPM)
0.
20.
40.
60.
80.
SR (PPM)
100.
200.
300.
400.
500.
48.
54.
60.
66.
72.
SIO2

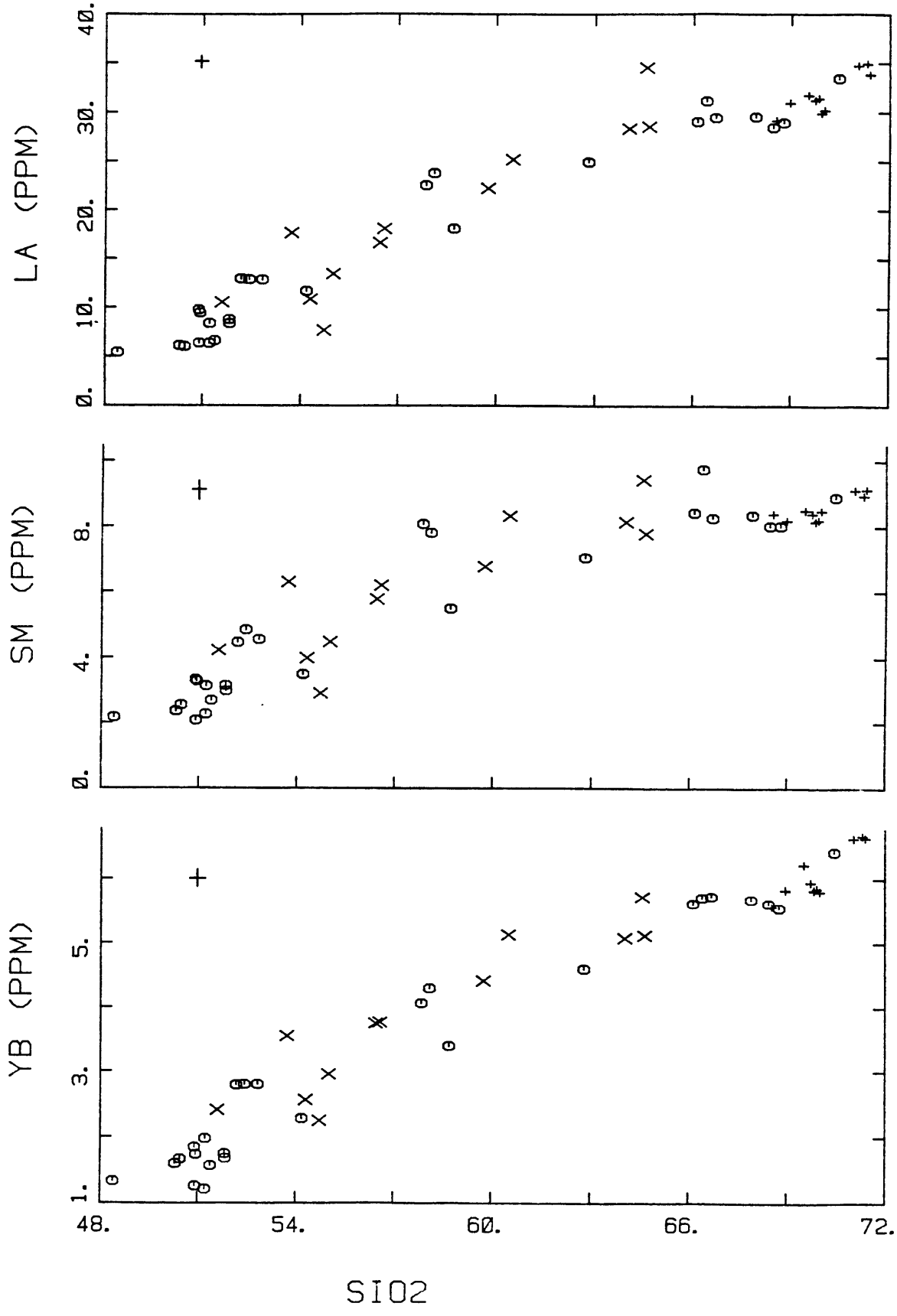
LA (PPM)
0.
10.
20.
30.
40.
SM (PPM)
0.
4.
8.
YB (PPM)
1.
3.
5.
48.
54.
60.
66.
72.
SIO2

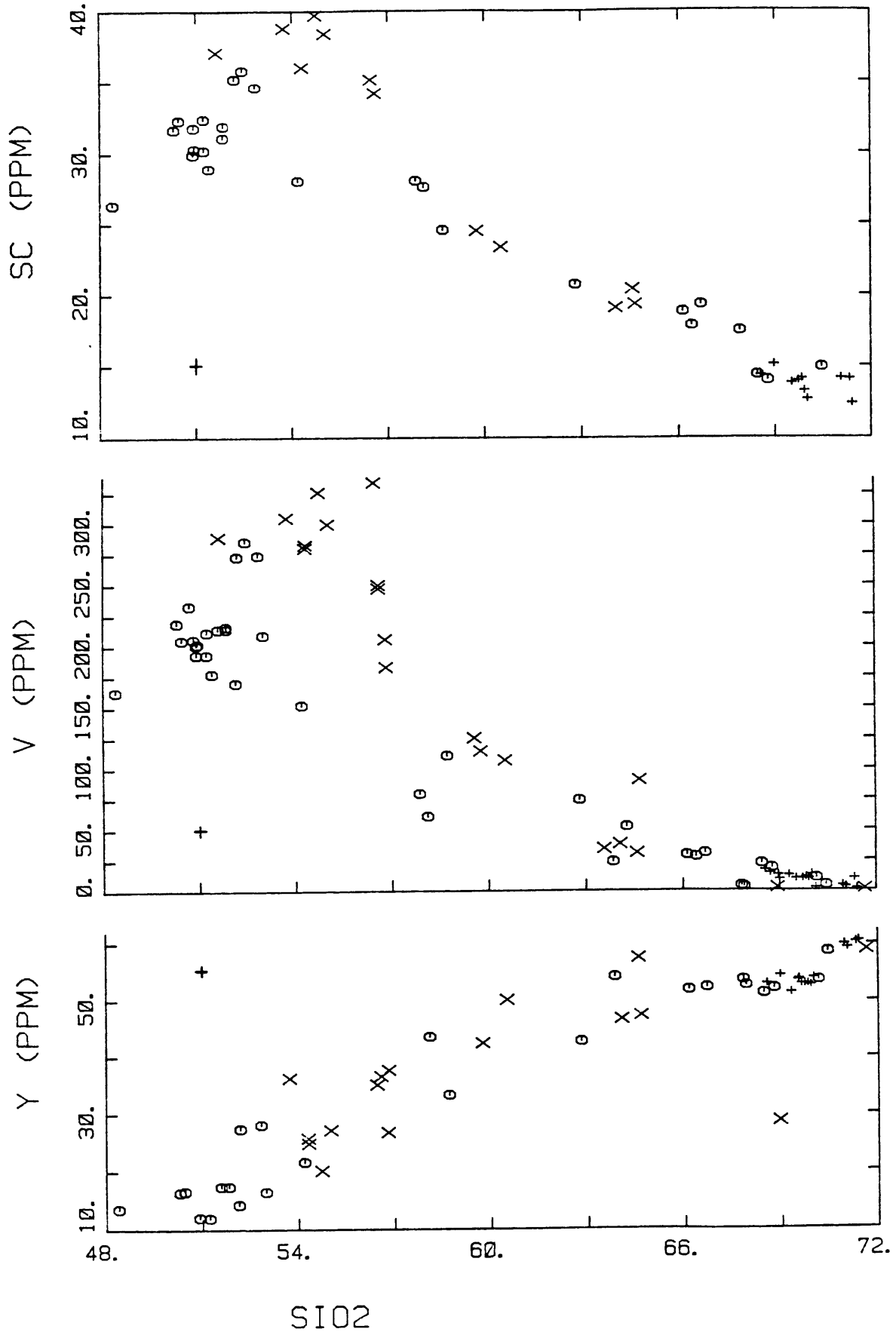
SC (PPM)
10.
20.
30.
40.
V (PPM)
0.
50.
100.
150.
200.
250.
300.
Y (PPM)
10.
30.
50.
48.
54.
60.
66.
72.
SIO2

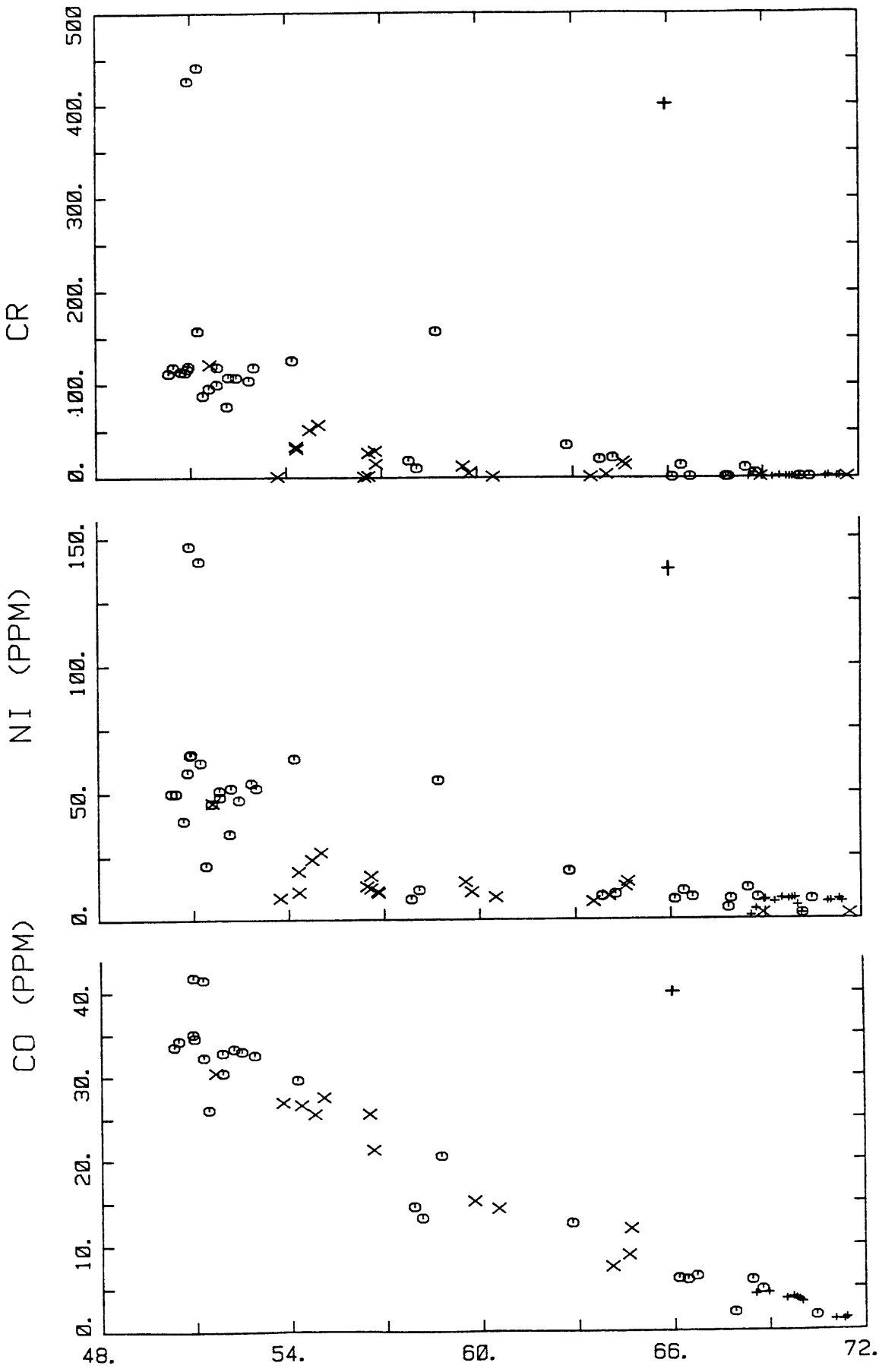
CR
0.
100.
200.
300.
400.
500
NI (PPM)
0.
50.
100.
150.
CO (PPM)
0.
10.
20.
30.
40.
48.
54.
60.
66.
72.
SIO2

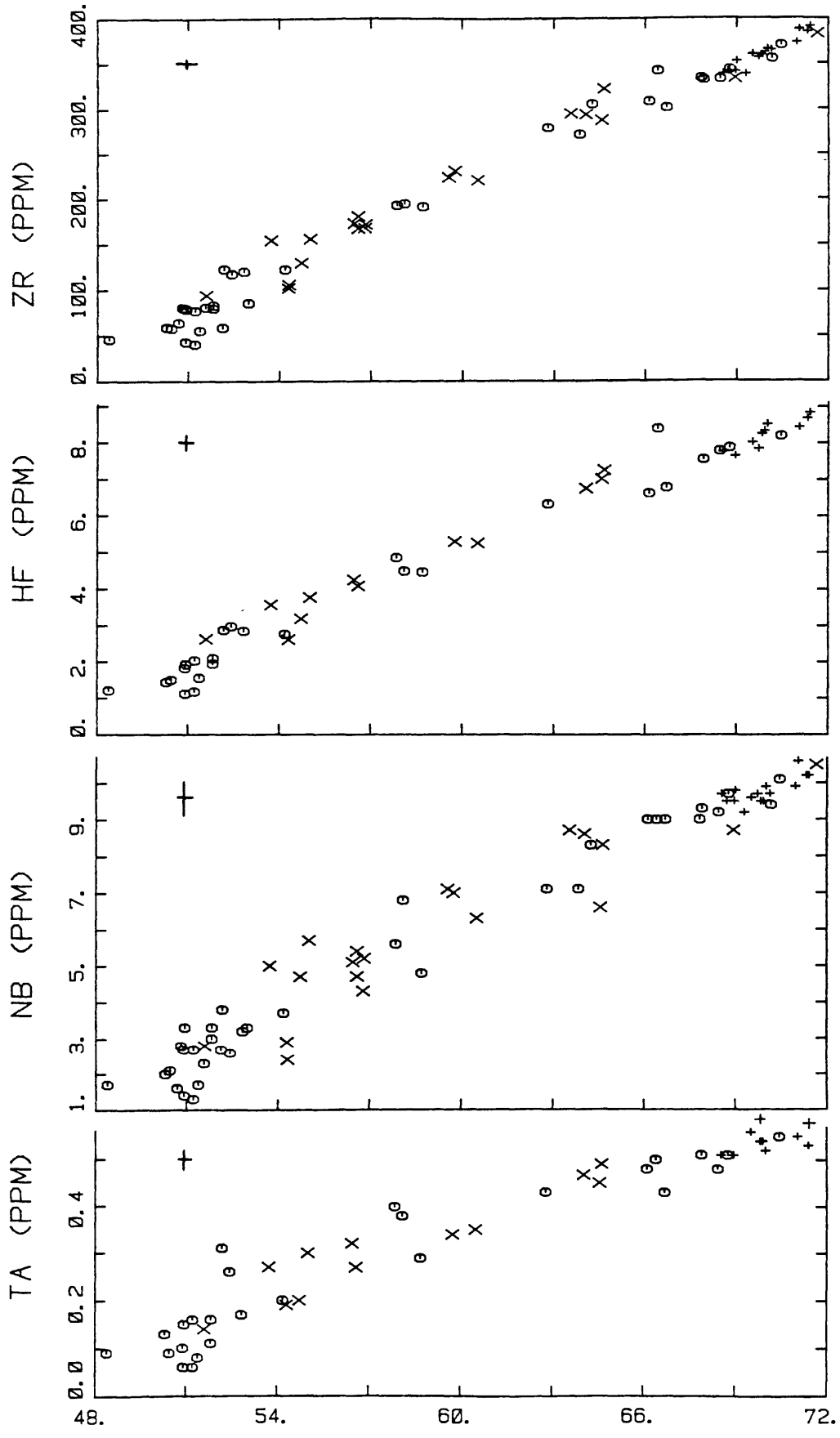
ZR (PPM)
0.
100.
200.
300.
400.
HF (PPM)
0.
2.
4.
6.
8.
NB (PPM)
1.
3.
5.
7.
9.
TA (PPM)
0.0
0.2
0.4
48.
54.
60.
66.
72.
SIO2

10 Variation or enrichment of LREE relative to HREE with increasing SiO_2 in Puyehue Volcano and Cordon Caulle lavas. (a) La/Sm vs. SiO_2 (b) La/Yb vs. SiO_2

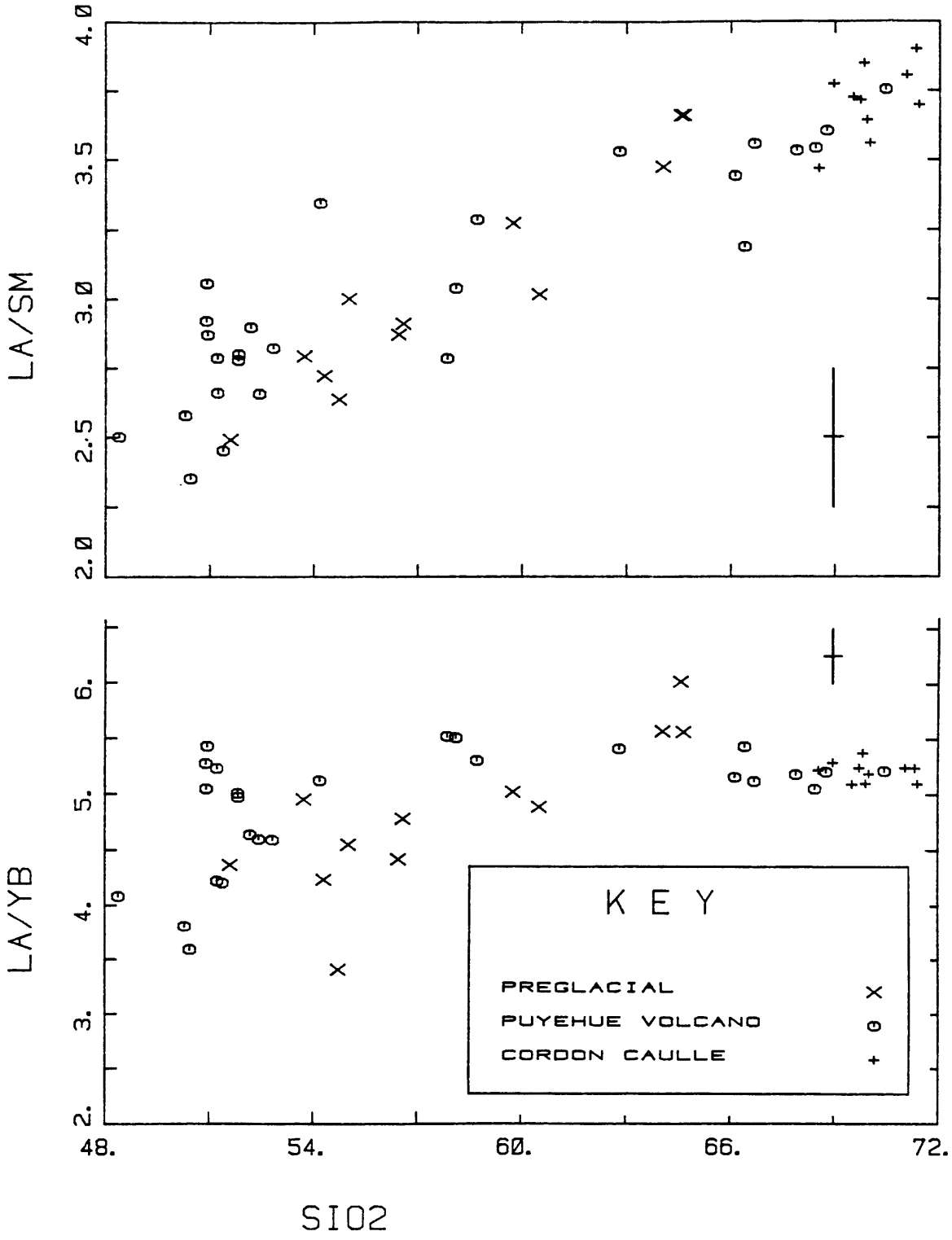
LA/SM
4.0
3.5
3.0
2.5
2.0
LA/YB
6.
5.
4.
3.
2.
48.
54.
60.
66.
72.
SIO2
KEY
PREGLACIAL
PUYEHUE VOLCANO
CORDON CAULLE

11 MgO-variation diagrams for abundances of selected trace elements (Rb, Th, and La) in basalts and basaltic andesites from Puyehue volcano.

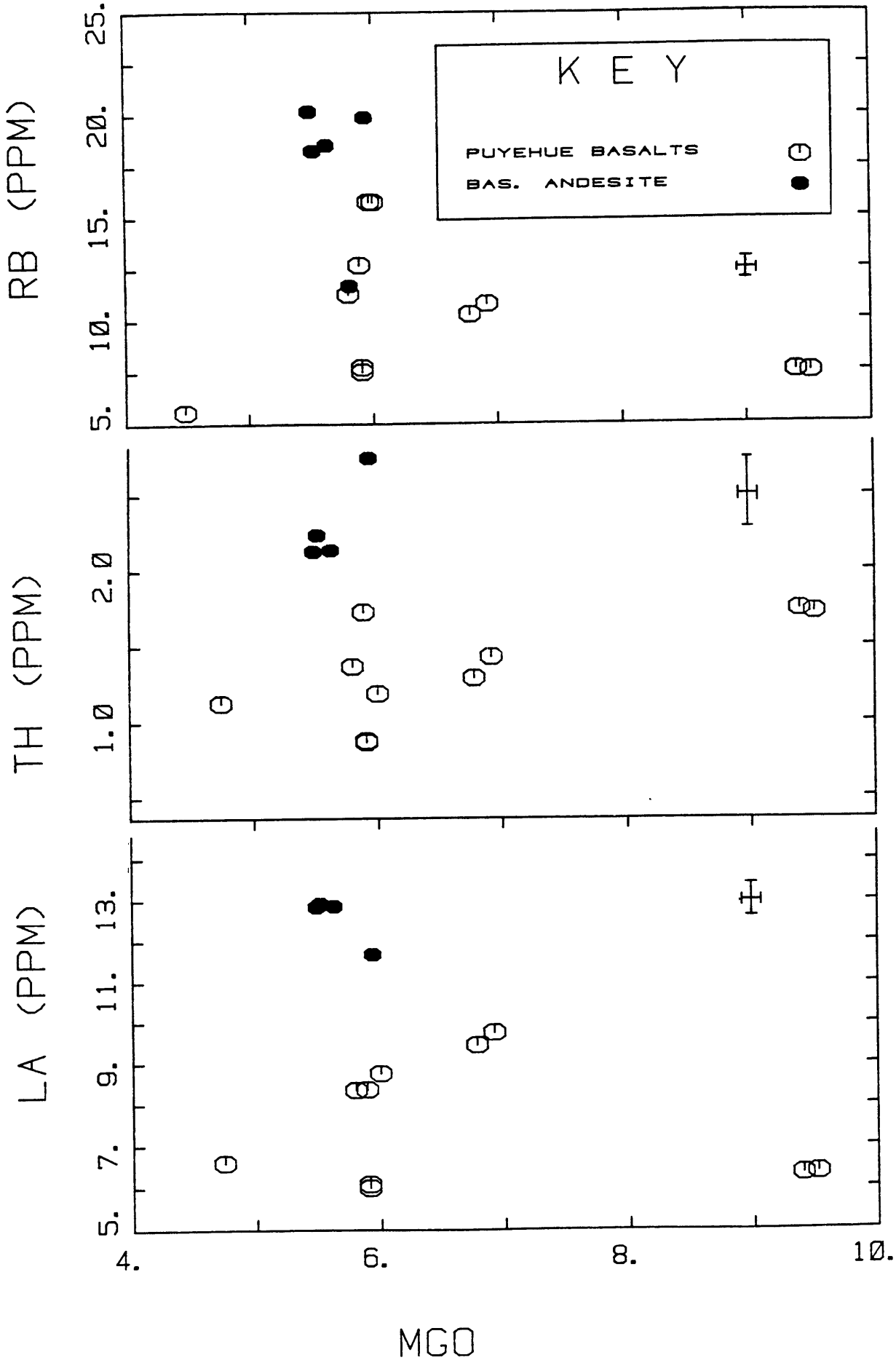
KEY
PUYEHUE BASALTS
BAS. ANDESITE
RB (PPM)
TH (PPM)
LA (PPM)
MGO
5.
10.
15.
20.
25.
1.0
2.0
7.
9.
11.
13.
4.
6.
8.
10.

other ratios such as Ba/La (22-26) are less variable. The basalts also display variable degrees of LREE-enrichment as reflected in La/Yb ratios ranging from 3.6 to 5.4 (La_N/Yb_N = 2.4-3.6) and this is nearly equivalent to the entire range of La/Yb ratios observed in all Puyehue samples.

Both preglacial and postglacial basaltic andesites (52-56 wt.% SiO_2) are similar in most respects, but preglacial basaltic andesites are higher in Sc and V (Fig. 9) and less LREE enriched (La/Yb = 3.4-5.0) than the younger postglacial basaltic andesites (La/Yb = 4.6-5.1).

Some preglacial basaltic andesites and andesites are lower in La, Th, and Ni and higher in V and Sc relative to younger postglacial basaltic andesites and andesites (Fig. 9). Three samples of postglacial PIV andesite (58-59 wt.% SiO_2) differ in their Ni (8-12 ppm vs. 55 ppm), Cr (10-18 vs. 158 ppm), Nb (5.6-6.8 vs. 4.8 ppm), Th (4.3-4.6 vs. 5.2 ppm), La (22-24 vs. 18 ppm), Co (13-14 vs. 20 ppm), V (60-80 vs. 111 ppm), Sc (28 vs. 24.5 ppm), and TiO_2 (1.44-1.57 vs. 0.85 wt.%) contents and FeO*/MgO ratios (3.0-3.4 vs. 1.6), but are similar in their Zr (191-194 ppm), Hf (4.5-4.9), Rb (35-39), Sr (~380 ppm), K_2O (1.45-1.53 wt.%), and Ba (408-446 ppm) abundances (Fig. 9, Table 4.

Postglacial dacites, rhyodacites, and rhyolites from Puyehue Volcano and Cordon Caulle display increasing Cs, Rb, Ba, Th, K, Nb, LREE, Hf, and Zr, and decreasing Sr, Sc, Co, and V abundances with increasing SiO_2 (Fig. 9, Table 4). Some samples of preglacial dacite and rhyodacite are slightly higher in Rb, Ba, Th, and La relative to compositionally equivalent younger PII and PIII lavas (Fig. 9). La/Yb ratios of 5.6 to 6.0 in preglacial dacites are higher than ratios of 5.0 to 5.3 observed in younger dacites, rhyodacites, and rhyolites in the PII, PIII, PIV, CCIV, CCV, and CCVI units.

4.4 Isotopic compositions

Representative samples from all stratigraphic units were analyzed for their Sr and Nd isotopic compositions (Table 5). The total range in $^{87}Sr/^{86}Sr$ is 0.70378±4 to 0.70416±4 and in $^{143}Nd/^{144}Nd$ is 0.512818±18 to 0.512900±31.

Basalts and basaltic andesites with lower La/Yb (3.6-4.6) display a restricted range in $^{87}Sr/^{86}Sr$ (0.70397-0.70406) and $^{143}Nd/^{144}Nd$ (0.51287-0.51288). Basalts higher in LREE (La/Yb = 5.0-5.4) span the entire range of $^{87}Sr/^{86}Sr$ (0.70378-0.70416) and extend to relatively lower $^{143}Nd/^{144}Nd$ (0.51282-0.51289). PIII and PIV samples ranging from andesites to rhyolites are somewhat restricted in $^{87}Sr/^{86}Sr$ (0.70397-0.70410) and display a relatively lower range of values of $^{143}Nd/^{144}Nd$ (0.51282-0.51286). Preglacial basaltic andesites and andesites range in $^{87}Sr/^{86}Sr$ (0.70402-0.70414) and $^{143}Nd/^{144}Nd$ (0.51282-0.51289) which overlap with all of the possible 'groups' distinguished above.

Rhyodacites and rhyolites from Cordon Caulle display narrow ranges in $^{87}Sr/^{86}Sr$ (0.70406-0.70415) and $^{143}Nd/^{144}Nd$ (0.51284-0.51290). Each of the three eruptive units, CCIV, CCV, and CVI, is homogeneous within analytical error with respect to $^{87}Sr/^{86}Sr$ and $^{143}Nd/^{144}Nd$. The CCIV and CCVI units are similar in their Sr and Nd isotopic compositions while two samples from the CCV unit are characterized by higher $^{87}Sr/^{86}Sr$ (0.70415) and lower $^{143}Nd/^{144}Nd$ (0.51284-0.51286) compared to the other two eruptive units (Table 5).

Eight representative samples of postglacial lavas from Puyehue Volcano and Cordon Caulle were selected for Pb-isotopic analysis (Table 5). All samples display relatively restricted ranges in

Table 5

Sr, Nd, and Pb isotopic compositions and abundances of selected trace elements (ppm) of representative samples from Puyehue Volcano

Unit	Sample	Ba	Cs	K	Rb	Sr	$^{87}Sr/^{86}Sr$[3]	Sm	Nd	$^{143}Nd/^{144}Nd$[4]	$^{206}/^{204}Pb$[5]	$^{207}/^{204}Pb$	$^{208}/^{204}Pb$
preglacial volcanics	1428212	[1]257.1 251.6	0.75 0.76	6389 6414	17.25 17.21	401.0 401.0	.70414±3	4.22	16.57	.512892±19			
	162828a	277.3	1.63	7412	20.60	391.7	.70408±5	3.05	11.50	.512836±19			
	82826b	333.1	2.00	10022	27.80	394.3	.70402±2	6.45	26.20	.512845±18			
	222821b	479.1	1.89	13605	40.90	353.5	.70413±5	8.31	35.61	.512849±17			
	82825	340.7	1.68	8503	23.23	423.3	.70412±3	-	-	.512832±15			
	82821	380.9	2.54	10917	33.87	347.6	.70407±3	-	-	.512820±18			
PII	13828	138.7	0.60	4030	7.48	496.3	.70381±3	2.27	9.25	.512861±17	18.551	15.578•	38.363
	272829	140.1	0.58	4129	7.49	494.8	.70378±4	2.26 2.27	9.23 9.23	.512881±21	18.558	15.589	38.403
	272825	146.4	0.58	3567	7.75	436.6	.70397±3	2.58	9.76	.512872±21			
	13826h	142.8	0.51	3570	7.52	434.5	.70398±3	2.54 2.54	9.66 9.67	.512879±26	18.570	15.592	38.454
	272824b	188.1	0.89 0.87	5547 5484	15.78 15.75	476.3 476.7	.70416±4	3.32	13.24	.512855±21	18.583	15.594	38.473
	220283-1	209.6	0.63	4627	10.29	462.2	.70401±25	3.23	13.37	.512818±18	18.576	15.594	38.466
	250283-2	195.4	0.94	4870	12.71	435.0	.70406±5	3.14	12.52	.512848±18			
	272827	269.7	1.46	7159	20.18	396.6 397.4	[1].70404±3 .70404±3	4.70	19.14	.512879±15			
	138212	271.3	1.46	6961	18.26	397.2	.70405±3	4.66	18.71	.512876±17			
	272826b	270.6	1.20 1.18	6805 6796	19.87 19.65	349.6 349.3	.70400±3	3.62	15.06	.512846±19			
	220283-3	273.5	1.45	7136	18.54	398.0	.70406±25	-	-	-			
	230283-2	209.0	0.65	4709	10.80	455.2	.70403±3	-	-	-			
	230283-5	218.1	0.68	4962	11.29	463.0	.70399±3	-	-	-			

Table 5 (continued)

Sr, Nd, and Pb isotopic compositions and abundances of selected trace elements (ppm) of representative samples from Puyehue Volcano

Unit	Sample	Ba	Cs	K	Rb	Sr	$^{87}Sr/^{86}Sr$[3]	Sm	Nd	$^{143}Nd/^{144}Nd$[4]	$^{206}/^{204}Pb$[5]	$^{207}/^{204}Pb$	$^{208}/^{204}Pb$
PIII	212824	667.5	4.70	21442	66.50	182.6	.70406±25	8.30	36.22	[2].512859±21 .512853±23			
	202825c	779.7	5.20	22538	68.34	161.2	.70409±3	9.17	40.18	.512850±23	18.581	15.597	38.477
PIV	220283-5	445.9	2.50	12284	35.13	377.8	.70407±3	7.93	33.21	.512837±16			
	272822	408.2	2.94	12682	38.90	374.7	.70388±4	5.68 5.69	24.17 24.19	[1].512832±28 .512819±30	18.581	15.593	38.469
	242824	549.9 555.0	3.62 3.67	17109 17212	53.98 54.08	289.5 288.2	.70410±5	7.19	31.21	.512827±30			
	212826	633.6	3.96	18582	56.53	230.4	.70402±3	8.67	37.25	[2].512857±17 .512869±27			
CIV	182821b	774.7	5.10	23432	71.21	141.6	.70409±3	9.28	40.81	.512880±21	18.583	15.599	38.488
	301821b	784.0	5.65	23016	70.39	143.1	.70409±3 .70411±3	9.34	41.07	.512899±26			
CCV	72822	690.9	4.77	21331	65.22	188.0	.70415±3	8.41	36.77	.512858±16			
	42821	687.4	4.78	21503	65.18	185.9	.70415±3	8.40	36.67	.512836±35			
CCVI	42824a	721.9 709.9	5.00 5.05	22408 22467	68.17 69.50	168.9 168.5	[1].70406±3 .70406±3	8.44 8.44	37.05 37.06	[1].512895±20 .512900±31			
	281822bh	735.1	5.15	22634	70.46	160.9	.70409±25	8.45	37.06	.512880±19			
	212823a	765.5	5.00	22578	69.66	162.8	.70407±3	8.44	37.00	.512866±18			

[1] Abundances determined by isotope dilution techniques (cf. Hart and Brooks, 1977). Duplicate analyses of abundances and annotated determinations of isotopic compositions were determined on different spike + samples mixtures in each case. Precision of duplicate analyses of the same spike + sample mixture is better than the uncertainty resulting from analysis of differing spike + sample mixtures.

[2] Duplicate analyses of spiked and unspiked samples.

[3] Normalized to $^{86}Sr/^{88}Sr = 0.1194$ and to E + A standard $^{87}Sr/^{86}Sr = 0.70800$. Errors are 2σ of the mean and correspond to least significant digits.

[4] Normalized to $^{146}Nd/^{144}Nd = 0.7219$ and to BCR-1 standard $^{143}Nd/^{144}Nd = 0.51263$. Errors are 2σ of the mean, and correspond to the least significant digits.

[5] Pb isotopic analyses are normalized for mass discrimination based on analyses of NBS SRM 981 and reproducibility is estimated to be better than 0.05% per a.m.u.

$^{206}Pb/^{204}Pb$ (18.551-18.583), $^{207}Pb/^{204}Pb$ (15.578-15.599), and $^{208}Pb/^{204}Pb$ (38.363-38.488) ratios.

5. General approach to petrogenetic modelling

A major goal of the present study is to outline the magmatic evolution of the volcano and to identify the various petrogenetic processes that produced the geochemical characteristics of the lavas. Identification of near-surface processess and evaluation of their efficacy will also aid in determining which samples are the most primitive in the sample suite and therefore reflective of source characteristics.

In the following sections, the importance of fractional crystallization and magma mixing and a lesser role for crustal contamination in producing the characteristics of the evolved lavas will be demonstrated. Basalts have variable geochemical characteristics, and different basalts may be identified as endmembers in specific hypothetical magma mixing phenomena or as parental lavas in certain fractional crystallization schemes. This is possible through combined use of major-element, trace element, and isotopic data.

5.1 Fractional crystallization models: identification of fractionating phases

The choice of mineral phases to be employed in fractional crystallization model calculations is well-constrained by the geochemical data. Decreasing CaO, Al_2O_3, and Sr with increasing SiO_2 throughout the sample suite indicate significant amounts of fractional crystallization of plagioclase (Table 4, Figs. 7 and 9). In the same manner, decreasing

MgO, Cr, and Ni contents indicate fractional crystallization of olivine, as Cr and Ni are preferentially incorporated in olivine (Leeman and Scheidegger, 1977; Leeman and Lindstrom, 1978). Small inclusions of Cr-spinel inclusions in olivine phenocrysts of basalts may deplete residual liquids in Cr but are inconsequential in most major-element model calculations. Relative enrichment of LREE as indicated by increasing La/Sm and La/Yb ratios with increasing SiO_2 (Fig. 10) suggests that fractional crystallization of clinopyroxene may have occurred, since middle to heavy REE are preferentially incorporated into clinopyroxene (Nicholls and Harris, 1980; Grutzeck et al., 1974). Moreover, fractional crystallization of clinopyroxene in the form of subcalcic augite was important in lavas containing greater than 54 wt.% SiO_2 as suggested by significant decreases in CaO/Al_2O_3 ratios with increasing SiO_2 (54 to 71 wt.% SiO_2). Initially increasing Ti and V abundances from basalt to basaltic andesites and decreasing abundances thereafter (Figures 8 and 9) indicate that fractional crystallization of Ti-magnetite was significant in evolved lavas (cf. Lindstrom, 1976). Increasing P_2O_5 contents from basalts to andesites and decreasing contents from andesites to rhyolites indicate that apatite fractionation was unlikely in basaltic to andesitic magmas but did occur in andesitic to rhyolitic magmas (Fig. 8).

Based on the above discussion and on petrographic observations, the chief crystallizing phases throughout the sequence include plagioclase, olivine, clinopyroxene (augite), orthopyroxene, minor pigeonite, and Ti-magnetite. Based on petrographic observations of phenocrysts covered earlier, the order of crystallization in lavas at Puyehue Volcano was plagioclase + olivine, plagioclase + olivine + augite ± spinel, plagioclase + augite + spinel, and plagioclase + augite + orthopyroxene +

12a. Experimentally determined phase relations for plagioclase-saturated compositions at 1-atm under anhydrous conditions after Grove et al. (1982). Liquid compositions are projected from plagioclase on to the pseudoternary olivine (oliv) - clinopyroxene (cpx) - quartz (qtz) using oxygen units as described by Grove et al. (1983). Cotectics and reaction curves determined by Walker et al. (1979), Grove et al. (1982), and Grove and Bryan (1983) are designated. Also shown are reaction points A (oliv + liq = pig + aug + plag) and B (oliv + liq = opx + pig + plag) separated by a thermal divide TD. Compositions of preglacial volcanics, and samples from Puyehue Volcano and Cordon Caulle are projected on the pseudoternary and represented by designated symbols.

12b. Bulk compositions of two basalts projected on the oliv-cpx-qtz pseudoternary. Groundmass compositions of the two basalts were calculated (see text) for comparison with original bulk compositions. Projected compositions of basaltic andesites are also shown for comparison.

12c. Projected bulk and groundmass compositions of two basalts are compared with those of basaltic andesites in the oliv-plag-qtz pseudoternary.

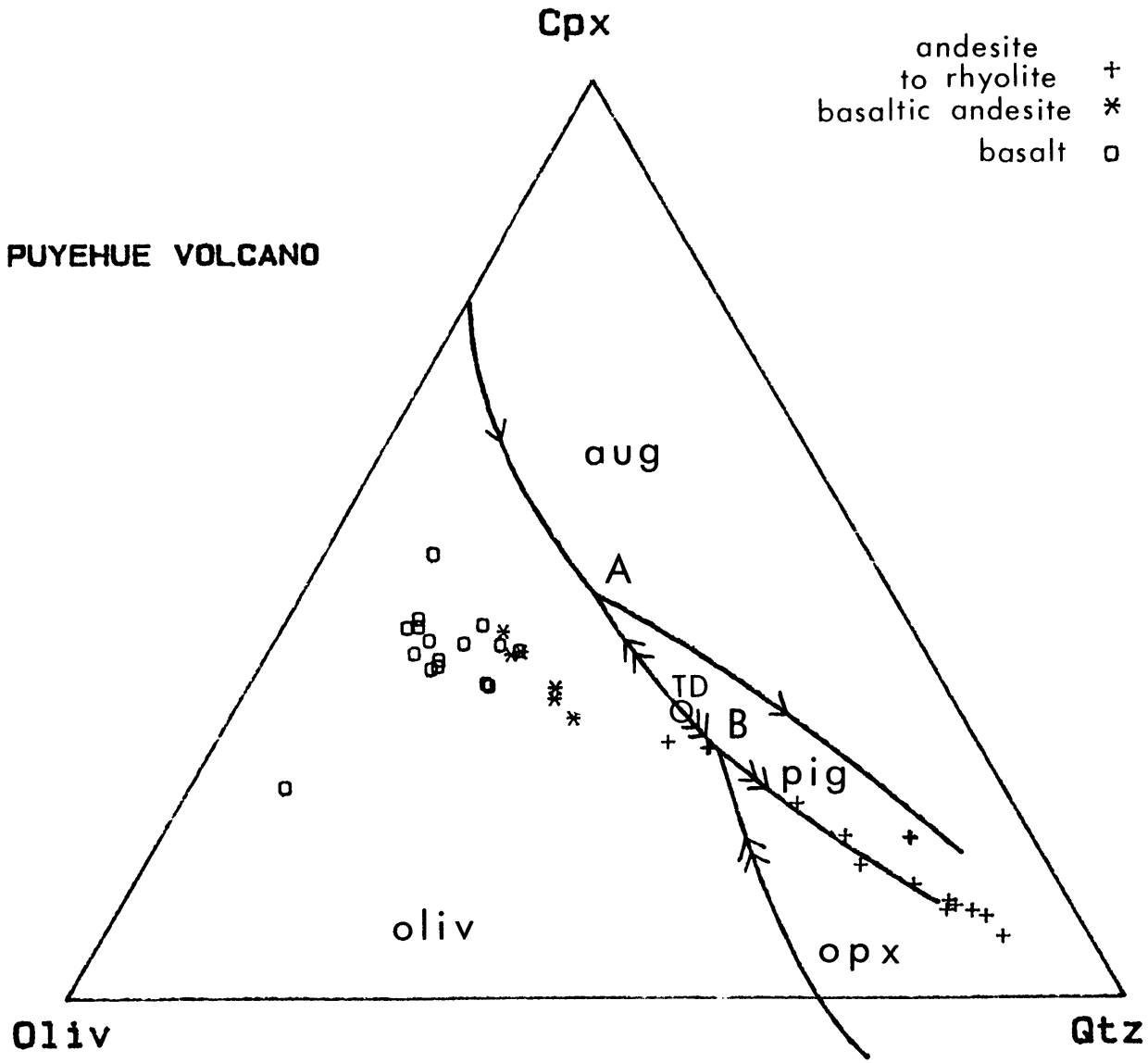
Cpx
andesite
to rhyolite +
basaltic andesite *
basalt o
PUYEHUE VOLCANO
aug
A
TD
B
pig
oliv
opx
Oliv
Qtz

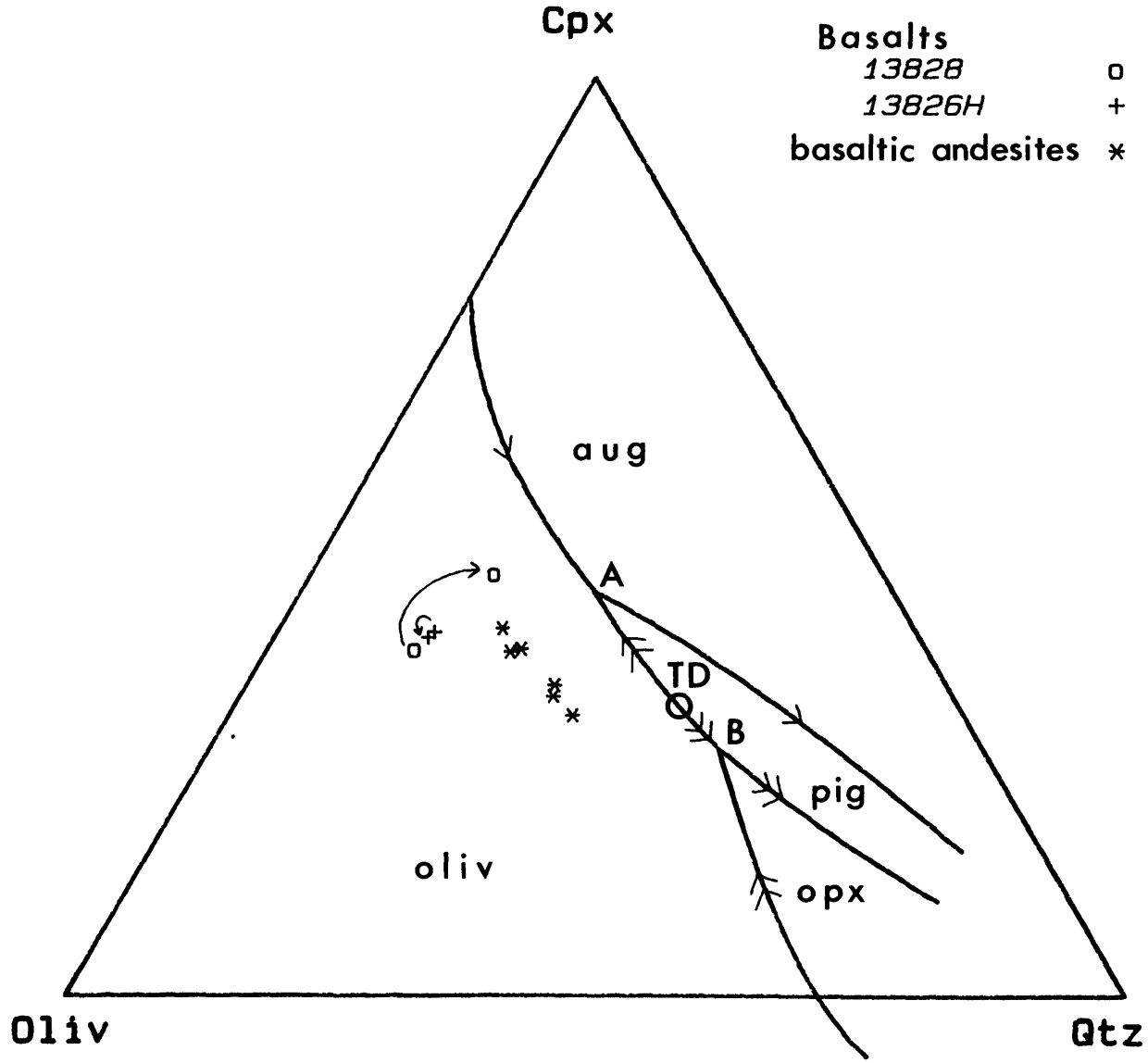
Cpx
Basalts
13828 o
13826H +
basaltic andesites *
aug
A
TD
B
pig
opx
oliv
Oliv
Qtz

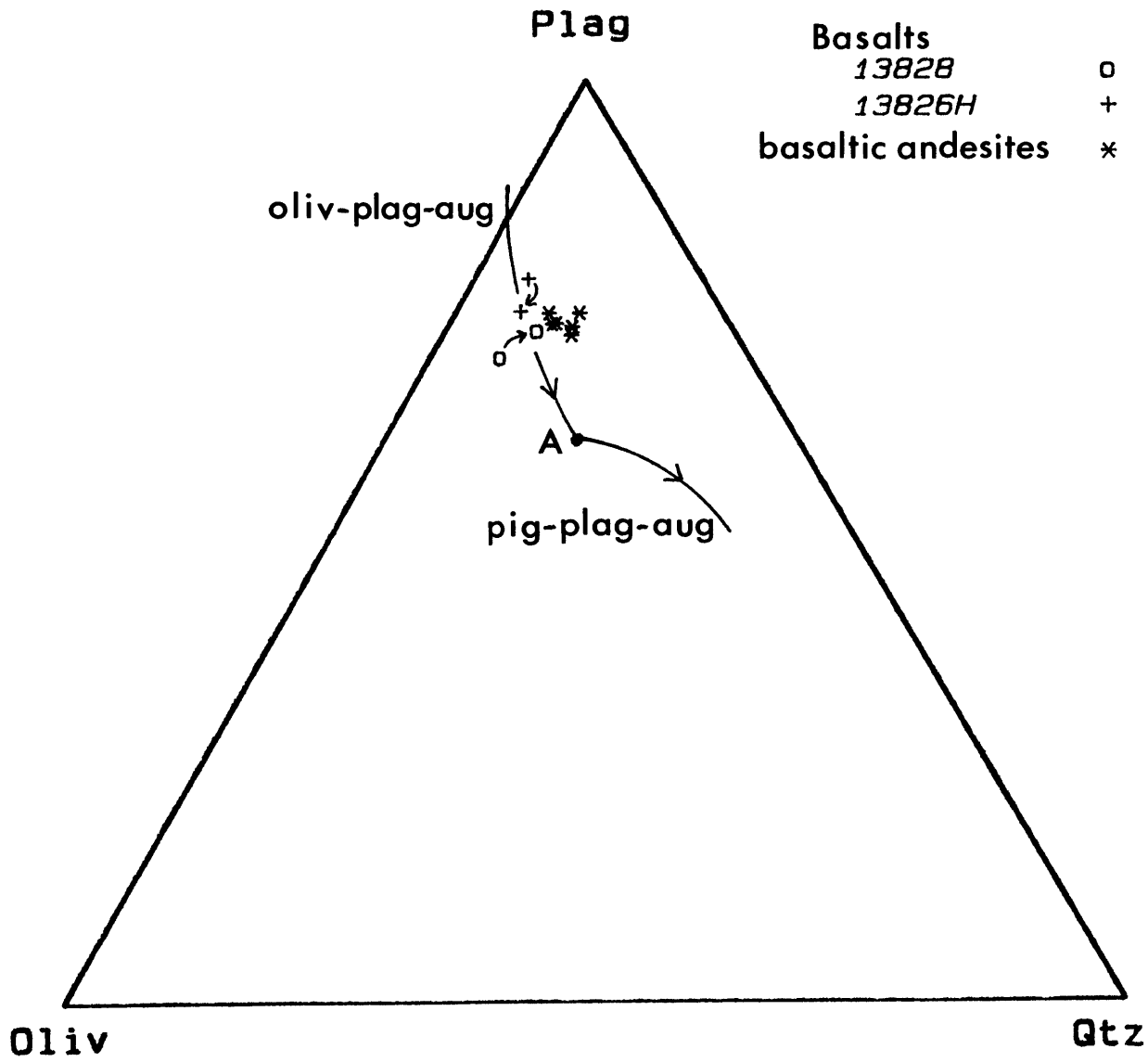
Plag
Basalts
13828 o
13826H +
basaltic andesites *
oliv-plag-aug
A
pig-plag-aug
Oliv
Qtz

spinel ± ilmenite. This reconstructed sequence of crystallization assumes a cogenetic relationship between all samples ranging from basalt to rhyolite and will be mainly applied to the interpretation of the post-glacial lavas. Both the overall sequence of crystallization and the approximate trend defined by the analyzed samples (Fig. 12a) on the projection olivine-cpx-SiO_2 at 1-atm after Grove et al. (1982) may suggest that fractional crystallization occurred at relatively low pressures. Although clinopyroxene is scarce or absent as phenocrysts in basalts and basaltic andesites (Table 2), a relatively early appearance and significant role for clinopyroxene may be justified by increasing relative LREE enrichment. If crystallization of clinopyroxene occurred simultaneously with plagioclase and olivine crystallization in basalt, i.e., the basaltic magmas were triply saturated with plagioclase, olivine, and clinopyroxene, this suggests moderate pressures of up to 5 kb (Spulber and Rutherford, 1983; Takahashi and Kushiro, 1983; Grove and Baker, 1984). Clinopyroxene is a primary liquidus phases and precedes olivine and plagioclase at pressures > 12 kb (Perfit and Gust, 1981).

5.2 Do the bulk compositions represent liquids?

Any fractional crystallization calculation scheme must assume that samples taken to represent parental and residual liquids are indeed liquids. Basalts are the most porphyritic (10% to 26% phenocrysts), and the question arises as to whether or not they represent liquids. Tests of fractional crystallization models will mostly concern major elements and incompatible trace elements, and it would be desirable to correct for phenocryst dilution. If phenocrysts have accumulated in a liquid by some

means such as gravitational settling, then the bulk composition of the resulting mixture does not represent a magmatic liquid composition. The exact bulk compositions of primitive or parental magmas for the basalts is unknown, and it is not possible to know the true relative crystallizing proportions of the phenocryst phases present. Modal olivine/plagioclase ratios vary from approximately 0.04 (sample 13826h) to 7 (sample 242822a) in the basalts, and this variation may be due to respective accumulations of plagioclase or olivine.

The possibility of plagioclase accumulation may be addressed in various plots in Figure 13. The positive correlation of Sr/Nd ratios versus Eu/Eu*, with most basalts displaying positive Eu anomalies (Eu/Eu* > 1.0) is an indication of plagioclase accumulation in many of the basalts. However, Eu/Eu* is not well correlated with modal abundances of plagioclase phenocrysts in the basalts. In Figures 13a, c, and d, abundances of Sr and Eu/Eu* were adjusted in the basalts for plagioclase accumulation assuming D_{plag}^{Sr} = 1.5 and Eu/Eu* = 10, the latter an average value based on experimental studies (Weill and Drake, 1973) and empirical studies (Fujimaki et al., 1984). If the basalt data are corrected for plagioclase phenocryst effects, as shown by calculated sample curves in Figure 13d, so that all samples featured little or no Eu anomaly (Eu/Eu* = 1.0), then the basalts still display a wide range in Sr/Nd ratios. This correction assumes that basaltic melts lack positive Eu anomalies. As seen in Figure 13a, b, and d, CaO/Al_2O_3 and Na_2O/K_2O ratios are relatively less sensitive to plagioclase accumulation.

Cores of plagioclase phenocrysts in the basalts range in composition from approximately An_{78} to An_{90} and are considerably more calcic than compositions (An_{50}-An_{55}) expected to be in equilibrium with the

13 Data for basalts and basaltic andesites from Puyehue Volcano displayed on selected ratio-ratio plots to both assess and display the effects of plagioclase accumulation. Trends for addition of plagioclase from arbitrary points are shown. Tickmarks refer to the % plagioclase added (by mass). In all plots, a basaltic liquid was assumed to have Na_2O = 2.90 wt.%, K_2O = 0.50 wt.%, Sr = 450 ppm, Nd = 10 ppm, Eu = 0.86 ppm, Sm = 2.54 ppm, Tb = 0.45 ppm, CaO = 9.5 wt.%, Al_2O_3 = 17.5 wt.%, and Eu/Eu* = 1.00. Plagioclase was assumed to have Na_2O = 1.10 wt.%, K_2O = 0.05 wt.%, CaO = 16.9 wt.%, Al_2O_3 = 33 wt.%, Nd = 0.1 ppm, Sm = 0.05 ppm, and Tb = 0.005 ppm. Eu/Eu* is calculated as

$= Eu_{C.N.}/[Sm_{C.N.} - 1/3(Sm_{C.N.} - Tb_{C.N.})]$. Eu/Eu*

for plagioclase is assumed to be 10.0 for the lower curve in (d), and 5.0 for the upper curve. Weill and Drake (1973) have demonstrated variation of Eu/Eu* in plagioclase with $^fO_2$. (a) Sr/Nd vs. Na_2O/K_2O (b) CaO/Al_2O_3 vs. Na_2O/K_2O (c) CaO/Al_2O_3 vs. Sr/Nd, and (d) Sr/Nd vs. Eu/Eu*. Filled circles refer to basalts and open circles refer to basaltic andesites.

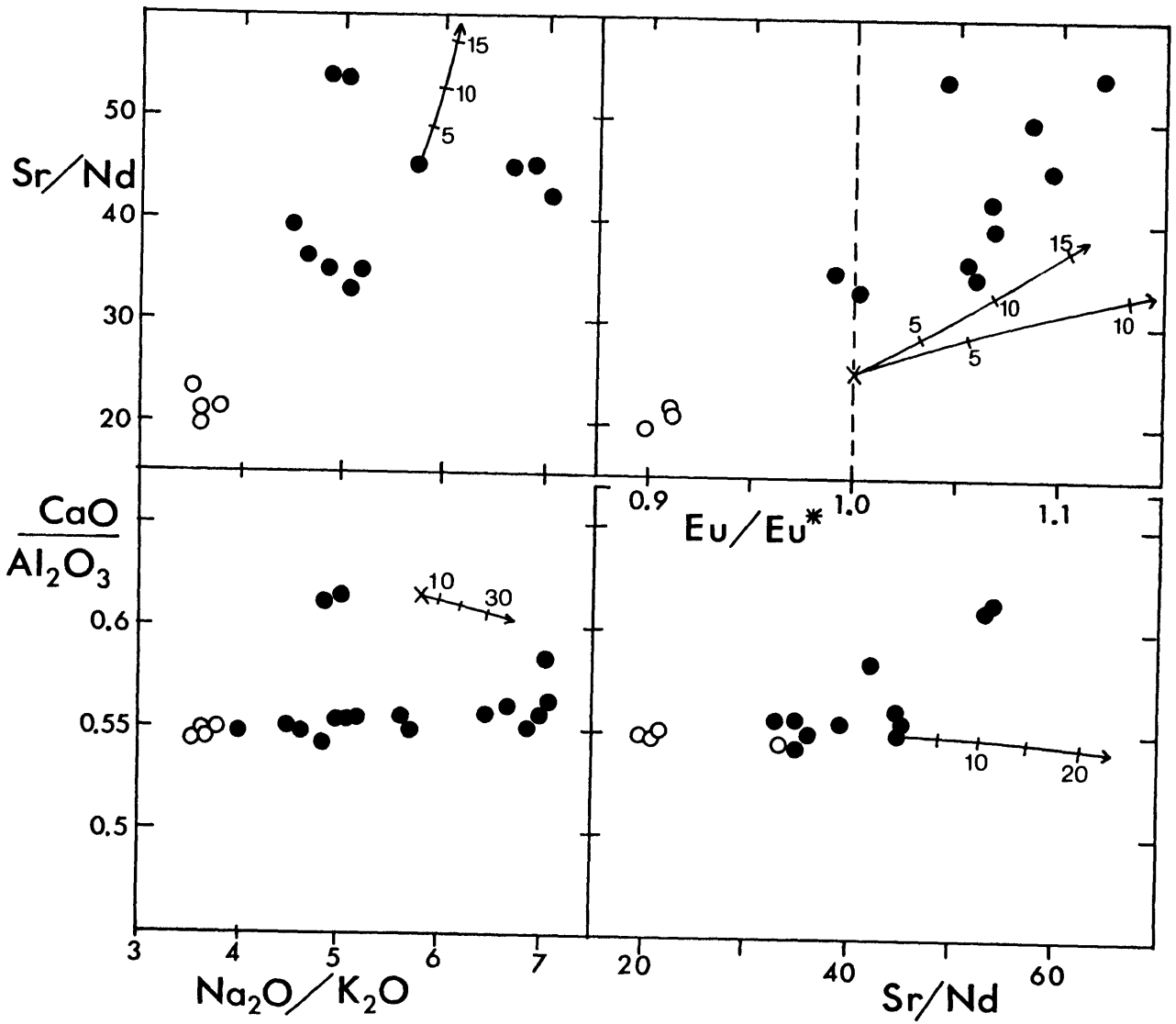
Sr/Nd
50
40
30
20
15
10
5
15
10
5
5
10
10
0.9
1.0
1.1
Eu/Eu*
CaO
Al2O3
0.6
0.55
0.5
10
30
10
20
3
4
5
6
7
Na2O/K2O
20
40
60
Sr/Nd

groundmass (here, crudely approximated by bulk composition) based on 1-atm experimental data (Grove et al., 1982). Since bulk compositions estimated in this manner are more calcic than actual groundmass compositions, the estimated range of An_{50} to An_{55} for equilibrium compositions is an upward limit. If the major-element bulk compositions of the basalts are corrected for accumulated phenocrysts, using plagioclase phenocryst microprobe analyses (Table 3) and modal analyses (Table 2), the disparity is increased. Thus, the plagioclase phenocrysts in the basalts may not be in equilibrium with the groundmass. Groundmass microphenocryst analyses may be more representative of equilibrium compositions and were used in modelling. The very calcic (An_{80}-An_{85}) phenocrysts are not necessarily xenocrysts but may be relict liquidus phases crystallized from more primitive basalts parental to the basalts analyzed in the present sample suite. Also, the combined effects of H_2O and higher total pressure would allow greater disparity in Ca-Na exchange between plagioclase and melt (Johannes, 1978) such that the more calcic plagioclase compositions are closer to being in equilibrium with the groundmass. This would necessitate use of higher K_D^{plag} ($X_{Ca}^{xl}X_{Na}^{liq}/X_{Na}^{xl}X_{Ca}^{liq}$) values in model calculations, but the precise variation of K_D^{plag} with varying total pressure and P_{H_2O} has not been determined. K_D^{plag} values of 0.75 to 1.5 were used in subsequent calculations because they result in calculated plagioclase compositions similar to analyzed phenocryst rim and groundmass compositions.

Olivine K_D^{oliv}'s may vary with pressure (Ford et al., 1983) and may be used with phenocryst compositions and bulk compositions to test whether or not olivine phenocrysts are accumulated in some of the basalts. Calculated K_D^{oliv}'s ($X_{Fe}^{oliv}X_{Mg}^{bulk}/X_{Mg}^{oliv}X_{Fe}^{bulk}$) assuming

total iron as Fe^{2+} for some samples such as basalt 242822a (23% olivine phenocrysts) are higher (0.55) than generally accepted values of 0.30 for low pressures and indicate olivine accumulation. These calculated K_D^{oliv}'s are also significantly higher than experimentally determined values of 0.40 at pressures of 30 kb (Ford et al., 1983). Other basalts (13826h, 138210) which contain a greater proportion of plagioclase phenocrysts relative to olivine phenocrysts yield lower calculated K_D^{oliv}'s (0.25 to 0.26). Higher calculated K_D^{oliv}'s for these samples would result if X_{Fe}^{bulk} was recalculated assuming a portion of the iron as Fe^{3+}. Basalts such as samples 220283-1 and 230283-5 are porphyritic (Table 2) but yield calculated K_D^{oliv}'s of approximately 0.31 and therefore may be representative of liquid compositions at low pressures at least where olivine phenocryst contents are concerned.

The major-element compositions of various basalts important in fractional crystallization models were adjusted assuming that all plagioclase and olivine phenocrysts were accumulated and results are listed in Table 6, with results of model calculations. Abundances of selected incompatible and moderately incompatible trace elements including La, Sm, Yb, Hf, Sc, Zr, Th, Nb, Rb, and Ba were also corrected for 'dilution' by olivine and plagioclase phenocrysts resulting in increased values proportional to total phenocryst content. Abundances of the compatible trace elements Sr, Cr, and Ni were adjusted assuming $D_{plag}^{Sr} = 1.5$, $D_{oliv}^{Cr} = 3.0$, and D_{oliv}^{Ni} estimated after the method and results of Hart and Davis (1978). If only a portion of the olivine and plagioclase phenocrysts were accumulated, then adjusted abundances of compatible elements such as Sr, Cr, and Ni should be considered minimum values and subject to some uncertainty.

The net effects on major elements of this adjustment for phenocrysts presumed to be accumulated is to increase SiO_2, TiO_2, Fe_2O_3, MgO, Na_2O, P_2O_5, and K_2O, and to lower Al_2O_3 and CaO, since plagioclase phenocrysts are volumetrically predominant in most basalts relative to olivine phenocrysts (Table 2). Correction of major-element compositions and trace element abundances at least for olivine phenocrysts appears to be justified by an example provided by basalt 13828. A calculated K_D^{oliv} of 0.44 for an uncorrected bulk composition of basalt 13828 is higher than that calculated (0.31) for groundmass composition. An independent calculation based on average phenocryst core compositions (Fo_{82}) and a K_D^{oliv} of 0.30 indicates that such olivine phenocrysts would be in equilibrium with a liquid characterized by an $X_{Mg}^{liq}/X_{Fe}^{liq}$ ratio of 1.42 and this is equivalent to that observed in a bulk composition of basalt 13828 which has been adjusted by removal of all phenocrysts.

In detail, projected compositions display differences between the original bulk compositions and adjusted compositions. This is shown in Figures 12b and 12c for two basalts, 13828 and 13826h. Adjusting the composition of 13828 results in a decreased olivine component and increases in clinopyroxene, plagioclase, and quartz components, while the adjusted composition of 13826h is characterized by a higher olivine component and lower plagioclase component relative to the original bulk composition (Figs. 12b and 12c). The adjusted compositions of the basalts are superficially similar to low-SiO_2 basaltic andesites such as sample 138212, although projected compositions of these basaltic andesites are distinct (Figs. 12b, 12c). Differences of 20-50% between basaltic andesites and adjusted basalt compositions yet remain in MgO, CaO, TiO_2, P_2O_5, and K_2O, and are even greater for trace element

abundances (cf., Table 6, Table 4). Thus, the aphyric basaltic andesites are dissimilar to calculated groundmass compositions of the basalts, i.e., basalts are not simply low-SiO_2 basaltic andesites with significant amounts of accumulated plagioclase and olivine phenocrysts. It is possible that not all of the olivine and plagioclase phenocrysts are accumulative, and adjustment of bulk compositions by removal of all phenocrysts may not be warranted. However, it is hoped that the estimated groundmass compositions of selected basalts are reasonable approximations of liquids which lie on the overall liquid line(s) of descent and which may be parental to evolved lavas.

5.3 Liquid lines of descent

A general approach in modelling one or more liquid lines of descent will be to consider restricted compositional ranges individually, i.e., basalt to basaltic andesite, basaltic andesite to andesite, and andesite to rhyolite. In choosing samples for modelling preference is given to samples which were more thoroughly analyzed. The geochemical variability in the basalts requires the application of a variety of criteria (Table 6) in selecting samples to model the derivation of basaltic andesites which are also variable in character. Choices of samples to be used in reconstructing the liquid line of descent from basaltic andesites to rhyolites are relatively restricted and will be discussed in later sections.

One of the more variable geochemical characteristics of the basalts is the large range in degree of relative LREE enrichment (La/Sm = 2.36-2.92, La/Yb = 3.64-5.43). Three samples of basaltic andesite (138212, 272827, 220283-3) are characterized by La/Sm ratios of

Table 6

Summary of geochemical criteria: basalts, basaltic andesites, and andesites

	basalts										
	13826h	272825	220283-4	242822a	250283-2	272824b	230283-5	272829	13828	230283-2	220283-1
La/Sm	2.36	2.36	2.45	2.50	2.66	2.64	2.80	2.79	2.80	2.92	2.93
La/Yb	3.59	3.81	4.20	4.08	4.22	5.01	4.97	5.23	5.05	5.28	5.43
La	6.00	6.09	6.60	5.43	8.36	8.76	8.35	6.33	6.36	9.76	9.45
Sm	2.54	2.58	2.69	2.17	3.14	3.32	2.98	2.27	2.27	3.34	3.23
Yb	1.67	1.60	1.57	1.33	1.98	1.75	1.68	1.21	1.26	1.85	1.74
Ni	50	50	22	302	62	51	49	141	147	65	65
Cr	118	112	88	640	158	100	119	441	426	117	120
MgO	5.91	5.91	4.74	14.32	5.89	6.00	5.80	9.40	9.52	6.92	6.78
TiO_2	0.83	0.85	0.70	0.70	0.93	0.89	0.96	0.66	0.65	0.90	0.94
$^{87}Sr/^{86}Sr$	.70398	.70397	-	-	.70406	.70416	.70399	.70378	.70381	.70403	.70402
$^{143}Nd/^{144}Nd$	.512879	.512872	-	-	.512848	.512855	-	.512881	.512861	.-	.512818

	basaltic andesites			
	220283-3	272827	138212	272826b
La/Sm	2.66	2.73	2.77	3.23
La/Yb	4.60	4.59	4.63	5.12
La	12.9	12.9	12.9	11.7
Sm	4.84	4.70	4.66	3.62
Yb	2.80	2.80	2.79	2.28
Ni	47	54	52	64
Cr	108	105	108	126
MgO	5.63	5.49	5.52	5.94
TiO_2	1.34	1.32	1.30	0.70
$^{87}Sr/^{86}Sr$	.70406	.70404	.70405	.70400
$^{143}Nd/^{144}Nd$	-	.512879	.512876	.512846

	andesites		
	220283-5	43821	272822
La/Sm	2.84	3.04	3.18
La/Yb	5.52	5.51	5.31
La	22.5	23.7	18.1
Sm	7.93	7.80	5.68
Yb	4.07	4.30	3.40
Ni	8	12	55
Cr	19	10	158
MgO	2.79	2.56	4.31
TiO_2	1.44	1.57	0.85
$^{87}Sr/^{86}Sr$	.70407	-	.70388
$^{143}Nd/^{144}Nd$	.512835	-	.51282

2.66 to 2.78 and La/Yb ratios of 4.59 to 4.63, and one sample (272826b) is relatively more LREE-enriched (La/Sm = 3.23, La/Yb = 5.12). Fractional crystallization of olivine and plagioclase will not increase LREE/HREE ratios in residual liquids, but may produce a slight decrease since $D_{Oliv}^{La} > D_{Oliv}^{Yb}$ and $D_{plag}^{La} > D_{plag}^{Yb}$ (cf., Fujimaki et al., 1984). Since partition coefficients for REE in olivine and plagioclase are generally quite low, this effect is negligible. Fractional crystallization of clinopyroxene will result in relative LREE enrichment in residual liquids. Since olivine, plagioclase, and clinopyroxene are the most probable fractionating phases in basalts, relatively LREE-enriched basalts (La/Yb = 4.97-5.43) cannot give rise to less LREE-enriched basaltic andesites (La/Yb = 4.59-4.63) by fractional crystallization, but may be parental to basaltic andesite 272826b (La/Yb = 5.12).

Basalts which are relatively less LREE enriched (La/Yb = 3.36-4.22) may be parental to the basaltic andesites except for basaltic andesite 272826b (Table 6). This sample has higher Ni and Cr abundances (64 ppm Ni, 126 ppm Cr) than several basalts such as 272825 and 13826h (50 ppm Ni, 112-118 ppm Cr); if 272826b were a product of fractional crystallization, bulk D^{Ni} and D^{Cr} should be >1.0 for most crystallizing assemblages and would result in lower Ni and Cr abundances in residual liquids. It is also unlikely that basalts 13826h and 272825 can yield such LREE-enriched residual liquids as 272826b by any reasonable degree of fractional crystallization even if clinopyroxene was the major crystallizing phase. Basalt samples such as 242822a (La/Yb = 4.1) and 220283-4 (La/Yb = 4.20) may represent parental liquids, but contain 25%-26% phenocrysts, and correction of their bulk compositions for accumulated phenocrysts may introduce too much uncertainty relative to

other, less porphyritic basalts. Basalt 250283-2 (La/Yb = 4.22, Ni 62 ppm, Cr 158 ppm) may not be parental to 272826b by fractional crystallization because it is isotopically different ($^{87}Sr/^{86}Sr$ = 0.70406) relative to 272826b ($^{87}Sr/^{86}Sr$ = .70400). Basalt 272824b (La/Yb = 5.0) is not a likely parental predecessor to 272826b due to low Ni and Cr (50 ppm, 100 ppm, respectively) abundances and higher $^{87}Sr/^{86}Sr$ (0.70416). If basaltic andesite 272826b was produced by fractional crystallization of basalt 250283-2 or 272824b, this would require concurrent contamination by crustal material with similar $^{143}Nd/^{144}Nd$ (0.51285) but much lower $^{87}Sr/^{86}Sr$ (< 0.70400). Based on above criteria, more likely parental basaltic magmas for the basaltic andesite 272826b may be represented by the relatively LREE enriched basalts such as 220283-1, 230283-2, 230283-5, 13828, and 272829. The latter two (13828 and 272829) are characterized by lower $^{87}Sr/^{86}Sr$ (0.70378 to 0.70381) relative to 272826b (0.70400) and the possibility of crustal contamination in this relationship will be discussed in a later section.

The relatively less LREE-enriched basaltic andesites (samples 138212, 272827, 220283-3) may have been derived from less LREE-enriched basalts (Table 6). Among these basalts, porphyritic samples 242822a and 220283-4 were not used for reasons stated earlier. If basaltic andesites such as 138212 and 272827 ($^{143}Nd/^{144}Nd$ = 0.51288) were produced by fractional crystallization of basalt 250283-2 ($^{143}Nd/^{144}Nd$ = 0.512848), this would require contamination by crustal material with similar $^{87}Sr/^{86}Sr$ (0.70404-0.70406) but lower $^{143}Nd/^{144}Nd$ (< 0.51285). As discussed in a later section, basalts such as 250283-2 and 272824b may themselves have been modified by crustal contamination relative to other

basalts, and it would involve more uncertainty in attempting to treat these basalts as parental magmas for the basaltic andesites. Of the remaining well-analyzed basalts, samples 13826h and 272825 may be the most likely representatives of magmas parental to basaltic andesites such as 138212.

Despite a higher SiO_2 content in basaltic andesite 272826b relative to basaltic andesite 138212, addition (by accumulation) or subtraction (by fractional crystallization) of any reasonable combination of phases cannot explain the higher Al_2O_3, MgO, CaO, and SiO_2 contents and lower TiO_2, P_2O_5, FeO, and Na_2O contents in 272826b relative to 138212.

In the following sections, the genetic relationships of specific basalts with the distinctive basaltic andesites as represented by samples 138212 (La/Sm = 2.78, La/Yb = 4.63, $^{87}Sr/^{86}Sr$ = 0.70405) and 272826b (La/Sm = 3.23, La/Yb = 5.12, $^{87}Sr/^{86}Sr$ = 0.70400) will be discussed. Modelling efforts will attempt to relate basalt 13826h to basaltic andesite 138212, and basaltic andesite 272826b to one or more of the relatively LREE-enriched basalts such as samples 13828 and 220283-1.

5.4 Modelling procedures: fractional crystallization

Fractional crystallization model calculations were carried out using a program RXNAFC written by T.L. Grove and employed by Grove *et al.* (1982) and Grove and Baker (1984). The approach followed is different than earlier least-squares mixing routines in that mineral-melt exchange coefficients (K_D's) based on experimentally determined values are used to calculate the compositions of phases in equilibrium with a starting liquid, i.e., parental magma. Compositions of phases to be removed by fractional crystallization are recalculated, or updated, for each successive residual liquid. This is considered to be a more realistic

approach in modelling the liquid line of descent. Compositionally zoned phenocrysts are straightforward evidence for fractional crystallization and indicate that for a given temperature and melt, diffusional reequilibration was ineffectual compared to crystal growth rates. Physically, the modelling approach can be envisioned as the immediate separation of crystallizing phenocrysts from remaining melt, or the production of compositionally zoned phenocrysts which are eventually removed.

Smaller steps (2% intervals) than those listed in Table 6 were used in the calculations to map out possible compositional paths. Infinitely small increments could be used, but beyond a point, the magnitude of the increments used makes little difference in the overall arguments.

Trace element partition coefficients are affected by bulk melt composition and phase compositions, and a rigorous approach would be to recalculate the partition coefficient for a given mineral phase and parental liquid at each increment in the modelled compositional evolution. Lacking adequate data for most trace element partitioning as a function of bulk compositions, this approach was taken only in calculating Ni abundances during fractional crystallization after Hart and Davis (1978). Mineral/melt partition coefficients for most incompatible and moderately incompatible trace elements increase with increasingly silicic melt compositions (Nagasawa and Schnetzler, 1971; Schnetzler and Philpotts, 1970; Drake and Weill,1976; Irving and Frey, 1984).

The low set of values (Table 8) is designed to be appropriate for basaltic compositions and the values were chosen or estimated from various empirical and experimental studies. Values for REE, Hf, and Zr

in plagioclase, olivine, clinopyroxene, orthopyroxene, magnetite and ilmenite were chosen based on a recent empirical study by Fujimaki et al. (1984). Results of this study are in agreement with those of earlier experimental studies (Drake and Weill, 1976; Grutzeck et al., 1984) and compilations of experimental results (Irving, 1978). Values for Rb, Sr, and Ba in various minerals were estimated from work of McKay and Weill (1976, 1977), Drake and Weill (1976), Sun et al. (1974); Lindstrom and Weill (1978), and were assumed to be negligible in oxide phases. Sources for Sc partition coefficients included Leeman (1976), Leeman et al. (1978), McKay and Weill (1977), and Lindstrom and Weill (1978), and Sc values for plagioclase were assumed to be negligible. Values for Nb in oxide phases werer estimated from McCallum and Charette (1978) and were assumed to be negligible in other phases. Thorium was assumed to be incompatible in all phases ($D^{Th} = 0.01$).

Higher values of REE, Hf, Zr, Sc, Nb, Rb, Sr, and Ba partition coefficients (Table 8) were taken from the same references as above, and Th values were again assumed to be $D^{Th} = 0.01$. Apatite REE and Sr partition coefficients are experimental (P = 7.5 kb) values for an andesitic composition (Watson and Green, 1981). A value for D_{apat}^{Th} was taken from Benjamin et al. (1980). Values of Sc, Hf, Nb, and Zr partition coefficients in apatite were estimated (cf. Baitis and Lindstrom, 1980).

Partition coefficients for Ni in olivine used in modelling were varied with composition (Hart and Davis, 1978). Values of partition coefficients for Ni and Cr in other mineral phases (Table 8) were estimated from a survey of various references including Leeman et al. (1978), Leeman and Lindstrom (1978), Lindstrom and Weill (1978), and the compilation by Irving (1978).

Extreme values (low and high) of mineral melt partition coefficients were assumed constant in the calculations. Use of both extreme values in some calculations results in a range of abundances possible for each residual liquid. This range includes values resulting from use of mineral/melt partition coefficients varying as a function of bulk composition, and at least serves to test specific parental liquid-residual liquid fractional crystallization models. The choice of specific phases in the crystallizing assemblage was based on the assumption that crystallization occurred at moderate to low pressures, and that the types of phenocrysts (though not necessarily their compositions) may be representative of the crystallizing phases at any given stage.

Proportions of fractionating phases in all calculated fractional crystallization models were estimated on the basis of which proportions subtracted yielded an approximation of the desired major-element composition of a residual liquid. Proportions chosen are not always equivalent to expected equilibrium phase proportions based on 1-atm experimental studies (Walker et al., 1979; Grove et al., 1982). This is because the effective separation of phenocrysts may be largely controlled by their respective density contrasts with the host liquid, e.g., if gravitational settling is the means of crystal-liquid separation, olivine phenocrysts may settle out, while plagioclase phenocrysts may be buoyant.

6. Petrogenesis of basalts to basaltic andesites

The general approach taken in deducing the origin of basaltic andesites was to first test models of closed-system fractional

crystallization of basaltic magma. It was recognized early on that approximate degrees of fractional crystallization of basaltic magma that would result in residual liquids similar in major-element composition to the basaltic andesites were inadequate to explain the abundances of incompatible trace elements in the latter. Therefore, only approximate matches between major-element compositions in calculated residual liquids and basaltic andesites were attempted. Open system fractional crystallization, or AFC models, involving crustal wallrock contamination accompanying fractional crystallization, can potentially produce an improved match in major-element compositions, trace element abundances and isotopic compositions between modelled residual liquids and basaltic andesites. However, since compositions of wallrock contaminants at depth are unknown, approximate matches between calculated liquids and basaltic andesites suffice only to demonstrate the possibility of AFC models. Magma mixing models were the next type of model attempted to explain the geochemical characteristics of the basalitc andesites. Mixing endmembers were selected from the data set, and if an approximate match was achieved between calculated mixtures and analyzed basaltic andesites, this was considered a demonstration of the possibility of magma mixing as a process that generated basaltic andesites.

6 .1 Basalt to basaltic andesite: 13826h to 138212

Olivine (40%) and plagioclase (60% of crystallizing assemblage) fractionation in a basalt such as sample 13826h results in residual liquid major-element compositions grossly similar to that of the low-SiO_2 basaltic andesite 138212 after approximately 10% fractional crystallization (Table 7a, Figure 14a), although TiO_2, P_2O_5, and K_2O

contents and FeO*/MgO ratios in the model residual liquid are lower than observed.

As plotted on the olivine-cpx-SiO_2 pseudoternary, Puyehue basalts do not fall near the 1-atm anhydrous olivine-augite-plagioclase cotectic (Fig. 12a). Fractional crystallization of clinopyroxene in addition to olivine and plagioclase may occur at moderate pressures (to 5 kb) if the oliv-aug-plag cotectic is shifted towards olivine as suggested by Grove and Baker (1984) based on earlier experimental works (Kushiro, 1973; Takahashi and Kushiro, 1983). The above model which involves fractional crystallization of only olivine and plagioclase is more consistent with the observed phenocryst assemblages in the basalts (Table 2) than a fractional crystallization model which includes clinopyroxene. However, clinopyroxene fractional crystallization is justified on the basis of geochemical data as discussed earlier. Approximately 30% fractional crystallization of an assemblage consisting of 14% olivine, 23% augite, 60% plagioclase, and 3% magnetite from basalt 13826h approximately reproduces the major-element composition of 138212 except that P_2O_5 and TiO_2 contents are still too low and FeO contents high in the calculated residual liquids (Table 7b). The misfit involving FeO and TiO_2 may be partly remedied by using a magnetite composition which is lower in TiO_2, although the composition used in the model is that of a phenocryst in basalt 272824b (Table 3a) and this approach seemed reasonable.

TiO_2 contents would increase more and FeO contents might be more effectively buffered by using smaller increments of fractional crystallization in the model calculations. This is because the compositions of all phases subtracted in each interval (2% used) are in equilibrium with the initial liquid and not a liquid intermediate in

14 Calculated major-element contents and trace element abundances normalized to observed values, for various models relating basalt 13826 to basaltic andesite 138212 by (a) fractional crystallization of olivine and plagioclase (Table 7a), (b) fractional crystallization of olivine, clinopyroxene, and plagioclase (Table 7b), (c) and AFC models (Table 7c), upper solid curve is for oliv+cpx+plag assemblage with r = 0.03, lower dashed curve corresponds to an oliv+plag assemblage with r = 0.18, and (d) mixing of basalitc (13826h) and andesitic (220283-5) magmas (Table 7d), as a means of comparing the results of each model.

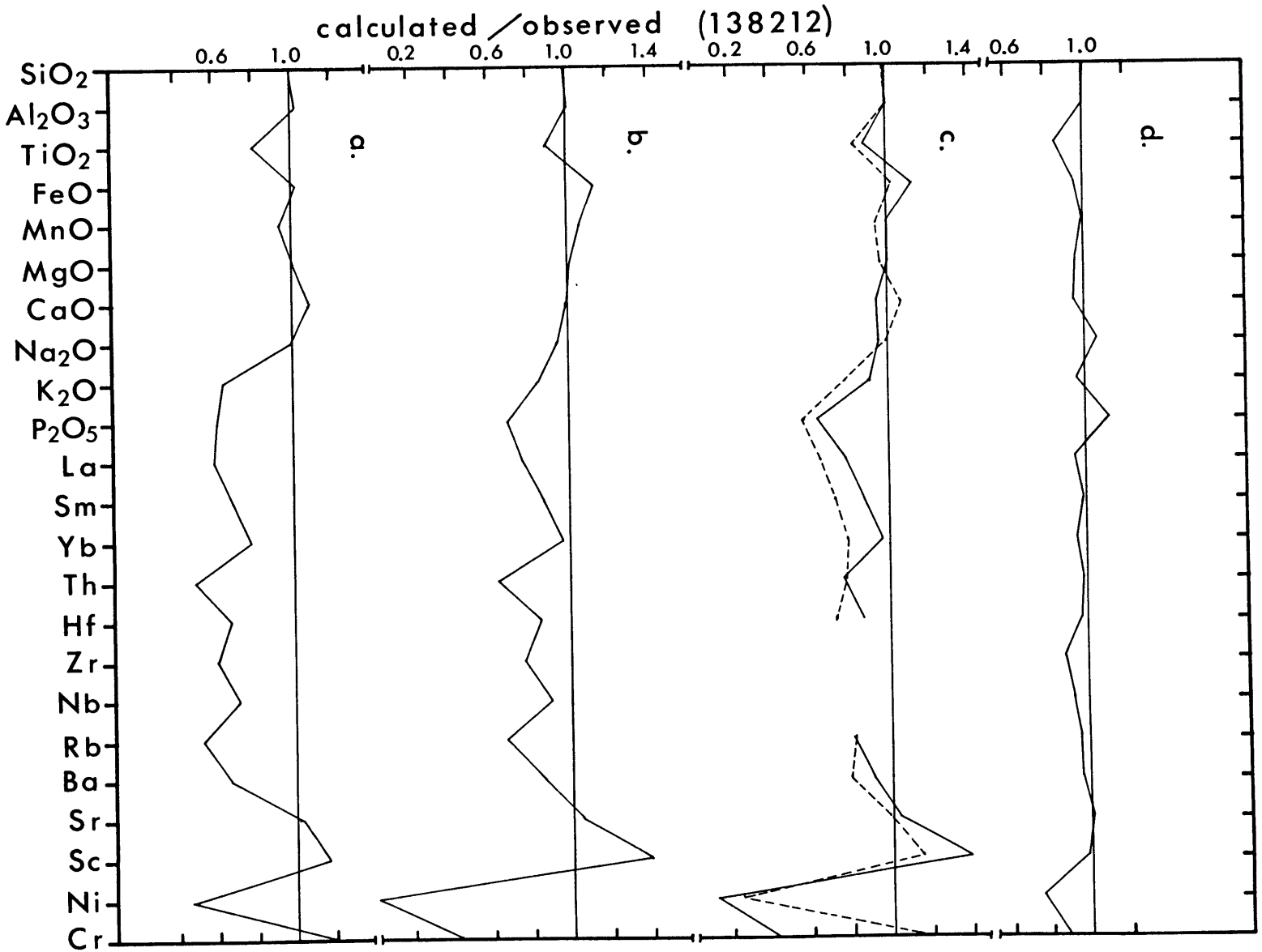
calculated / observed (138212)
0.6
1.0
0.2
0.6
1.0
1.4
0.2
0.6
1.0
1.4
0.6
1.0
SiO2
Al2O3
TiO2
FeO
MnO
MgO
CaO
Na2O
K2O
P2O5
La
Sm
Yb
Th
Hf
Zr
Nb
Rb
Ba
Sr
Sc
Ni
Cr
a.
b.
c.
d.

composition between parental and residual liquids for the interval. This results in the subtraction of phases more magnesian or more calcic than may be required, and a slight underestimation of the degree of fractional crystallization when compared to results based on use of smaller increments. This would not make any substantial changes to the major arguments of this section. Calculated compositions of ferromagnesian phases in fractional crystallization models are similar to the composition of groundmass phases or phenocryst rims analyzed in the basalts and this suggests that this approach in fractional crystallization modelling is reasonable.

In the fractionation scheme involving augite, a lower plagioclase K_D of 0.75 was used, as compared with the first model which employed a value of 1.7 for K_D^{plag} (Table 7a). This was necessary to prevent a rapid decline of CaO contents to effect a better CaO match while crystallizing a relatively large amount of plagioclase (60% of the assemblage). The latter is suggested by decreasing Al_2O_3 and Sr contents, and approximately constant, or even buffered CaO/Al_2O_3 ratios from 13826h to 138212. Even so, CaO/Al_2O_3 ratios in calculated liquids are slightly lower than that observed in 138212 (Table 7b). Thus, the main justification for a low plagioclase K_D of 0.75 is that a better match is achieved between model calculations and observed values. Application of plagioclase K_D's of 1.7 and 0.75 in the two modelling schemes results in relatively more calcic or more sodic (Table 7a, 7b) equilibrium plagioclase compositions, respectively. Calculated plagioclase compositions using K_D^{plag} of 0.75 are more sodic than observed groundmass plagioclase compositions in basalts but are similar to those observed in basaltic andesite 138212 (cf., Table 7b, Fig. 3a). A smaller proportion

of clinopyroxene would allow use of a higher K_D^{plag} and reduce the gap between calculated and observed plagioclase compositions, but this in turn would increase the disagreement in trace element abundances and abundance ratios, which are affected by clinopyroxene fractionation, between calculated residual liquids and basaltic andesites. Johannes (1978) demonstrated that increasing P_{H_2O} expands the plagioclase binary solvus, resulting in increasing values of K_D^{plag}. The two fractional crystallization schemes for basalt 13826h to basaltic andesite 138212 imply different physical conditions, i.e., olivine + plagioclase ($K_D^{plag} \cong 1.7$) occurring at very low pressures (< 2 kb) and relatively more hydrous conditions, and olivine + augite + plagioclase ± magnetite ($K_D^{plag} \cong 0.75$) occurring at relatively higher pressures (> 5 kb) and more anhydrous conditions.

The approximate fits with regard to major-element compositions in the above fractional crystallization calculations yield estimates of the degree (%) of crystallization which may then be used in further tests with trace element abundances. For the two basic modelling schemes, distinguished by the absence or presence of augite, the degree of fractional crystallization is estimated at approximately 10% and 30% respectively. For incompatible trace element abundances adjusted (raised) for phenocryst dilution, 10-30% fractional crystallization falls short of producing the trace element abundances observed in basaltic andesites such as sample 138212, as shown in Tables 7a and 7b and Figure 14a and 14b even using the lower values of partition coefficients (Table 8). This is also true for K_2O, TiO_2, and P_2O_5 contents (Figures 14a and 14b) even though K_2O is unrealistically treated as totally incompatible by its arbitrary omission from the composition of

calculated equilibrium plagioclase compositions. Although preliminary studies have been made concerning partitioning of Mn (e.g., Leeman and Scheidegger, 1977), MnO was also treated as incompatible in fractional crystallization models. Certain abundance ratios of trace element pairs differing only slightly in their respective estimated incompatibilities (La/Sm, Ba/Rb, Zr/Sm, etc.) vary much more in analyzed samples of basaltic andesite than predicted in the calculated crystallization models (Tables 7a and 7b). For example, basalts such as 13826h which are less LREE-enriched are characerized by Ba/Rb ratios of 18 to 19 and Zr/Sm ratios of 21 to 23, while basaltic andesites such as 138212 display lower Ba/Rb (13 to 15) and higher Zr/Sm (24 to 26) ratios. Use of higher mineral/melt partition coefficients as listed in Table 8 will serve to decrease Ba/Rb and increase La/Sm ratios with fractional crystallization (Tables 7a and 7b), but use of these larger partition coefficients in turn only further aggravates the problem of achieving the trace element abundances observed in the basaltic andesites since high D values suppress their enrichment in the residual liquids. Based on many empirical and experimental studies, such high D values are probably unrealistic for basalts and basaltic andesites.

The disparity between estimated degrees of fractional crystallization based on major-element modelling and those based on trace element abundances may be alleviated by contamination by, or assimilation by the magma of wallrock during fractional crystallization (AFC). The bulk composition of wallrock contaminant in such a model must be specified, if taking a direct approach, and to this end, it is probably reasonable to use an analyzed sample of country rock from the immediate area. This consists of a virtually intact xenolith of granite from a

1979 eruption of Mirador in the Carran-Los Venados Volcanic Group just north of Puyehue Volcano. The granite is characterized by high Rb and Ba abundances, and rather fractionated REE abundances with La/Yb = 17.2 (Frey, unpubl. data). Using low values of partition coefficients, a crystallizing assemblage closely similar to that used in a closed-system models (Tables 7a and 7b), and varioius ratios of assimilated wallrock/amount crystallized (r), calculated major-element compositions, trace element abundances (aside from Sc and Sr), and trace element abundance ratios begin to approach those of basaltic andesite 138212 for approximately 11-34% crystallization (Table 7c, Fig. 14c). AFC models which include fractional crystallization of only olivine and plagioclase approximately reproduce the major-element composition of 138212 after only 11% fractional crystallization (Table 7c). In these models, abundances of incompatible trace elements (La, Sm, Yb, Th, Hf, Rb, and Ba) are below observed abundances (Table 7c, Fig. 14c), even with relatively higher r values (0.10, 0.18). An AFC model which includes fractional crystallization of olivine, clinopyroxene, plagioclase, and magnetite results in trace element abundances in a residual liquid which are more similar to observed abundances after 34% fractional crystallization with an r value of 0.03 (Table 7c). A major difference between the AFC models presented in Table 7c is that different values of K_{plag}^{Na-Ca} are required for different fractionating assemblages in order to match CaO contents in modelled residual liquids vs. that of 138212. In all models, contents of P_2O_5 and TiO_2 in calculated residual liquids are too low, and FeO contents are higher than observed values (Fig. 14c, Table 7c). For the given granite wallrock composition, a larger value of r in model calculations may lead to improved matches between modelled

liquids and basaltic andesites on the basis of certain trace element abundances (La, Sm, Yb, Hf, Th, Rb, Sr, and Ba). However, the disparity in TiO_2, P_2O_5, MgO, and CaO contents, CaO/Al_2O_3 ratios, and Ni and Cr abundances between modelled liquids and basaltic andesite 138212 is increased (Table 7c). As in the closed-system fractional crystallization models, a higher proportion of Ti-magnetite in the fractionating assemblage will reduce FeO contents in residual liquids and reverse the subdued iron-enrichment as shown (Tables 7a to 7c), but will result in a lessened increase in TiO_2 contents in residual liquids, or may possibly result in decreasing TiO_2 contents with fractional crystallization. Higher values of K_D^{Fe-Mg} for olivine and clinopyroxene would result in more Fe-rich calculated compositions which on removal may produce a better FeO match between calculated and observed FeO contents in residual liquids.

The calculated AFC model is inconsistent with $^{87}Sr/^{86}Sr$ ratios in the presumed parental (13826h) and residual (138212) liquids. The composition of wallrock contaminant is the least constrained parameter in the AFC model calculations. Less silicic volcanic or plutonic contaminants with higher Sr abundances would require higher, though possibly not unreasonable, r values. Less evolved wallrock compositions with higher Sr abundances, and in terms of a basalt to basaltic andesite AFC model, would be characterized by lower required $^{87}Sr/^{86}Sr$ ratios. High $^{87}Sr/^{86}Sr$ ratios for wallrocks at depths corresponding to a moderate pressure regime (~ 5 Kb) consistent with the fractionating mineral assemblages are not unlikely since basement rocks of Paleozoic and Mesozoic age are exposed east of Puyehue Volcano. In any case, the Nd isotopic compositions of basalt 13826h ($^{143}Nd/^{144}Nd$ = 0.512879±26) and

basaltic andesite 138212 (0.512876±17) are identical, requiring that wallrock contaminants, regardless of Nd abundances, be characterized by identical Nd-isotopic ratios and relatively higher Sr-isotopic ratios, and would then lie well to the right of the mantle array on a plot of $^{143}Nd/^{144}Nd$ vs. $^{87}Sr/^{86}Sr$. A likely contaminant endmember with these characteristics may consist of altered volcanic rocks or metasediments of oceanic affinity which have been subjected to seawater alteration. The probability of this special condition cannot be evaluated further without a better knowledge of the geochemical characteristics of basement rocks in the area.

Although AFC models are a slight improvement over closed-system fractional crystallization models, several inconsistencies remain unsolved, as outlined above. Simple bulk mixing of basaltic magma with evolved magmas may provide the best explanation of the geochemical characteristics of basaltic andesites such as 138212, and the best agreement for all data, including major-element compositions, trace element abundances, trace element abundance ratios, and isotopic compositions. Magma mixing is also a likely process that may occur in crustal-level magma chambers, in addition to fractional crystallization and AFC processes.

The characteristics of basaltic andesite 138212 are best explained by mixing of approximately 67% basalt (sample 13826h) with relatively low La/Sm (2.37), high Ba/Th (165), high Ba/Rb (19), and moderate $^{87}Sr/^{86}Sr$ (.70398) with 33% andesite such as sample 220283-5 (Table 7d, Figures 14d). The andesite has sufficiently high trace element abundances and TiO_2 (1.47 wt.%) and P_2O_5 (0.63 wt.%) contents, and appropriately low abundance ratios (e.g., Ba/Rb = 12.7, Ba/Th = 98, La/Sm

= 2.84) to serve as a likely mixing endmember. Abundances of Ni and Cr are low in the calculated mixture (Table 7d), but may be due to inaccuracies in corrections for phenocryst dilution in the basalt. Sr isotopic compositions of mixtures are also slightly lower than observed values but are within analytical error. Abundances of La, Zr, Nb, Rb, Ni, and Cr, and La/Sm ratios in the calculated mixture containing 33% of the andesite endmember are lower than observed values. The TiO_2 contents in a calculated mixture (1.14 wt.%) are also low relative to observed values but the mismatch would be reduced if another sample of andesite (sample 43821) was assumed as an endmember. Sample 43821 is slightly higher in TiO_2 (1.57 wt.%) and was collected from the same late-stage PIV cinder cone (Fig. 2) as sample 220283-5. It is also possible that andesitic magmas with still higher TiO_2 contents were available as mixing endmembers, since some preglacial andesites contain up to 2.56 wt.% TiO_2. A more appropriate basaltic endmember would be characterized by higher TiO_2 contents and higher abundances of La, Zr, Ni, and Cr, but it is not represented in the data set. There is no reason to exclude the possibility of mixing of different basaltic magmas with one another, in addition to their mixing with more evolved magmas, resulting in a spectrum of basalts with similar major-element compositions characterized by variable trace element abundances and abundance ratios.

6.2 Basaltic andesite 272826b

The major-element composition of the relatively LREE-enriched basaltic andesite 272826b contrasts with that of less LREE-enriched basaltic andesites such as 138212, and this difference leads to corresponding differences in fractional crystallization modelling.

Compared to 138212, basaltic andesite 272826b is lower in FeO, P_2O_5, TiO_2, and Na_2O, and higher in Al_2O_3, CaO, SiO_2, and MgO. Also relative to 138212, 272826b contains lower abundances of REE, Sc, Co, V, and Sr, and higher abundances of Ni, Cr, and Th. Fractional crystallization of only clinopyroxene from basalt may explain higher Al_2O_3 and lower MgO, FeO, and CaO contents in 272826b. However, FeO and TiO_2 contents are too high and K_2O and MgO contents too low in a modelled residual liquids (Table 7e).

Fractional crystallization of only clinopyroxene will result in increasing Al_2O_3 and decreasing CaO contents in residual liquids. Phenocryst-corrected compositions of relatively LREE-enriched basalts such as samples 13828 and 220283-1 are low in Al_2O_3 relative to basaltic andesite 272826b (Table 7e) and fractional crystallization of clinopyroxene (13% and 3% respectively) reproduces SiO_2, Al_2O_3, and CaO contents observed in 272826b, but FeO and TiO_2 contents in calculated residual liquids are high relative to those in 272826b (Table 7e, Figure 15a). Abundances of incompatible trace elements in a residual liquid produced by fractional crystallization of basalt 13828 are lower than those observed in basaltic andesite 272826b (Fig. 15a). A small amount of clinopyroxene fractionation from basalt 220283-1, which contains higher abundances of most incompatible trace elements than basalt 13828, fails to increase Th, Rb, and Zr abundances to those observed in 272826b (Fig. 15b). In both models, Sr and Sc abundances are too high in calculated residual liquids, and in addition, P_2O_5 contents are too high assuming basalt 220283-1 as a parental magma, and Cr contents are too high in calculated residual liquids assuming basalt 13828 as a parental magma. Most of the relatively more LREE-enriched

15 Calculated major-element contents and trace element abundances normalized to observed values, for various models of the derivations of basaltic andesite 272826b. These include clinopyroxene fractionation from (a) basalt 13828 and (b) basalt 220283-1, and fractional crystallization of olivine, clinopyroxene, plagioclase, and magnetite (c) from basalt 13828; all are presented in Table 7e. Results of an AFC model (Table 7f) are shown in (d), and those of magma mixing models (Table 7g) are shown in (e) and (f).

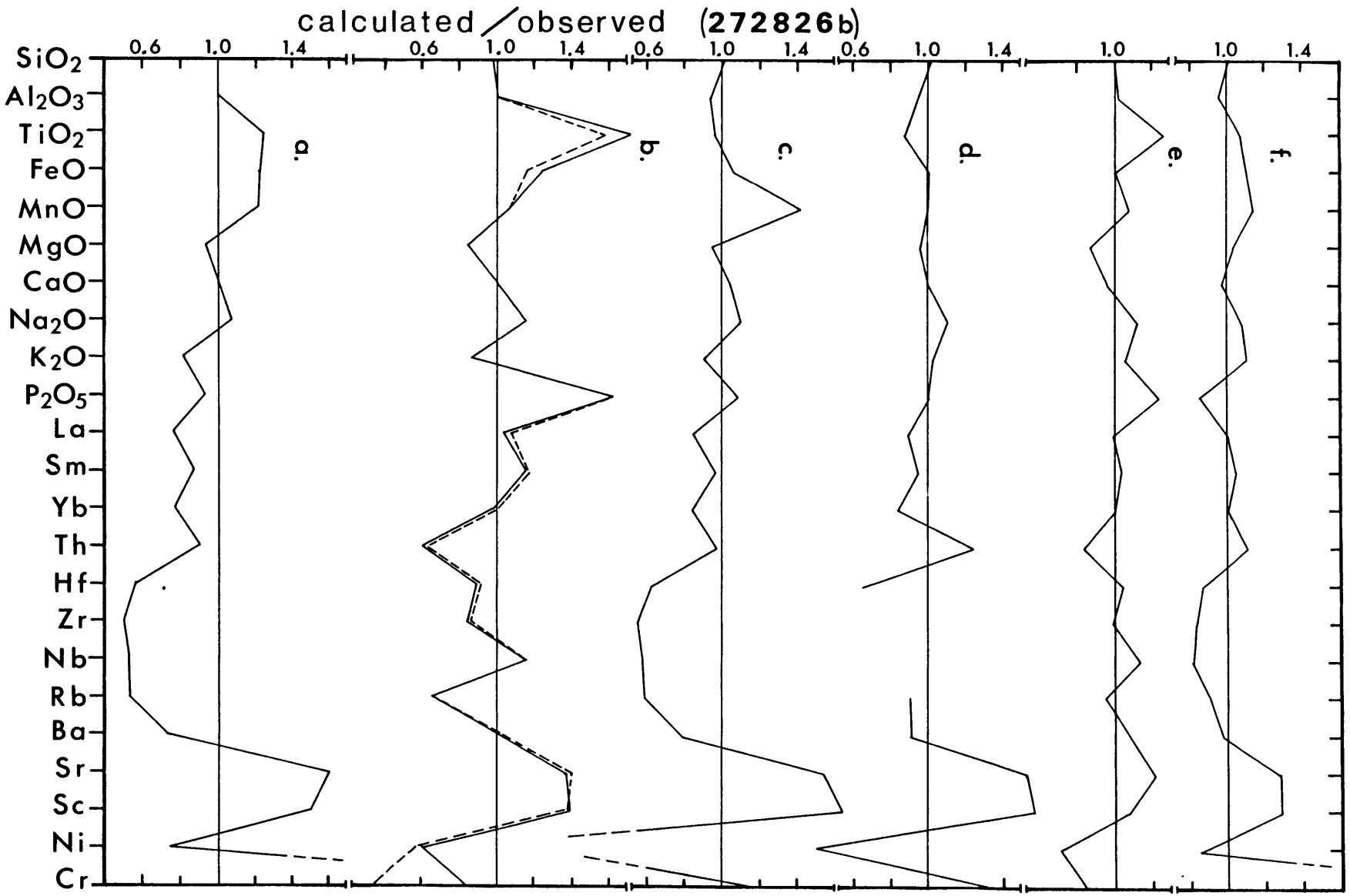
calculated / observed (272826b)
0.6
1.0
1.4
SiO2
Al2O3
TiO2
FeO
MnO
MgO
CaO
Na2O
K2O
P2O5
La
Sm
Yb
Th
Hf
Zr
Nb
Rb
Ba
Sr
Sc
Ni
Cr
a
b
c
d
e
f

basalts such as 220283-1 are higher in TiO_2, P_2O_5, and Na_2O relative to basaltic andesite 272826b, and fractional crystallization of any reasonable mineral assemblages will only result in still higher Na_2O and P_2O_5 contents. Thus, basalts such as 13828 are more likely representative of parental magmas. Clinopyroxene fractionation would occur at pressures > 12 Kb (Perfit and Gust, 1981). Since pyroxene phenocrysts are generally not observed in the basalts, but instead only olivine and plagioclase, such a model for derivation of basaltic andesite 272826b is probably not reasonable.

Approximately 20% fractional crystallization of a polyphase assemblage (20% olivine, 30% clinopyroxene, 40% plagioclase, 10% magnetite) from basalt 13828 results in a calculated residual liquid major-element composition similar to that of 272826b (Table 7e, Figure 15c). Aside from Sm and Th, however, abundances of other incompatible trace elements and Ni as calculated are too low, and calculated Sr and Sc abundances are too high, relative to observed values (Fig. 15c). Trace element abundance ratios (e.g., La/Sm, Zr/Sm) which are low or high (e.g., Ba/Rb) in basaltic mixing endmembers do not approach those observed in basaltic andesite 272826b for closed system fractional crystallization models (Table 7e). Fractional crystallization of magnetite reduces FeO and TiO_2 in calculated residual liquids and may be a significant fractionating phase due to its presence (up to 3.5%) in some basalts (Table 2).

In the above fractional crystallization model, one major drawback is that the assumed parental magma is not isotopically similar to basaltic andesite 272826b. If this presumed parental magma is correct, modification of the isotopic compositions of residual liquids must have

occurred. The most likely means would be assimilation of country rock or wall rock with higher $^{87}Sr/^{86}Sr$ and lower $^{143}Nd/^{144}Nd$ during fractional crystallization (AFC). If such wall rocks are granitic in composition, abundances of incompatible trace elements will be increased more effectively than in a situation of closed-system fractional crystallization. Modelling calculations for an AFC process were carried out as before in section 5.2.1 and as shown in Table 7c, assuming basalt 13828 as a parental magma and the Mirador granite xenolith as representative of a wall rock contaminant. Phase proportions of olivine, clinopyroxene, plagioclase and magnetite used were similar to those in the polyphase closed-system fractional crystallization model (cf. Tables 7e and 7f). Three values of the mass ratio (r) of granite assimilated to amount crystallized ranging from 0.05 to 0.15 were used. The major-element compositions of calculated residual liquids in each case are approximately similar to that of basaltic andesite 272826b (Table 7f, Fig. 15d). For the highest value of r (0.15) in this model, abundances of La, Yb, Hf, Rb, Ba, and Ni are too low, and those of Th, Sr, Sc, and Cr are too high, relative to those in 272826b (Fig. 15d).

The $^{87}Sr/^{86}Sr$ ratios of residual liquids were calculated after the method of DePaolo (1981) and are low relative to that of 272826b (0.70400). This is related to the low D_{plag}^{Sr} (1.5) used and the proportion of plagioclase used in the modelling calculations. This results in a bulk $D^{Sr} < 1.0$, increasing abundances of Sr in residual liquids, and little change in the $^{87}Sr/^{86}Sr$ ratio of residual liquids. A subordinate proportion of plagioclase in the fractionating assemblage is required in the model to increase Al_2O_3 contents in residual liquids. However, in the model, Sr abundances must decrease from approximately

500 ppm to 350 ppm as observed in basaltic andesite 272826b. In the model of polyphase closed-system fractional crystallization D_{plag}^{Sr} would have to be 6.5, and in the AFC models, higher values of 10 to 11 for D_{plag}^{Sr} are required (cf. eqn. 15b, DePaolo, 1981) assuming basalt 13828 as a parental magma and the Mirador granite as a wall rock composition. Such high values of D_{plag}^{Sr} are not appropriate for fractional crystallization of basalts (cf. Drake and Weill, 1976). The mismatch of calculated vs. observed isotopic compositions in the AFC model could be improved by using a $D_{plag}^{Sr} > 1.5$, and assuming an older, more radiogenic wall rock contaminant with higher Sr abundances. Low $^{87}Sr/^{86}Sr$ and high Sr, Sc, and Cr abundances in basalt 13828 produce misfits in the AFC model (Table 7f, Fig. 15d). Basalts such as 13826h are characterized by only slightly lower $^{87}Sr/^{86}Sr$ (0.70397-0.70398) relative to basaltic andesite 272826b, but these basalts are higher in Al_2O_3 and are relatively less LREE-enriched such that no reasonable, i.e., plagioclase-dominated fractional crystallization or AFC model could give rise to 272826b. AFC models employing other, relatively LREE-enriched basalts are generally not suitable on the basis of other criteria as discussed earlier and would require a wall rock contaminant with relatively lower $^{87}Sr/^{86}Sr$ and/or higher $^{143}Nd/^{144}Nd$, since most of these basalts have higher $^{87}Sr/^{86}Sr$ and/or lower $^{143}Nd/^{144}Nd$ relative to basaltic andesite 272826b.

Fractional crystallization and AFC models illustrate the difficulty in producing the Sr, Cr, Ni, Th, Zr, Hf, and Sc abundances observed in basaltic andesite 272826b, despite success in deriving its major-element composition. The characteristics of this basaltic andesite may be explained if the composition of this lava was the result of magma mixing.

A mixing model for basaltic andesite 272826b must chiefly explain the higher Al_2O_3, CaO, Ni, and Cr contents and higher La/Sm (3.2), Zr/Sm (33.8), and Rb/Sr ratios observed in this sample relative to basaltic andesite 138212. This distinct composition is best explained as a mixture of approximately 85-87% basalt and 13-15% rhyolite (Table 7g, Figure 15e). A basalt such as sample 230283-5 with an intermediate Sr-isotopic composition ($^{87}Sr/^{86}$ = 0.70399) and slightly higher trace element abundances relative to basalt 13828 may serve as a reasonable basaltic mixing endmember.

A calculated mixture of basalt 230283-5 with a silicic magma represented by rhyolite 202825c is isotopically similar, but high in TiO_2, Na_2O, and P_2O_5 contents and Sr abundances, and low in MgO contents and abundances of Th and Ni relative to 272826b (Table 7g, Fig. 15e). A calculated mixture of basalt 13828 and the rhyolite is a reasonable approximation of the major-element composition of 272826b, however abundances of Sr, Sc, and Cr are high and abundances of Zr, Hf, and Nb and the calculated $^{87}Sr/^{86}Sr$ ratio are low relative to 272826b. Given the geochemical variability of the basalts, however, a more appropriate basaltic magma endmember may exist but is not represented in the data set, and a magma mixing process for the petrogenesis of basaltic andesite 272826b remains a possibility.

In summary, the composition and geochemical characteristics of basaltic andesite 272826b are not adequately explained by closed-system fractional crystallization of basaltic magmas as represented by basalts in the data set. Mixing of basaltic and rhyolitic magmas may potentially explain the characteristics of 272826b. Combined assimilation and fractional crystallization is also a likelihood due to the lack of

Table 7a
Fractional crystallization model: basalt to andesite

	F (fraction of residual liquid)							
	13826h	.90	.81	.60	.51	.42	138212	220283-5
[1]SiO_2	51.67	52.35	53.00	55.26	56.69	58.78	53.06	58.96
Al_2O_3	17.23	16.96	16.81	16.43	16.12	15.70	16.56	15.62
TiO_2	0.97	1.07	1.19	1.43	1.43	1.43	1.32	1.47
FeO	9.86	10.01	10.13	10.02	9.69	9.10	9.78	8.45
MnO	0.16	0.14	0.15	0.18	0.19	0.20	0.18	0.22
MgO	6.65	5.62	4.69	2.94	2.73	2.41	6.61	2.84
CaO	9.90	9.96	9.86	8.72	7.73	6.32	9.12	6.09
Na_2O	3.06	3.21	3.38	3.94	4.21	4.56	3.24	4.23
K_2O	0.50	0.55	0.61	0.83	0.97	1.19	0.85	1.48
P_2O_5	0.13	0.16	0.19	0.25	0.29	0.36	0.26	0.63
[2]La	6.92	7.68	8.54	11.4	13.4	16.2	12.9	22.5
Sm	2.92	3.23	3.58	4.72	5.47	6.52	4.66	7.93
Yb	1.93	2.14	2.37	3.12	3.61	4.30	2.79	4.07
Hf	1.73	1.92	2.13	2.83	3.31	3.99	2.88	4.87
Sc	37	41	45	57	64	74	35	28
Zr	67	74	83	111	130	157	123	192
Th	1.00	1.11	1.23	1.66	1.95	2.36	2.24	4.56
Nb	2.4	2.7	3.0	4.0	4.6	5.6	3.8	5.6
Rb	8.7	9.7	10.7	14.45	17.0	20.6	18.3	35.1
Sr	410	414	421	441	449	460	397	378
Ba	165	183	203	271	317	383	271	446
Ni	53	25	14	3	2	<1	52	8
Cr	133	130	125	33	5	<1	108	19
CaO/Al_2O_3	0.575	0.587	0.587	0.531	0.480	0.403	0.551	0.390
[2]La/Sm	2.37	2.38	2.38	2.41	2.45	2.48	2.77	2.84 12.7
Ba/Rb	19.0	18.9	18.9	18.8	18.6	18.6	14.8	98
Ba/Th	165	164	164	163	163	162	121	24.2
Zr/Sm	22.9	22.9	23.2	23.5	23.7	24.1	26.4	
[3]La/Sm		2.35	2.40	2.71	2.97	3.32		
Ba/Rb		18.2	17.6	15.8	14.9	13.8		
Ba/Th		158	152	135	126	116		
Zr/Sm		22.9	23.7	27.5	30.5	34.5		
proportions:								
oliv:		40%	40%	15%	-	-		
cpx:		-	-	25%	35%	35%		
plag:		60%	60%	55%	55%	55%		
mag:		-	-	5%	10%	10%		
[4]compositions:								
oliv(Fo%)		78	73	63	-	-		
cpx (En%)		43	40	35	34	33		
plag(An%)		75	73	67	62	55		

[1]major-element composition and trace element abundances adjusted for phenocryst content, total iron as FeO, and analysis normalized to 100%.
[2]trace element abundances and abundance ratios calculated using set of low values of partition coefficients (see Table 8).
[3]calculated using high values of partition coefficients (Table 8).
[4]K_{plag}^{Na-Ca} of 1.7, K_{oliv}^{Fe-Mg} of 0.32, and K_{aug}^{Fe-Mg} of 0.26 were assumed. Values of K_D^{Mn} of 1.0 were assumed for olivine and cpx, and 3 for magnetite.

Table 7b

Fractional crystallization model: basalt to basaltic andesite 138212

	F (fraction of residual liquid)						
	13826h	.90	.81	.74	.70	.66	138212
[1]SiO_2	51.67	51.81	52.02	52.26	52.39	52.52	53.06
Al_2O_3	17.23	17.06	16.88	16.71	16.63	16.53	16.56
TiO_2	0.97	1.02	1.08	1.15	1.18	1.22	1.32
FeO	9.86	10.18	10.50	10.85	11.01	11.16	9.78
MnO	0.16	0.17	0.18	0.19	0.19	0.20	0.18
MgO	6.65	6.36	6.08	5.78	5.63	5.48	5.61
CaO	9.90	9.65	9.39	9.13	8.98	8.84	9.12
Na_2O	3.06	3.07	3.08	3.08	3.08	3.08	3.24
K_2O	0.50	0.55	0.61	0.68	0.72	0.75	0.85
P_2O_5	0.13	0.15	0.16	0.17	0.18	0.19	0.26
[2]La	6.92	7.67	8.51	9.30	9.82	10.40	12.9
Sm	2.92	3.22	3.55	3.86	4.06	4.29	4.66
Yb	1.93	2.13	2.35	2.55	2.68	2.83	2.79
Hf	1.73	1.91	2.12	2.31	2.44	2.58	2.88
Sc	37	40	44	47	49	52	35
Zr	67	74	82	90	95	101	123
Th	1.00	1.11	1.23	1.35	1.42	1.51	2.24
Nb	2.4	2.7	2.9	3.2	3.4	3.6	3.8
Rb	8.7	9.7	10.7	11.7	12.4	13.1	18.3
Sr	410	413	415	418	419	420	397
Ba	165	183	202	221	233	246	271
Ni	53	25	14	8	6	4	52
Cr	133	97	74	54	49	40	108
CaO/Al_2O_3	0.575	0.566	0.556	0.546	0.540	0.535	0.551
[2]La/Sm	2.37	2.38	2.40	2.41	2.42	2.42	2.77
Ba/Rb	19.0	18.9	18.9	18.9	18.8	18.8	14.8
Ba/Th	165	165	164	164	164	163	121
Zr/Sm	22.9	23.0	23.1	23.3	23.4	23.5	26.4
	oliv: cpx: plag: mag = .14/.23/.60/.03						
[3]olivine(Fo%)		78	76	75	74	73	
cpx(En%)		43	42	41	41	41	
plag(An%)		57	56	55	55	55	

[1]major-element composition and trace element abundances adjusted for phenocryst content, total iron as FeO, and analysis normalized to 100%.

[2]calculated using low values of partition coefficients (Table 8).

[3]K_{plag}^{Na-Ca} of 0.75, K_{oliv}^{Fe-Mg} of 0.32, and K_{aug}^{Fe-Mg} of 0.26 were assumed. Values of K_D^{Mn} of 1.0 were assumed for olivine and cpx, and 3 for magnetite.

Table 7c

Assimilation-fractional crystallization models:
basalt to basaltic andesite 138212

	F (fraction of residual liquid)					
	13826h	.89	.89	.66	138212	Mirador granite
[1]SiO_2	51.67	52.86	53.00	52.79	53.06	76.23
Al_2O_3	17.23	16.87	16.62	16.56	16.56	13.19
TiO_2	0.97	1.10	1.10	1.21	1.32	0.13
FeO	9.86	9.91	9.98	11.20	9.78	1.31
MnO	0.16	0.17	0.17	0.19	0.18	0.04
MgO	6.65	5.20	5.37	5.48	5.61	0.34
CaO	9.90	9.87	9.75	8.50	9.12	0.89
Na_2O	3.06	3.25	3.22	3.10	3.24	3.48
K_2O	0.50	0.62	0.66	0.84	0.85	4.36
P_2O_5	0.13	0.15	0.15	0.18	0.26	0.06
[2]La	6.92	8.12	8.46	10.8	12.9	25.7
Sm	2.92	3.31	3.33	4.32	4.66	2.33
Yb	1.93	2.19	2.20	2.85	2.79	1.49
Hf	1.73	2.00	2.05	2.64	2.88	3.9
Sc	37	41	40	52	35	3.0
Zr	67	-	-	-	123	-
Th	1.00	1.44	1.75	1.87	2.24	23
Nb	2.4	-	-	-	3.8	-
Rb	8.7	12.4	15.0	16.2	18.3	191
Sr	410	413	406	19	397	195
Ba	165	199	214	464	271	1114
Ni	53	11	12	2 4	52	-
Cr	133	124	124	38	108	2
CaO/Al_2O_3	0.575	0.585	0.587	0.513	0.551	0.067
[2]La/Sm	2.37	2.45	2.54	2.50	2.77	11.0
Ba/Rb	19.0	16.0	14.3	16.3	14.8	5.8
Ba/Th	165	138	122	41	121	48
Zr/Sm	22.9	-	-	-	26.4	-
phase proportions						
oliv		.45	.42	.13		
cpx		-	-	.26		
plag		.64	.76	.61		
mag		-	-	.03		
r ratio		.10	.18	.03		
phase compositions						
[3]olivine(Fo%)		75	75	73		
cpx(En%)		-	-	41		
plag(An%)		70	70	54		
K_{plag}^{Na-Ca}		1.8	1.8	0.75		
$^{87}Sr/^{86}Sr$	.70398	.70400	.70403	.70400	.70405	.70453
Sr (D_{plag}^{Sr} = 1.8)		399	394	394		

[1]major-element composition and trace element abundances adjusted for phenocryst content, total iron as FeO and analysis normalized to 100%.
[2]calculated using low values of partition coefficients (Table 7).
[3]K_{oliv}^{Fe-Mg} of 0.32, and K_{aug}^{Fe-Mg} of 0.26 were assumed.

Table 7d

Magma mixing model: basalt + andesite = basaltic andesite 138212

	proportion of evolved endmember						
	[1]13826h (endmember)	+20%	+30%	+33%	+40%	138212	220283-5 (endmember)
SiO_2	51.67	53.13	53.86	54.08	54.59	53.06	58.96
Al_2O_3	17.23	16.91	16.75	16.70	16.59	16.56	15.62
TiO_2	0.97	1.07	1.12	1.14	1.17	1.32	1.47
FeO	9.86	9.58	9.44	9.39	9.30	9.78	8.45
MnO	0.16	0.17	0.18	0.18	0.18	0.18	0.22
MgO	6.65	5.89	5.51	5.39	5.13	5.61	2.84
CaO	9.90	9.14	8.76	8.64	8.38	9.12	6.09
Na_2O	3.06	3.29	3.41	3.44	3.53	3.24	4.23
K_2O	0.50	0.70	0.79	0.82	0.89	0.85	1.48
P_2O_5	0.13	0.23	0.28	0.29	0.33	0.26	0.63
La	6.92	10.0	11.6	12.1	13.2	12.9	22.5
Sm	2.92	3.92	4.42	4.57	4.92	4.66	7.93
Yb	1.93	2.36	2.57	2.64	2.79	2.79	4.07
Hf	1.73	2.36	2.67	2.77	2.99	2.88	4.87
Sc	37	35	34	34	33	35	28
Zr	67	92	105	108	117	123	192
Th	1.0	1.71	2.07	2.17	2.42	2.24	4.56
Nb	2.4	3.0	3.4	3.5	3.7	3.8	5.6
Rb	8.7	14.0	16.6	17.4	19.3	18.3	35.1
Sr	410	404	400	399	397	397	378
Ba	165	221	249	258	277	271	446
Ni	53	44	40	39	35	52	8
Cr	133	110	99	95	87	108	19
CaO/Al_2O_3	0.575	0.541	0.523	0.518	0.505	0.551	0.390
La/Sm	2.37	2.55	2.62	2.65	2.68	2.77	2.84
Ba/Rb	19.0	15.8	15.0	14.	14.4	14.8	12.7
Ba/Th	165	129	120	119	114	121	98
Zr/Sm	22.9	23.5	23.8	23.7	23.8	26.4	24.2
$^{87}Sr/^{86}Sr$	.70398	.70400	.70401	.70401	.70402	.70405	.70407

[1]major-element composition and trace element abundances adjusted for phenocryst content, total iron as FeO, and analysis normalized to 100% on anhydrous basis.

Table 7e

Fractional crystallization models: basalt to basaltic andesite 272826b

	13828	F .87	220283-1	F .97	F .96	13828	F 80%	272826b
[1]SiO_2	52.97	53.31	53.22	53.27	53.69	52.97	55.27	54.80
Al_2O_3	15.97	17.63	16.97	17.38	17.51	15.97	16.29	17.48
TiO_2	0.82	0.88	1.19	1.22	1.12	0.82	0.68	0.71
FeO	8.91	9.07	9.17	9.20	8.65	8.91	7.82	7.43
MnO	0.16	0.18	0.15	0.15	0.15	0.16	0.20	0.14
MgO	7.24	5.58	5.31	5.03	5.04	7.24	5.70	6.01
CaO	10.51	9.48	9.78	9.42	9.47	10.51	9.91	9.51
Na_2O	2.81	3.17	3.29	3.39	3.42	2.81	3.24	2.95
K_2O	0.61	0.69	0.70	0.72	0.73	0.61	0.76	0.84
P_2O_5	0.11	0.12	0.21	0.21	0.21	0.11	0.14	0.13
[2]La	7.91	9.03	11.9	12.2	12.4	7.91	9.83	11.7
Sm	2.82	3.15	4.06	4.16	4.20	2.82	3.46	3.62
Yb	1.57	1.76	2.18	2.23	2.25	1.57	1.92	2.28
Hf	1.39	1.58	2.42	2.49	2.51	1.39	1.72	2.77
Sc	39.5	42.3	38	39	38.7	39.5	46	28
Zr	53	61	100	103	104	53	66	122
Th	2.14	2.46	1.62	1.67	1.69	2.14	2.67	2.75
Nb	1.7	1.95	4.1	4.2	4.3	1.7	2.1	3.7
Rb	9.2	10.6	12.9	13.3	13.4	9.2	11.5	19.9
Sr	500	562	472	484	489	500	540	350
Ba	173	199	263	271	274	173	214	271
Ni	63	48	43	39	36	63	3	64
Cr	403	305	110	105	45	403	149	126
CaO/Al_2O_3	0.658	0.538	0.576	0.542	0.541	0.658	0.608	0.544
[2]La/Sm	2.80	2.87	2.93	2.93	2.95	2.80	2.84	3.23
Ba/Rb	18.8	18.8	20.4	20.4	20.4	18.8	18.6	13.6
Ba/Th	81	81	162	162	162	81	80.1	99
Zr/Sm	18.8	19.4	24.6	24.8	24.8	18.8	19.1	33.7
Phase proportions (%)								
oliv		-		-	-		20	
cpx		100		100	80		30	
plag		-		-	-		40	
mag		-		-	20		10	

[1]major-element composition and trace element abundances adjusted for phenocryst content, total iron as FeO, and analysis normalized to 100%.
[2]trace element abundances and abundance ratios calculated using set of low values of partition coefficients (see Table 8).

Table 7f

Assimilation-fractional crystallization model (AFC):
basalt to basaltic andesite 272826b

		F (fraction of residual liquid)				
	13828	F=.82	F=.82	F=.83	272826b	Mirador granite
SiO_2	52.97	55.24	55.40	55.76	54.80	76.23
Al_2O_3	15.97	16.42	16.42	16.44	17.48	13.19
TiO_2	0.82	0.68	0.68	0.62	0.71	0.13
FeO	8.91	7.91	7.89	7.54	7.43	1.31
MnO	0.16	0.19	0.19	0.18	0.14	0.04
MgO	7.24	5.77	5.71	5.76	6.01	0.34
CaO	10.51	9.63	9.51	9.46	9.51	0.89
Na_2O	2.81	3.24	3.25	3.25	2.95	3.48
K_2O	0.61	0.79	0.82	0.86	0.84	4.36
P_2O_5	0.11	0.13	0.13	0.13	0.13	0.06
La	7.91	9.88	10.1	10.4	11.7	25.7
Sm	2.82	3.40	3.42	3.41	3.62	2.33
Yb	1.57	1.89	1.90	1.90	2.28	1.49
Hf	1.39	1.73	1.75	1.80	2.77	3.9
Sc	39.5	45	45	44	28	3.0
Zr	53	-	-	-	122	-
Th	2.14	2.87	3.04	3.40	2.75	23
Nb	1.7	-	-	-	3.7	-
Rb	9.2	13.4	14.8	18.0	19.9	191
Sr	500	537	536	534	350	195
Ba	173	222	230	247	271	1114
Ni	63	28	27	26	64	-
Cr	403	198	194	167	126	2
CaO/Al_2O_3	0.658	0.586	0.579	0.575	0.544	0.067
La/Sm	2.80	2.91	2.95	3.05	3.23	11.0
Ba/Rb	18.8	16.6	15.5	13.7	13.6	5.8
Ba/Th	81	77.4	75.7	72.6	99	48
Zr/Sm	18.8	-	-	-	33.7	-
Phase proportions (%)						
oliv		17.1	16.7	15.7		
cpx		36.2	37.0	37.4		
plag		37.1	37.0	35.7		
mag		9.5	9.3	11.3		
r		.05	.08	.15		
$^{87}Sr/^{86}Sr$		.70381	.70381	.70382	.70400	.70453

Table 7g

Magma mixing models: basalt + rhyolite = basaltic andesite 272826b

proportion of rhyolite given in %

	[1]230283-5 (endmember)	+13%	13828 (endmember)	+15%	272826b	202825c (endmember)
SiO_2	52.66	55.02	52.97	55.65	54.80	70.82
Al_2O_3	18.41	17.84	15.97	16.67	17.48	13.99
TiO_2	0.98	0.90	0.82	0.76	0.71	0.41
FeO	7.91	7.44	8.91	8.21	7.43	4.26
MnO	0.16	0.15	0.16	0.16	0.14	0.13
MgO	5.89	5.16	7.24	6.20	6.01	0.28
CaO	10.21	9.15	10.51	9.24	9.51	2.02
Na_2O	3.00	3.30	2.81	3.18	2.95	5.27
K_2O	0.60	0.88	0.61	0.93	0.84	2.75
P_2O_5	0.17	0.16	0.11	0.11	0.13	0.10
La	8.35	11.6	7.91	11.7	11.7	33.4
Sm	2.98	3.78	2.82	3.77	3.62	9.17
Yb	1.68	2.29	1.57	2.30	2.28	6.41
Hf	2.09	2.88	1.39	2.41	2.77	8.20
Sc	32	29.8	39.5	36	28	14.9
Zr	83	120	53	101	122	370
Th	1.37	2.27	2.14	3.06	2.75	8.25
Nb	3.3	4.2	1.7	3.0	3.7	10.1
Rb	11.3	18.7	9.2	18.1	19.8	68.3
Sr	463	423	500	449	350	161
Ba	218	291	173	264	271	780
Ni	49	44	63	55	64	8
Cr	119	104	403	342	126	1
CaO/Al_2O_3	0.555	0.513	0.658	0.554	0.544	0.144
La/Sm	2.80	3.07	2.80	3.10	3.23	3.64
Ba/Rb	19.3	15.6	18.8	14.6	13.7	11.4
Ba/Th	159	128	81	86	99	94
Zr/Sm	27.8	31.7	18.8	26.8	33.7	40.3
$^{87}Sr/^{86}Sr$	.70399	.70400	.70381	.70383	.70400	.70409

[1]Major-element composition as analyzed. Total iron as FeO and normalized on anhydrous basis to 100%. Trace element abundances as analyzed.

Table 8

Mineral/melt partition coefficients used in fractional crystallization calculations

a. low values

	oliv	opx	cpx	plag	mag
La	0.011	0.015	0.06	0.012	0.03
Ce	0.01	0.024	0.15	0.011	0.032
Nd	0.01	0.030	0.20	0.01	0.038
Sm	0.01	0.031	0.22	0.01	0.053
Eu	0.01	0.054	0.30	0.34	0.055
Tb	0.01	0.125	0.35	0.01	0.092
Dy	0.01	0.130	0.30	0.01	0.10
Yb	0.01	0.130	0.25	0.01	0.12
Hf	0.005	0.005	0.10	0.008	0.01
Sc	0.20	1.4	0.5	0.01	1.0
Zr	0.005	0.005	0.10	0.008	0.10
Th	0.001	0.001	0.001	0.001	0.001
Nb	0.005	0.005	0.01	0.001	0.10
Rb	0.001	0.001	0.001	0.01	0.001
Sr	0.001	0.001	0.001	1.5	0.001
Ba	0.001	0.001	0.001	0.10	0.001
Cr	3.0	3.0	1.5	0.01	31
Ni	*	3.0	3.0	0.01	11

b. high values

	oliv	opx	cpx	plag	mag	ilm	apat
La	0.013	0.04	0.20	0.22	0.04	0.05	6.4
Ce	0.012	0.04	0.25	0.20	0.042	0.06	10
Nd	0.011	0.04	0.38	0.15	0.05	0.07	17
Sm	0.011	0.045	0.48	0.12	0.06	0.08	19.1
Eu	0.011	0.045	0.50	1.0	0.07	0.10	3
Tb	0.012	0.06	0.52	0.10	0.10	0.13	16
Dy	0.013	0.08	0.52	0.10	0.12	0.16	15.2
Yb	0.015	0.12	0.52	0.10	0.15	0.19	8.5
Hf	0.01	0.08	0.40	0.08	0.25	1.0	0.11
Sc	0.4	2.0	7.0	0.01	4.0	4.0	0.01
Zr	0.01	0.08	0.42	0.08	0.25	1.4	0.10
Th	0.01	0.01	0.01	0.01	0.01	0.01	1.3
Nb	0.01	0.08	0.03	0.01	0.50	0.80	0.10
Rb	0.01	0.01	0.01	0.01	0.01	0.01	0.01
Sr	0.01	0.01	0.10	3.0	0.01	0.01	1.3
Ba	0.01	0.01	0.10	0.35	0.01	0.01	0.01
Cr	3.0	2.0	2.5	0.01	150	7	0.01
Ni	*	2.0	8.0	0.01	10	30	0.01

* D_{Oliv}^{Ni} calculated after the method of Hart and Davis (1978).

knowledge of the geochemical characteristics of the basement rocks in the area.

6.3 Possible open-system fractional crystallization: general considerations

The problem of anomalously elevated trace element abundances and different abundance ratios in the basaltic andesites than expected given their major-element compositions may be explained by open-system fractional crystallization in a magma chamber that is periodically replenished and periodically tapped, termed an 'RTF' magma chamber by O'Hara (1984). Decoupling of trace element abundances and abundance ratios and major-element compositions are likely in an RTF magma chamber (O'Hara and Matthews, 1981). Major-elements may actually be buffered to some extent if the mass fraction (z) of new melt entering the chamber is greater than the sum of the mass fraction (y) of melt withdrawn and the mass fraction (x) crystallized. If the amount y withdrawn is small relative to x and z, these conditions may produce a series of lavas with seemingly anomalously high incompatible element abundances which would otherwise appear to be best explained by varying degrees of partial melting. The elevated incompatible element abundances in the basaltic andesites at Puyehue suggest that they were produced by approximately 50% fractional crystallization while major-element compositions suggest a maximum of 30% fractional crystallization. This decoupled increase in trace element abundances in the basaltic andesites may be modelled as an RTF phenomenon, but many assumptions must be made regarding the input parameters such that no unique solution is to be obtained, i.e., each may be varied to produce the same answer. Values for x, y, z, w (optional

mass fraction of wallrock contaminant), and bulk partition coefficient D must be assumed. Further assumptions are made regarding the choice of the compositions of initial parental magmas and subsequent (replenishing) parental magmas. For the relationship to be evaluated for the data set in this study, it seems intuitive that amounts of magma withdrawn should be small relative to the crystallizing fraction x and input fraction z. Over the long term, this is supported by the predominance of more evolved lavas as late stage eruptives. Over the short term, these relative values of x, y, and z, are suggested by the geochemical characteristics of the basalts and basaltic andesites, if indeed they are genetically related by processes occurring within an RTF magma chamber.

A major problem to be resolved is the dramatic changes in abundance ratios of incompatible (I) and highly incompatible (HI) elements. This problem may be also resolved by postulating open-system behavior in an RTF magma chamber. Values of input (z), fractional crystallization (x), and output (y) cannot be uniquely determined, but the number of cycles (n) of replenishment, followed by crystallization and then eruption withdrawal may be estimated and realistically evaluated, as in an example presented by O'Hara and Matthews (1981, p. 248). In this example, for y = 0 or near zero, an abundance ratio of an HI element (D^{HI} = 0.001) to an incompatible element (D^{I} = 0.1) will be increased nearly twofold after 100 cycles in an RTF chamber. This phenomenon may be observed in the basalts and basaltic andesites at Puyehue, in that many basalts have Th/Ba ratios of .0061 to .0072 amd Rb/Ba ratios of 0.045 to 0.054 and the basaltic andesites display higher ratios (Th/Ba = 0.0083 to 0.010 and Rb/Ba = 0.068 to 0.075). These data may indicate open system behavior but differences in bulk partition coefficients for Ba as compared to Rb

and Th, presumed to be highly incompatible, may not be as extreme as two orders of magnitude as in the example above. An additional problem in this example is that in achieving a nearly twofold increase in ratios of HI elements vs. I elements after approximately 100 cycles, the abundances of each are increased in the magma chamber 8 to 10 times the original levels. Thus, with application to Puyehue basalts and basaltic andesites, a particular balance must be struck between all variable parameters in any RTF modelling scheme to explain the somewhat drastic changes in abundance ratios with only twofold increases in abundances from basalts to basaltic andesites. Assuming a constant composition for new replenishing magams, greater fractions of input z may relatively suppress progressive enrichment in HI and I elements in each cycle, but again, it would seem that unreasonably high differences in D^{HI} and D^{I} are required to explain the apparent progressive increase in abundance ratios C_n^{HI}/C_n^{I}. For constant parameters x, y, z, and D^{HI} and D^{I}, the ratio C_n^{HI}/C_n^{I} increases with increasing numbers of cycles (n), and for infinite n (as $n \to \infty$), the maximum (or 'steady state') values of C_n^{HI}, C_n^{I}, and C_n^{HI}/C_n^{I} for the magma chamber may be estimated (eqns. 13 and 15, O'Hara and Matthews, 1981). These assumptions may be unrealistic with regard to application of such a model to Puyehue lavas. If basalt 13826h is assumed to be representative of initial parental and subsequent replenishing melts input in amounts of 10% of the proportion of the total magma chamber, an infinite number of cycles of 10% input, 5% fractional crystallization and 1% erupted will achieve abundances of 4.9 ppm Th, 43 ppm Rb, and 652 ppm Ba in the final steady state magma chamber for $D^{Ba} = 0.05$ and D^{Rb}, $D^{Th} = 0.001$. Abundances in this sample calculation are two to three times those observed in the basaltic andesites, though

ratios of Th/Ba (.0076) and Rb/Ba (0.065) are equivalent to those observed in the basaltic andesites. If the basalts and basaltic andesites are related by complex processes in an RTF magma chamber, explanations for such a calculated mismatch may include: (1) the possibility that basalt 13826h is not representative of parental of replenishing magmas which may instead have been characterized by lower (more primitive) trace element abundances, (2) that the composition of replenishing magmas was not constant with time, (3) that assumed values of x, y, and z are not correct, (4) that $D^{Ba}-D^{HI(Th,Rb)} > 0.05$, and (5) that magmas assimilated some small proportion of country rock. The suggestion in (2) above is supported by the highly variable characteristics of the basalts alone, in which some C^{HI}/C^{I} ratios vary. This may be due to their derivation from different sources, or open-system processes in a deeper, intermediate magma chamber. If the latter were true, this would provide some explanation for the variability in the basalts.

With the present data set, it is not possible to adequately quantify a model of open-system magmatism in an RTF magma chamber, especially with the various possible complexities as suggested above. For such an effort to be attempted, it would be desirable to have 100% outcrop exposure to allow stratigraphically controlled sampling of extensive continuous sequences of lavas. This would facilitate evaluation of possible megacycles in any RTF magma chamber processes.

The total volume of PII basalts and basaltic andesites is estimated at 30 km^3, which may be considered a maximum if there exists a significant proportion of pyroclastic and vesicular lavas in this unit. If lava flows average 10 m in thickness, 100 m in breadth and 2 km in length, then the total number of extruded lava flows may be as high as

15000, which may correspond to an equivalent number of individual cycles of replenishment, fractional crystallization, and eruption. This large number of possible cycles, given a judicious choice of model input parameters, may be adequate to produce anomalously enriched trace element abundances and variable C^{HI}/C^{I} abundance ratios, especially if the eruptive activity increases on occasion, which would define and separate a number of 'megacycles' seen in the chemistry of the lavas. However, basaltic andesites are randomly interbedded with the highly variable basalts, suggesting that such 'megacycles' may not be adequate in duration to explain the observed decoupling of major elements, incompatible trace elements, and highly incompatible trace elements in these lavas. The result is that abrupt geochemical 'breaks' are observed rather than gradually increasing abundances and abundance (C^{HI}/C^{I}) ratios. Open-system magmatism at Puyehue Volcano may have occurred to some extent, but alone, may be inadequate in explaining the geochemical characteristics of the basalts and basaltic andesites.

7. Mixed andesites

7.1 Petrographic and geochemical criteria

Direct evidence for magma mixing is seen in the form of disequilibrium phenocryst assemblages in andesite 272822 and dacitic andesite 242824 (Figures 3a, 4, and 5a). Sample 272822 is characterized by higher TiO_2, P_2O_5, Ni, and Cr abundances and lower $^{87}Sr/^{86}Sr$ (0.70388±3) relative to 242824, in which $^{87}Sr/^{86}Sr$ = .70410±4. These differences are significant in that they are the chief factors by which possible mixing endmembers among the sample suite were determined.

The composition of andesite 272822 may represent a mixture of approximately 45% basalt and 55% dacite (Table 9a). The high Ni, Cr, and Th abundances and low $^{87}Sr/^{86}Sr$ in sample 13828 indicate this basalt to be the most likely mixing endmember in the data set. Compositions of olvine and plagioclase phenocrysts in 272822 are similar to those in 13828 (Figures 3a and 4). A complementary silicic endmember for a mixing origin of 272822 must contain higher TiO_2 and P_2O_5 contents, higher $^{87}Sr/^{86}Sr$, higher abundances of incompatible trace elements (Rb, Ba, Th, Nb, La, Sm, Yb, Zr, Hf) and lower abundances of compatible trace elements (Sc, Sr, Ni, Cr) and dacite sample 212826 has the required characteristics. Compositions of relatively more sodic disequilibrium plagioclase phenocrysts in 272822 are similar to those in dacite 212826 (Fig. 3a), and augite phenocryst compositions overlap in both samples (Fig. 5a). However, pigeonite phenocrysts in andesite 272822 are similar to those in rhyolites such as samples 182821b and 202825c (cf., Figs. 5a, 5c). As seen in Table 9a, and Figure 16a, a calculated mixture containing 55% dacite is higher in MgO content and Ni and Cr abundances and lower in Th. A partial correction to the bulk composition of 13828 to account for accumulated olivine phencrysts would alleviate this small disparity in calculated vs. observed values. Attempting to totally correct the bulk composition of 13828 for accumulated olivine, however, would result in Ni and Cr abundances too low: a simple calculation suggests that the basaltic endmember contained about 350 ppm Cr. As discussed earlier, it is difficult to assess what proportion of phenocrysts are accumulated and which phenocrysts, how many of them, or what portion of the phenocrysts grew in situ and therefore constitute a complementary component of the magma. Based on approximate knowledge of

16 Calculated major-element contents and trace element abundances normalized to observed values in magma mixing models for (a) andesite 242824 (Table 9b), and (b) andesite 272822 (Table 9a).

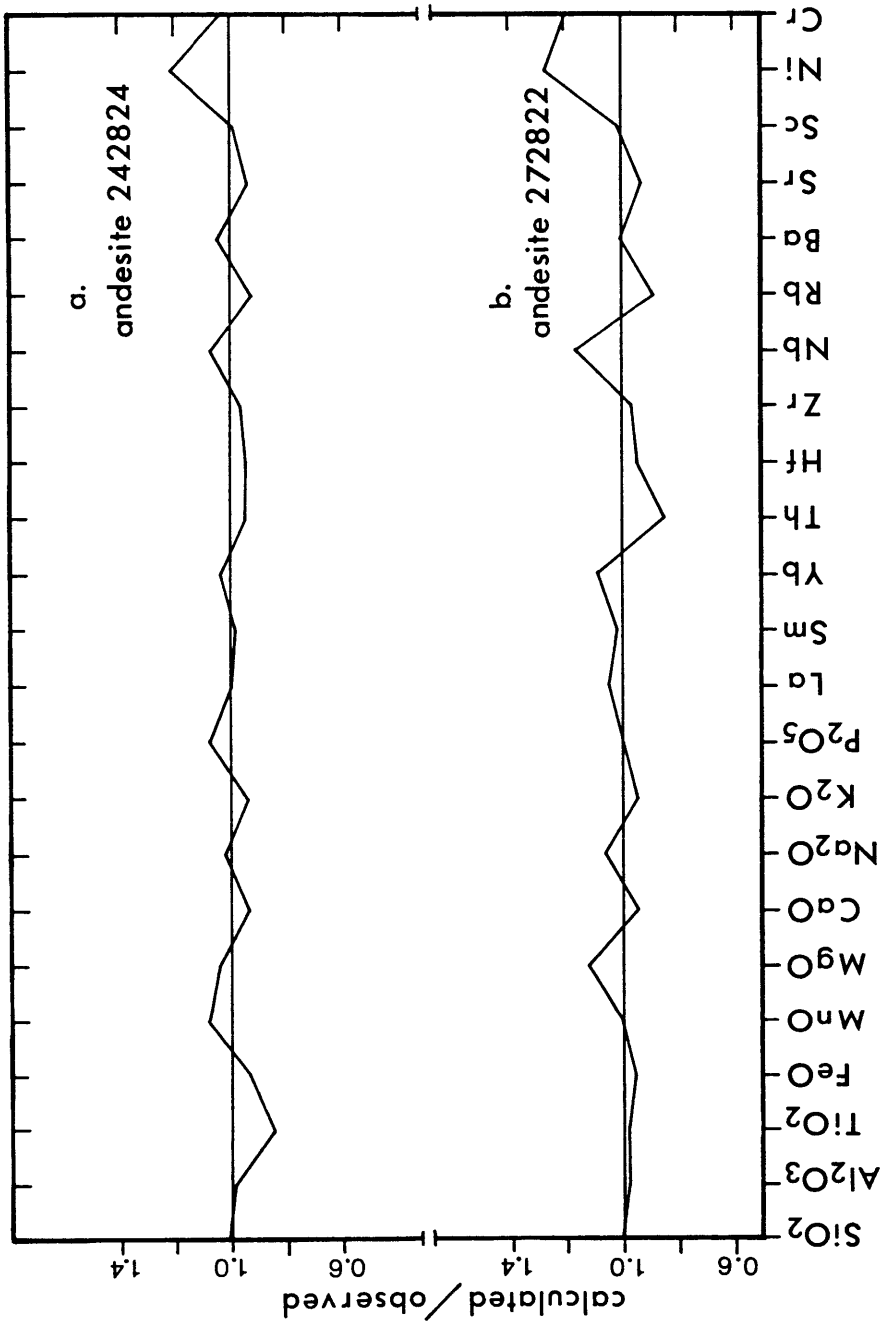
a.
andesite 242824
b.
andesite 272822
calculated / observed
0.6
1.0
1.4
SiO2
Al2O3
TiO2
FeO
MnO
MgO
CaO
Na2O
K2O
P2O5
La
Sm
Yb
Th
Hf
Zr
Nb
Rb
Ba
Sr
Sc
Ni
Cr

Table 9a

Magma mixing model: basalt + dacite = andesite

	13828[1] (endmember)	proportion of evolved endmember +30%	+40%	+50%	+55%	272822	212826 (endmember)
SiO_2	51.82	56.21	57.67	59.13	59.86	59.26	66.44
Al_2O_3	16.79	16.06	15.82	15.58	15.46	15.86	14.37
TiO_2	0.66	0.76	0.79	0.82	0.84	0.86	0.98
FeO	8.27	7.46	7.19	6.92	6.79	7.12	5.57
MnO	0.13	0.14	0.14	0.15	0.15	0.15	0.16
MgO	9.69	7.07	6.20	5.33	4.89	4.35	0.97
CaO	10.55	8.36	7.63	6.90	6.54	6.87	3.25
Na_2O	2.50	3.33	3.60	3.88	4.01	3.77	5.25
K_2O	0.50	1.02	1.20	1.37	1.46	1.54	2.24
P_2O_5	0.13	0.18	0.19	0.21	0.22	0.22	0.29
La	6.36	13.3	15.6	17.9	19.0	18.1	29.4
Sm	2.26	4.18	4.82	5.46	5.78	5.68	8.66
Yb	1.26	2.60	3.05	3.50	3.72	3.40	5.74
Hf	1.12	2.82	3.38	3.95	4.23	4.48	6.78
Sc	32	28.2	26.9	25.7	25.0	24.5	19.3
Zr	43	120	146	172	185	191	301
Th	1.72	3.18	3.67	4.16	4.40	5.18	6.60
Nb	1.4	3.7	4.4	5.2	5.6	4.8	9.0
Rb	7.4	22.1	27.0	32.0	34.4	38.9	56.5
Sr	496	416	390	363	350	375	230
Ba	139	288	337	387	411	408	634
Ni	147	106	92	78	71	55	9
Cr	426	299	256	214	192	158	1
CaO/Al_2O_3	0.628	0.521	0.482	0.443	0.423	0.433	0.226
La/Sm	2.81	3.18	3.24	3.28	3.29	3.19	3.40
Ba/Rb	18.8	13.0	12.5	12.1	11.9	10.5	11.2
Ba/Th	81	91	92	93	93	79	96
Zr/Sm	19.0	28.7	30.3	31.5	32.0	33.6	34.8
$^{87}Sr/^{86}Sr$	.70381	.70384	.70386	.70388	.70389	.70388	.70402

[1]Major-element composition as analyzed. Total iron as FeO and normalized on anhydrous basis to 100%. Trace element abundances as analyzed.

Table 9b

Magma mixing model: basalt + rhyolite = andesite

		proportion of evolved endmember				
	272824b[1]	+50%	+60%	+65%	242824	202825c
SiO_2	52.17	61.50	63.36	64.29	63.33	70.82
Al_2O_3	18.41	16.20	15.76	15.54	15.70	13.99
TiO_2	0.90	0.66	0.61	0.58	0.69	0.41
FeO	8.32	6.29	5.88	5.68	6.12	4.26
MnO	0.16	0.15	0.14	0.14	0.13	0.13
MgO	6.04	3.16	2.58	2.30	2.22	0.28
CaO	10.10	6.06	5.25	4.85	5.19	2.02
Na_2O	3.04	4.16	4.38	4.49	4.41	5.27
K_2O	0.65	1.70	1.91	2.02	2.14	2.75
P_2O_5	0.20	0.15	0.14	0.14	0.13	0.10
La	8.76	21.1	23.5	24.8	24.9	33.4
Sm	3.32	6.25	6.83	7.12	7.19	9.17
Yb	1.75	4.08	4.55	4.78	4.60	6.41
Hf	1.94	5.07	5.70	6.01	6.32	8.20
Sc	31	23.0	21.3	20.5	20.7	14.9
Zr	80	225	254	269	279	370
Th	1.04	4.65	5.37	5.73	6.06	8.25
Nb	3.0	6.6	7.3	7.6	7.1	10.1
Rb	15.8	42.1	47.3	49.9	54.0	68.3
Sr	476	319	287	271	290	161
Ba	188	484	543	573	550	780
Ni	51	30	25	23	19	8
Cr	100	51	41	36	35	1
CaO/Al_2O_3	0.549	0.374	0.333	0.312	0.331	0.144
La/Sm	2.64	3.38	3.44	3.48	3.46	3.64
Ba/Rb	11.9	11.5	11.5	11.5	10.2	11.4
Ba/Th	181	104	101	100	91	94
Zr/Sm	24.1	36.0	37.2	37.8	38.8	40.3
$^{87}Sr/^{86}Sr$	.70416	.70414	.70414	.70413	.70410	.70409

[1]Major-element composition as analyzed. Total iron as FeO and normalized on anhydrous basis to 100%. Trace element abundances as analyzed.

the partitioning of Cr in olivine, olivine phenocrysts contribute most of the Cr (~75-80%) in the bulk analysis. High Cr abundances required in the mixing model in Table 8a may suggest that the basaltic component did contain olivine or a high-Cr basaltic endmember, and in addition, the mere presence of olivine phenocrysts and calcic plagioclase phenocrysts in andesite 272822 is evidence that this basaltic endmember was porphyritic. A reasonable match in most major- and trace elements is observed in Figure 16a, however the magma mixing process that produced andesite 272822 may not have been one of simple two-component (basalt + dacite) mixing but may have included rhyolitic magma as indicated by the pigeonite phenocrysts.

A porphyritic basaltic endmember is also called for in a magma mixing model for dacitic andesite 242824, as demonstrated again by the phenocrysts themselves. A rhyolitic, rather than dacitic endmember is suggested on the basis of (1) relatively high trace element abundances, significantly higher (La/Sm, Zr/Sm) abundance ratios, and (2) Fe-rich pyroxene phenocrysts and sodic plagioclase phenocrysts which are compositionally similar to those in rhyolite 202825c (Figs. 3a and 5a). Sample 242824 may have been produced by mixing with a silicic endmember even more evolved than 202825c. Fe-rich olivines (Fo_{26}) found in 242824 are not observed in 202825c, although they would be in equilibrium with the latter based on an Fe-Mg olivine-liquid exchange K_D of 0.31. Olivines of this composition are observed in recent rhyolites of the nearby Cordon Caulle (Fig. 5c, Table 3b), and these rhyolites are slightly more evolved than 202825c (section 3.3.5). A basalt such as 272824b fits most requirements for a hypothetical endmember in this example, especially the requirement that, because of relatively higher

$^{87}Sr/^{86}Sr$ in 242824 relative to the presumed rhyolitic mixing endmember, the $^{87}Sr/^{86}Sr$ ratio of the basaltic endmember cannot be lower than that in 242824, but instead must be characterized by higher $^{87}Sr/^{86}Sr$. As seen in Table 9b, the characteristics of the mixed dacitic andesite may be explained by mixing of 35-40% basalt with 60-65% rhyolite. Abundances of K, Th, Hf, and Zr are slightly low, and $^{87}Sr/^{86}Sr$ ratios slightly high in calculated mixtures compared to observed values (Table 9b), but again, given the demonstrated variability in the basalts, a basalt with even more ideal characteristics could be chosen, but is not necessarily represented in the analyzed sample suite.

7.2 Magma mixing: isotopic criteria

Isotopic (Sr) and trace element abundance ratio criteria for each of four mixing models explaining the various basaltic andesite and andesite compositions are illustrated in Figure 17. Sr-isotopic data agree reasonably well in all examples and Nd-isotopic data also match reasonably well for basaltic andesites being mixtures of specific magmas as outlined earlier. However, the andesites with disequilibrium phenocryst assemblages display lower $^{143}Nd/^{144}Nd$ ratios (.512818-.512833) than their respective inferred basaltic ($^{143}Nd/^{144}Nd$ = .512885-.512861) and silicic ($^{143}Nd/^{144}Nd$ = .512850-.512869) mixing endmembers. A few accidental, intact inclusions of various sizes consisting of older volcanics are observed, but on the basis of representative analyses of preglacial exposed volcanics, these may be isotopically very similar and would not be expected to substantially affect the isotopic composition of the mixed host lava. Inclusions of granite, though not observed, may contribute Nd of lesser radiogenic character, in addition to Th, K, Zr,

17 $^{87}Sr/^{86}Sr$ vs. Rb/Sr and La/Sm systematics in lavas from Puyehue Volcano. Dashed lines are mixing lines between magmas of different compositions that may be endmembers in producing certain basaltic andesites and andesites by magma mixing. These are keyed to specific models discussed earlier. Mixing line (1) refers to mixing of basalt 13826h and andesite 220283-5 to produce basaltic andesite 138212 (Table 7d, Figure 14d). Mixing line (3) corresponds to a model for basaltic andesite 272826b by mixing of basalt 230283-5 and rhyolite 202825c (Table 7g). Mixing lines (2a) and (2) correspond to magma mixing models for andesite 242824 (Table 9b) and andesite 272822 (Table 9a), respectively.

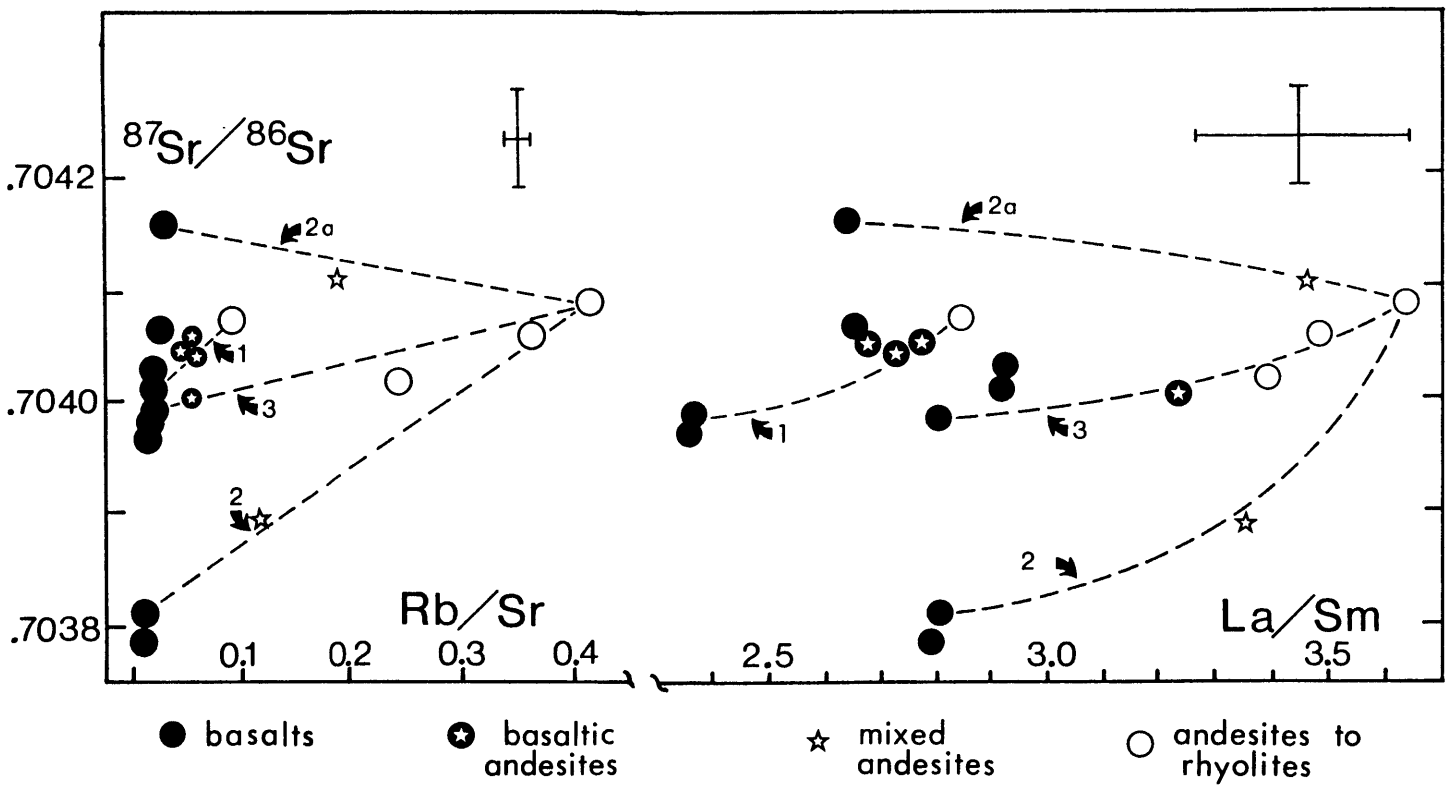
$^{87}Sr/^{86}Sr$
.7042
.7040
.7038
2a
1
3
2
Rb/Sr
0.1
0.2
0.3
0.4
2a
1
3
2
La/Sm
2.5
3.0
3.5
basalts
basaltic andesites
mixed andesites
andesites to rhyolites

and Rb, the abundances of which are slightly lower in the calculated mixtures vs. observed values. By the same token, it may be speculated that the silicic magma mixing endmember for the mixed andesites is not strictly represented in the sample suite and had lower $^{143}Nd/^{144}Nd$ and higher Th, K, Zr, and Rb relative to those selected to partly represent such an endmember (212826 and 202825c), and that these characteristics may reflect some component derived from melting of older granitic plutonic rocks.

8. Petrogenesis of evolved lavas:

8.1 Basaltic andesites to andesites

Most lavas from Puyehue, including basalts to rhyolites, are relatively Fe-rich and fall into the 'tholeiitic' field on a plot of FeO^*/MgO vs. SiO_2 (Fig. 6b). The exceptions which fall into the calcalkaline field include a few samples of basalt and basaltic andesite. One basaltic andesite in particular, sample 272826b, was interpreted as a product of mixing of basaltic and rhyolitic magmas or an AFC process. Other basaltic andesites were interpreted as products of mixing of basaltic and andesitic magmas. The two mixed andesites with disequilibrium phenocryst assemblages also plot in the calcalkaline field. It has been suggested that many subduction zone related lavas which plot in the calcalkaline field as in Figure 6b, are those which are produced by magma mixing (Sakuyama, 1981; Kay et al., 1982) although many may also be produced by fractional crystallization at moderate pressures (cf., Grove and Baker, 1984). However, most samples in this study do not have low FeO^*/MgO ratios similar to those of sample suites discussed by Kay et al. (1982) and Sakuyama (1981). A tendency to plot in the calcalkaline field may be seen more often in mixed andesites and dacites,

and is also dependent on the characteristics of the mixing endmembers. Basaltic andesites such as 138212, in which both the presumed basaltic and high-TiO_2 andesitic mixing endmembers are characterized by relatively higher FeO*/MgO ratios, plot in the tholeiitic field.

Andesites such as samples 43821 and 220283-5 with high TiO_2 (1.44-1.57 wt.%) and P_2O_5 (0.62-0.68 wt.%) contents and high FeO*/MgO (3.0-3.4) ratios seem likely products of fractional crystallization processes. These andesites display no textural or occult geochemical evidence of an origin by magma mixing, and their origin will be addressed through fractional crystallization modelling. The most immediate parental precursors, basaltic andesites, are aphyric. Phases in crystallizing assemblages which may be used in fractional crystallization models for the derivation of the andesites are suggested by phenocrysts in basalts (olivine, plagioclase, magnetite) and in dacites (plagioclase, augite, orthopyroxene, magnetite). The andesite compositions plot near reaction point 'B' (Fig. 18a) in the 1-atm oliv-cpx-qtz pseudo-ternary projection (Grove et al., 1982, 1983). Since Puyehue basalts plot to the left of a line from olivine to reaction point A, fractional crystallization of basalts at low pressure would consist of olivine + plagioclase crystallization driving residual liquid compositions to near point A and then toward the plag-pig-aug cotectic. However, without exception, evolved Puyehue lavas (andesite to rhyolite) plot mostly along the opx-pig-plag reaction curve (Fig. 18a). This would seem to preclude the derivation of these andesitic liquids by low-pressure fractional crystallization of basaltic magma. Fractional crystallization of basaltic magmas at higher pressure may explain the trend from basalt to basaltic andesite to andesite suggested on the oliv-cpx-qtz projection, by early crystallization of oliv+plag+augite along a hypothetical

18(a) Compositions of samples from Puyehue Volcano projected on the oliv-cpx-SiO_2 pseudoternary as in Figure 12a.

(b) Compositions of basaltic andesites from Puyehue Volcano projected on the oliv-cpx-SiO_2 pseudoternary. Curves labelled (1) and (2) represent two possible compositional paths of residual liquids produced by fractional crystallization of low-SiO_2 basaltic andesites, as discussed in text.

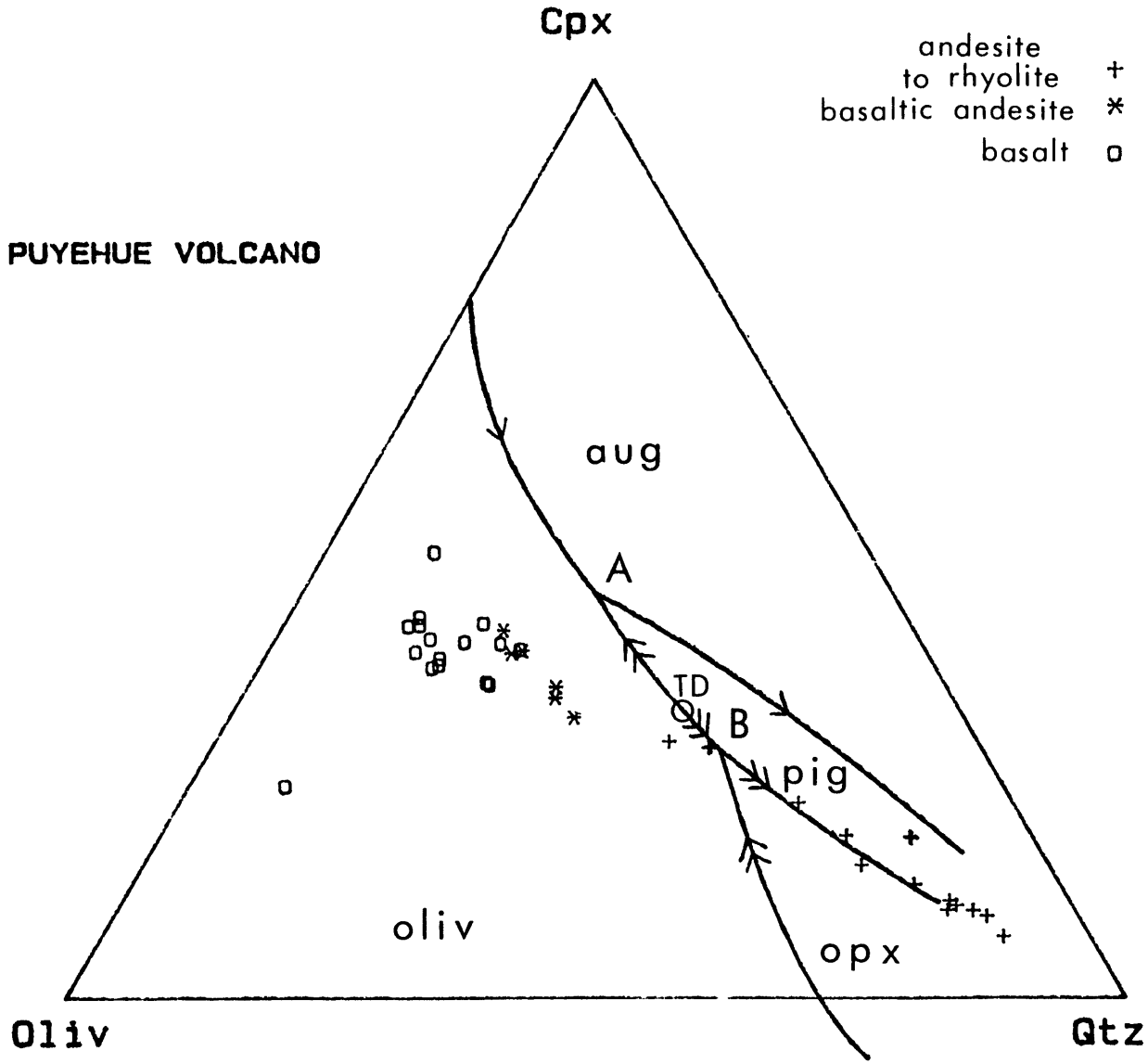
Cpx
andesite to rhyolite +
basaltic andesite *
basalt o
PUYEHUE VOLCANO
aug
A
TD
B
pig
oliv
opx
Oliv
Qtz

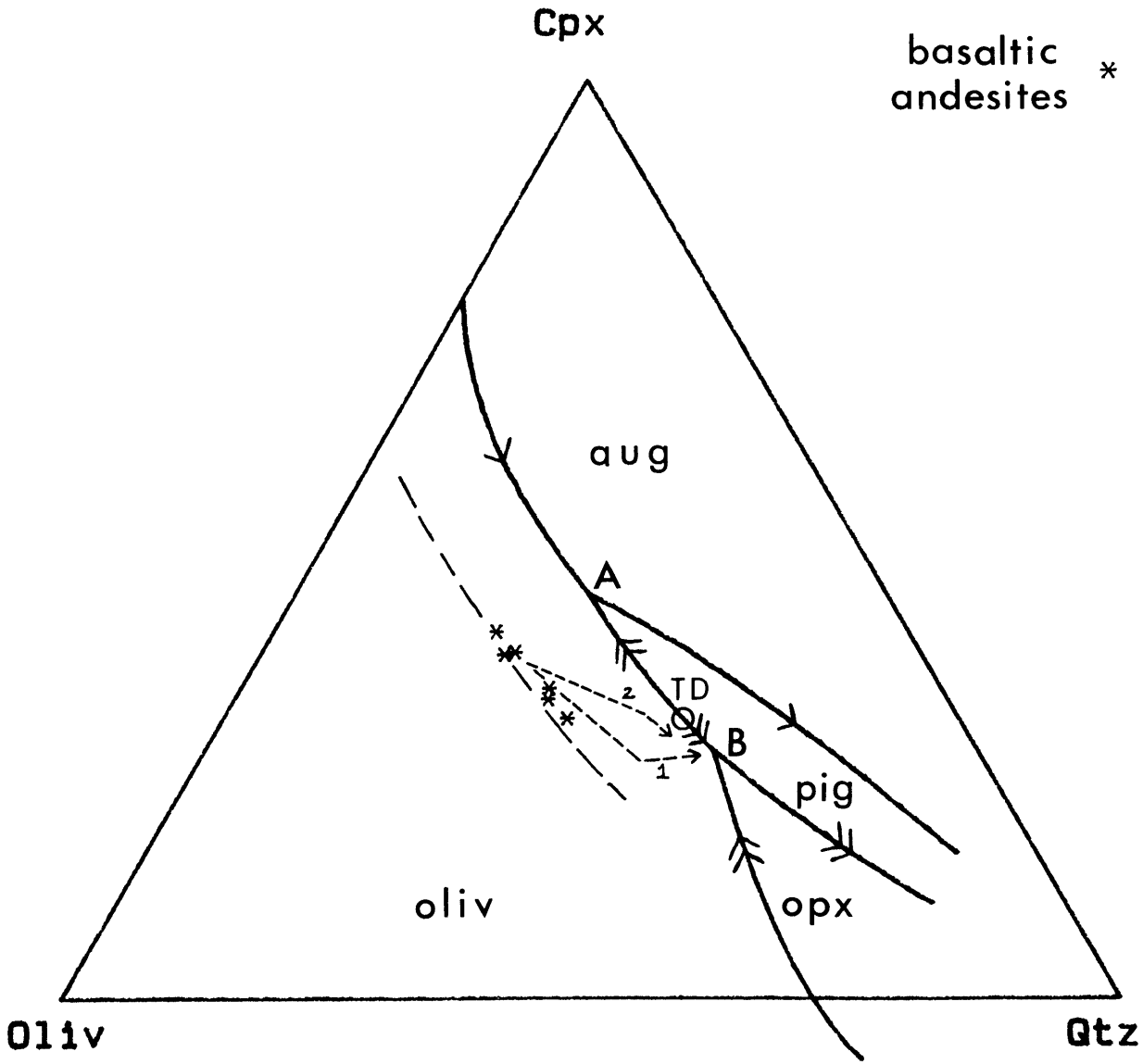
Cpx
basaltic
andesites
*
aug
A
TD
B
pig
opx
oliv
2
1
Oliv
Qtz

high-pressure cotectic thus avoiding reaction point A (Grove and Baker, 1984). This could produce basaltic andesites with projected compositions as represented by those sampled, however these liquids would not be as enriched in incompatible trace element abundances, a problem discussed earlier when attempting to relate the basaltic andesites to various basalts as parental magmas.

The basaltic andesites as projected in Figure 18a may coincide with an oliv-cpx-plag cotectic which is more appropriate at moderate pressures, and which may be subparallel to the 1-atm oliv-cpx-plag cotectic (Fig. 18b), as predicted by Grove and Baker (1984). Fractional crystallization of these basaltic andesites at low pressures (near 1-atm) would drive compositions of residual liquids toward the olivine-pig-plag reaction curve and into the pigeonite-plagioclase phase field. This could occur if magmas of basaltic andesite composition are transferred to a low-pressure environment after their generation at relatively higher pressures by fractional crystallization of basaltic magma. It is also possible that fractional crystallization of basaltic andesites continued at the same location or the same magma reservoir at moderate pressures, and the crystallizing assemblage would consist of oliv+augite+plag ±magnetite. This assemblage may occur at pressures of 2kb<P<5kb based on experimental results under anhydrous conditions (Takahashi and Kushiro, 1983; M. Baker, pers. comm.). These pressures may be above the stability range of pigeonite, and liquids of basaltic andesite to andesitic compositions are not saturated with pigeonite.

Fractional crystallization models were tested assuming basaltic andesite 138212 as a magma composition parental to the high-TiO_2, high-P_2O_5 andesites. P_2O_5 contents and to a lesser extent, TiO_2

contents, served as important criteria in determining the most appropriate samples which may be representative of parental magmas for the andesites. Abundances of incompatible trace elements and P_2O_5 contents in high-TiO_2, high-P_2O_5 andesites 220283-5 and 43821 are enriched three to four times above abundances in the basalts. However, the basalts are variable such that no one basalt may represent an appropriate parental magma, e.g., some basalts such as 220283-1 are sufficiently high in REE to generate the observed REE abundances in the andesites by approximately 60% fractional crystallization, however Th and P_2O_5 contents would require 70%-80% fractional crystallization. Examining basaltic andesites as potential parental magmas to andesites may result in more precise determination of liquid line(s) of descent. A basaltic andesite such as 272826b is characterized by incompatible trace element abundances requiring 50% fractional crystallization, i.e., a two-fold increase, if it is parental to the andesites. However the andesites (P_2O_5 = 0.63-0.68 wt.%) contain more than six times the P_2O_5 content in basaltic andesite 272826b. Basaltic andesites such as 138212 are sufficently high in incompatible trace elements and P_2O_5 (also assumed to be incompatible) such that these elements are uniformly enriched about two times in the andesites, and these basaltic andesites are the best candidates for parental magmas in discussing the compositional liquid line of descent leading to the andesites. High-TiO_2, high-P_2O_5 basaltic andesites such as 138212 ($^{87}Sr/^{86}Sr$ = 0.70405) are also isotopically similar to the high-TiO_2, high-P_2O_5 andesites such as 220283-5 ($^{87}Sr/^{86}Sr$ = 0.70407). Models involving other basaltic andesites and most basalts require extra complexities such as crustal contamination to serve as parental magma representatives.

Results of one of two fractional crystallization model calculations (Table 10a) are based on a crystallization scheme with a first stage at moderate pressure followed by further fractional crystallization at relatively low pressure. Fractional crystallization of predominantly plagioclase with subequal proportions of olivine and augite will drive residual liquids in a direction subparallel to the hypothetical cotectic represented in Figure 18b. At lower pressures (however, > 1 atm), the olivine phase field expands, and fractional crystallization of a slightly different assemblage with clinopyroxene subordinate to olivine (25% oliv, 10% cpx, 55% plag, 10% mag) will drive compositions of residual liquids towards point B. Except for MgO, P_2O_5 contents, and Th, Ni, Sr, Sc, and Cr abundances, an andesitic residual liquid roughly similar to andesite 220283-5 is produced (Table 10a, Fig. 19a). However, CaO/Al_2O_3 ratios are too high in this modelled residual liquid. A significantly better match of CaO/Al_2O_3 ratios and most elements in general is observed for a second fractional crystallization model outlined in Table 10b and Figure 19b. The first stage of this model involves subequal proportions of olivine, plagioclase, and clinopyroxene and is the same as in Table 10a. In the second stage, the proportion of clinopyroxene was arbitrarily increased at the expense of olivine. In contrast to the second stage of the model in Table 9a, this second stage develops while the magma is under constant moderate pressure (2-5 Kb), rather than a low-pressure second stage. Both models are capable of producing andesitic liquids which project near reaction point B, and approximate compositional paths of residual liquids for these two models are illustrated and compared in Figure 18b. However, the model addressed in Table 10b occurs at moderate pressures where the 1-atm phase relations no

19 Calculated major-element contents and trace element abundances normalized to observed values for two models of the derivation of andesite 220283-5 from basaltic andesite by fractional crystallization. Normalized results in (a) correspond to a two-stage moderate pressure to low pressure model (Table 10a, Figure 18b), and those in (b) correspond to a moderate pressure fractional crystallization scheme (Table 10b, Figure 18b).

a.
b.
calculated / observed andesite (220283-5)
0.6
1.0
1.4
1.8
SiO2
Al2O3
TiO2
FeO
MnO
MgO
CaO
Na2O
K2O
P2O5
La
Sm
Yb
Th
Hf
Zr
Nb
Rb
Ba
Sr
Sc
Ni
Cr

Table 10a

Fractional crystallization model:
basaltic andesite to andesite

	138212	F (fraction of residual liquid) .81	.67	.58	220283-5	43821
[1]SiO_2	53.06	54.14	56.39	58.45	58.96	58.74
Al_2O_3	16.56	16.17	15.85	15.59	15.62	15.63
TiO_2	1.32	1.61	1.55	1.50	1.47	1.59
FeO	9.78	10.42	9.34	8.22	8.45	8.82
MnO	0.18	0.21	0.24	0.27	0.22	0.20
MgO	5.61	4.40	3.28	2.37	2.84	2.59
CaO	9.12	8.17	7.86	7.61	6.09	6.00
Na_2O	3.24	3.56	3.85	4.11	4.23	4.28
K_2O	0.85	1.06	1.26	1.45	1.48	1.46
P_2O_5	0.26	0.32	0.39	0.44	0.63	0.69
[2]La	12.9	15.9	19.0	21.9	22.5	23.7
Sm	4.66	5.67	6.80	7.80	7.93	7.80
Yb	2.79	3.39	4.05	4.64	4.07	4.30
Hf	2.88	3.53	4.24	4.88	4.87	4.50
Sc	35	41.	48	54	28.	28
Zr	123	151.	180	205	192.	194
Th	2.24	2.76	3.33	3.84	4.56	4.35
Nb	3.8	4.7	5.5	6.3	5.6	6.8
Rb	18.3	22.6	27.2	31.4	35.1	35.1
Sr	397	411.	424	435	378.	381
Ba	271	331.	394	450	446.	443
Ni	52	20	5	1	8	12.
Cr	108	105	7	<1	18.5	10.
FeO^*/MgO	1.74	2.37	2.85	3.47	2.98	3.40
CaO/Al_2O_3	0.551	0.505	0.496	0.488	0.390	0.384
[2]La/Sm	2.77	2.80	2.80	2.80	2.84	3.04
Ba/Rb	14.8	14.6	14.5	14.3	12.7	12.6
Ba/Th	121	120	118	117	97.8	102
Zr/Sm	26.4	26.6	26.5	26.3	24.2	24.9
proportions:						
oliv:		20%	25%	25%		
cpx:		25%	10%	10%		
plag:		55%	55%	55%		
mag:		-	10%	10%		
[3]compositions:						
oliv(Fo%)		71	66	62		
cpx(En%)		42	39	38		
plag(An%)		60	56	52		

[1] total iron as FeO, analysis normalized to 10 %
[2] calculated with low values for partition coefficients (Table 7)
[3] K_{plag}^{Na-Ca} of 1.3, K_{oliv}^{Fe-Mg} of 0.32, and K_{aug}^{Fe-Mg} of 0.25 were assumed. D_{Mn}^{oliv} was assumed to be 1.0.

Table 10b

Fractional crystallization model:
basaltic andesite to andesite

		F (fraction of residual liquid)				
	138212	.81	.66	.55	220283-5	43821
[1]SiO_2	53.06	54.14	56.16	58.27	58.96	58.74
Al_2O_3	16.56	16.17	16.01	15.95	15.62	15.63
TiO_2	1.32	1.61	1.53	1.44	1.47	1.59
FeO	9.78	10.42	9.73	8.89	8.45	8.82
MnO	0.18	0.21	0.24	0.27	0.22	0.20
MgO	5.61	4.40	3.68	2.97	2.84	2.59
CaO	9.12	8.17	7.04	5.93	6.09	6.00
Na_2O	3.24	3.56	3.92	4.25	4.23	4.28
K_2O	0.85	1.06	1.29	1.55	1.48	1.46
P_2O_5	0.26	0.32	0.39	0.48	0.63	0.69
[2]La	12.9	15.9	19.2	23.1	22.5	23.7
Sm	4.66	5.67	6.82	8.11	7.93	7.80
Yb	2.79	3.39	4.06	4.81	4.07	4.30
Hf	2.88	3.53	4.27	5.12	4.87	4.50
Sc	35	41.	48	55	28.	28
Zr	123	151.	181	215	192.	194
Th	2.24	2.76	3.37	4.06	4.56	4.35
Nb	3.8	4.7	5.5	6.6	5.6	6.8
Rb	18.3	22.6	27.6	33.2	35.1	35.1
Sr	397	411.	431	453	378.	381.
Ba	271	331.	398	476	446.	443.
Ni	52	20	7	2	8	12.
Cr	108	105	4	<1	18.5	10.
FeO^*/MgO	1.74	2.37	2.64	2.99	2.98	3.40
CaO/Al_2O_3	0.551	0.505	0.440	0.372	0.390	0.384
[2]La/Sm	2.77	2.80	2.82	2.85	2.84	3.04
Ba/Rb	14.8	14.6	14.4	14.3	12.7	12.6
Ba/Th	121	120	118	117	97.8	102
Zr/Sm	26.4	26.6	26.5	26.5	24.2	24.9
proportions:						
oliv:		20%	10%	10%		
cpx:		25%	30%	30%		
plag:		55%	50%	50%		
mag:		-	10%	10%		
[3]compositions:						
oliv(Fo%)		71	67	65		
cpx(En%)		42	41	40		
plag(An%)		60	56	51		

1 total iron as FeO, analysis normalized to 100%
2 calculated with low values for partition coefficients (Table 1-7)
3 K_{plag}^{Na-Ca} of 1.3, K_{oliv}^{Fe-Mg} of 0.32, and K_{aug}^{Fe-Mg} of 0.25 were assumed. D_{Mn}^{oliv} was assumed to be 1.0.

longer apply. In summary, the two models in Tables 10a and 10b may represent two extremes, of which that in Table 10b is relatively more successful. A third, and simpler model may be that single-stage fractional crystallization of an assemblage consisting of plagioclase, magnetite, and subequal proportions of clinopyroxene and olivine from basaltic andesite magma produces high-TiO_2, high-P_2O_5 andesitic liquids. There are no samples intermediate between the low-SiO_2 basaltic andesites such as sample 138212 and andesite 220283-5, and a relatively greater likelihood of any one of these three schemes cannot be addressed further.

It is certainly possible that magmas which may have been produced by mixing need not be erupted, in which case they may remain behind and undergo fractional crystallization. As discussed earlier, high-TiO_2, high P_2O_5 basaltic andesites such as 138212 appear to be produced by mixing of basaltic magma and high-TiO_2, high P_2O_5 andesitic magma. This suggests that either (1) these andesitic magmas were initially present and available as endmembers to derive the basaltic andesites by mixing, or (2) the basaltic andesites were not produced by magma mixing but by fractional crystallization of a basaltic magma not represented by any of the basalts sampled in this study. Projected compositions of basaltic andesites appear to lie on mixing lines between basaltic endmembers and more evolved endmembers ranging from andesite to rhyolite (Fig. 18a). In any case, the anomalously enriched basaltic andesites are the most likely magmas parental to the high-TiO_2, high-P_2O_5 andesites. The enriched basaltic andesites, although represented by only a few samples, may represent a major intermediate magma type in the evolution of Puyehue Volcano in that they essentially link the basalts and andesites. The

suggested origin of the enriched basaltic andesites by predominantly magma mixing is a further demonstration of the conclusions of Grove et al. (1982) and Grove and Baker (1984), based on low-pressure phase equilibria, that magma mixing is a major process in producing intermediate to silicic lavas in many calcalkaline volcanic suites. In the present study, magma mixing was apparently significant in producing magmas parental to more evolved lavas.

8.2 Andesites to rhyolites

Lavas ranging in composition from andesites to rhyolites plot along the opx-pig-plag reaction curve (Fig. 20a) as projected in the oliv-cpx-qtz pseudoternary taken from Grove et al., (1983). Suites of calcalkaline (Medicine Lake Volcano) and transitional tholeiitic/calcalkaline (Witu Islands, cf. Johnson and Arculus, 1978) suites selected for discussion by Grove and Baker (1984) do not clearly display this trend.

The trend of evolved Puyehue lavas along the opx-pig-plag reaction curve is only coincidental, since textural and compositional data for phenocrysts in the silicic lavas do not support this, i.e., pigeonite phenocrysts are not observed in andesites to rhyodacites. As shown in Figure 20b, projected compositions of andesites to rhyolites do not coincide with the plag-pig-aug reaction curve. Andesites 43821 and 220283-5 discussed in the last section, are more likely representatives of magma parental to dacites, rhyodacites, and rhyolites, rather than the mixed andesites 272822 and 242824. Andesites 43821 and 220283-5 are aphyric and provide no evidence of phases involved in fractional crystallization. Augite, orthopyroxene, pigeonite, plagioclase, and

20(a) Compositions of andesites to rhyolites from Puyehue Volcano, and of rhyodacites and rhyolites from Cordon Caulle projected on the oliv-cpx-qtz pseudoternary, as in Figure 12a.

(b) Compositions of Puyehue andesites to rhyolites, and Cordon Caulle rhyodacites and rhyolites projected on the oliv-plag-qtz pseudoternary with 1-atm augite-saturated cotectics after Grove et al. (1982, 1983).

(c) A series of oliv-cpx-qtz pseudoternary projections for dacite 212826 (opx+aug phenocrysts) and rhyolite 202825c (aug+pig phenocrysts) with hypothetical phase equilibria for varying conditions based on data of Grove et al. (1982, 1983), Spulber and Rutherford (1983), Takahashi and Kushiro (1983), and M. Baker (pers. comm.).

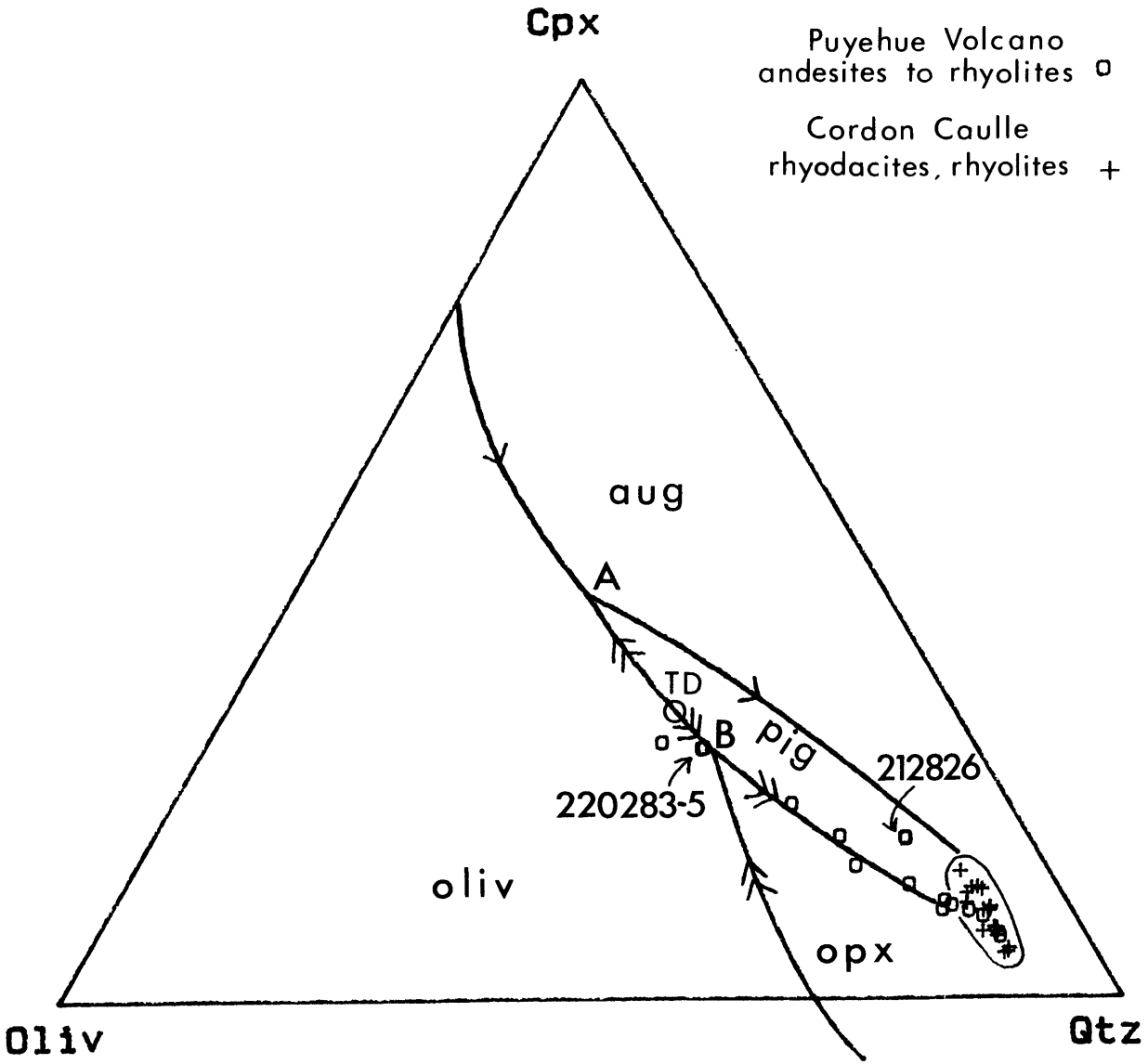
Cpx
Puyehue Volcano
andesites to rhyolites
Cordon Caulle
rhyodacites, rhyolites
aug
A
TD
B
pig
212826
220283-5
oliv
opx
Oliv
Qtz

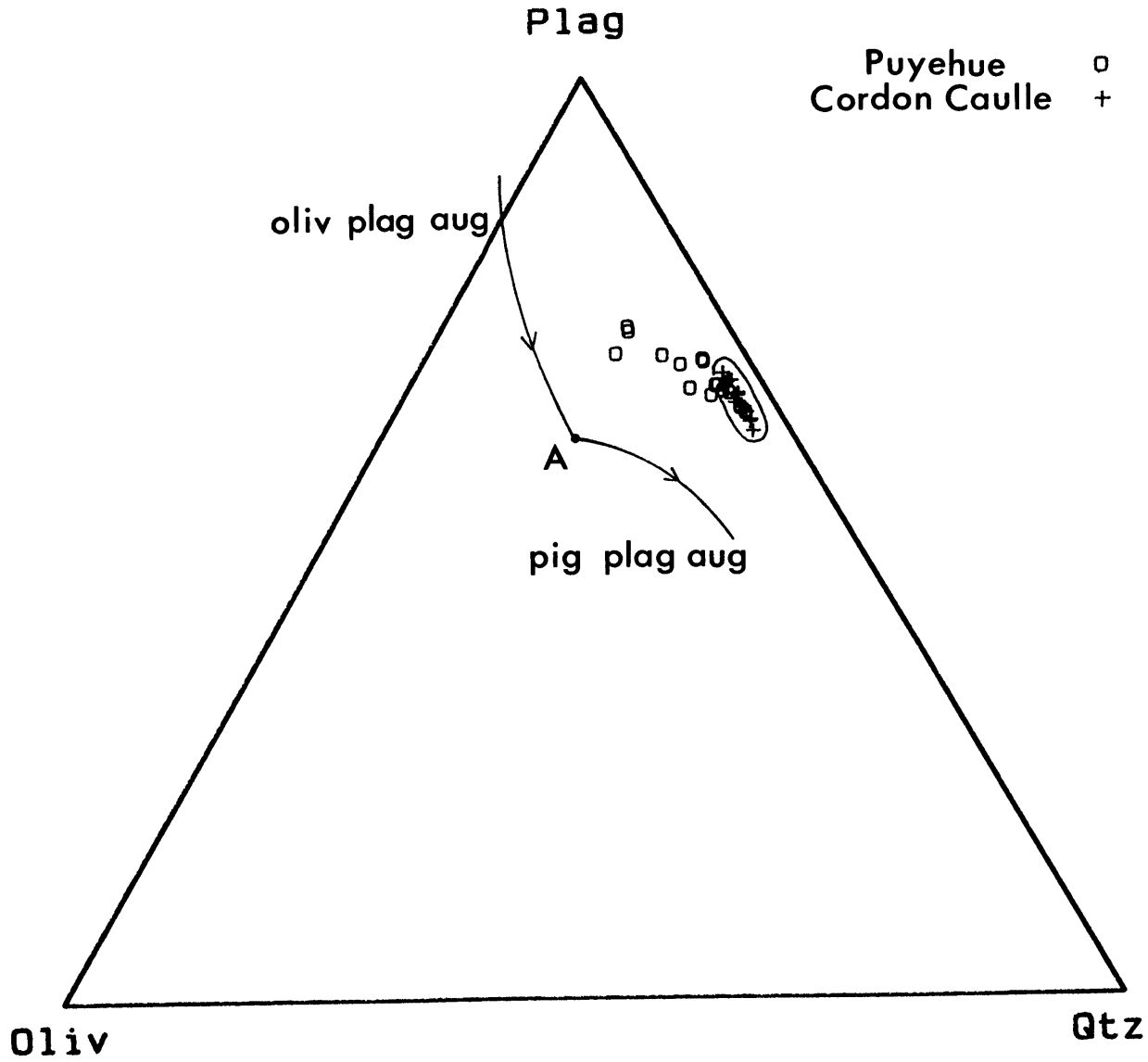
Plag
Puyehue
Cordon Caulle
oliv plag aug
A
pig plag aug
Oliv
Qtz

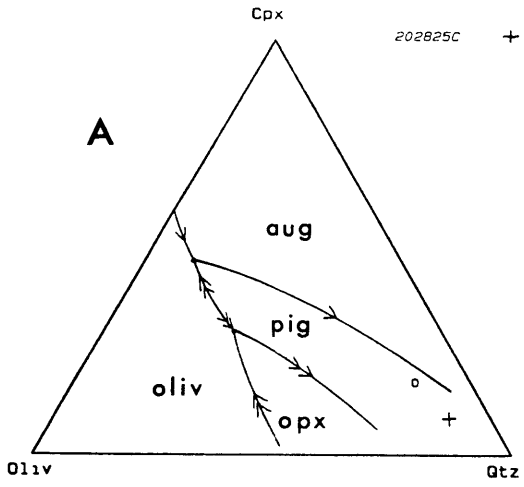

$P_{tot} \approx 2$ kb

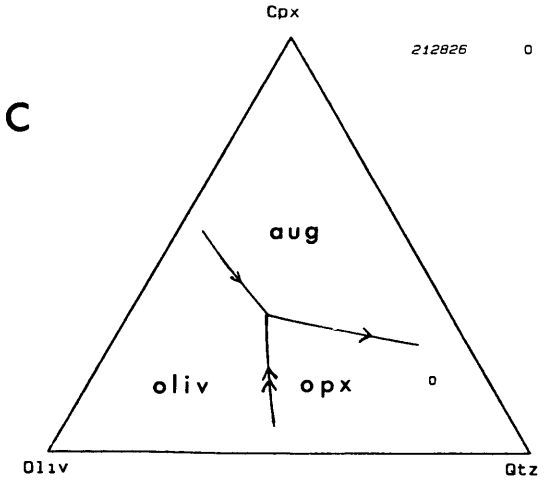

$2\text{ kb} < P_{tot} < 5\text{ kb}$

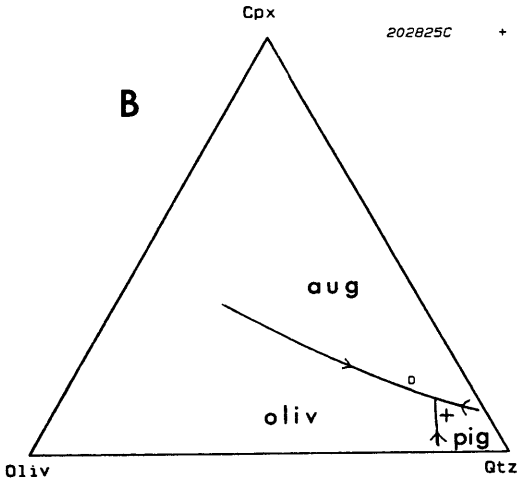

$P_{tot} \approx 1$ kb

$P_{H_2O} \leq P_{tot}$

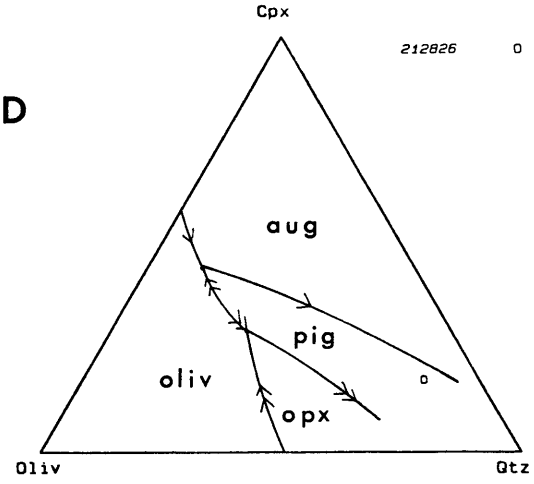

$P_{tot} \approx 2$ kb

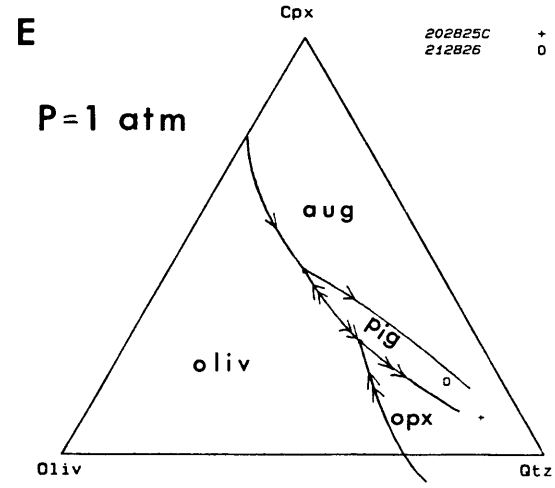

magnetite are phenocryst phases in dacites, rhyodacites, rhyolites, and mixed andesites, and are likely phases for consideration of a model of fractional crystallization of andesitic magma in derived more evolved, silicic lavas. The types of phenocrysts and particular phenocryst assemblages observed in specific samples may provide clues concerning the pressures under which crystallization occurred and the relevant phase equilibria at these pressures.

Fractional crystallization of andesitic magma at low pressures near 1 atm may commence with a short interval of plag+oliv±magnetite fractional crystallization. This would drive compositions of residual liquids to either the plag-pig-oliv reaction curve or the plag-opx-oliv reaction curve. Residual liquid composition would then proceed through the plag-pig phase volume to the plag-aug-pig cotectic, or first through the opx-plag primary phase volume to the opx-pig-plag reaction curve, then across the pig-plag phase volume to the pig-aug-plag cotectic (Grove et al., 1983; Grove and Baker, 1984). Discrete phenocrysts of pigeonite, or phenocrysts of orthopyroxene mantled by rims of pigeonite or augite might be observed in lavas produced by such a fractional crystallization sequence. This is not clearly indicated by phenocrysts in the evolved lavas. In dacites, particularly sample 212826, coexisting augite and orthopyroxene are nearly homogeneous in composition (Fig. 5a) and are observed in clusters with plagioclase and magnetite. If these clusters represent a cognate crystallizing equilibrium assemblage in the host lava or a slightly less silicic lava, this is not in accordance with 1-atm phase equilibria (E in Fig. 20c). Instead, this crystallizing assemblage may be characteristic of moderate pressures in the absence of a pigeonite stability field as illustrated in C in Figure 20c.

Clinopyroxene phenocrysts in rhyolite 202825c are relatively iron-rich and display patchy zones or intergrowths of calcic and subcalcic ferroaugite, and pigeonite (section 3.3.4). These phenocrysts may have crystallized under conditions of varying P_{H_2O} or total pressure. If the ferroaugite phenocrysts in 202825c were crystallizing under anhydrous conditions between 2 Kb to 5 Kb total pressure (Fig. 20c), a gradual or sudden change to lower pressures (e.g., C to D to E, Fig. 20c) will result in pigeonite crystallization as shown by the projected composition of 202825c plotting approximately in the low-pressure (1 atm to 2 Kb) pigeonite phase field (E in Fig. 20c). Alternatively, a change from moderate pressures and anhydrous conditions to low pressures (~ 1 Kb) and relatively higher P_{H_2O} (C to B, Fig. 20c) will also stabilize pigeonite. An additional possibility is that augite and pigeonite phenocrysts in rhyolite 202825c initially crystallized at ~ 1 Kb under water-undersaturated conditions and that outgassing of H_2O prior to eruption effectively changes conditions whereby 1-atm anhydrous-basis phase equilibria apply and pyroxene phenocrysts would react to this change in conditions (B to E in Fig. 20c). Any of the above processes may explain the complex intergrowths or zones observed in the pyroxene phenocrysts of rhyolite 202825c.

If an andesitic magma with a projected composition at point B represents a common parental magma to all relatively more evolved lavas, differing proportions of orthopyroxene, pigeonite, or clinopyroxene in crystallizing assemblages will drive compositions of residual liquids in directions which are a function of these relative proportions. For example, the projected composition of dacite 212826 falls slightly above the main 'trend' that mimics the 1-atm opx-pig-plag reaction curve and

plots in the pigeonite phase volume (Fig. 20a). This sample may have been produced by fractional cyrstallization of andesite with a crystallizing assemblage relatively higher in orthopyroxene relative to assemblages leading to other dacite or rhyodacite projected compositions which plot nearer the 1-atm opx-pig-plag reaction curve. An alternative explanation for the apparent overall trend of silicic Puyehue lavas along the low-pressure opx-pig-plag reaction curve may be that this overall trend generally reflects near-constant proportions of subcalcic pyroxenes and calcic pyroxenes removed by fractional crystallization at relatively higher pressures. For example, fractional crystallization of augite and pigeonite from andesitic magma would drive liquid compositions on a trajectory away from augite and pigeonite compositions as projected in the oliv-cpx-qtz pseudoternary, and this trajectory may mimic the pig-aug-plag boundary determined by Spulber and Rutherford (1983), and the 1-atm anhydrous opx-pig-plag reaction curve determined by Grove et al. (1982, 1983), (cf., Fig. 20a and 20c). Thus, the compositional trend of evolved lavas projected on the oliv-cpx-SiO_2 pseudoternary is not necessarily indicative of equilibrium crystallization at low pressures (1-atm).

Other experimental studies (Eggler, 1972; Merzbacher and Eggler, 1984) suggest that clinopyroxene and orthopyroxene are coexisting equilibrium phases in silicic lavas at very low pressures. This is suggested by dacitic and rhyodacitic liquids assumed to be in equilibrium with plag+cpx+opx+magnetite in recent 1 atm anhydrous experiments by Merzbacher and Eggler (1984). This conflicts with the experimental results of Grove et al. (1982, 1983) which suggest that orthopyroxene and pigeonite are in reaction relationship and that a pigeonite primary phase

volume lies between orthopyroxene and augite primary phase volumes at 1 atm. Although observed 2-pyroxene phenocryst assemblages in silicic lavas from Puyehue Volcano and many other calcalkaline suites may support the experimental results of Merzbacher and Eggler (1984), experiments in this study may not have been conducted at sufficiently long enough run times to achieve near-equilibrium conditions or at least nucleation and growth of pigeonite, compared to the studies conducted by Grove et al. (1982, 1983).

Fractional crystallization of andesitic magma represented by sample 220283-5 approximately reproduces the liquid line of descent represented by dacites, rhyodacites, and rhyolite. Fractional crystallization of assemblages consisting of plagioclase, augite, orthopyroxene, magnetite, ilmenite, and apatite approximate the major-element compositions of the silicic lavas (Tables 11a and 11b). Dacites such as sample 212826 may represent residual liquids after 40-45% fractional crystallization, while rhyodacites such as 172822b and rhyolite 202825c may represent residual liquids after 45-50% and 55-60% fractional crystallization respectively. Ratios of FeO*/MgO and CaO/Al_2O_3 in the model calculations are similar to those observed in the dacites to rhyolites. Ranges of calculated compositions of plagioclase, orthopyroxene, and to a lesser degree augite, based on experimentally determined exchange K_D's, are similar to those of the phenocrysts analyzed in the silicic lavas.

Fractional crystallization models with andesite 220283-5 as a parental magma are presented in Tables 11a through 11c. Proportions of plagioclase (57-58%), clinopyroxene (15-17%), orthopyroxene (15%), magnetite (6-10%), and apatite (3%), are similar in two models which differ mainly in the absence or inclusion of ilmenite in the

Table 11a

Fractional crystallization model: andesite to rhyolite

	F (fraction of residual liquid)					analyses for comparison			
	220283-5	.67	.59	.53	.49	230283-3	212826	172822b	202825c
[1]SiO_2	58.96	65.02	67.03	69.03	70.64	65.17	66.77	68.32	70.74
Al_2O_3	15.62	14.67	14.36	14.17	13.99	15.29	14.44	14.62	13.98
TiO_2	1.47	1.23	1.12	1.04	0.96	0.64	0.98	0.65	0.41
FeO	8.45	6.33	5.37	4.45	3.59	5.64	5.60	5.29	4.28
MnO	0.22	0.19	0.18	0.18	0.17	0.16	0.16	0.16	0.13
MgO	2.84	1.62	1.20	0.84	0.55	1.70	0.97	0.45	0.28
CaO	6.09	3.71	3.19	2.40	1.94	4.23	3.26	2.64	2.02
Na_2O	4.23	4.79	4.91	5.01	5.07	4.73	5.28	5.19	5.29
K_2O	1.48	2.24	2.53	2.81	3.05	2.31	2.25	2.51	2.76
P_2O_5	0.63	0.21	0.11	0.04	0.02	0.13	0.29	0.16	0.10
[2]La	22.5	29.1	31.6	33.8	35.6		29.4	29.5	33.4
Sm	7.93	8.85	9.16	9.43	9.64		8.67	8.35	9.17
Yb	4.07	5.13	5.52	5.87	6.14		5.74	5.69	6.41
Hf	4.87	6.86	7.64	8.38	8.96		6.78	7.55	8.20
Sc	28.0	20.7	18.8	17.3	16.3		19.3	17.4	14.9
Zr	192.	270	301	330	352	305.	301	332	370
Th	4.56	6.67	7.53	8.34	8.99		6.60	7.32	8.25
Nb	5.6	8.1	9.1	10.1	10.8	8.3	9.0	9.3	10.1
Rb	35.1	52.2	59.2	65.8	71.1		56.5	65.0	68.3
Sr	378.	278	252	232	219	268	230.	234	161.
Ba	446.	610	674	733	780	613	634.	684	780.
FeO^*/MgO	2.98	3.91	4.48	5.30	6.53	3.32	5.77	11.8	15.3
CaO/Al_2O_3	0.390	0.253	0.222	0.169	0.139	0.277	0.226	0.181	0.145
[2]La/Sm	2.84	3.29	3.45	3.58	3.69	-	3.39	3.53	3.64
Ba/Rb	12.7	11.7	11.4	11.1	11.0	-	11.2	10.5	11.4
Ba/Th	97.8	91.5	89.5	87.9	86.8	-	96.1	90.6	94.5
Zr/Sm	24.2	30.5	32.9	35.0	36.5		34.7	39.8	40.3
Zr/Nb	34.3	33.3	33.1	32.7	32.6	36.7	33.4	35.7	36.6

cpx: plag: opx: mag: apat = 0.15/0.57/0.15/0.10/0.03

[3]compositions				
opx(En%)	55	54	52	50
cpx(En%)	37	36	35	33
plag(An%)	46	42	38	34

[1] total iron as FeO, analysis normalized to 100%
[2] calculated with high values for partition coefficients (Table 7)
[3] K_{plag}^{Na-Ca} of 1.1, K_{aug}^{Fe-Mg} of 0.25, and K_{opx}^{Fe-Mg} of 0.27 were assumed.

Table 11b

Fractional crystallization model: andesite to rhyolite

		F (fraction of residual liquid)				analyses for comparison			
	220283-5	.67	.57	.50	.45	230283-3	212826	172822b	202825c
[1]SiO_2	58.96	64.44	66.98	69.05	70.83	65.17	66.77	68.32	70.74
Al_2O_3	15.62	14.59	14.19	13.93	13.73	15.29	14.44	14.62	13.98
TiO_2	1.47	1.13	0.96	0.80	0.65	0.64	0.98	0.65	0.41
FeO	8.45	7.27	6.42	5.58	4.70	5.64	5.60	5.29	4.28
MnO	0.22	0.19	0.18	0.17	0.15	0.16	0.16	0.16	0.13
MgO	2.84	1.64	1.12	0.74	0.44	1.70	0.97	0.45	0.28
CaO	6.09	3.53	2.51	1.74	1.18	4.23	3.26	2.64	2.02
Na_2O	4.23	4.76	4.90	4.97	4.95	4.73	5.28	5.19	5.29
K_2O	1.48	2.23	2.64	2.98	3.31	2.31	2.25	2.51	2.76
P_2O_5	0.63	0.21	0.09	0.02	0.01	0.13	0.29	0.16	0.10
[2]La	22.5	29.1	32.2	35.0	37.5		29.4	29.5	33.4
Sm	7.93	8.83	9.22	9.54	9.81		8.67	8.35	9.17
Yb	4.07	5.12	5.61	6.05	6.42		5.74	5.69	6.41
Hf	4.87	6.81	7.80	8.70	9.51		6.78	7.55	8.20
Sc	28.0	20.6	18.1	16.4	15.1		19.3	17.4	14.9
Zr	192.	267	306	341	372	305.	301	332	370
Th	4.56	6.67	7.78	8.82	9.75		6.60	7.32	8.25
Nb	5.6	8.1	9.4	10.6	11.7	8.3	9.0	9.3	10.1
Rb	35.1	52.2	61.2	69.7	77.4		56.5	65.0	68.3
Sr	378.	275	242	218	200	268	230.	234	161.
Ba	446.	609	691	765	830	613	634.	684	780.
FeO^*/MgO	2.98	4.43	5.73	7.54	10.7	3.32	5.77	11.8	15.3
CaO/Al_2O_3	0.390	0.242	0.177	0.125	0.086	0.277	0.226	0.181	0.145
[2]La/Sm	2.84	3.30	3.49	3.67	3.82	-	3.39	3.53	3.64
Ba/Rb	12.7	11.7	11.3	11.0	10.7	-	11.2	10.5	11.4
Ba/Th	97.8	91.3	88.8	86.7	85.1	-	96.1	90.6	94.5
Zr/Sm	24.2	30.2	33.2	35.7	37.9		34.7	39.8	40.3
Zr/Nb	34.3	33.0	32.6	32.2	31.8	36.7	33.4	35.7	36.6

cpx: plag: opx: ilm: mag: apat = 0.165/0.58/0.146/0.06/0.02/0.03

[3]compositions				
opx(En%)	55	53	51	49
cpx(En%)	36	35	33	31
plag(An%)	45	39	33	28

1 total iron as FeO, analysis normalized to 100%
2 calculated with high values for partition coefficients (Table 7)
3 K_{plag}^{Na-Ca} of 1.1, K_{aug}^{Fe-Mg} of 0.25, and K_{opx}^{Fe-Mg} of 0.27 were assumed.

Table 11c

Fractional crystallization model: andesite to rhyolite

	F (fraction of residual liquid)				analyses for comparison		
	220283-5	.56	.50	.45	212826	172822b	202825c
[1]SiO_2	58.96	66.72	68.57	70.73	66.77	68.32	70.74
Al_2O_3	15.62	14.34	14.29	14.16	14.44	14.62	13.98
TiO_2	1.47	0.92	0.68	0.38	0.98	0.65	0.41
FeO	8.45	6.16	5.34	4.08	5.60	5.29	4.28
[2]MnO	0.22	0.17	0.16	0.15	0.16	0.16	0.13
MgO	2.84	0.97	0.65	0.32	0.97	0.45	0.28
CaO	6.09	3.04	2.47	2.09	3.26	2.64	2.02
Na_2O	4.23	4.72	4.73	4.74	5.28	5.19	5.29
K_2O	1.48	2.66	2.94	3.26	2.25	2.51	2.76
[3]P_2O_5	0.63	0.29	0.16	0.10	0.29	0.16	0.10
[4]La	22.5	33.9	36.4	39.7	29.4	29.5	33.4
Sm	7.93	10.4	10.8	11.6	8.67	8.35	9.17
Yb	4.07	5.99	6.40	6.97	5.74	5.69	6.41
Hf	4.87	7.93	8.65	9.53	6.78	7.55	8.20
Sc	28.0	18.2	16.9	15.6	19.3	17.4	14.9
Zr	192.	311	339	372	301	332	370
Th	4.56	7.98	8.83	9.89	6.60	7.32	8.25
Nb	5.6	9.6	10.6	11.8	9.0	9.3	10.1
Rb	35.1	62.3	69.1	77.6	56.5	65.0	68.3
Sr	378.	235.	217.	198.	230.	234	161.
Ba	446.	699.	759.	831.	634.	684	780.
FeO^*/MgO	2.98	6.35	8.22	12.8	5.77	11.8	15.3
CaO/Al_2O_3	0.390	0.212	0.173	0.148	0.226	0.181	0.145
[4]La/Sm	2.84	3.26	3.37	3.42	3.39	3.53	3.64
Ba/Rb	12.7	11.2	11.0	10.7	11.2	10.5	11.4
Ba/Th	97.8	87.6	86.0	84.0	96.1	90.6	94.5
Zr/Sm	24.2	29.9	31.4	32.1	34.7	39.8	40.3
Zr/Nb	34.3	32.4	32.0	31.5	33.4	35.7	36.6

phase proportions:

plag	.594	.576	.584
aug	.161	.137	.138
opx	.149	.166	.168
mag	.059	.059	.059
ilm	.019	.039	.039
apat	.019	.024	.012

[5]compositions

opx(En%)	50	44	37
cpx(En%)	32	28	25
plag(An%)	39	30	27

[6]calculated bulk D's:

La	0.54	0.97	<0
Sm	0.85	1.34	0.11
Yb	0.41	1.08	<0
Th	0.36	0.07	<0
Sr	1.86	0.84	4.5
Ba	0.39	0.32	<0

1 total iron as FeO, analysis normalized to 100%
2 calculated with assumed K_D^{Mn}'s: aug(3), opx(4), mag(5), and ilm(4).
3 apatite was assumed saturated in all liquids and proportions of apatite removed were calculated from P_2O_5 contents; thus, P_2O_5 contents of modelled analogous residual liquids were taken as analyzed values.
4 calculated with high values for partition coefficients (Table 8)
5 K_{plag}^{Na-Ca} of 1.3, K_{aug}^{Fe-Mg} of 0.26, and K_{opx}^{Fe-Mg} of 0.28 were assumed.
6 calculated for each interval of fractional crystallization using analyzed abundances.

crystallizing assemblage. A model with a small amount (2%) of ilmenite (Table 11b and a lower proportion of magnetite is more successful in that FeO*/MgO ratios increase more and TiO_2 contents are decreased more rapidly relative to the model in Table 11a. K_2O contents in model calculations are slightly higher than observed values, and this may be primarily due to the unrealistic exclusion of K_2O from calculated plagioclase compositions in the major-element models. The relative effects of ilmenite accompanied by a slightly greater proportion of augite (Table 11b) in the fractionating assemblage relative to a model lacking ilmenite (Table 11a) are compared in Figure 21 for fractions of residual liquids designed to reproduce the bulk composition of dacite 212826. FeO contents are high and CaO contents low in model liquids derived by ilmenite fractionation relative to the observed composition, while TiO_2 and MgO contents are high in model liquids relative to observed liquids for a fractionating assemblage lacking ilmenite (Figure 21). P_2O_5 contents in model liquids (Tables 11a, 11b) are lower than observed values. A smaller proportion (<3%) in the fractionating assemblage would reduce this descrepancy, though in order to maintain a reasonable match in modelled vs. observed REE abundances, higher partition coefficients for REE in apatite would be required. Those used (Table 8) are based on experimental studies in andesitic and granitic bulk compositions by Watson and Green (1981) and were considered reasonable. Based on more recent experiments by Harrison and Watson (1984) conducted at 8 Kb under water-undersaturated conditions, andesites (220283-5 and 43821) with 0.63 to 0.68 wt.% P_2O_5 are not saturated with apatite, despite estimates made earlier by Watson and Capobianco (1981) that andesites with 0.4 wt.% P_2O_5 may be saturated with apatite.

Nevertheless, apatite saturation may have occurred in the andesites especially at higher pressures (Watson, 1980) and indicated by decreasing P_2O_5 from andesites to rhyolites. An alternative calculation was carried out assuming that apatite is saturated in andesite to rhyolite and results are presented in Table 11c. The major-element compositions of dacite, rhyodacite, and rhyolite are similar to modelled residual liquids after 44%, 50%, and 55% fractional crystallization of andesitic magma, respectively. Proportions of apatite in the fractionating assemblage were then calculated using observed differences in P_2O_5 contents and it may be seen that the proportion of apatite varies (Table 11c). A larger proportion of ilmenite in fractionating assemblages from dacite to rhyolite is suggested by the rapidly decreasing TiO_2 contents. The relatively larger proportion of apatite from dacite to rhyodacite is consistent with the suppression of REE abundances from dacite to rhyodacite (Table 11c). The models presented in Table 11 represent the extremes that may be taken in modelling apatite fractionation in these silicic lavas.

Discrete phenocrysts of apatite are not observed in the andesites, which are aphyric, nor in dacites. If present, they would provide evidence that apatite was indeed a liquidus phase. Harrison and Watson (1981) determined that diffusion of P in silicic melts may be slow such that localized saturation of apatite may occur in the interface region between a growing crystal and host melt, and suggested that apatite fractionation may occur by this mechanism. This is supported by observations of small apatite inclusions in plagioclase and pyroxene phenocrysts in dacitic to rhyolitic lavas. Apatite saturation may occur in dacites to rhyodacites (0.29 to 0.16 wt.% P_2O_5) in the study suite based on the suggestion by Watson and Capobianco (1981) that felsic melts

21 Calculated major-element contents and trace element abundances normalized to observed values for two fractional crystallization models for the derivation of dacite 212826. Model in (a) corresponds to that in Table 11a, and (b) corresponds to model presented in Table 11b.

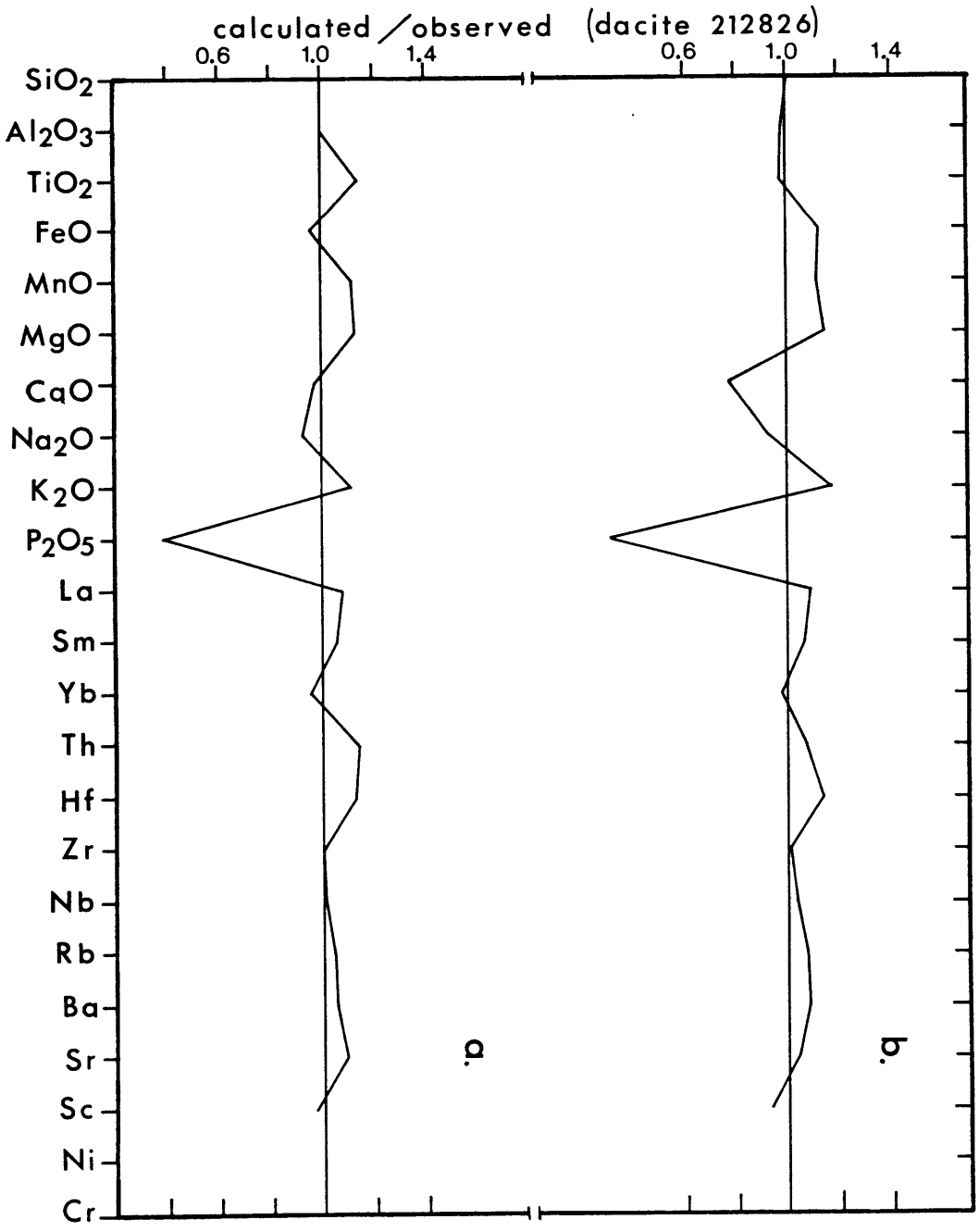
calculated / observed (dacite 212826)
0.6
1.0
1.4
0.6
1.0
1.4
SiO2
Al2O3
TiO2
FeO
MnO
MgO
CaO
Na2O
K2O
P2O5
La
Sm
Yb
Th
Hf
Zr
Nb
Rb
Ba
Sr
Sc
Ni
Cr
a.
b.

with 0.14 wt.% P_2O_5 may be saturated with apatite. It is possible that segregation of apatite in andesitic magma was chiefly accomplished by localized P_2O_5 saturation and crystallization of apatite as inclusions in major phenocryst minerals.

Based on major-element compositions (Tables 11a to 11c) samples 212826, 172822b, and 202825c may constitute a sequence of silicic lavas representing residual liquids produced by approximately 40-45%, 45-50%, and 50-55% fractional crystallization of andesitic magma respectively. Using observed abundances and estimated values of F, apparent bulk partition coefficients for selected trace elements were calculated (Table 12). If the proportions of all phases (plagioclase, augite, orthopyroxene, magnetite, and apatite) remain approximately constant, then calculated bulk D's for incompatible trace elements (La, Sm, Yb, Hf, Zr, Th, Nb, Rb, and Ba) should consistently increase from sample 212826 to 202825c, based on empirical studies (Mahood and Hildreth, 1983; Fujimaki et al., 1984) and experimental studies (e.g., Drake and Weill, 1975). This is not strictly observed for all of the above elements Tables 11c, 12), and may be due in part to analytical error or other problems related to assumptions in the fractional crystallization model. Enrichment factors calculated for most trace element abundances in the three representative silicic lavas (samples 212826, 172822b, and 202825c) ranging from dacite to rhyolite relative to the presumed parental andesite 220283-5 display increasing values (Table 12).

For the compositional interval ranging from dacites (212826) to rhyodacites (172822b) however, LREE (La) and HREE (Yb) abundances were buffered while MREE (Sm) abundances decreased, as indicated by plateaux or kinks in variations of REE vs. Th, Zr, and P_2O_5 for the compositional

Table 12

a. Calculated bulk partition coefficients for selected trace elements based on fractional crystallization models (Tables 10a and 10b)

	212826	172822b	202825c
	dacite	rhyodacite	rhyolite
estimated F	.57 - .59	.50 - .53	.45 - .49
La	0.49 - .0.52	0.57 - 0.61	0.45 - 0.51
Sm	0.84 - 0.85	0.92 - 0.93	0.79 - 0.81
Yb	0.35 - 0.39	0.47 - 0.51	0.37 - 0.44
Hf	0.38 - 0.41	0.31 - 0.37	0.27 - 0.35
Sc	1.66 - 1.70	1.69 - 1.75	1.80 - 1.89
Zr	0.15 - 0.20	0.14 - 0.21	0.08 - 0.18
Th	0.30 - 0.34	0.25 - 0.31	0.17 - 0.26
Nb	0.10 - 0.15	0.20 - 0.27	0.18 - 0.26
Rb	0.10 - 0.15	0.03 - 0.11	0.06 - 0.16
Sr	1.88 - 1.94	1.69 - 1.75	2.06 - 2.18
Ba	0.34 - 0.38	0.33 - 0.39	0.22 - 0.30

b. Enrichment factors relative to andesite 220283-5.

	212826	172822b	202825c
La	1.31	1.31	1.48
Sm	1.09	1.05	1.16
Yb	1.41	1.40	1.57
Hf	1.39	1.55	1.68
Sc	0.69	0.62	0.53
Zr	1.57	1.73	1.93
Th	1.45	1.61	1.81
Nb	1.61	1.66	1.80
Rb	1.61	1.85	1.95
Sr	0.61	0.62	0.43
Ba	1.42	1.53	1.75

22(a) Th, Zr, and P_2O_5 variation diagrams for selected trace element abundances in andesites to rhyolites from Puyehue Volcano.

(b) La/Sm, La/Yb, and Zr/Sm ratios vs. Th and P_2O_5 in dacites, rhyodacites, and rhyolites from Puyehue Volcano.

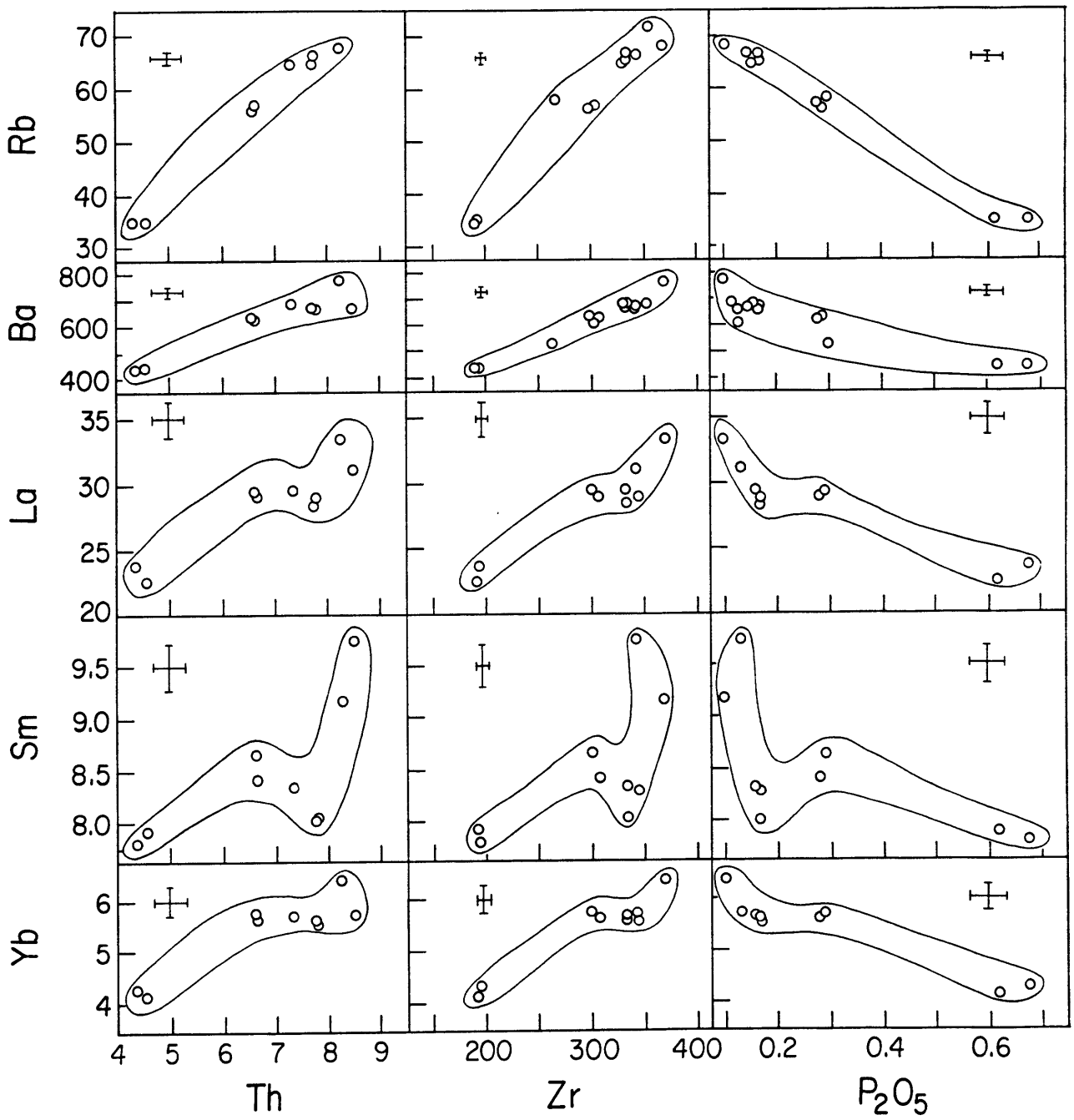
Rb
Ba
La
Sm
Yb
Th
Zr
P_2O_5
70
60
50
40
30
800
600
400
35
30
25
20
9.5
9.0
8.5
8.0
6
5
4
4 5 6 7 8 9
200 300 400
0.2 0.4 0.6

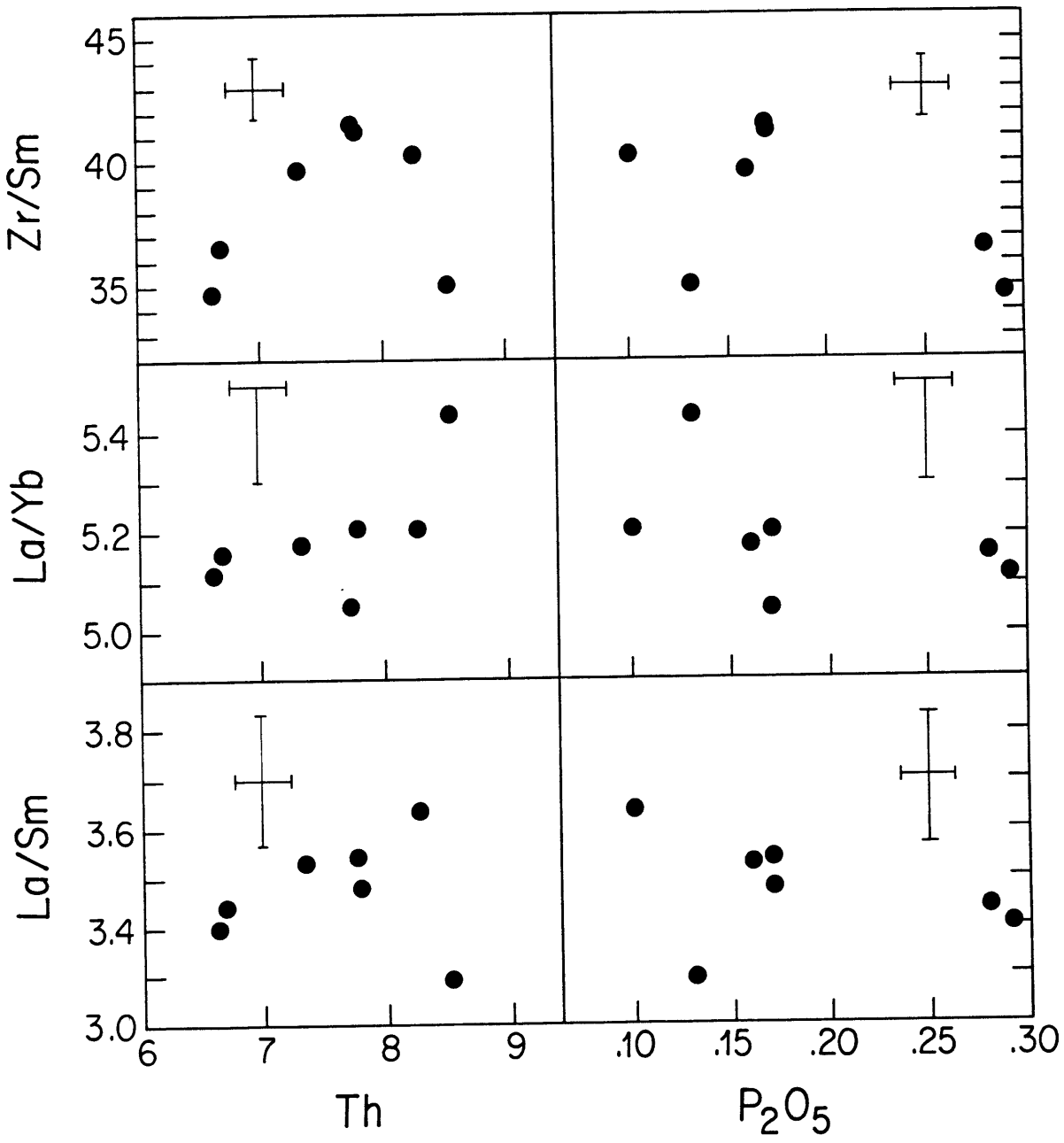
Zr/Sm
45
40
35
La/Yb
5.4
5.2
5.0
La/Sm
3.8
3.6
3.4
3.0
6
7
8
9
Th
.10
.15
.20
.25
.30
P2O5

interval andesites to rhyolites (Fig. 22a). Since partition coefficients for REE in apatite are high, the magnitude of bulk D^{REE} in silicic magmas is largely controlled by the relative proportions of apatite in crystallizing assemblages. High apparent bulk D^{REE} (Tables 11c, 12) and trends in Figure 22 suggest $D_{apat}{}^{REE}$ were considerably higher or the proportions of apatite in the fractionating assemblage and resulting bulk D^{REE} was higher in the compositional interval dacites to rhyodacites. Assuming that apatite was saturated, a difference in 0.13 wt.% P_2O_5 between dacite 212826 and rhyodacite 172822b for only ~5% fractional crystallization also indicates a greater proportion of apatite fractionation (Table 11c) as mentioned earlier in this compositional interval relative to that defined by 172822b to rhyolite 202825c; here a reduction of 0.06 wt.% P_2O_5 occurred over approximately 5-10% fractional crystallization. An alternative or additional explanation may be that crystallization rates were relatively more rapid and increased the effective localized saturation of P_2O_5 at growing phenocryst crystal faces during a period of fractional crystallization which may have produced rhyodacitic residual liquids from dacitic magma. This may have resulted in increased nucleation and crystal fractionation of apatite. For the interval rhyodacites to rhyolites, P_2O_5 contents in residual liquids may have been saturated such that apatite did not crystallize or crystallization rates were relatively slow such that significantly lesser amounts of fractional crystallization of apatite as inclusions in other phenocrysts occurred.

The silicic lava with the highest Sm and Th abundances is not a rhyolite but is a dacite, sample 230283-6. This dacite is largely similar in major-element composition to other dacites, e.g., sample

212826, but is lower in TiO_2 and P_2O_5 and higher in K_2O. Dacite 230283-6 is also comparatively higher in Ba, Zr, Hf, Ta, Th, and LREE abundances. If derived by a similar degree of fractional crystallization (57-59%, cf., Tables 11a to 11c), from an andesitic magma represented by sample 220283-5, relatively lower bulk D's for these trace elements are implied to explain the relatively greater enrichments in some incompatible elements in 230283-6. Alternatively, magmas parental to dacite 230283-6 may have been higher in incompatible trace element abundances. This suggests the possibility of multiple liquid lines of descent among the silicic lavas, i.e., the compositional range andesite to rhyolite, however, based on previous arguments, this may be just as easily explained by variations in trace element bulk partition coefficients, which in turn are caused by variations in proportions of minor or accessory phases such as apatite. Abundances of Zr and Th increase steadily from andesite to rhyolite (Table 12b, Fig. 22a), or at least lack any discontinuities as seen in REE abundances. This precludes allanite or zircon as minor phases which controlled REE abundances in the silicic magmas and further indicates apatite as the major cause of this effect.

Both calculated bulk D's and enrichment factors in Table 12 for certain elements support the importance of specific minerals in the crystallizing assemblage. Decreasing Sc abundances and a consistently high D^{Sc} as indicated are coupled with pyroxene fractionation. High D^{Sr} is associated with plagioclase fractionation, and a slight increase in D^{Sr} from 212826 to 202825c as suggested in model calculations (Tables 11, 12) is probably a result of decreasing temperature as is the slight increase in D^{Ba} indicated (Drake and Weill, 1975). Calculated values for

D^{Th} seem high and may suggest small amounts of allanite fractionation or that the value of D_{apat}^{Th} (1.3) used is too low. Decreasing V and TiO_2 contents are indicative of fractional crystallization of magnetite and ilmenite in the evolved lavas.

Variations in most trace element abundance ratios such as La/Sm, La/Yb, Ba/Rb, and Ba/Th with increasing degrees of fractional crystallization as seen by comparing values observed in rhyodacites and rhyolites to those in andesites are consistent with the present knowledge of specific mineral/melt partition coefficients. The nearly twofold increase in Zr/Sm ratios (24.2 to 40.3) from andesites to rhyodacites and rhyolites (Fig. 22b, 23a) may be explained as a result of apatite fractionation, since $D_{apat}^{Sm} >> D_{apat}^{Zr}$ (Table 8). La/Sm, La/Yb, and Zr/Sm ratios increase from dacite to rhyodacite (Fig. 22b). A lesser proportion of apatite in the crystallizing assemblage leading to rhyolite 202825c may be responsible for a slight lowering of Zr/Sm in rhyolite. Zr/Hf ratios range from 39.4 to 46.5 in andesite to rhyolite, though not smoothly, due to analytical uncertainty, or variations in magnetite and ilmenite proportions in fractionating assemblages. Based on a recent, comprehensive study of phenocryst/matrix partitioning of REE, Zr, and Hf (Fujimaki et al., 1984), fractional crystallization of ordinary mineral phases (olivine, plagioclase, pyroxenes, and spinel) should not produce large variations in Zr/Hf ratios. The results of the above study demonstrated that for most minerals except ilmenite, D^{Zr} is only slightly less or nearly equal to corresponding mineral/melt partition coefficients for Sm and Hf. Inclusion of ilmenite in the crystallizing assemblage then tends to decrease Zr/Hf and Zr/Nb ratios with fractionation (Table 11b). Zr/Hf ratios are widely scattered in more basic rocks but

23 (a) Zr/Sm ratios vs. SiO_2 and (b) Zr/Hf ratios vs. SiO_2 for all Puyehue and Cordon Caulle lavas.

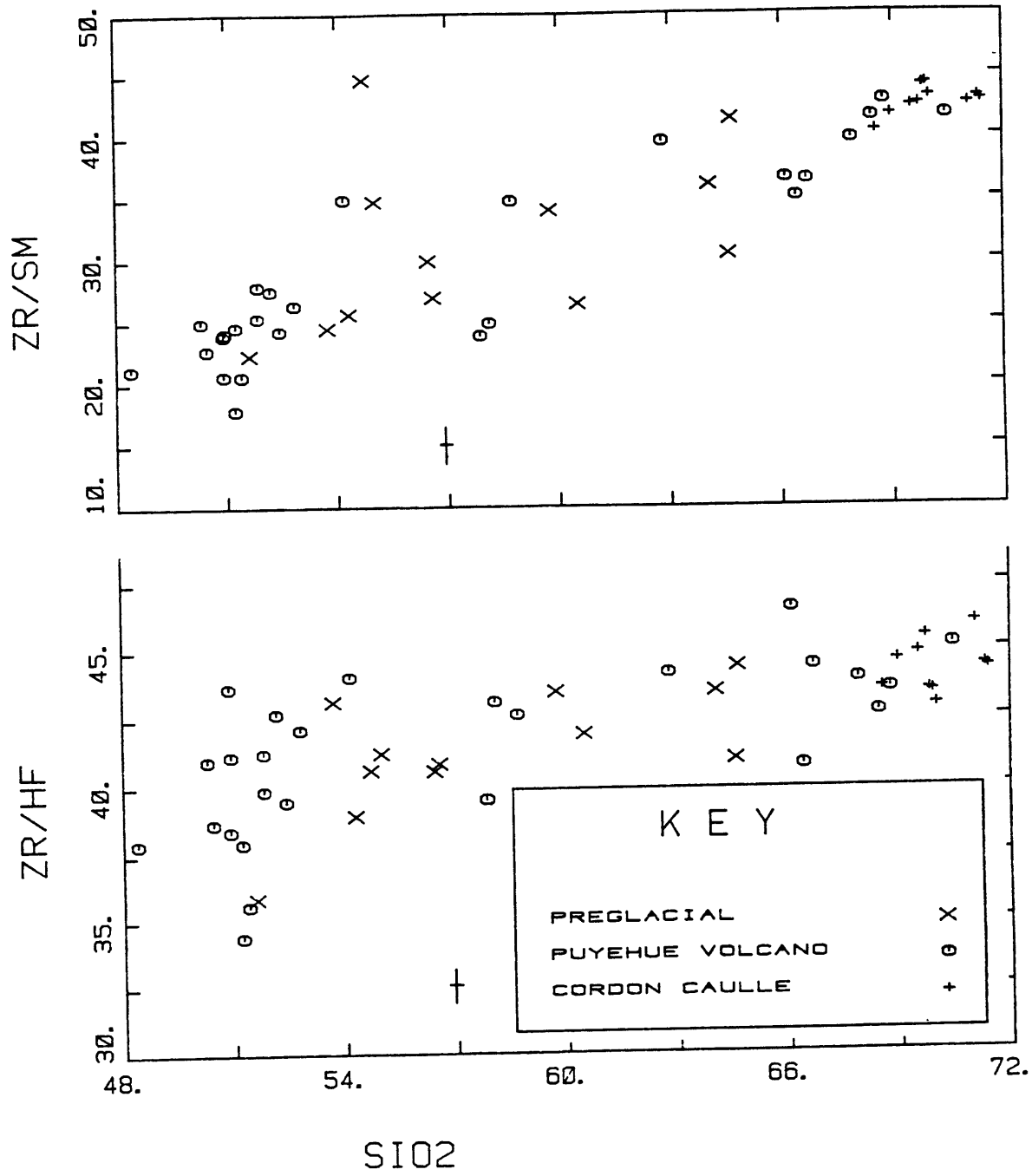
ZR/SM
50.
40.
30.
20.
10.
ZR/HF
45.
40.
35.
30.
48.
54.
60.
66.
72.
SIO2
KEY
PREGLACIAL
PUYEHUE VOLCANO
CORDON CAULLE

increase slightly from andesite to rhyolite (Figure 23b) and indicate that bulk D^{Zr} is generally less than bulk D^{Hf}.

Fractional crystallization of plagioclase, augite, orthopyroxene, magnetite, apatite, and possibly ilmenite can produce most major-element and trace element characteristics of the silicic lavas. This is demonstrated by model calculations, positive intercorrelations of selected incompatible trace elements, and depletion of compatible trace elements such as Sr, Sc, and V, which may be identified as being preferentially incorporated into specific crystallizing phases. Irregular variations in REE abundances with increasing fractional crystallization are linked with variations in the proportion of apatite in the crystallizing assemblage as discussed above. The increasing predominance of silicic lavas and pyroclastic eruptions in the later stages of Puyehue Volcano suggests that repose times between eruptions may have been adequate to allow extensive fractional crystallization and that the rate or volume of new magma input into the system had possibly diminished with time.

9. Petrogenesis of prehistoric and historic Cordon Caulle eruptions

Rhyodacites and rhyolites of the adjacent Cordon Caulle volcanic group (Figure 1, Plate I) are petrographically and geochemically similar to late-stage rhyodacites and rhyolites sampled from Puyehue Volcano. It is probable that Cordon Caulle lavas are the latest phase of magmatism that built Puyehue Volcano, as suggested by earlier workers (Katsui and Katz, 1967; Moreno, 1977).

9.1 Eruption characteristics

Three eruptive units are recognized. The largest unit (CCIV, after Moreno, 1978) consists of approximately 1.2 km^3 (Katsui and Katz, 1967) of thick (~ 20-30 m) rhyolite flows and domes, and the southernmost of these domes occurs on the NW flank of Puyehue Volcano (Figure 1, Plate I). Katsui and Katz (1967) tentatively designated these volcanics as the 1921-1922 Cordon Caulle eruption. Portions of the CCIV flows display some vegetative growth while all portions are covered by varying thicknesses of pumice. Since the pumice from the later 1960 eruption was deposited (blown) mainly in a SE direction (Katsui and Katz, 1967), the pumice cover on the older CCIV rhyolite may be from the 1921-1922 eruption. The assumption that the pumice overlying these older rhyolites is not from the same eruptive event that produced the rhyolites is based on direct observation of the 1960 eruption, which began with emission of water vapor, ash, and pumice, followed by extrusion of lava flows (Veyl, 1960; Saint Amand, 1960; Katsui and Katz, 1967). Thus, the CCIV rhyolite is distinguished from products of the 1921-1922 and 1960 eruptions, and is henceforth referred to as 'prehistoric', although this unit may be no more than 100 to 200 years old.

Lava flows (total estimated volume 0.1 km^3) assigned to the 1921-1922 eruption (CCV unit, after Moreno, 1977) were erupted from the NW portion of a NW-SE trending fissure (Plate I), and those assigned to the 1960 eruption (estimated volume 0.1 km^3) were erupted from the SE end of the fissure (Moreno, 1977). Neither group of lava flows displays any pumice cover, which may have led Katsui and Katz (1967) to assume that all of these flows were erupted in 1960, and the CCIV rhyolites represent the 1921-1922 eruption. The chief difference betweeen the 1921-1922

(CCV) and 1960 (CCVI) flows as mapped by Moreno (1977) is that the craters, or vents associated with the latter currently exhibit significant amounts of solfatara activity in the form of sulphurous vapors and hydrothermal springs. In addition, there are small, but significant compositional differences (Table 13), as determined in this study, between the CCV and CCVI units as mapped by Moreno (1977). This does not necessarily constrain the time of eruption, because it may be possible that the magma chamber that produced these lavas was slightly zoned with respect to composition. Whether or not the lavas with different compositions were extruded during the same eruption or 38 years apart is important in identifying and evaluating petrogenetic processes and magma chamber conditions. Moreno (1977) has compiled eyewitness observations and accounts from earlier workers (Stone, 1935; Hantke, 1940). These, in combination with his field observations and those conducted in the present study, indicate that indeed, the CCV lavas represent a major eruption that occurred in December 1921 to February 1922, and that the CCVI lavas as mapped are products of the well-documented eruption in May, 1960.

Values of temperature and log $^{f}O_2$ were estimated from suitable magnetite-ilmenite pairs analyzed in samples 72822, a CCV lava, and 212821 and 42824a, both CCVI lavas. Although errors on temperature estimates may be as high as ±50°C, the difference in calculated temperatures for 72822 (975°C) and 42824a and 212821 (915°C) is believed to be significant. Estimated log $^{f}O_2$ values are -10.9 and -12.3 respectively, and fall consistently between the NNO and QFM buffers. This suggests that the lavas were erupted under the same redox conditions although at different temperatures. If lavas of both eruptions were

Table 13

Average compositions of the 3 Cordon Caulle eruptive units

	CCV	n		CCVI	n		CCIV	n		Puyehue rhyolite 202825c	
SiO_2	68.88(.33)	4	69.13	69.65(.31)	7	70.03	70.98(.51)	5	71.38	70.46	70.72
Al_2O_3	14.35(.09)	4	14.40	14.14(.05)	7	14.22	13.89(.07)	5	13.97	13.92	13.97
TiO_2	0.77(.03)	4	0.77	0.68(.02)	7	0.68	0.37(.01)	5	0.37	0.41	0.41
FeO	-	-	4.00	-	-	3.76	-	-	3.67	-	3.97
Fe_2O_3	4.83(.11)	4	0.40	4.47(.07)	7	0.31	4.37(.09)	5	0.31	4.73	0.34
MgO	0.62(.06)	4	0.62	0.48(.07)	7	0.48	0.18(.08)	5	0.18	0.28	0.28
CaO	2.48(.07)	4	2.49	2.18(.07)	7	2.19	1.79(.06)	5	1.80	2.02	2.03
Na_2O	5.25(.15)	4	5.27	5.28(.16)	7	5.31	5.25(.16)	5	5.28	5.27	5.29
K_2O	2.61(.01)	4	2.62	2.74(.04)	7	2.76	2.80(.04)	5	2.82	2.75	2.76
MnO	0.13(.01)	4	0.13	0.11(.01)	7	0.11	0.14(.01)	5	0.14	0.13	0.13
P_2O_5	0.16(.01)	4	0.16	0.14(.01)	7	0.14	0.08(.01)	5	0.08	0.10	0.10
total	100.08		100	99.87		100	99.85		100	100.07	100
CO_2	0.02(.03)	4		0.04(.02)	7		0.08(.06)	5		0.09	
H_2O^+	0.15(.05)	4		0.14(.04)	7		0.20(.06)	5		0.12	
Sc	14.7(0.5)	2		13.6(0.6)	5		13.5(1.0)	3		14.9	
V	14.2(1.9)	4		10.6(1.5)	7		4.3(3.3)	5		4	
Cr	1.5(2.1)	4		0.9(0.3)	6		1.2(0.5)	5		0.9	
Co	4.32(.11)	2		3.65(0.2)	5		1.24(.10)	3		1.70	
Ni	4.7(2.7)	4		7.4(1.1)	6		5.9(2.2)	5		8	
Zn	93.7(2.4)	4		86.0(1.3)	6		118.5(2.0)	5		116	
Ga	17.8(0.5)	3		17.6(0.4)	6		18.7(.33)	4		19.2	
K	21417(122)	2		22524(101)	3		23224(294)	2		22538	
Rb	66.3(1.8)	3		70.8(1.6)	6		72.2(1.7)	4		68.3	
Sr	185(2.3)	4		164(4.4)	7		145(2.8)	4		161.2	
Cs	4.78(.01)	2		5.05(.09)	3		5.37(.39)	2		5.20	
Ba	684(7.2)	4		726(26)	6		756(25)	5		779.7	
Y	52.9(1.5)	3		53.2(0.5)	6		60.0(0.5)	4		58.6	
Zr	340(1.7)	4		359(4.6)	6		380(11)	5		370	
Nb	9.5(0.2)	4		9.7(0.2)	6		10.1(0.3)	5		10.1	
Hf	7.71(.08)	2		8.20(.26)	5		8.65(.20)	3		8.20	
Ta	0.51(0)	2		0.55(.03)	5		0.55(.03)	3		0.55	
Pb	21.4(0.8)	3		23.0(0.8)	6		23.9(0.5)	4		22	
Th	7.83(.16)	3		8.42(.13)	6		8.70(0.11)	4		8.25	
La	30.0(1.3)	2		30.9(0.8)	5		34.5(0.59)	3		33.4	
Ce	71.6(0.5)	2		75.3(2.2)	5		83.2(4.9)	3		84.0	
Nd	36.7(.07)	2		37.6(0.8)	5		40.0(1.6)	3		40.2	
Sm	8.41(.01)	2		8.40(.13)	5		9.25(.10)	3		9.17	
Eu	1.78(.07)	2		1.72(.06)	5		1.80(.02)	3		1.84	
Tb	1.25(.13)	2		1.30(.07)	5		1.44(.05)	3		1.32	
Yb	5.71(.19)	2		5.94(.17)	5		6.64(.02)	3		6.41	
Lu	0.86(.01)	2		0.91(.01)	5		0.99(.01)	3		0.96	
$^{87}Sr/^{86}Sr$	.70415	2		.70408	3		.70409	2		.70409	
$^{143}Nd/^{144}Nd$	.51285	2		.51289	3		.51289	2		.51285	

[1] Numbers in parentheses represent one standard deviation(s) about the mean. Analyses listed to right have iron recalculated as FeO and Fe_2O_3 after the method of Kilinc et al. (1983), using temperature and f_{O_2} estimates (see text).

[2] General note: all available data were averaged in each case. As in Table 4, more major-element analyses are available relative to most trace elements. Numbers of samples averaged for each element is = n.

related to a common parental magma, this magma may have undergone closed-system cooling with a constant, buffered oxygen fugacity. Alternatively, if the magma chamber was initially zoned with respect to composition and temperature, then the oxygen fugacity was buffered throughout.

The lack of hydrous phases in any of the Cordon Caulle lavas suggests relatively low magmatic H_2O contents, as in late-stage silicic lavas at Puyehue Volcano. For a temperature of 975°C, a multiply-saturated lava such as 72822 may contain a maximum of only 2.0-2.5 wt.% H_2O at pressures of 4kb H_2O based on results of Merzbacher and Eggler (1984), or even lower contents at lower pressures. If water contents in Cordon Caulle magmas increased by intratelluric crystallization, subsequent cooling or mechanisms of heat loss must be sufficiently effective to cause exsolution of H_2O as vapor and outgassing of the magma, preventing the accumulation of H_2O contents to levels adequate for stabilization of hydrous phases such as hornblende. Buildup of vapor pressure is evident in the initial, steam-dominated explosive phases of each eruption. This suggests in turn that magma chambers feeding each eruption may be located at relatively shallow depths and that pressures are too low for retention of significant amounts of H_2O in the magmas.

9.2 Geochemical characteristics, comparison with late-stage Puyehue lavas, and petrogenesis

The compositions of phenocrysts analyzed in Cordon Caulle lavas are similar to those in late-stage silicic lavas of Puyehue Volcano (Table 3, Figures 3 to 5). As may be expected for fractional crystallization,

increasingly iron-rich ferromagnesian mineral compositions are correlated with increasing FeO*/MgO and SiO_2 in the Cordon Caulle lavas. However, Fe-Mg exchange K_D's ($K_D^{xl} = X_{Fe}^{xl} X_{Mg}^{liq}/X_{Mg}^{xl} X_{Fe}^{liq}$) for olivine (0.32), augite (0.25), pigeonite (0.25), and orthopyroxene (0.27) based on experimental data (Grove et al., 1983; Grove and Bryan, 1983) suggest that the phenocrysts are consistently too Mg-rich to represent phases in equilibrium with the nearly aphyric host lavas (Table 14). Plagioclase is, as usual, the predominant phenocryst phase, and the addition of a small amount of ferromagnesian phenocrysts, even if in equilibrium with the groundmass would cause a slight decrease in the FeO*/MgO ratio of the resulting mixture relative to a crystal-free liquid as may be represented by the groundmass composition. However, this effect may be cancelled out by the presence of accumulated magnetite phenocrysts. Thus, it may be a safe assumption that bulk compositions of Cordon Caulle lavas are representative of liquid compositions. The question of whether or not the ferromagnesian phenocrysts in Cordon Caulle lavas are accumulated or the extent or amount of accumulation may depend on the reliability of experimentally determined exchange K_D's. Values of X_{Fe} for averaged bulk compositions (Table 13) were calculated for each, with a correction for Fe^{3+} based on the method of Kilinc et al. (1983) and using temperature and f_{O_2} information derived from coexisting oxides in the lavas. Phenocryst compositions for each of the three eruptive units are also presented in Table 14. Values of X_{Fe} in liquids expected to be in equilibrium with all phenocrysts are relatively lower than the actual bulk rock X_{Fe}, and this difference seems greater than can be accounted for by mere addition of small amounts of phenocrysts as stated above. Moreover, the calculated X_{Fe} of liquids based on augite analyses and a

Table 14

Comparison of bulk compositions vs. expected equilibrium liquid compositions for phenocrysts in Cordon Caulle lavas

	X_{Fe}^{xl} in phenocrysts			
	oliv	augite	pig	opx
CCV	-	.33-.34	-	.42-.43
CCVI	-	.38-.40	-	.43-.46
CCIV	.75-.77	.52-.57	.61-.62	-
PIII(202825c)	-	.46-.48	.55-.58	-

		expected[1] X_{Fe}^{liq} based on X_{Fe}^{xl} and[2] K_D^{xl}:			
	actual X_{Fe}^{liq}	oliv	augite	pig	opx
CCV	.782	-	.66-.67	-	.73-.74
CCVI	.814	-	.71-.73	-	.74-.76
CCIV	.920	.90-.91	.81-.84	.86-.87	-
PIII (202825c)	.889	-	.77-.79	.83-.85	-

1 $X_{Fe}^{liq} = (1 + K_D^{xl} (1 - X_{Fe}^{xl}/X_{Fe}^{xl}))^{-1}$

2 $K_D^{xl} = (X_{Fe}^{xl} X_{Mg}^{liq})/(X_{Mg}^{xl} X_{Fe}^{liq})$

3 Actual X_{Fe}^{liq} estimated based on recalculated analyses (Table 13) after the method of Kilinc *et al.* (1983)

K_D^{aug} of 0.25 is lower than that calculated for orthopyroxene analyses and a K_D^{opx} of 0.27, for average compositions of the CCV and CCVI lavas (Table 14). For example in CCV rhyodacites, orthopyroxenes may have crystallized in a liquid more Fe-rich than that in which the augite phenocrysts crystallized and this would be consistent with fractional crystallization of dacitic magmas at moderate pressures (2-5 kb) as discussed earlier (Figs. 20a, 20c). The occurrence of both pyroxenes in phenocryst clots or clusters in dacites and rhyodacites suggests that they are co-precipitated, however, and that perhaps there may be some error in the values assumed for exchange K_D's or at least some doubt with regard to their applicability in highly silicic lavas. A similar problem may be apparent for augite vs. pigeonite phenocrysts (or zones within phenocrysts) in CCIV rhyolite. The assumed value of K_D^{oliv} indicates that the iron-rich olivine phenocrysts (Fo_{25}) in CCIV rhyolites are approximately in equilibrium with the bulk composition, but that augite and pigeonite phenocrysts are not, based on their respective exchange K_D's. Augite compositions may be more out of equilibrium than the pigeonite compositions (Table 14), and this is consistent with a change in physical conditions during crystallization (Fig. 20c) such that pigeonite is stabilized relative to augite, as proposed earlier for augite-pigeonite phenocrysts in a sample of rhyolite (202825c) from Puyehue Volcano.

As with many mineral/melt trace element partition coefficients, exchange K_D's may be different for silicic magmas compared to basaltic and intermediate magmas. Analyses of the phenocrysts may not be representative of mineral compositions in equilibrium with the host liquid especially if the phenocrysts are zoned. Rim compositions are most desirable in resolving this question.

Regardless of whether or not the phenocrysts in each sample are in equilibrium with the groundmass, the co-variation of phenocryst composition with bulk composition suggests that processes of fractional crystallization operated and that this may be an important mechanism in producing the range (albeit narrow) of compositions observed in Cordon Caulle lavas. As Hildreth (1979, 1981) has pointed out, the high viscosities of very silicic magmas may effectively inhibit crystal separation by settling. In both Cordon Caulle lavas and late-stage silicic lavas of Puyehue Volcano, phenocrysts may occur in clusters or clots of attached or intergrown crystals. If the mean density of such a cluster consisting of plagioclase, magnetite, clinopyroxene and orthopyroxene is greater than that of the host magma, then crystal settling can occur. Higher temperatures and low H_2O contents indicated in these lavas relative to values determined in other silicic lavas such as Mt. St. Helens dacite (Merzbacher and Eggler, 1984) and the Bishop Tuff (Hildreth, 1979, 1981) suggest that silicic lavas of Puyehue and Cordon Caulle may be relatively less viscous as a result, and crystal settling may be facilitated.

If the three eruptive units of Cordon Caulle are comagmatic and related by crystal fractionation, some problems may arise in considering petrographic observations vs. prediction based on low-pressure experimental results (Grove et al., 1982, 1983). Projected compositions of lavas from all three units appear to define a short trend which crosscuts the 1-atm pigeonite field and which might suggest fractional crystallization of augite and minor pigeonite at very low pressures (Fig. 20a). The absence of pigeonite phenocrysts and coexistence of augite and orthopyroxene in CCV and CCVI lavas suggests that pigeonite is

not stable at the conditions under which CCV and CCVI lavas were crystallizing. The pigeonite stability field may be substantially reduced and shifted at pressures higher than 1-atm and may be nonexistent at even higher pressures (Fig. 20c). By contrast, CCIV rhyolites do contain augite and pigeonite in addition to Fe-rich olivine. These lavas may have experienced fractional crystallization under relatively lower total pressures and nearly anhydrous conditions. Alternatively, the patchy zones or intergrowths of augite and pigeonite in pyroxene phenocrysts in the CCIV rhyolites may have resulted from sudden changes in P_{H_2O} or total pressure during crystallization as suggested earlier.

An additional difference displayed by CCIV lavas relative to CCV and CCVI lavas is that phenocrysts of ilmenite are lacking and magnetite phenocrysts are relatively more titaniferous. This suggests that either TiO_2 contents in the CCIV magmas had been reduced by fractional crystallization of magnetite + ilmenite to levels insufficient for further saturation of ilmenite, or that temperatures were sufficiently high and redox conditions relatively more reducing. This latter condition may have partially suppressed fractional crystallization of magnetite, and effectively produced the extreme late-stage Fe-enrichment in residual liquids necessary for stabilization of Fe-rich olivine in CCIV rhyolite magmas. These conditions may also apply to late-stage PIII rhyolite from Puyehue Volcano as represented by sample 202825c. This sample displays Fe-enrichment just short of that for CCIV lavas (Table 13). Fe-rich olivine phenocrysts are not observed in 202825c and augite and pigeonite phenocrysts are slightly less Fe-rich than those in CCIV lavas (Figs. 5a and 5c, Table 14).

Bulk compositions of Cordon Caulle lavas, including major element contents and trace element abundances, suggest that the three eruptive units may be related by varying amounts of fractional crystallization of the observed phenocryst phases. A sequence consisting of CCV, CCVI, and CCIV lavas may respectively represent products of increasing amounts of fractional crystallization. The absence of pigeonite in phenocryst assemblages in CCV and CCVI rhyodacite lavas does not necessarily preclude the possibility of these lavas as representative of earlier magmas parental to the relatively older CCIV rhyolites. Decreasing CaO/Al_2O_3 ratios and Sc and Co abundances and increasing FeO*/MgO ratios are linked with pyroxene fractionation, and decreasing Na_2O/K_2O and Eu/Eu* ratios, Al_2O_3 contents, and Sr abundances are diagnostic of plagioclase fractionation (Tables 13 and 15). Decreasing TiO_2 contents and V abundances are coupled with magnetite ± ilmenite fractionation. Most incompatible and moderately incompatible trace element abundances consistently increase within this sequence, except for Sm and Eu (Table 13).

Most trace element abundance ratios are constant between the three eruptive units, except for Rb/Sr, La/Sm, La/Yb, Sm/Nd, and Eu/Eu* ratios (Table 15). Increasing Rb/Sr ratios and decreasing Eu/Eu* ratios are associated with plagioclase fractionation, while increasing La/Sm and La/Yb ratios and variable Sm/Nd ratios are attributed to the combined effects of augite, orthopyroxene, magnetite, apatite, and ilmenite fractionation. In detail however, La/Sm ratios consistently increase from CCV to CCVI to CCIV.

For a fractional crystallization process between CCV and CCVI lavas, the crystallizing assemblage consisted of plagioclase, augite,

Table 15

Relevant abundance ratios and enrichment factors for Cordon Caulle eruptive units.(1)

	CCV	CCVI	CCIV
CaO/A_2O_3	0.173	0.154	0.129
FeO^*/MgO	7.01	8.38	21.9
Na_2O/K_2O	2.01	1.93	1.88
K/Rb	323	318	322
Rb/Sr	0.358	0.432	0.498
Ba/Rb	10.3	10.3	10.5
Zr/Nb	35.8	37.0	37.6
Zr/Hf	44.1	43.8	43.9
Zr/Sm	40.4	42.7	41.1
Ba/Th	87.4	86.2	86.9
Ba/Nb	72.0	74.8	74.9
Ba/La	22.8	23.5	21.9
La/Ce	0.42	0.41	0.41
La/Sm	3.57	3.68	3.73
La/Yb	5.25	5.20	5.20
Sm/Nd	0.229	0.223	0.231
Eu/Eu^*	0.656	0.628	0.596
Sc		(2)0.93	(2)0.92
V		0.75	0.30
Cr		0.6	0.8
Co		0.84	0.29
Ni		1.57	1.26
K		1.05	1.08
Rb		1.07	1.09
Sr		0.89	0.78
Cs		1.06	1.12
Ba		1.06	1.11
Y		1.006	1.13
Zr		1.056	1.12
Nb		1.02	1.06
Hf		1.06	1.12
Ta		1.08	1.08
Pb		1.07	1.12
Th		1.075	1.11
La		1.03	1.15
Ce		1.05	1.16
Nd		1.025	1.09
Sm		0.999	1.10
Eu		0.966	1.01
Tb		1.04	1.15
Yb		1.04	1.16
Lu		1.06	1.15

(1) based on average compositions presented in Table 13.
(2) enrichment factors relative to CCV average composition.

24(a) Th, Zr, and P_2O_5 variation diagrams for selected trace element abundances in Cordon Caulle rhyodacites and rhyolites. Samples from the CCIV eruptive unit are designated by filled circles, while those from the CCV and CCVI units are represented by plus (+) symbols and crosses (x), respectively.

(b) La/Sm, La/Yb, and Zr ratios vs. Th and P_2O_5 in Cordon Caulle rhyodacites and rhyolites. The three eruptive units are distinguished by same symbols as in Figure 24a. Samples from Puyehue Volcano ranging from dacite to rhyolites are represented by open circles.

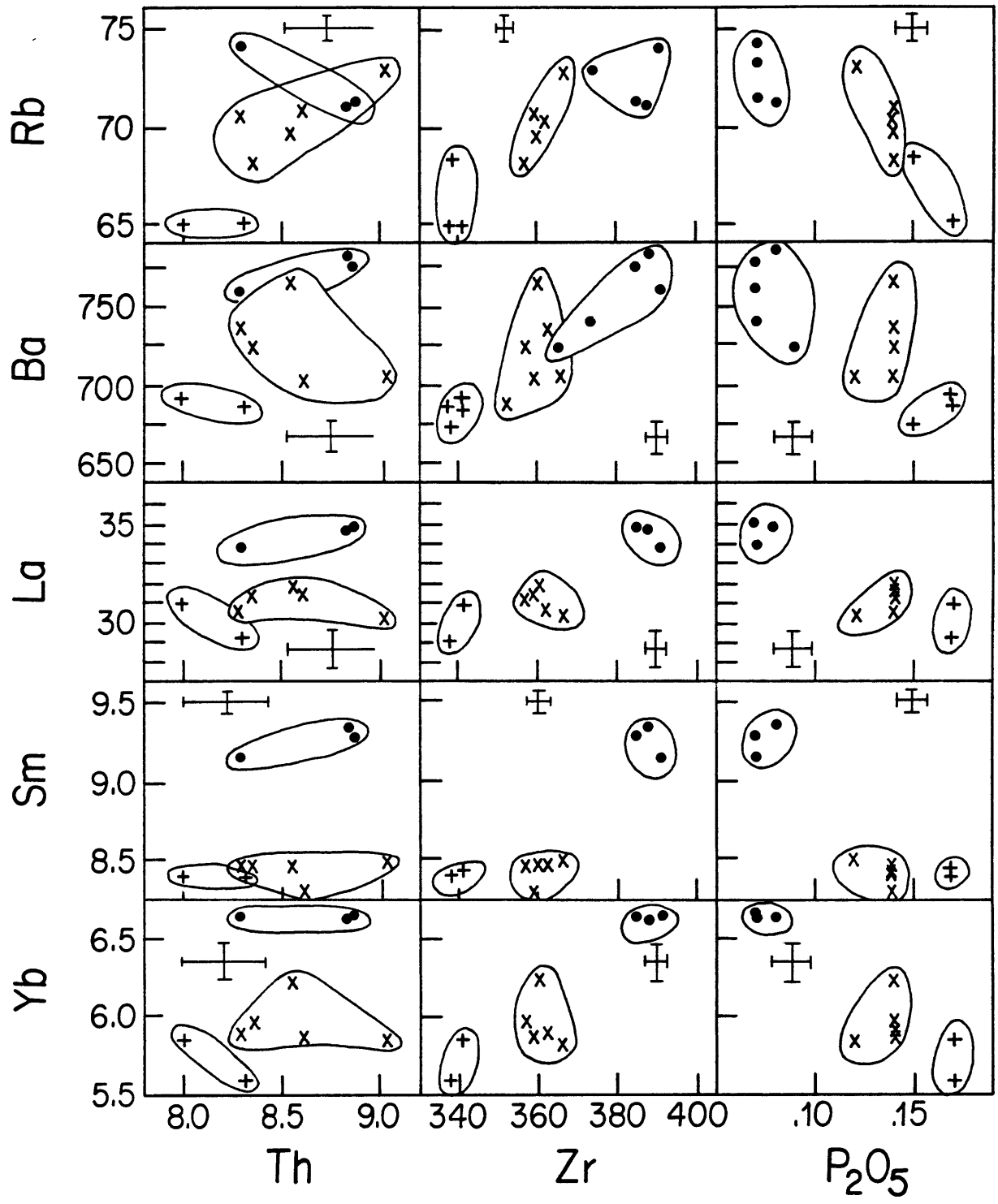
Rb
Ba
La
Sm
Yb
75
70
65
750
700
650
35
30
9.5
9.0
8.5
6.5
6.0
5.5
8.0
8.5
9.0
340
360
380
400
.10
.15
Th
Zr
P2O5

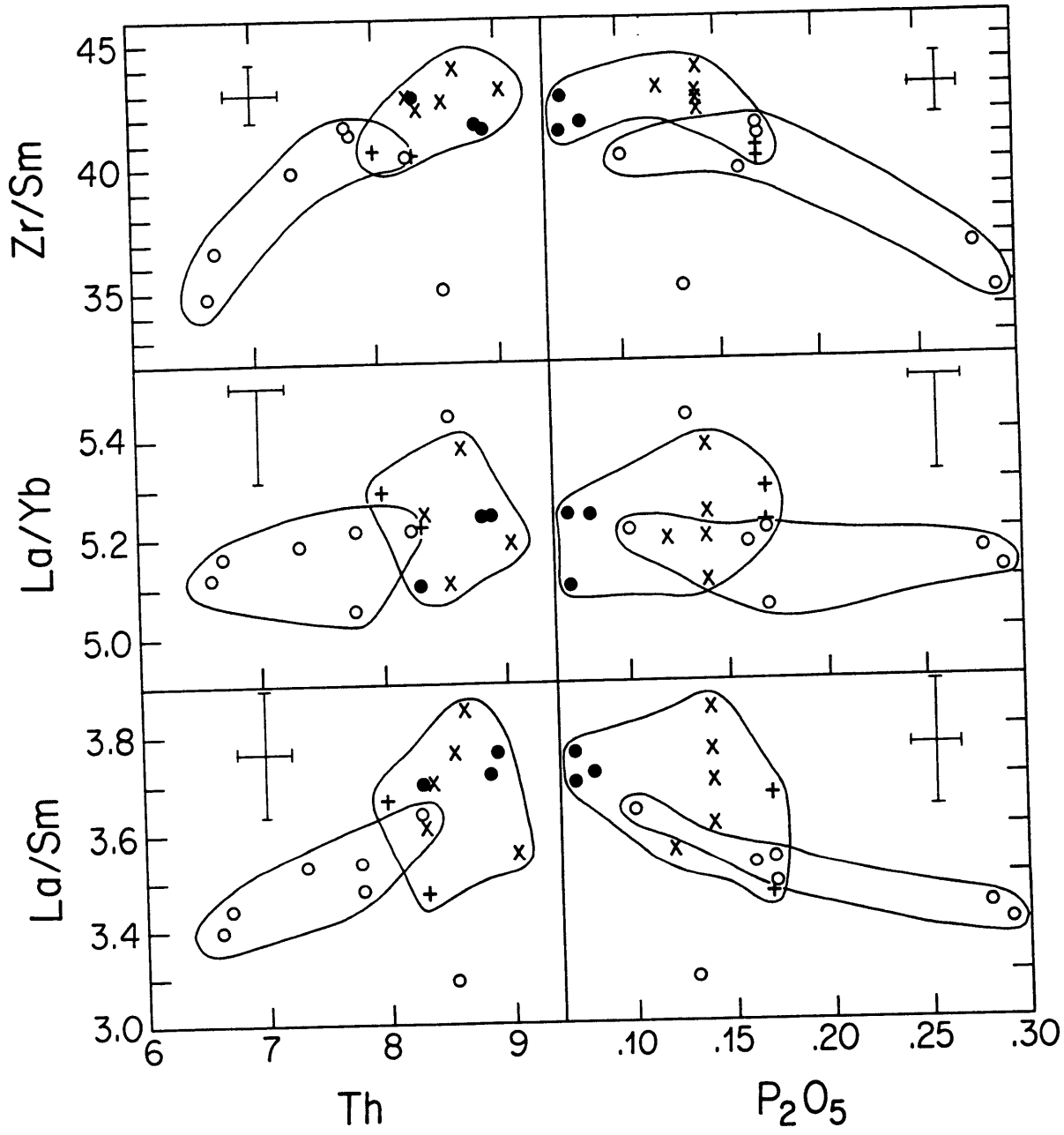
Zr/Sm
45
40
35
La/Yb
5.4
5.2
5.0
La/Sm
3.8
3.6
3.4
3.0
6
7
8
9
Th
.10
.15
.20
.25
.30
P2O5

orthopyroxene, magnetite, ilmenite, and apatite, as suggested by combined consideration of petrography, major-element contents, and trace element constraints. Bulk REE partition coefficients for this assemblage would be relatively higher for the middle REE (MREE) compared to LREE and HREE, reflecting the influence of high apatite REE partition coefficients. The suppression of MREE relative to LREE and HREE is also suggested by enrichment factors for CCVI lavas relative to CCV lavas (Table 15) and trends shown in Figure 24a. For a fractional crystallization process between CCVI and CCIV lavas, the crystallizing assemblage consisted of plagioclase, augite, pigeonite, magnetite, possibly Fe-rich olivine, and relatively less apatite, as suggested earlier in discussion relating Puyehue rhyodacites to rhyolites. Bulk partition coefficients for this assemblage may have been somewhat different in that those for middle REE and HREE were subequal, i.e., $D_{La} < D_{Sm} \cong D_{Yb}$, reflecting the predominant effect of the clinopyroxenes. These conjectures regarding mineral/melt and bulk partition coefficients are in agreement with results of recent empirical determinations (Fujimaki et al., 1984).

Bulk partition coefficients for REE differed not only for CCV to CCVI fractional crystallization vs. CCVI to CCIV fractional crystallization, but must have been relatively higher during CCV to CCVI fractional crystallization. Abundances of Sm and to a lesser degree, La, are suppressed somewhat between CCV and CCVI lavas resulting in a concave rather than sublinear trends on Th and Zr variation plots for the 3 eruptive units (Fig. 24a, 24b). As in late-stage Puyehue rhyodacites and rhyolites, the presence of apatite in the crystallizing assemblage results in bulk D_{Sm} near or greater than one, and its relatively lower proportion in crystallizing assemblages leading to rhyolitic CCIV liquids

resulted in lower bulk D_{Sm} and sharp increases in all REE abundances over this relatively narrow compositional interval.

Cordon Caulle lavas include more silicic rhyolites than were sampled in late-stage Puyehue lavas although the compositions of CCV and CCVI rhyodacites overlap with Puyehue lavas. Keeping in mind that Puyehue and Cordon Caulle rhyodacites and rhyolites are roughly similar in their major-element compositions, some Cordon Caulle lavas appear to display higher Th and Zr abundances for a given Sm abundance relative to late-stage silicic lavas sampled from Puyehue Volcano (Figure 24b). Four explanations are possible: (1) Th and Zr abundances in Cordon Caulle lavas are enriched relative to those in Puyehue lavas by a relatively greater extent of some liquid-state enrichment process, (2) crystallizing assemblages were similar in both groups of lavas and changes in proportions occurring in each group were similar, but bulk D_{Sm} was, for some reason, consistently higher in Cordon Caulle lavas relative to Puyehue lavas, (3) ilmenite and allanite or zircon fractionation created lower abundances of Zr and Th respectively, in Puyehue lavas relative to Cordon Caulle rhyodacites and lavas or (4) apatite fractionation was more pervasive in Cordon Caulle rhyodacites and rhyolites compared to Puyehue rhyodacites and rhyolites. Case (3) does not seem likely, since Zr abundances in the lavas may not be high enough to saturate zircon (Watson and Harrison, 1983), and ilmenite phenocrysts are present in both Puyehue and Cordon Caulle lavas. It is not possible with available data to demonstrate a role for the process suggested in (1) above in Cordon Caulle lavas. The compositions of pyroxene phenocrysts in both Puyehue and Cordon Caulle rhyodacites are similar, and it is therefore difficult to justify a higher bulk D_{Sm} for the parental magmas that gave rise to

Cordon Caulle lavas relative to Puyehue lavas as suggested in case (2) above. An additional possibility may simply be that the parental precursors of Cordon Caulle lavas are slightly lower in Sm, or inherited relatively more concave REE patterns, relative to those of late-stage Puyehue lavas. Since CCIV and CCVI lavas have higher Zr/Sm and Th and lower P_2O_5, they form an extension of the Puyehue trend (Figure 24b) suggesting that continuing apatite fractionation is the cause.

The chronology of the 3 eruptive units does not correlate with the proposed evolutionary sequence, but the above discussion concerning compositional trends serves to illustrate fractional crystallization as an important process in their petrogenesis. The most evolved, silicic unit, consisting of the CCIV rhyolites, is the earliest of the 3 eruptive units. The CCIV rhyolites are slightly more evolved than the most silicic lava (202825c) sampled from uppermost unit PIII of Puyehue Volcano, and if comagmatic with late-stage Puyehue lavas, may indicate further that (1) a magma chamber beneath the general area was evolving to more silicic compositions and (2) the frequency of eruptions was diminishing, allowing more time for more extensive fractional crystallization between eruptions, relative to earlier stages in the evolution of the volcano.

Rhyolitic magmas may have coexisted with andesitic and basaltic magmas, if only for short periods of time, in the late stages of Puyehue Volcano. Mixed andesites and dacites of the PIV unit on Puyehue Volcano are the youngest eruptives of Puyehue Volcano and may be largely contemporaneous with the earliest unit, CCIV of Cordon Caulle. Rhyolitic magmas as represented by CCIV lavas may have served as a mixing endmember as indicated by Fe-rich olivine phenocrysts in the mixed andesite 242824,

one of the youngest eruptive products of Puyehue Volcano. CCIV rhyolites are characterized by higher $^{143}Nd/^{144}Nd$ ratios relative to the PIV mixed andesites. Thus, the CCIV rhyolites cannot be precisely representative of the silicic mixing endmember required for the mixed andesites, since the Nd-isotopic composition of the mixture would be dominated by that of the silicic endmember. Presumed basaltic mixing endmembers for the PIV mixed andesites are characterized by slightly higher $^{143}Nd/^{144}Nd$, therefore the silicic endmember must have lower $^{143}Nd/^{144}Nd$ than the mixed andesites.

Isotopic compositions of Cordon Caulle lavas and selected late-stage silicic lavas from Puyehue Volcano are compared in Figure 25a. Rhyodacites and rhyolites of Puyenue Volcano are similar to rhyodacites and rhyolites of the CCVI and CCIV units, respectively, on the basis of their Sr isotopic compositions, although differences are observed with respect to Nd isotopic compositions. CCV rhyodacites are distinguished by higher $^{87}Sr/^{86}Sr$ and slightly lower $^{143}Nd/^{144}Nd$ ratios relative to other Cordon Caulle lavas (Figure 25b). Among the Cordon Caulle eruptive units, there are vague correlations between bulk composition and isotopic composition, especially $^{143}Nd/^{144}Nd$ (Figure 25b). These trends are opposite to those that may result from crustal contamination or an AfC process involving a crustal component with relatively higher $^{87}Sr/^{86}Sr$ and lower $^{143}Nd/^{144}Nd$, and may be related to slight differences in magmas from different magma chambers.

The close proximity of the southernmost CCIV lava dome and the crater of Puyehue Volcano (Figure 1, Plate I) also suggests that Cordon Caulle lavas and late-stage Puyehue lavas may be comagmatic, or at least genetically related. The shift in the locus of volcanism may be related

25(a) Rb/Sr and Sm/Nd ratios and Th abundances vs. $^{87}Sr/^{86}Sr$ and $^{143}Nd/^{144}Nd$ in dacite, rhyodacite, and rhyolite from Puyehue Volcano, and in Cordon Caulle rhyodacites and rhyolites. Symbols are the same as in Figures 24a and 24b. Large crosses represent estimated analytical uncertainty.

(b) Rb/Sr, Sm/Nd ratios and Th abundances vs. $^{87}Sr/^{86}Sr$ and $^{143}Nd/^{144}Nd$ as in 24a for Cordon Caulle rhyodacites and rhyolites only. Same symbols as in Figure 24a. Large crosses represent estimated analytical uncertainty.

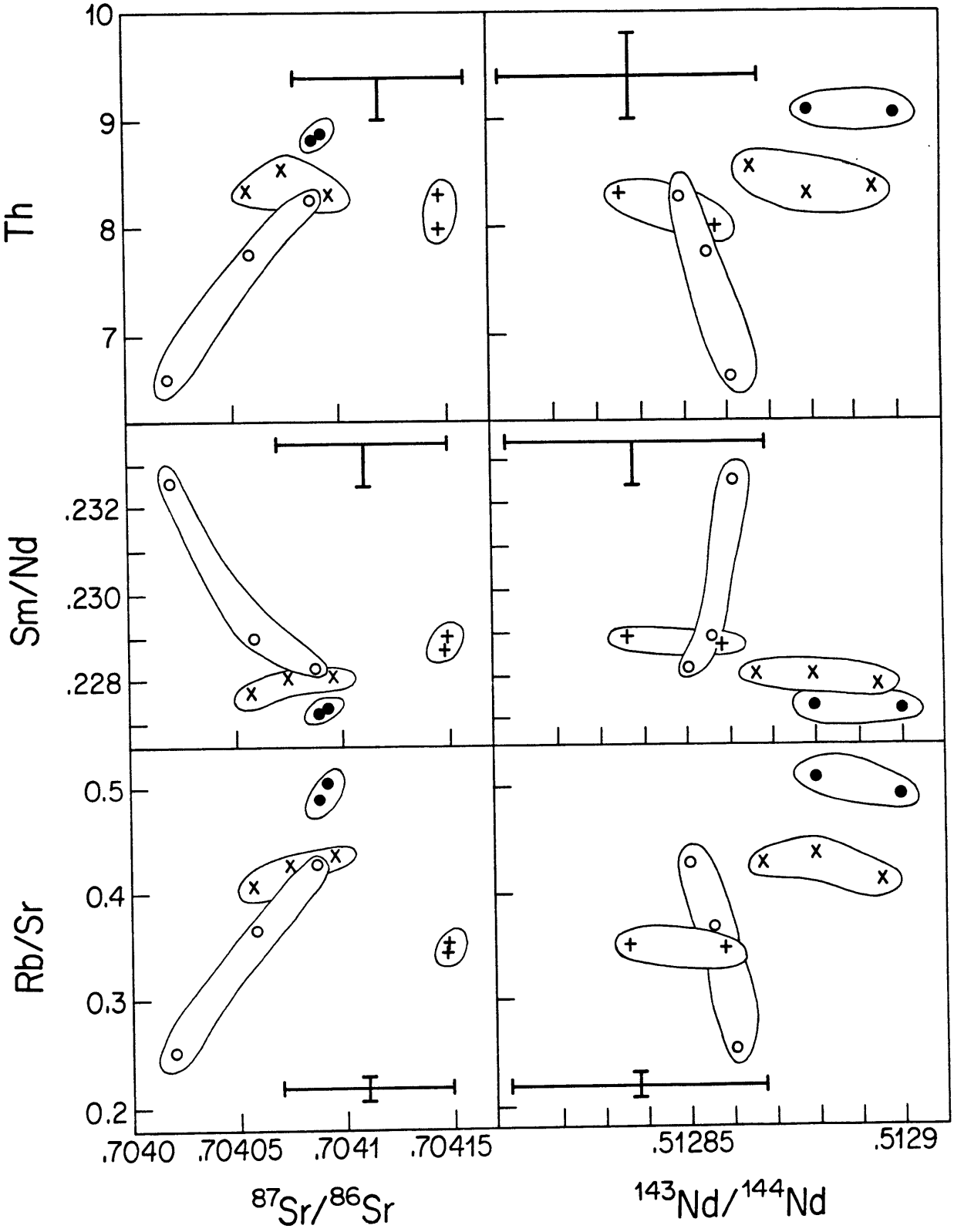
Th
Sm/Nd
Rb/Sr
10
9
8
7
.232
.230
.228
0.5
0.4
0.3
0.2
.7040
.70405
.7041
.70415
.51285
.5129
87Sr/86Sr
143Nd/144Nd

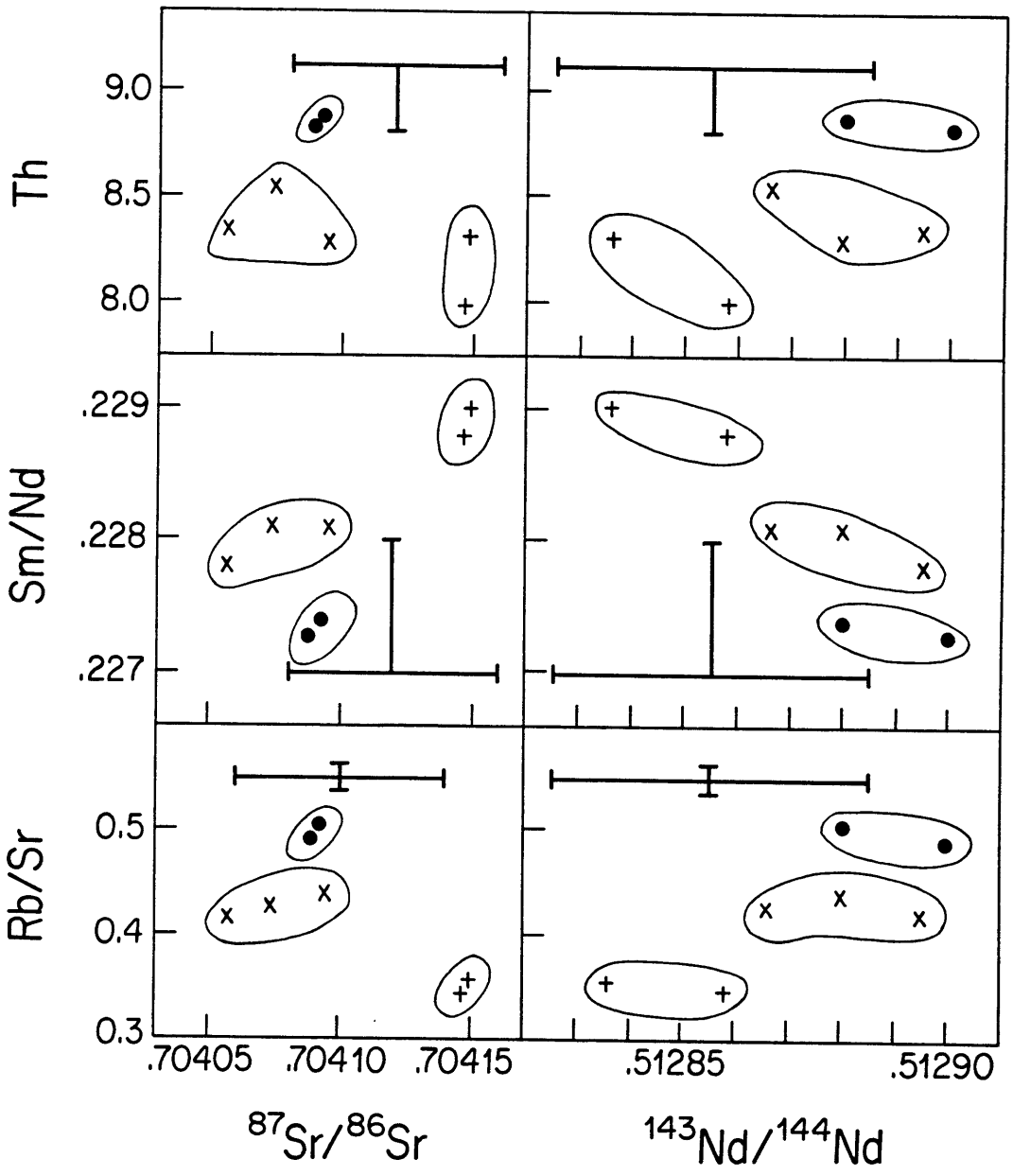
Th
9.0
8.5
8.0
Sm/Nd
.229
.228
.227
Rb/Sr
0.5
0.4
0.3
.70405
.70410
.70415
.51285
.51290
87Sr/86Sr
143Nd/144Nd

to either changes in the geometry of a magma chamber, a suppressing overburden effect of the volcanic pile of Puyehue Volcano, or structural controls. With regard to the latter possibility, Moreno (1977) suggested that Cordon Caulle eruptions are vented through fissures associated with recently activated NW trending faults.

If CCIV rhyolites (volume approximately 1.2 km^3) represent only the upper portion, i.e., a small fraction, of a magma chamber possibly zoned with respect to composition, then a chamber of considerable size existed, and may still exist at depth. If the size of the magma chamber was static at this time, an equivalent volume of magma, possibly basaltic in composition, should have been replenished at the base of the magma chamber after the CCIV eruption. This may have catalyzed instability in overlying portions of the magma chamber and effectively triggered the next eruption, represented by CCV lavas. The CCV lavas are less silicic than CCIV lavas, and may in turn represent a less silicic zone of magma remaining behind after the eruption of the CCIV rhyolites. However, in a continuously zoned magma chamber, some slight compositional gradation would be expected in any given single eruption. CCIV rhyolites are compositionally uniform throughout (cf. Table 4 and sample localities, Plate I), which may imply that some amount of magma with this composition may have been retained in the magma chamber after the eruption. The less silicic and less uniform CCV rhyodacites (Table 13) may have been produced by turbulent, though fairly thorough, mixing of residual CCIV rhyolite magma with rhyodacitic or dacitic magma. Plagioclase phenocrysts in CCV lavas vary in composition (Figure 3b) and more calcic phenocrysts (section 3.3.5) may have been largely derived from dacitic magma if this scenario is correct.

The CCV rhyodacites are characterized by higher $^{87}Sr/^{86}Sr$ and lower $^{143}Nd/^{144}Nd$ ratios relative to the CCIV rhyolites (Table 13). If CCV lavas were produced in the same magma chamber as CCIV rhyolites, this further implies that the magma chamber was zoned, or at least variable, with respect to isotopic composition. If CCV rhyodacites ($^{87}Sr/^{86}Sr$ = .70415) were produced by mixing of CCIV rhyolitic ($^{87}Sr/^{86}Sr$ = .70409) magma with dacitic magma containing approximately 230 ppm Sr, the $^{87}Sr/^{86}Sr$ ratio of the latter would be .70419. Such an amount of isotopic zoning within a single magma chamber is modest compared to other reported instances (cf. Hildreth, 1983). Higher $^{87}Sr/^{86}Sr$ in lower portions of the magma chamber may either be caused by partial mixing of replenishing magmas with higher $^{87}Sr/^{86}Sr$, or by relatively greater amounts of assimilation of wallrock with higher $^{87}Sr/^{86}Sr$, aided at deeper levels of the magma chamber by higher temperatures relative to upper levels.

If the above scenario is true, this poses a problem in explaining the geochemical characteristics of the CCVI lavas. The CCVI rhyodacites may be explained as produced by fractional crystallization of residual CCV rhyodacitic magma. However, CCVI lavas are characterized by lower $^{87}Sr/^{86}Sr$ and higher $^{143}Nd/^{144}Nd$ relative to CCV lavas and are isotopically similar to the CCIV rhyolites. This suggests that if all 3 eruptive units issued from the same magma chamber, the isotopic composition of at least the upper portion of such a magma chamber from which CCVI lavas were withdrawn had been 'restored' to earlier values. Whatever process required must have taken effect in only 38 years, the time between the CCV and CCVI eruptions. Assimilation of wallrock with lower $^{87}Sr/^{86}Sr$ and higher $^{143}Nd/^{144}Nd$ relative to CCV lavas seems

improbable and requires a change in the isotopic characteristics of the wallrock with time, or a sudden decrease or increase in the rate of assimilation, depending on the assumed isotopic characteristics of the wallrock. Another possibility may be that the post-1922 magma chamber was replenished with magma characterized by relatively lower $^{87}Sr/^{86}Sr$ and higher $^{143}Nd/^{144}Nd$, and that this magma thoroughly mixed and reset the isotopic composition of the entire magma chamber. A period of fractional crystallization may then have occurred in at least the upper portion of the magma chamber to produce the relatively more silicic CCVI lavas. It seems unlikely that such a complex, two-stage process could have occurred to produce such compositionally uniform lavas as sampled from the 1960 eruption. Taking into account various fractors such as slow settling rates of crystals in very silicic magams, 38 years may be inadequate to derive CCVI lavas from magma of CCV composition, disregarding for the moment the differences in isotopic composition.

A reasonable possibility is that the 1921-1922 and 1960 eruptions tapped small, separated, compositionally distinct magma chambers. In connection with this possibility, CCIV rhyolite lavas may have been derived from the same magma chamber as CCVI lavas. To carry this further, CCIV rhyolites may represent the most silicic and uppermost magmas in a compositionally zoned magma chamber and were tapped first and CCVI rhyodacites may represent a lower, less evolved portion of this same magma chamber that was tapped later. If CCIV rhyolites and CCVI rhyodacites represent erupted portions of a contiguous magma body, it may be that portions of the magma resided in branching reservoirs subject to different total pressures, as suggested by differences in phenocryst mineralogy. Since CCIV lavas and vent locations overlap spatially with

those of the CCV lavas, a question may arise as to how the separation or isolation of separate magma chambers was maintained. An alternative may be that the CCV and CCVI lavas were respectively tapped from different portions of a single magma body zoned with respect to composition, including isotopic character. For some reason, lower, less silicic portions of this magma were tapped first during the 1921-1922 CCV eruption. Only a small amount of fractional crystallization and mixing in the upper, more silicic portion of the magma chamber may then have followed prior to the 1960 CCVI eruption. Geochemical and other data in this study cannot be used to choose between any of the possibilities discussed above with regard to single or multiple magma chambers. Triggering of eruptions by magma replenishment may not be necessary or characteristic of Cordon Caulle eruptions as there is some evidence that the 1960 eruption was triggered by the large earthquake that occurred in the nearby city of Valdivia only two days prior to the eruption (Katsui and Katz, 1967; Moreno, 1977).

10. Petrogenesis of basalts from Puyehue Volcano

10.1 Relevant geochemical characteristics of the basalts

The basalts are roughly similar in their major-element compositions, except some samples are characterized by higher CaO/Al_2O_3 ratios and lower FeO*/MgO ratios as noted earlier (section 4.2). Other variations, such as MgO contents ranging from 6.0 to 14.3 wt.%, are due to variations in phenocryst contents between samples, e.g., correction for phenocryst contents illustrates that groundmass of samples 13826h and 13828 may contain 6.65 and 7.24 wt.% MgO, while the bulk rocks contain 5.91 and 9.52 wt.%, respectively. However, CaO and Al_2O_3 contents, and FeO and Mg contents, while not different by >1 wt.% between these samples, are inversely correlated such that differences in CaO/Al_2O_3 and FeO*/MgO ratios still persist. Na_2O, K_2O, Al_2O_3, and TiO_2 contents are also inversely correlated between the two samples, resulting in different Al_2O_3/TiO_2 (17.8 vs. 19.5) and Na_2O/K_2O (6.42 vs. 4.61) ratios. As discussed earlier (section 5.2), samples of basalt may contain varying amounts of accumulated phenocrysts and the resulting bulk major-element composition is not representative of a liquid. Correcting the bulk compositions of some of the basalts was helpful in attempts to identify the processes or liquid line(s) of descent which led to relatively more evolved lavas. In subsequent discussion, abundance ratios of incompatible trace elements and isotopic compositions of the basalts will be used in identifying processes or components involved in basalt genesis. Since these data are unaffected by fractional crystallization or accumulation, the question of whether or not the analyzed samples are representative of liquids becomes immaterial. Abundances of Sr are important in later models, and were corrected for plagioclase phenocryst accumulation in selected basalts assuming $D_{plag}^{Sr} = 1.5$.

When compared to the most primitive basalts located in continental or oceanic arcs, basalts from Puyehue Volcano are not as primitive with regard to their major-element composition (Table 16). Puyehue basalts are characterized by intermediate values of Mg#, FeO*/MgO, and CaO/Al_2O_3 ratios, but contain more SiO_2 relative to other basalts listed. One Puyehue basalt listed (242822a) may have accumulated a significant amount of olivine phenocrysts as suggested by high Mg, Cr, Ni, MgO content, and lowered CaO and Al_2O_3 contents relative to other basalts (Table 4, Table 16). In general, Mg# and FeO*/MgO are variable in Puyehue basalts, because of their sensitivity to olivine phenocryst content, but CaO/Al_2O_3 ratios are less sensitive, since CaO/Al_2O_3 in plagioclase phenocrysts is $\cong$ 0.50-0.53, similar or slightly lower than ratios observed in many basalts. As seen in Table 16, CaO/Al_2O_3 ratios vary from 0.55 to 0.92, and this large range may be due to different degrees of high-pressure clinopyroxene fractionation in primitive magmas of each locality. In addition to FeO*/MgO ratios (Fig. 6b), K_2O contents and total alkali (Na_2O+K_2O) have been used to distinguish 'tholeiitic' and 'calcalkaline' basalts associated with subduction zones. Among those listed in Table 16, there is no correlation between K_2O contents, FeO*/MgO ratios, or CaO/Al_2O_3 ratios. These compositional parameters may be affected locally by any of several possible processes that may modify primitive magmas, and general conclusions concerning arc magma genesis on the basis of major elements are inhibited unless the effects of such processes are assessed.

Trace element abundances in basalts from Puyehue Volcano are intermediate with respect to the range observed in arc basalts. Normalized abundances of incompatible and moderately incompatible trace

Table 16

Comparison of major-element compositions of arc basalts with basalts from Puyehue Volcano

	1	2	3	4	5	6	7	8	9	10
SiO_2	47.68	48.56	47.51	48.20	48.97	47.42	48.17	48.39	50.91	50.45
TiO_2	0.71	1.47	1.12	1.06	0.72	0.97	0.52	0.70	0.65	0.83
Al_2O_3	17.74	17.47	18.10	16.90	16.27	15.67	16.40	14.64	16.49	18.94
FeO		11.67	10.77		8.78					
[1]Fe_2O_3	9.72			11.36		11.17	10.88	10.78	9.02	9.48
MgO	9.35	6.57	8.57	8.82	9.62	7.07	8.59	14.32	9.52	5.91
CaO	11.74	9.58	9.89	10.52	12.86	14.37	13.43	8.55	10.36	10.53
Na_2O	2.30	3.65	3.50	2.89	2.00	2.16	1.86	2.19	2.46	2.90
K_2O	0.09	0.56	0.23	0.18	0.54	0.64	0.30	0.31	0.49	0.42
MnO	0.16	0.16	0.18	0.16	0.18	0.17	0.19	0.17	0.13	0.14
P_2O_5	0.06	0.15	0.10	0.13	0.13	0.13	0.12	0.13	0.11	0.13
total:	99.54	99.85	99.97	100.22	100.07	99.77	100.46	99.87	100.14	99.73
Mg/Mg+ΣFe	0.656	0.501	0.586	0.606	0.661	0.556	0.610	0.703	0.676	0.552
FeO*/MgO	0.936	1.78	1.26	1.16	0.913	1.422	1.140	0.678	0.853	1.44
CaO/Al_2O_3	0.662	0.548	0.546	0.622	0.790	0.917	0.819	0.584	0.628	0.556

[1] total iron as Fe_2O_3 or FeO for selected samples.

1. Modoc high-alumina basalt, Medicine Lake Highland, California (Gerlach and Grove, 1982).
2. Cave basalt, Mt. St. Helens, Washington (D. R. Smith, unpub. data)
3. Indian Heaven basalt, Washington (D. R. Smith, unpub. data)
4. Average of olivine basalts, Edgecumbe Volcanic Field, Alaska (Myers et al., 1984)
5. Ashishik basalt, Okmok Volcano, Alaska (Byers, 1961)
6. C-series basalt, Grenada, Lesser Antilles (Thirlwall and Graham, 1984)
7. West Epi basalt, New Hebrides (Dupuy et al., 1982)
8. (242822a) basalt from Puyehue Volcano, Chile (this study)
9. (13828)
10. (13826h)

elements for three representative samples are summarized and displayed in Figure 26. The normalized abundances are plotted in an order (after Hofmann, 1983) based on increasing compatibility (or bulk partition coefficient) for an upper mantle assemblage believed to be representative of the common source for parental magmas of MORB. Relative to OIB and E-type and N-type MORB, Puyehue basalts display typical characteristics of most arc lavas, namely, enrichments in alkalies and alkaline earths (Cs, Rb, Ba, K), positive Sr 'spikes,' and depletions or negative anomalies in high-field strength elements (HFSE), such as Ta, Nb, Hf, Zr, and Ti (Fig. 26). Except for HFSE anomalies, overall increases are observed from La to Cs. There is no well-defined flattening or decrease from K to Rb in Puyehue basalts, as seen in OIB. This was noted in other arc basalts and also in OIB by Morris (1984), and was a basis for suggesting that, in general, arc basalts and OIB may display similar alkali element abundance ratios. In detail, the three Puyehue basalts display variability in Figure 26, in that the normalized patterns are not subparallel. Abundances of Th and HFSE vary, and one sample (13828) is relatively depleted in HREE.

Abundances of alkali elements in the basalts display vague positive correlations (Fig. 27). On detailed inspection, a few basalts with intermediate Ba abundances (188-198) display higher Cs, Rb, and K abundances than the remainder of the basalts. Basalts with the lowest Ba abundances (133-146) contain the lowest (0.81-0.88 ppm) and highest (1.72-1.74 ppm) Th abundances (Fig. 27). Abundances of the HFSE (Zr, Hf, Ti, Nb) are positively correlated, and small scatter in the data can be attributed to analytical uncertainty (10-25% estimated) for Nb (Fig. 27). The scatter observed in the covariation among REE and Y, however, is

26 Trace element abundances in oceanic basalts compared with representative basalts from Puyehue Volcano, normalized to chondritic abundances using values from Sun and Nesbitt (1977), Sun et al. (1979), and Masuda et al. (1976). Normalizing values are given in wt. % for TiO_2 and P_2O_5 and in ppm (μg/g) for all other elements along the abscissa. Abundances in Nazca Plate basalts (Thompson et al., 1976; Rhodes et al., 1976; Hart, 1976) are shown as a shaded region and are representative of N-type MORB. Abundances in an E-type MORB from the mid-Atlantic Ridge (M.A.R.) at 45°N are shown and are taken from Tarney et al. (1980). Abundance patterns for three Puyehue basalts (samples 13828, 13826h, and 220283-1) are shown, and are distinguished by open symbols.

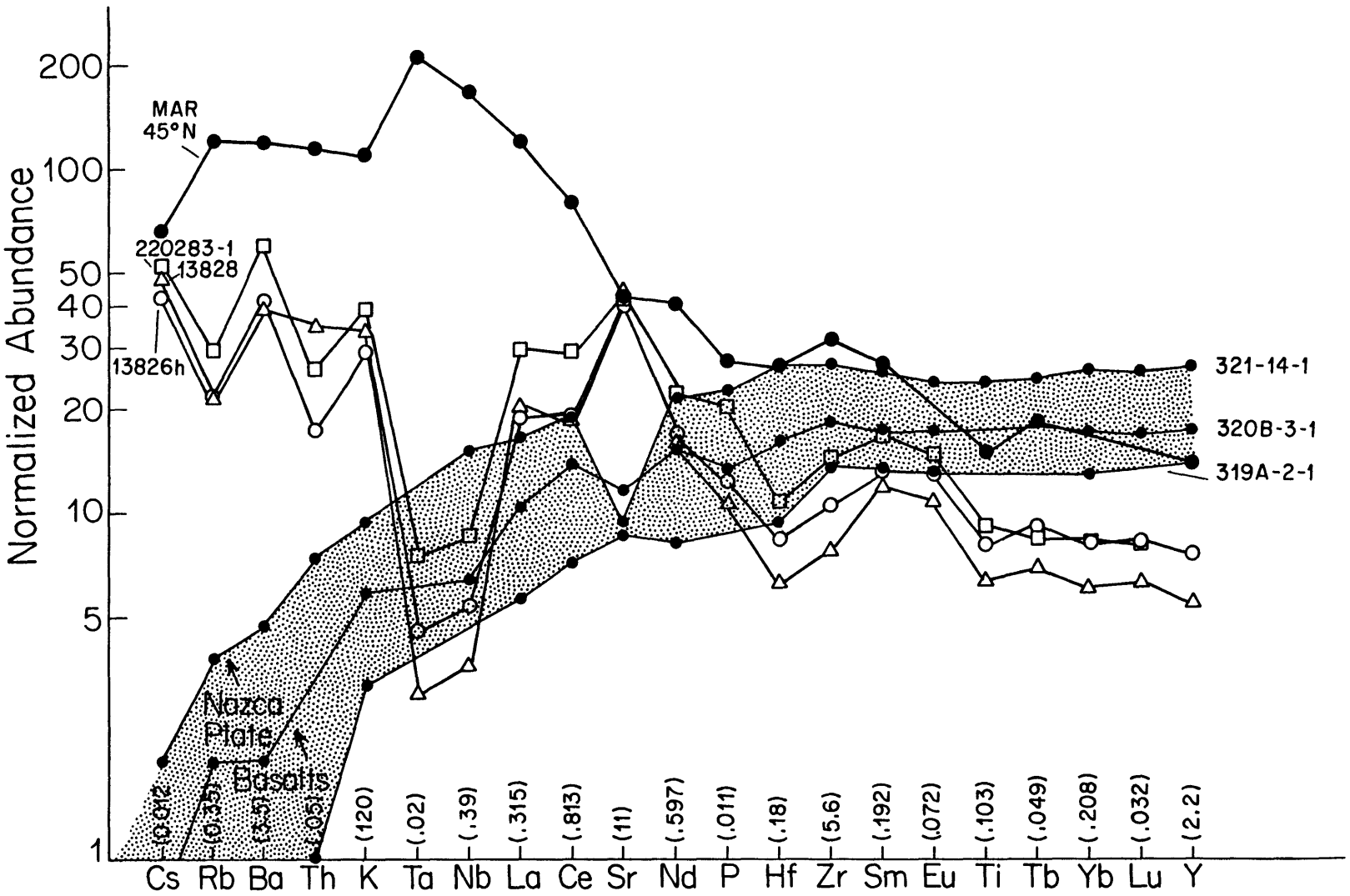
Normalized Abundance
200
100
50
40
30
20
10
5
1
MAR
45°N
220283-1
13828
13826h
321-14-1
320B-3-1
319A-2-1
Nazca
Plate
Basalts
(.012)
(.135)
(.5)
(.05)
(120)
(.02)
(.39)
(.315)
(.813)
(11)
(.597)
(.011)
(.18)
(5.6)
(.192)
(.072)
(.103)
(.049)
(.208)
(.032)
(2.2)
Cs Rb Ba Th K Ta Nb La Ce Sr Nd P Hf Zr Sm Eu Ti Tb Yb Lu Y

27 Relative variations in alkali (LIL) elements, Th, high-field strength (HFSE) trace elements, and rare earth group (REE) elements in basalts from Puyehue Volcano. Estimated analytical uncertainty represented by a cross (+) in each diagram.

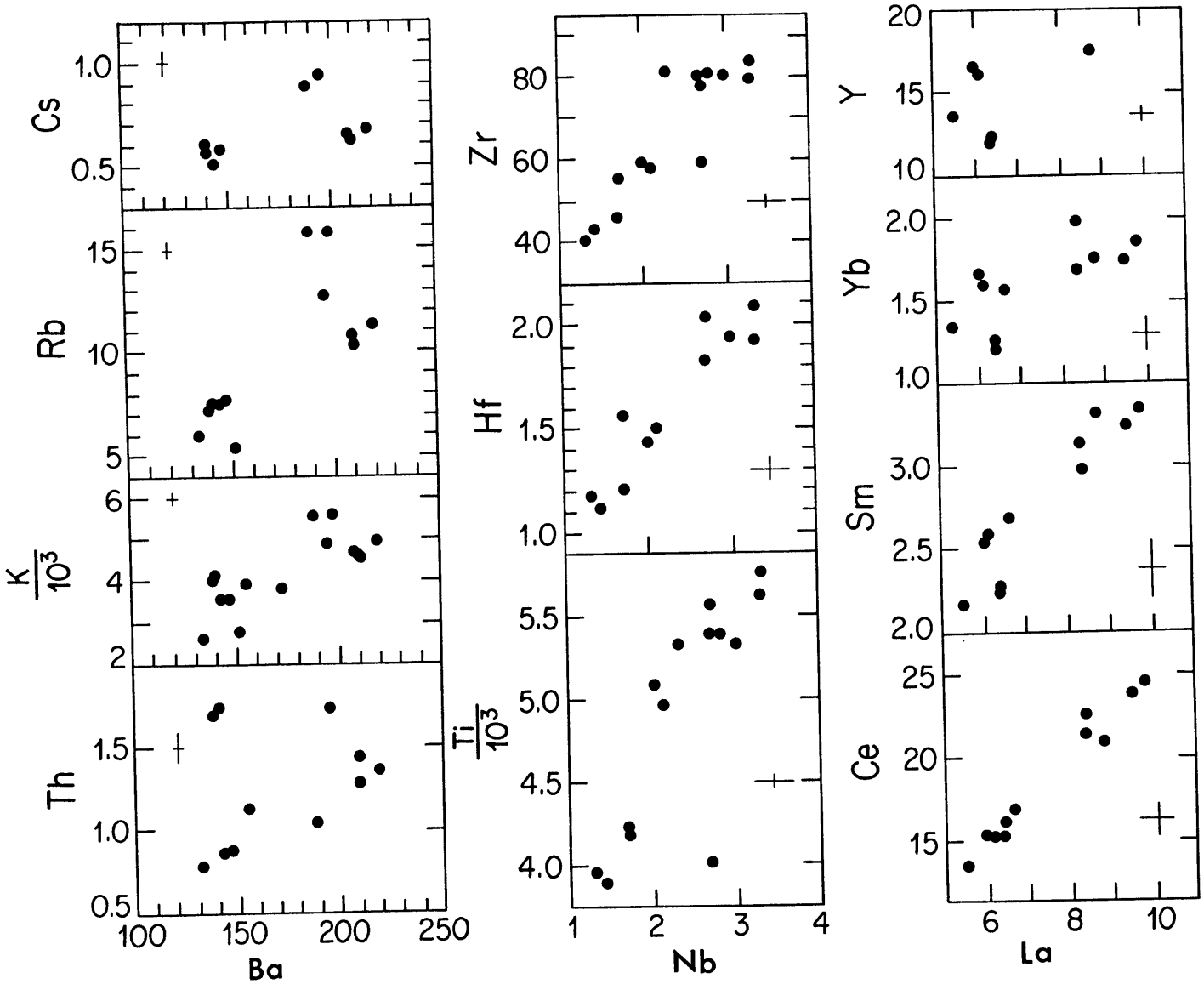
Cs
Rb
K/10³
Th
Ba
Zr
Hf
Ti/10³
Nb
Y
Yb
Sm
Ce
La

somewhat greater than analytical error. The scatter is greater in plots of LREE vs. HREE (La vs. Yb, La vs. Y) than in other plots of REE closer in atomic number (La vs. Ce, La vs. Sm). In particular, basalts with similar La abundances (6.0-6.4 ppm) display a ~ 40% difference in Yb abundances (1.2-1.7 ppm) which are inversely correlated with La, resulting in crossing REE patterns, e.g., samples 13826h and 13828 in Figure 26.

Trace element abundances in the basalts vary greater than 2x for some incompatible trace elements (Rb, Th, Nb) and nearly twofold for other incompatible and moderately incompatible trace elements such as Cs, La, and Zr. The range of trace element abundances in the basalts or enrichment factors (highest abundance/lowest abundance), using corrected abundances as above, may be used to rank the trace elements in the basalts based on their observed degree of incompatibility. Such a ranking of decreasing incompatibility (Rb (E.F. = 2.61) > Nb(2.41) > Th(2.25) > Zr(1.92) > Cs(1.86) > La(1.74) > Ba(1.69) ≥ K(1.66) > Nd(1.59) > Yb(1.45) ≥ Y(1.42) ≥ Sm(1.40) > Sr(1.24)) is different from that suggested by Hofmann (1983) based on bulk partition coefficients assumed for upper mantle MORB sources and trace element abundances observed in MORB (Fig. 26). This ranking of trace elements in Puyehue basalts is also different than the incompatible element order suggested for MORB by other workers (Wood et al., 1979; Tarney et al., 1980). Hofmann's (1983) ranking is based on trace element systematics within MORB. It may be true that arc basalts are generated under quite different conditions relative to MORB and thus a different order of incompatible elements for arc basalts may be expected. Nevertheless, the order observed in Puyehue basalts is very different from what may be expected based on mineral/melt

trace element partitioning in most reasonable mantle assemblages and this may suggest additional complexities other than partial melting to explain the variability in Puyehue basalts. For example, Zr abundances would not be expected to range more widely than Cs abundances, or La abundances more than K abundances, if all of the basalts were related by repeated melting episodes of a single source, or by varying degrees of melting of separated sources all with the same composition.

Trace element abundance ratios do not display many well-defined correlations with selected trace element abundances (Figures 28-30). Alkali element (LIL) abundance ratios are not well-correlated with LIL abundances (Fig. 28). Crude negative correlations of K/Rb and Ba/Rb vs. Rb may be interpreted as mixing trends, or if the basalts were produced by varying degrees of partial melting, that $D^{K}>D^{Rb}$. Increasing K abundances may be positively correlated with increasing K/Ba ratios in the basalts also signifying a mixing trend or that $D^{Ba}>D^{K}$.

Abundance ratios of HFSE display correlations with HFSE abundances, except where Nb may be involved, due to analytical uncertainty (Fig. 29). An increase in Zr/Hf and Zr/Ti ratios with increasing Zr abundances, as above, suggests either a mixing trend or that Zr is incompatible relative to Hf and Ti. Negative correlations of Ti/Nb, Hf/Nb, and possibly Zr/Nb vs. Nb abundances (Fig. 29) may also be mixing trends or at least clearly indicate that Nb may be the most incompatible element among the HFSE. REE abundance ratios display poor, if any, correlations with REE abundances (Fig. 30). It is especially noteworthy that basalts with relatively lower abundances of LREE (La = 5.4-6.4 ppm) display a wide range in degree of relative LREE enrichment. The low-abundance basalts are characterized by wide ranges of La/Sm (2.36-2.81) and La/Yb

28 Alkali (LIL) element abundance ratios vs. selected abundances in basalts from Puyehue Volcano.

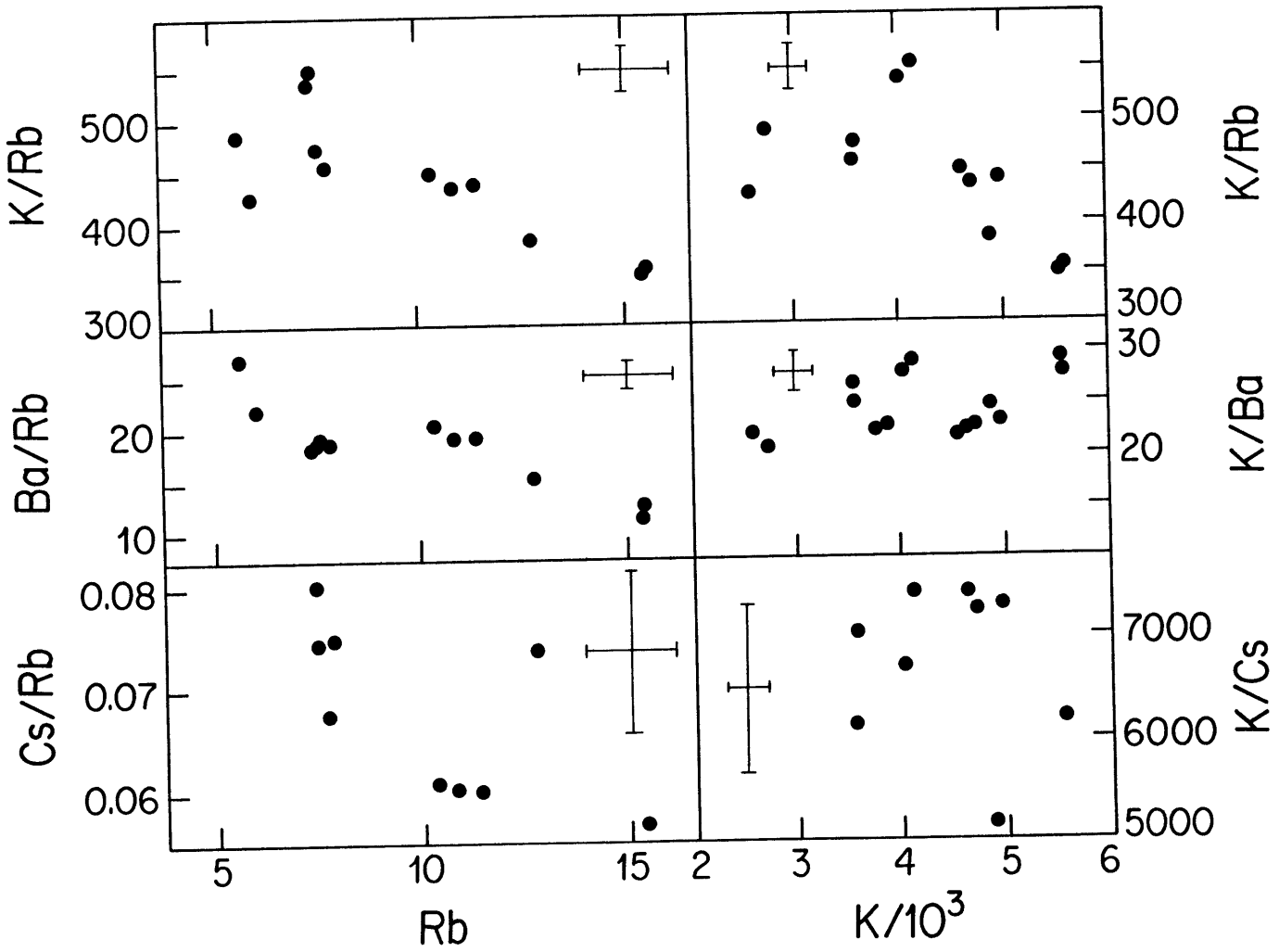
K/Rb
500
400
300
Ba/Rb
20
10
Cs/Rb
0.08
0.07
0.06
5
10
15
Rb
2
3
4
5
6
K/10^3
500
400
300
K/Rb
30
20
K/Ba
7000
6000
5000
K/Cs

29 High-field strength (HFSE) trace element abundance ratios vs. selected abundances in basalts from Puyehue Volcano.

Zr/Nb
35
30
25
20
Zr/Hf
45
40
35
Zr/Ti
0.014
0.012
0.010
40
50
60
70
80
Zr
Hf/Nb
1.0
0.9
0.8
0.7
0.6
Ti/Nb
3000
2000
1000
1
2
3
4
Nb

30 Rare earth element (REE) and Y abundance ratios vs. selected abundances in basalts from Puyehue Volcano.

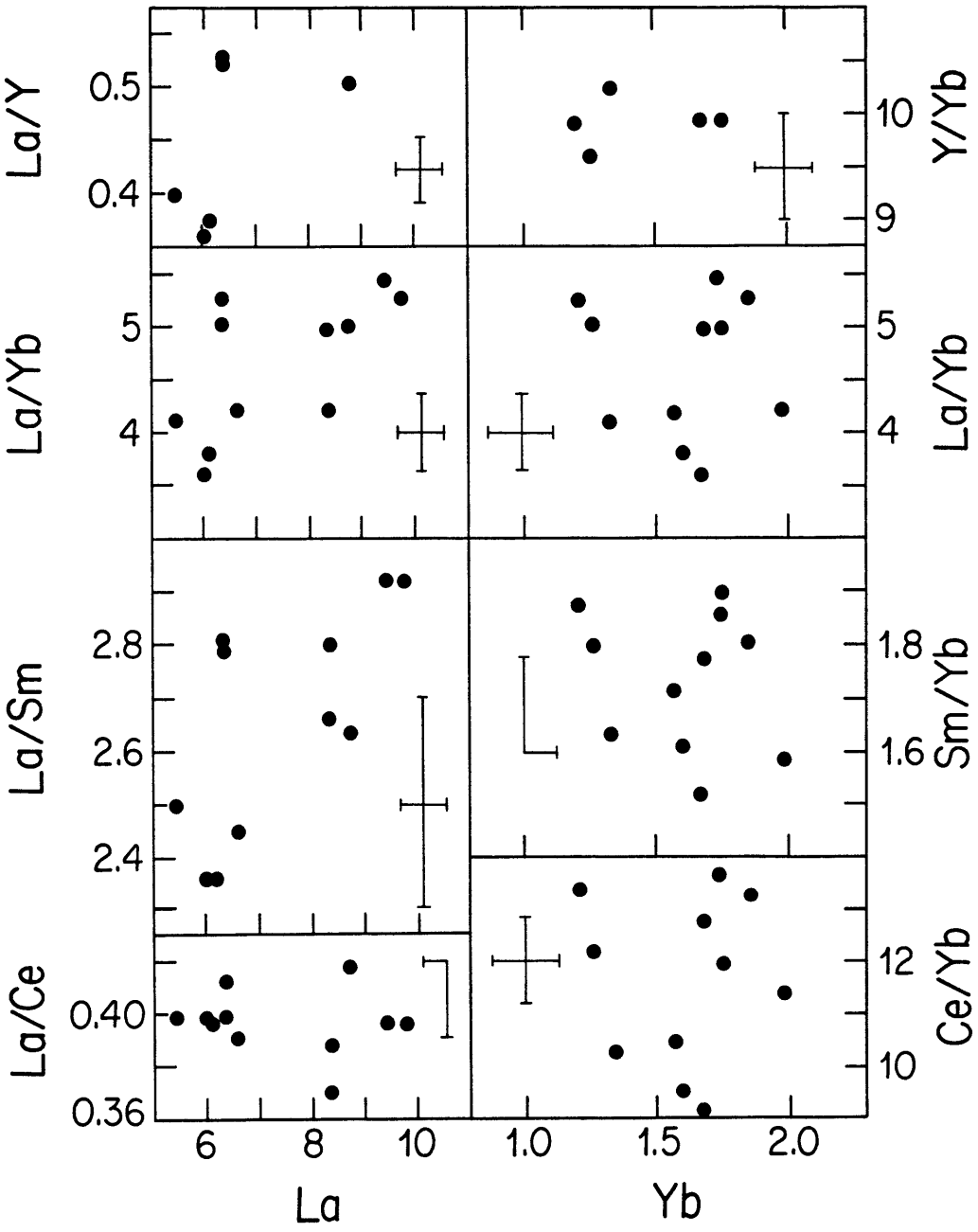
La/Y
0.5
0.4
Y/Yb
10
9
La/Yb
5
4
La/Yb
5
4
La/Sm
2.8
2.6
2.4
Sm/Yb
1.8
1.6
La/Ce
0.40
0.36
Ce/Yb
12
10
6
8
10
La
1.0
1.5
2.0
Yb

(3.59-5.23) ratios which are nearly equivalent to the total ranges observed (La/sm = 2.36 to 2.92, La/Yb = 3.59-5.43) for all of the basalts.

Abundances of HFSE, REE, and alkalis generally display positive correlations. This is partly illustrated by plots of La and Ba vs. Nb, and of La and Ba vs. Rb (Fig. 31). Abundances of Th are not simply correlated with REE, HFSE, or alkalis. Basalts with the lowest abundances of Nb (1.3-2.1 ppm), Rb (6.0-7.7 ppm), La (5.4-6.4 ppm) and Ba (133-146 ppm) also contain the most extreme Th abundances (Fig. 31). It is these basalts which are also characterized by extreme abundance ratios such as Ba/Th (81 vs. 166), La/Th (3.6 vs. 6.9), and Nb/Th (0.75 vs. 2.41). Basalts with relatively low abundances of La (6.0-6.4 ppm) and Ba (139-147 ppm) vary in Nb (1.3 to 2.1 ppm); as a result, these basalts display extreme Ba/Nb (68 vs. 108) and La/Nb (2.86 vs. 4.87) ratios. In general, LIL/LREE abundance ratios are less variable than LIL/HFSE, LIL/Th, or HFSE/Th abundance ratios, none of which display clear correlations with any abundances.

Incompatible element abundance ratios in the basalts vary widely but do not display good correlations (Fig. 26). The best trend observed is a negative correlation between Ba/Th and La/Nb ratios and the linearity of a 'companion' plot (after Langmuir et al., 1979) of Ba/Th vs. Nb/Th suggests that the basalts may be explained by mixing of two distinct sources or mixing of parental magmas derived from two distinct sources. The linear correlations observed in other companion plots in Figure 32 may be fortuitous. Mediocre to nonexistent correlations are observed in corresponding ratio-ratio plots and element-element plots (Figures 31 and 32). Calculated, arbitrary mixing curves assuming specific basalts as

31 Selected covariations of alkali (LIL) elements, HFSE, REE, and Th in basalts from Puyehue Volcano.

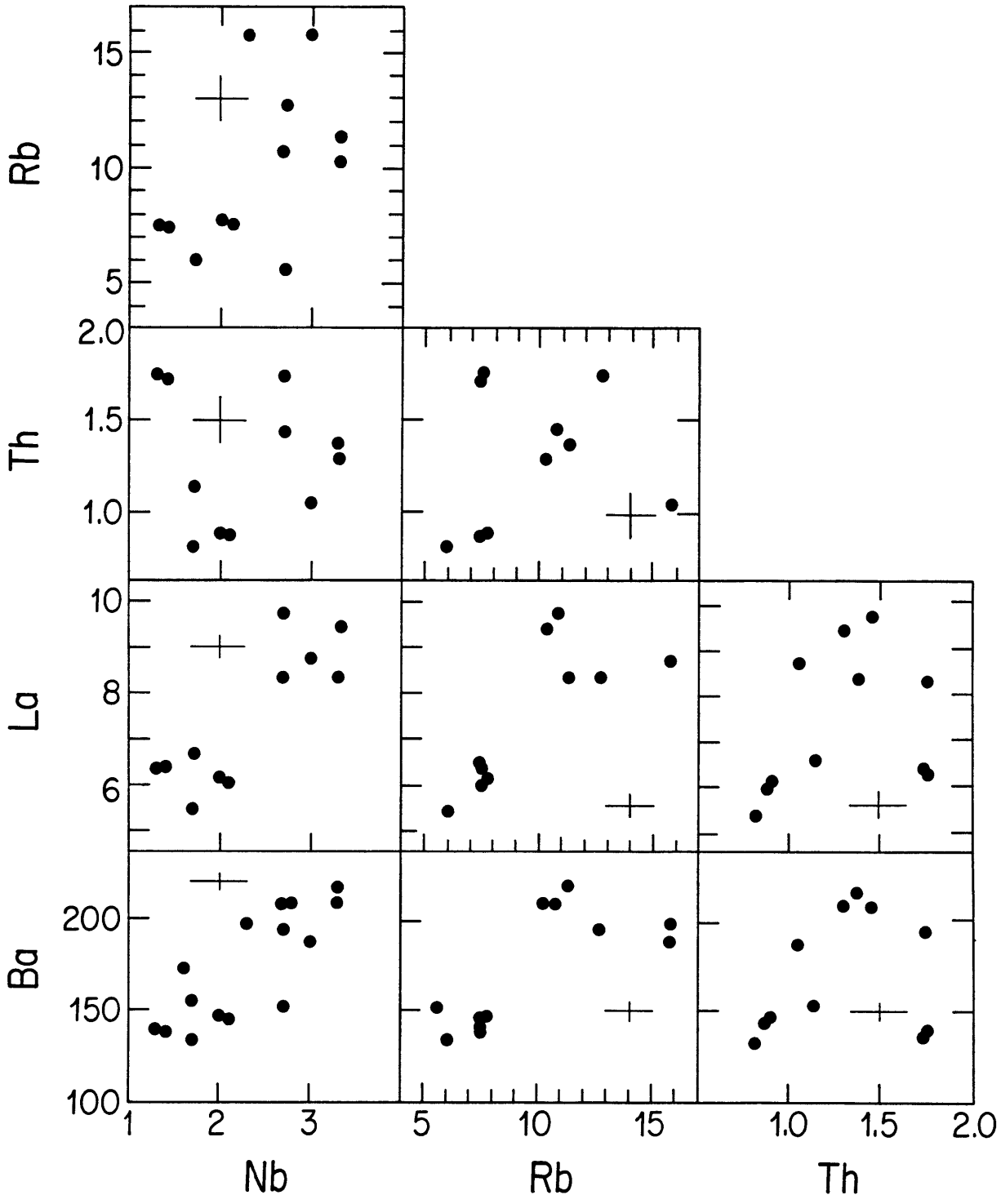
Rb
15
10
5
Th
2.0
1.5
1.0
La
10
8
6
Ba
200
150
100
1
2
3
Nb
5
10
15
Rb
1.0
1.5
2.0
Th

32 Co-variations in selected trace element abundance ratios for basalts from Puyehue Volcano. Arbitrary mixing curves attempting to relate the basalts by mixing of two or three endmembers were calculated using abundances in specific basalts presumed to lie on mixing lines (cf. Langmuir et al., 1978). Complementary diagrams to test for mixing relationships are shown at the right and suggest that two of three possible mixing endmembers may be characterized by similar abundance ratios (see text).

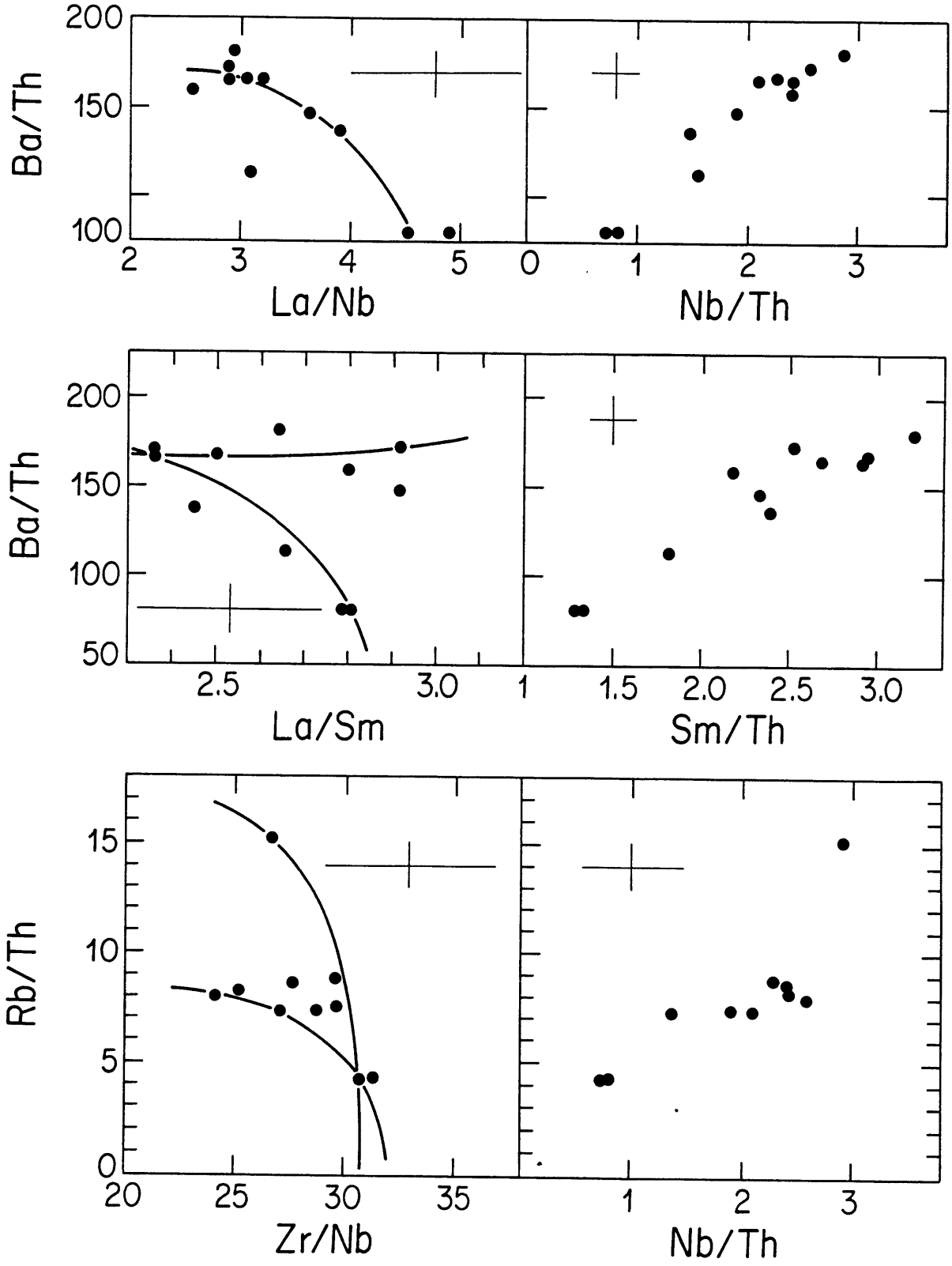
Ba/Th
200
150
100
2
3
4
5
La/Nb
0
1
2
3
Nb/Th
Ba/Th
200
150
100
50
2.5
3.0
La/Sm
1
1.5
2.0
2.5
3.0
Sm/Th
Rb/Th
15
10
5
0
20
25
30
35
Zr/Nb
1
2
3
Nb/Th

mixtures do not pass through all data points in ratio-ratio plots (Fig. 32), but two mixing curves between three components may explain the scatter. The linear correlations on each of the three companion plots in Figure 32 signifies, then, that two of the three components are similar in one abundance ratio. The lack of any observed correlations between alkali abundance ratios (K/Rb, Rb/Sr, Ba/Rb, etc.) or ratios such as Ba/Th, Ba/Nb, Ba/Zr, or K/La and degree of relative LREE enrichment (e.g., La/Sm and La/Yb ratios) suggests that variations in alkali elements may be decoupled from variations in REE and HFSE.

The basalts are slightly variable with respect to Sr-isotopic composition, but nearly homogeneous in Nd- and Pb-isotopic compositions. Although absolute abundances of incompatible trace elements may be affected by phenocryst dilution, $^{87}Sr/^{86}Sr$ ratios in basalts display crude positive (vs. Cs, Rb, K, and La) or negative correlations (vs. Th) with trace element abundances (Fig. 33). Positive correlations of incompatible trace elements with $^{87}Sr/^{86}Sr$ in the basalts may be consistent with either magma mixing, crustal contamination, or AFC processes, however, a vague negative correlation of Th vs. $^{87}Sr/^{86}Sr$ may support magma mixing, assuming that Th abundances, along with other incompatible trace elements, may be increased during crustal contamination or AFC processes. The boundary or 'cutoff' for basalts (<52 wt.%) and basaltic andesites (>52 wt.%) based on SiO_2 contents is somewhat arbitrary. Despite slightly overlapping MgO contents in basalts (4.7-9.5 wt.%) and basaltic andesites (5.5-6.0 wt.%), abundances of most incompatible trace elements are uniformly higher in basaltic andesites relative to basalts which have similar MgO contents or $^{87}Sr/^{86}Sr$ (Figs. 11 and 33). Two basalt samples with the highest $^{87}Sr/^{86}Sr$ (.70406

33 Variations in selected trace element abundances with $^{87}Sr/^{86}Sr$ in basalts (filled circles) and basaltic andesites (open circles) from Puyehue Volcano. Estimated analytical uncertainty noted by crosses (+).

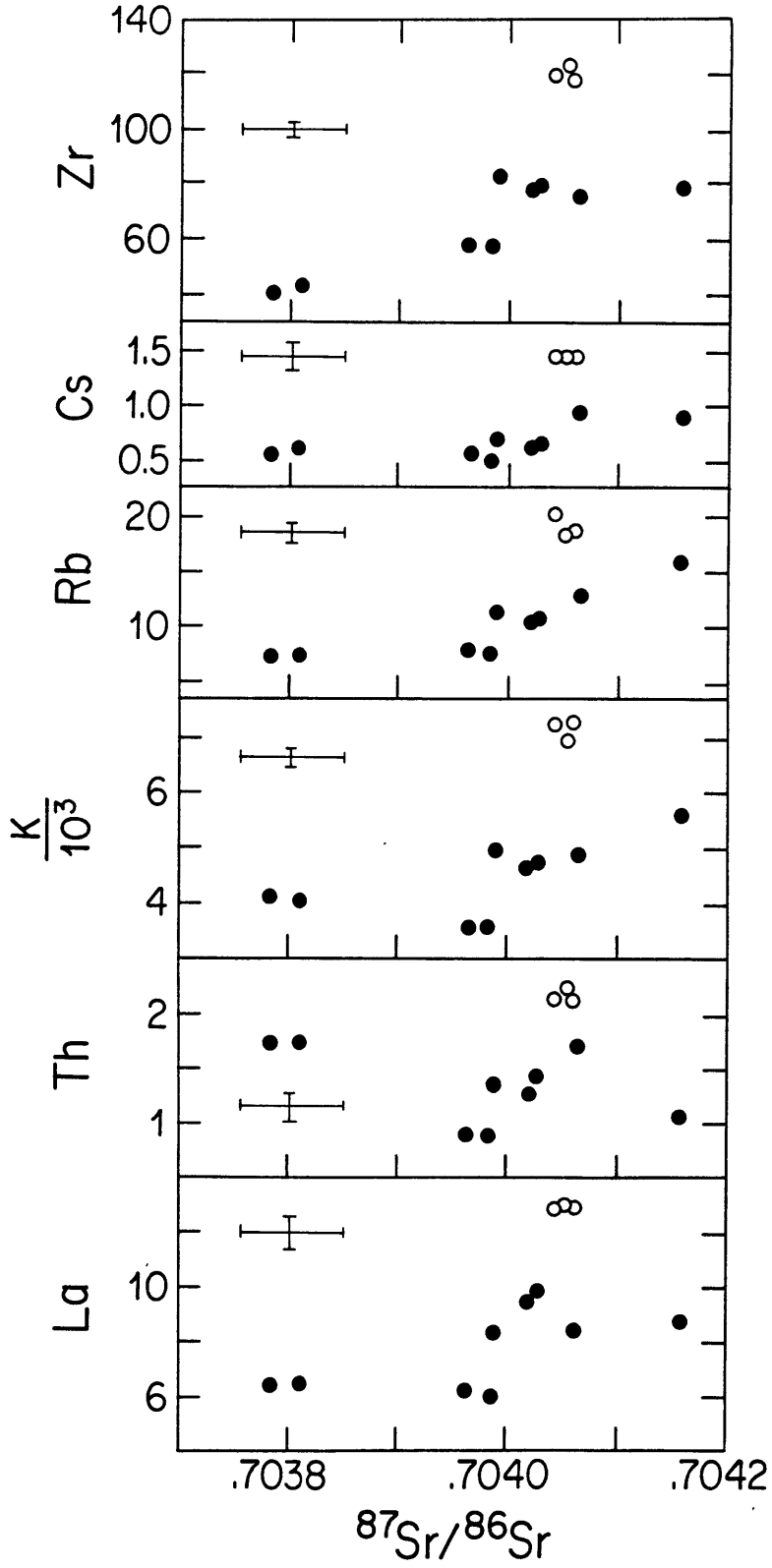
140
100
60
Zr
1.5
1.0
0.5
Cs
20
10
Rb
6
4
K/10³
2
1
Th
10
6
La
.7038
.7040
.7042
87Sr/86Sr

and .70416) are characterized by Cs, Rb, and K abundances which are high relative to most other basalts but still lower than most basaltic andesites. The basalt (sample 272824b) with Rb and K abundances similar to basaltic andesites is distinguished from the latter by relatively higher $^{87}Sr/^{86}Sr$ and lower Cs, Th, and La abundances (Fig. 33).

Selected trace element abundance ratios are correlated with isotopic compositions of the basalts. Among LIL elements, trends are apparent in plots of K/Rb and Rb/Sr vs. $^{87}Sr/^{86}Sr$, though a single trend is not observed for Ba/Rb vs. $^{87}Sr/^{86}Sr$ (Fig. 34a, 34b). While it is obvious that a single mixing line cannot explain the relationships (or lack thereof) of $^{87}Sr/^{86}Sr$ with Ba/Rb ratios, it is not as obvious for $^{87}Sr/^{86}Sr$ vs. K/Rb (Fig. 34a). Utilizing abundance data, single mixing lines assuming two basalts as mixtures consisting of respectively varying proportions of unspecified endmembers do not include, or pass through all data points. Two mixing curves are necessary (Fig. 34a). The linear correlation on the companion plot of K/Rb vs. $^{87}Sr/^{86}Sr$ indicates that two of the three endmembers required may have similar Rb/Sr ratios but different $^{87}Sr/^{86}Sr$ ratios. A plot of Rb/Sr (corrected for plagioclase phenocrysts as described earlier) vs. $^{87}Sr/^{86}Sr$ also requires more than one mixing curve (Fig. 34b). Not necessarily apparent on a plot of K/Rb vs. $^{86}Sr/Rb$, but suggested on a plot of K/Rb vs. $^{87}Sr/^{86}Sr$ and Rb/Sr vs. $^{87}Sr/^{86}Sr$ is the possibility that basalts with intermediate $^{87}Sr/^{86}Sr$ (0.70397-0.70403) define a mixing curve between endmembers with different Rb/Sr ratios in addition to different $^{87}Sr/^{86}Sr$ ratios (Fig. 34a). Due to elevated Rb abundances, the two basalts with the highest $^{87}Sr/^{86}Sr$ (0.70406 and 0.70416) are characterized by lower K/Rb and Ba/Rb ratios and higher Rb/Sr ratios than the remainder of the basalts. These are the

34(a) Variations in selected trace element abundance ratios with $^{87}Sr/^{86}Sr$ in basalts from Puyehue Volcano. Complementary diagrams (cf., Langmuir et al., 1978) are shown for K/Rb and Ba/Rb vs. $^{87}Sr/^{86}Sr$. Evidence of single two-component mixing trends is lacking for Ba/Rb $^{87}Sr/^{86}Sr$. For K/Rb vs. $^{87}Sr/^{86}Sr$, the lack of single, two-component mixing relationships is more subtle, and is demonstrated by plotting two possible mixing curves. The linearity of K/Rb vs. $^{86}Sr/Rb$ suggests that two of the three possible mixing endmembers or components may be characterized by similar K/Rb but different $^{87}Sr/^{86}Sr$ ratios.

(b) Variations in Rb/Sr and La/Sm vs. $^{87}Sr/^{86}Sr$ in basalts from Puyehue Volcano. As in (a), K/Rb vs. $^{87}Sr/^{86}Sr$, a single mixing curve is not clearly indicated for Rb/Sr vs. $^{87}Sr/^{86}Sr$. As seen in La/Sm vs. $^{87}Sr/^{86}Sr$, Sr-isotopic compositions of the basalts are not correlated with degree of relative LREE enrichment.

(c) Variations in La/Nb, K/Nb, Zr/Sm, and Hf/Sm ratios with $^{87}Sr/^{86}Sr$ ratios in basalts from Puyehue Volcano. Complementary diagrams (cf., Langmuir et al., 1978) are shown for each plot as a test for possible mixing relationships.

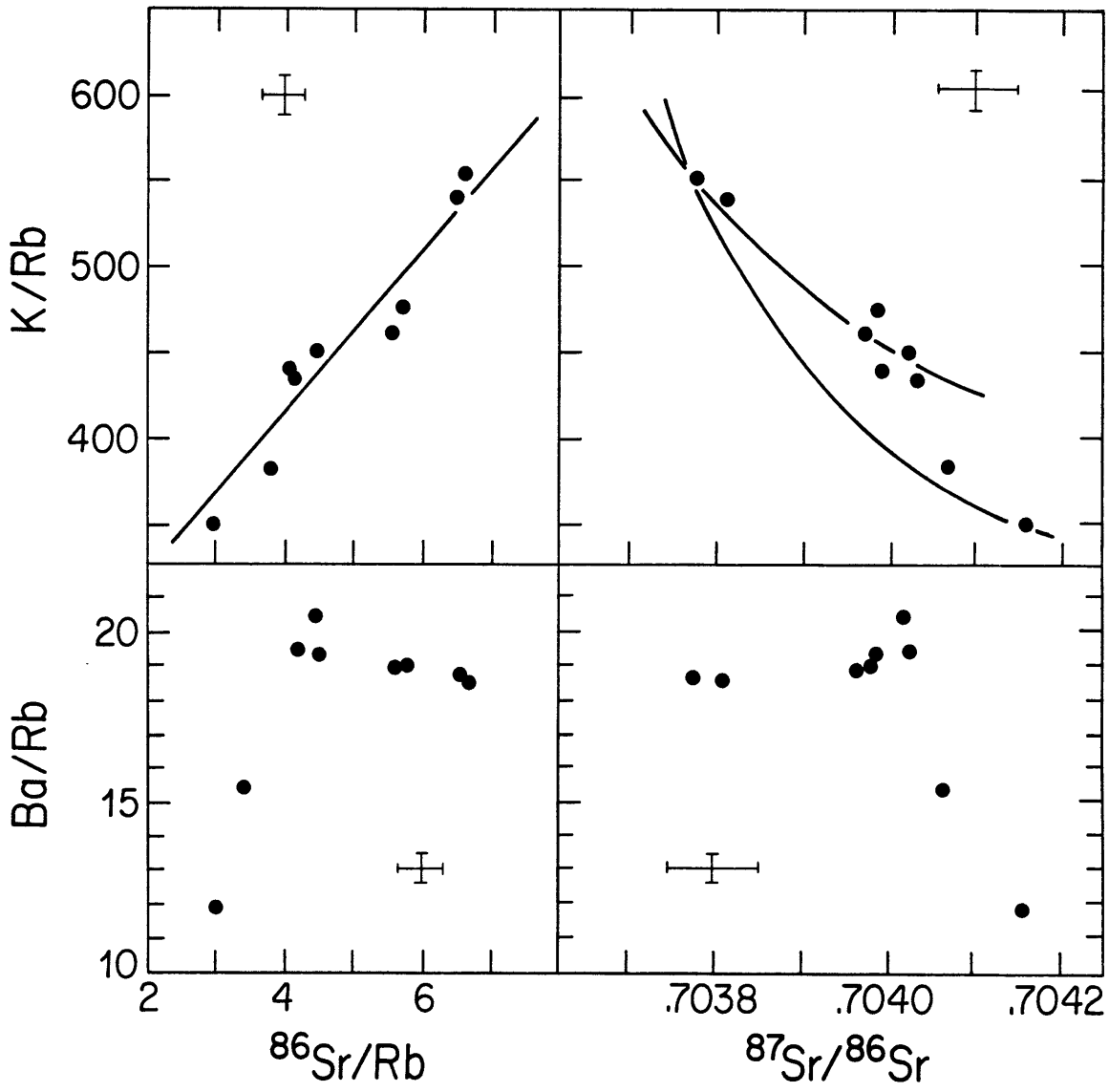
600
500
400
K/Rb
20
15
10
Ba/Rb
2
4
6
$^{86}Sr/Rb$
.7038
.7040
.7042
$^{87}Sr/^{86}Sr$

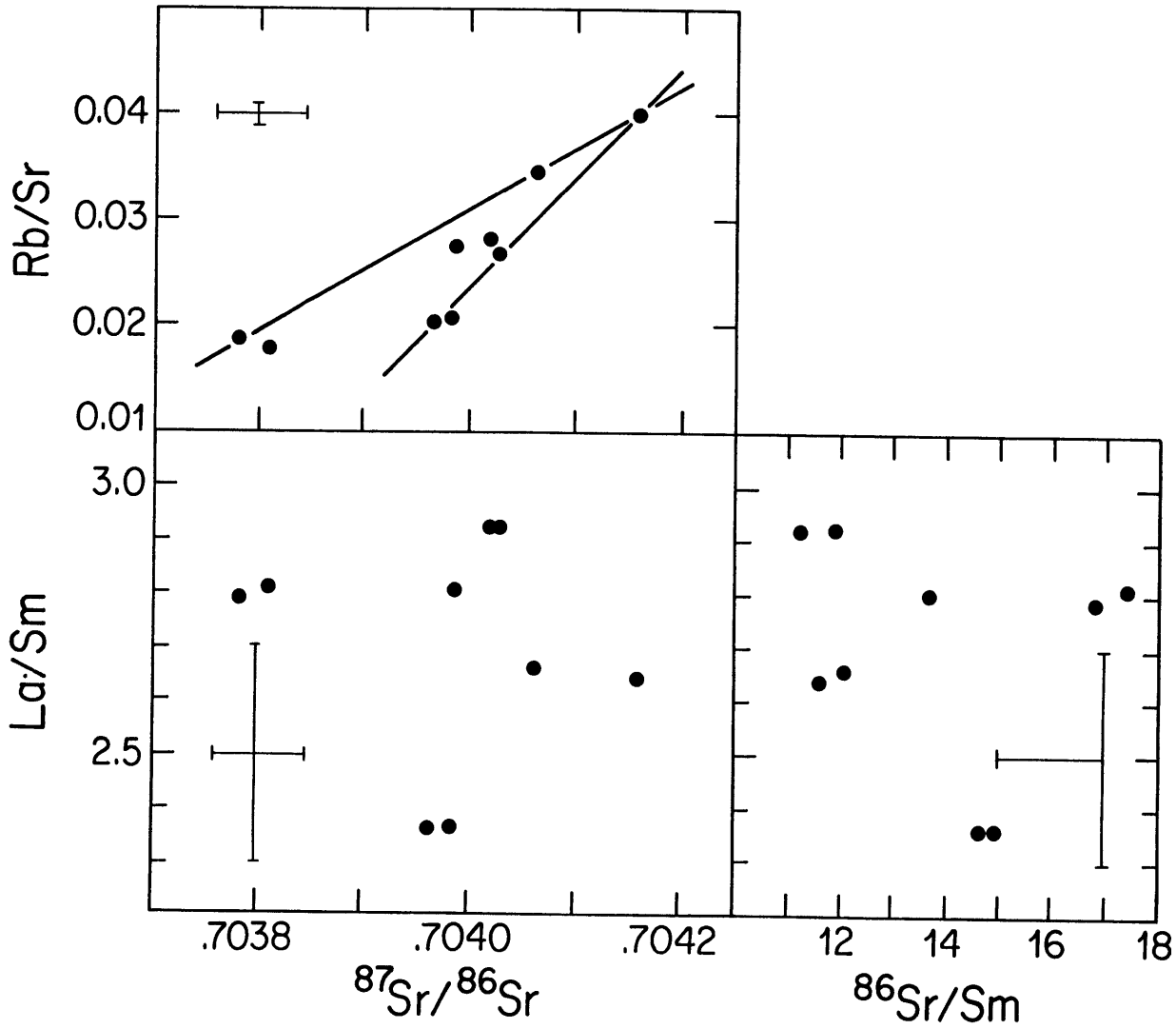
0.04
0.03
0.02
0.01
Rb/Sr
3.0
2.5
La/Sm
.7038
.7040
.7042
87Sr/86Sr
12
14
16
18
86Sr/Sm

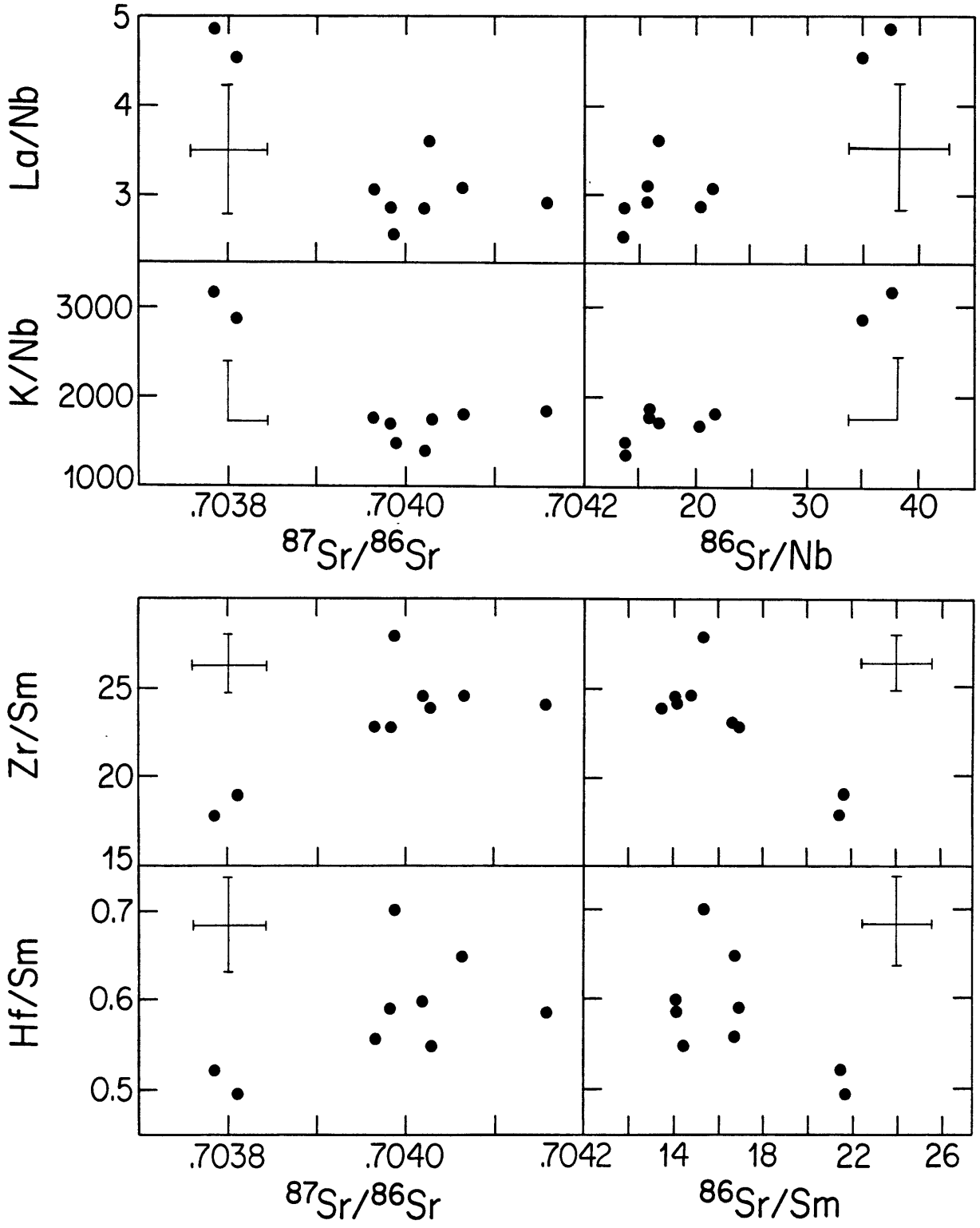
La/Nb
5
4
3
K/Nb
3000
2000
1000
.7038
.7040
.7042
87Sr/86Sr
20
30
40
86Sr/Nb
Zr/Sm
25
20
15
Hf/Sm
0.7
0.6
0.5
.7038
.7040
.7042
87Sr/86Sr
14
18
22
26
86Sr/Sm

chief distinguishing factors for these two basalts, however, these two samples are intermediate in most trace element abundances and undistinguished by most other trace element abundance ratios.

The relative degree of LREE enrichment in the basalts is not correlated with their isotopic composition as shown in a plot of La/Sm vs. $^{87}Sr/^{86}Sr$ (Fig. 34b). Abundances and abundance ratios, e.g., Nb/Hf, Zr/Hf, and Zr/Ti, of HFSE are positively correlated, though crudely, with $^{87}Sr/^{86}Sr$. Ratios of alkali elements and REE with HFSE serve to semi-quantify the relative magnitudes of HFSE depletions if elements chosen are similar in their respective bulk partition coefficients at least in upper mantle lithologies. Ratios such as Zr/Sm and Hf/Sm display crude positive correlations with $^{87}Sr/^{86}Sr$, and K/Nb and La/Nb are inversely correlated with $^{87}Sr/^{86}Sr$ in the basalts (Fig. 34c), suggesting that the magnitude of negative HFSE depletions decreases with increasing $^{87}Sr/^{86}Sr$. No continuous correlation of Sr-isotopic composition with Ba/Nb ratios is observed, only a general division between basalts with high Ba/Nb (99-108) ratios and low $^{87}Sr/^{86}Sr$ (.70378-.70381) and basalts with relatively lower Ba/Nb (63-77) ratios and higher $^{87}Sr/^{86}Sr$ (.70397-.70416). In summary, the Sr-isotopic composition of basalts varies with the abundances and abundance ratios of alkalis (LIL) and HFSE, but is generally decoupled from variations in REE abundances and degree of relative LREE enrichment.

10.2 Components of arc magma genesis

Volcanic rocks from a single center or a number of centers over a finite region associated with a subduction zone have been produced and modified by any number of complex processes that may involve many

components. This is an inherent property of volcanic arcs in general. In a continental arc such as the southern Andes of Chile (34°-46°S), several components may have contributed to sources of the magmas, or subsequently modified primary magmas during ascent and emplacement. These include:

1) Sub-arc mantle, either
   (a) depleted mantle formed as a residue from production of mid-ocean ridge basalts (MORB).
   (b) mantle enriched relative to (a), variable in trace-element and isotopic characteristics, and suitable as a source for oceanic island basalts (OIB) or MORB.
2) Subducted oceanic crust, consisting of a few km thickness of MORB basalts, gabbroic cumulates, ultramafic cumulates, and minor OIB basalts.
3) Sediments, which may be found in two specific localities in an arc setting:
   (a) sediments may comprise a small fraction of the subducted oceanic crust, (2) above. Depending on the tectonic setting (the size of the oceanic basin, and uplift and erosion rates of the overriding continental mass), the relative proportions of abyssal (pelagic) sediments and continentally derived sediments may vary, an important consideration because each has differing geochemical characteristics.
   (b) sediments may comprise a significant portion of the continental crust, and as above, may be variable, consisting of continental, marine, or volcanogenic sediments, depending on local tectonic and geologic history.

4) continental crust comprising the uppermost portion of the overriding plate is typically subdivided into two components:
   (a) upper crust, which may include a wide variety of rock types of widely ranging age, and
   (b) lower crust, generally thought to consist of high-grade metamorphic rocks relatively older than (a), unless the lower crust is largely comprised of crystal cumulates of basaltic magmas in which case it is of similar age and possibly isotopic character.

Because of the characteristic structure of a subduction zone, or Wadati-Benioff zone, the effects of component (4) above must be identified and evaluated, before assessment of the relative roles of components (1), (2), and (3), all of which may have contributed to the subcrustal source of primary magma generation. In subsequent sections, the signature and mechanism of crustal contamination in basalts from Puyehue Volcano will be investigated. The petrogenesis of basalts unaffected by a secondary process such as crustal contamination will then be addressed in an attempt to estimate the geochemical characteristics of the subcrustal arc source. The basalts have been shown to exhibit variable geochemical characteristics which may reflect geochemically distinct subcrustal sources, or more specifically, sources which vary in their relative proportions or contributions of sub-arc mantle, subducted oceanic crust, and subducted sediments. This two-stage investigative procedure will make use of geochemical characteristics unique to each major component listed above.

10.3 Processes and environment of magma contamination

The best evidence of crustal contamination is indicated by systematic correlations between isotopic compositions and other

compositional parameters in a series of lavas believed to be cogenetic or comagmatic on the basis of geologic evidence. If preexisting crustal rocks are relatively young or at least not drastically different in isotopic composition relative to intruding magmas, then derivative plutonics or volcanics which have experienced crustal contamination may display little or no diagnostic isotopic signature. This may be true at least in part for the Puyehue-Cordon Caulle region. Granitic xenoliths ($^{87}Sr/^{86}Sr$ = .70453) from the 1979 Mirador eruption indicate the presence of relatively young plutonic bodies at depth. However, Tertiary and older plutonic rocks related to the Panguipulli batholith crop out immediately to the north of the study area, and metamorphic basement rocks as old as Paleozoic crop out to the east and south (Fig. 1, Plate I). Thus, the wide variety of pre-Quaternary rocks exposed suggest that at relatively shallow depths of up to a few km, magmas in the Puyehue-Cordon Caulle area may be in contact with a variety of upper crustal wall rocks characterized by a large range of isotopic compositions. Although the continental lithosphere in this region may be thin (~30 km; Herron et al., 1981) relative to the Central Andes, the presence of relatively older, high-grade metamorphic lower crustal lithologies cannot be ruled out.

Wallrock contamination of magmas may take place by three major mechanisms and these include: (1) bulk assimilation of wallrock, (2) adulteration of magmas by partial melts extracted from wall rock, and (3) solid-liquid diffusion between wallrock and magma. All three of these mechanisms may occur both within the continental crust and in the subcrustal environment. Recognition of crustal contamination is dependent on contrasting geochemical characteristics of crustal lithologies and upper mantle lithologies and possibly a difference in which processes are most prevalent in each environment respectively.

One of the three mechanisms by which magmas may be contaminated is that of bulk assimilation of surrounding wallrock, and this may be necessary for magmas to create space in which to aggregate, ascend, and eventually create a magma chamber in which they may reside prior to eruption. Difference in the physical conditions between the upper mantle environment and the crustal environment may dictate whether or not contamination by bulk assimilation is relatively more effective, or at least likely to occur. At any point in the history of ascending magma, there must be a thermal contrast between magma and wallrock. The first type or stage of bulk assimilation may take place in the form of complete melting of surrounding upper mantle lithologies by contact with primary melts. This creates more interconnected pore space to facilitate the aggregation of magma and instabilities related to density differences lead to diapiric uprise. Magmas may rise adiabatically, but excess heat is required for continuous melting of wallrock in transit. This may be facilitated by continuous replenishment of melt from greater depths which may effectively maintain a thermal contrast between magma and wallrock. Stoping of wallrock is a process by which magmas may progress, however, as Marsh (1980) has pointed out, if the magma is constant in volume, stoping may proceed to a point where the conduit is choked and the magma can ascend no further. This problem is circumvented if there is a continuous supply of replenishing melt from below, and if some degree of bulk assimilation (complete melting) of stoped wallrock takes place. However, stoping without melting of wallrock may be more likely during transit through the upper mantle since the thermal contrast between magma and wallrock may not be large. The thermal contrast between magma and continental crust may be greater so that bulk assimilation is relatively

more possible in this environment although this depends on the thermal budget of the magma and the physical properties of both the magma and the enclosing wallrocks. This may occur in a magma chamber which represents the final endpoint of ascent, and stoping may not be occurring at this stage. If dissipation of heat within the wallrock is relatively rapid and the solidus of the wallrock relatively high, then crustal contamination of the magma may be minimized in the crustal environment. The geochemical characteristics of the magma source and the upper mantle wallrock which is intruded or traversed may be similar and contamination of the magma in this environment may not produce any diagnostic geochemical signature in ascending the magmas. The composition of the crust in a continental arc setting is expected to be geochemically distinct compared to primitive magmas and a geochemical signature in the magma resulting from bulk melting of wallrock would be recognizable.

Contamination of a magma by mixing with partial melts extracted from wallrock as in category (2) rather than bulk assimilation, may also be a consequence during ascent and emplacement of a magma. If the composition of the wallrock is known, then the geochemical effects of bulk assimilation vs. contamination by partial melting of the wall rock may be discerned, assuming that the composition of the partial melt may be inferred. Within the upper mantle 'hanging wall' portion of a Wadati-Benioff subduction zone, contamination by partial melts of peridotitic wall rock may increase the abundances of incompatible trace elements in primary magmas such that they appear to represent a smaller degree of partial melting relative to the degree of melting in the initial stage of their production. If melt extraction from wall rock residue is relatively rapid, non-equilibrium melts may be added to magma

in transit and these melts will differ in compositions from partial melts produced by batch melting. The characteristics of contaminating non-equilibrium melts extracted from wall rock may be governed by different rates of solid-liquid diffusion for different elements and various minerals, grain size, and magma-wall rock thermal contrast. This would be manifest as selective enrichment in magmas by the most diffusive, or volatile elements, such as alkalis, leading to apparent lower effective bulk partition coefficients for these elements relative to other elements such as REE and HFSE. Finally, additional complications may result if the upper mantle is not constant in lithology throughout, and differences in proportions or types of phases will result in different trace element characteristics in wall rock partial melts. Thus, contamination of primitive magmas by mixing in transit with partial melts of upper mantle wall rock may not be easily recognized and may change the geochemical characteristics of the magmas so that the characteristics of their initial sources cannot be ascertained. Contamination of magmas by mixing with wall rock partial melts within the continental crust may be more easily recognized, again primarily due to the expected compositional contrast between primitive mantle-derived magmas and continental crust. However, some compositional parameters such as certain trace element abundance ratios may be similar in both the upper mantle and the continental crust. Similar changes in the abundance ratios in primitive magmas may be brought about by contamination either in the upper mantle or in the crustal environment, as will be discussed in a later section concerning subcrustal arc processes.

Solid-liquid diffusion as a means of contaminating primitive magmas contrasts with the previous two mechanisms. In order for diffusion

between magma and wallrock to be defined as an independent mechanism, no melting of wallrock can occur. For most wall rock lithologies, diffusion in solids, even in a monominerallic assemblage, is relatively slow at subsolidus temperatures and only the most readily diffusive elements, possibly alkalis, may be added to magma by this mechanism. This is a selective contamination process in that a magma may be enriched in certain trace elements with little or no change in major-element bulk composition. Alternatively, if magma is enriched relative to wallrock in elements which diffuse readily, diffusion may occur in an opposite sense such that the magma may lose elements to wallrock. If magma ascent is sufficiently slow relative to diffusion rates, then the magma may continually re-equilibrate with unmelted wallrock. Within the upper mantle environment, however, changes in the magma composition due to this process would result only if there is a difference in composition and/or modal mineralogy between wallrock and the primary source of the magma. Diffusion as the sole means of contamination of magma requires that solid wallrock within the upper mantle or continental crust must be porous or must deform plastically to allow passage of magma. Since continental crust is relatively more brittle than upper mantle material, magma ascent by plastic deformation is less likely within the crust than forceful intrusion or stoping.

In summary, it may not be possible to state which of the three types of wallrock contamination, i.e., bulk assimilation, contamination by partial melts, or contamination by solid-liquid diffusion, is relatively more prevalent in the subcrustal/upper mantle environment or the continental Diffusion between magma and solid wall rock may be an effective means of contamination of magmas at relatively shallow crustal

levels. Processes of partial melting or complete melting of wall rock may be prevalent at relatively deeper levels within the lower crust and upper mantle in order for magmas to ascend. Without accurate knowledge of the means by magmas aggregate and ascend, contamination of magmas within the upper mantle, if recognizable as such, cannot be unambiguously attributed to one of the three methods of contamination discussed above. Testing for contamination within the continental crust depends on the contrasting geochemical characteristics between upper mantle and continental crust. The average bulk composition of the continental lithosphere, or at least that of potential contaminating materials may be granodioritic to granitic. This may be assumed even if the average bulk composition is relatively more mafic than granodiorite, since minimum or partial melts should be largely granitic in bulk composition.

10.4 Crustal contamination in Puyehue basalts

Two basalts in this study (samples 272824b and 250283-2) display characteristics which may be interpreted as resulting from crustal contamination. The major-element compositions of these basalts are similar to those of the remainder of the basalts. These basalts are not distinguished by any aberrant petrographic characteristics save a slight variation in olivine phenocryst compositions (Fo_{70} to Fo_{80}) which is large relative to the range of composition in other basalts (Fig. 4). Basalts 272824b and 250283-2 are characterized by relatively intermediate abundances of most incompatible trace elements. The most noteworthy characteristics include : anomalously elevated Cs and Rb abundances (Fig. 27) and higher $^{87}Sr/^{86}Sr$ relative to the remainder of the basalts. In addition to higher $^{87}Sr/^{86}Sr$ ratios, these basalts are characterized

by ratios of Ba/Rb (11.9-15.4) and K/Rb (352-383) which are lower than those of the remainder of the basalts (Ba/Rb = 18.7-27, K/Rb = 429-551. Bulk assimilation of granitic wallrocks such as Mirador granite (Table 7c) in amounts required to explain the observed relative increases in Rb and Cs abundances and lower Ba/Rb and K/Rb ratios would not greatly affect the major-element composition of contaminated basalts. However, other incompatible trace elements enriched in granite such as Th, Ba, and La are not higher in these basalts (250283-2 and 272824b) relative to other basalts. Another way of explaining some of the characteristics of these two basalts is if they consist of mixtures of basaltic magma and rhyolitic magma, a process akin to bulk assimilation of granite. Rhyolites analyzed from this area have similar or lower $^{87}Sr/^{86}Sr$ than these two basalts, however.

In some ways, these two basalts (especially sample 250283-2) are similar to the low-SiO_2 basaltic andesites discussed earlier (section 5.2). The basaltic andesites were explained as a result of mixing basaltic magmas with evolved magmas such as rhyolite or high-TiO_2, high-P_2O_5 andesite. Figure 35 consists of a series of trace element abundance ratios vs. $^{87}Sr/^{86}Sr$ designed to illustrate both similarities and differences between the basaltic andesites and the two basalts (272824b and 250283-2), and mixing curves for a mixing model presented in Table 7d. In most plots (Fig. 35) mixing of any of the basalts with either rhyolite or andesite cannot duplicate the characteristics of the two basalts 250283-2 and 272824b. This is mainly indicated by ratios in these two basalts of Cs/La, Rb/La, Ba/Rb, K/La, and $^{87}Sr/^{86}Sr$ which are similar to, or are higher than those observed in the basaltic andesites. Mixing curves between any of the basalts and granite (Mirador xenolith)

35 Selected trace element abundance ratios vs. $^{87}Sr/^{86}Sr$ for basalts, basaltic andesites, andesite, and rhyolite from Puyehue Volcano and a granitic xenolith from Mirador Volcano. Mixing curves for a specific model of mixing (Table 7d) of basaltic and andesitic magmas to produce basaltic andesite are shown as a dashed line in each diagram. The compositions of basalts (samples 250283-2 and 272824b as labelled) presumed to be affected by processes of crustal contamination differ from those of basaltic andesites and do not plot on the mixing curve shown between basalt 13826h and andesite 220283-5, nor on mixing curves between other basalts with rhyolite 202825c (see text). The composition of the Mirador granitic xenolith is presented as a speculated endmember for crustal contamination processes.

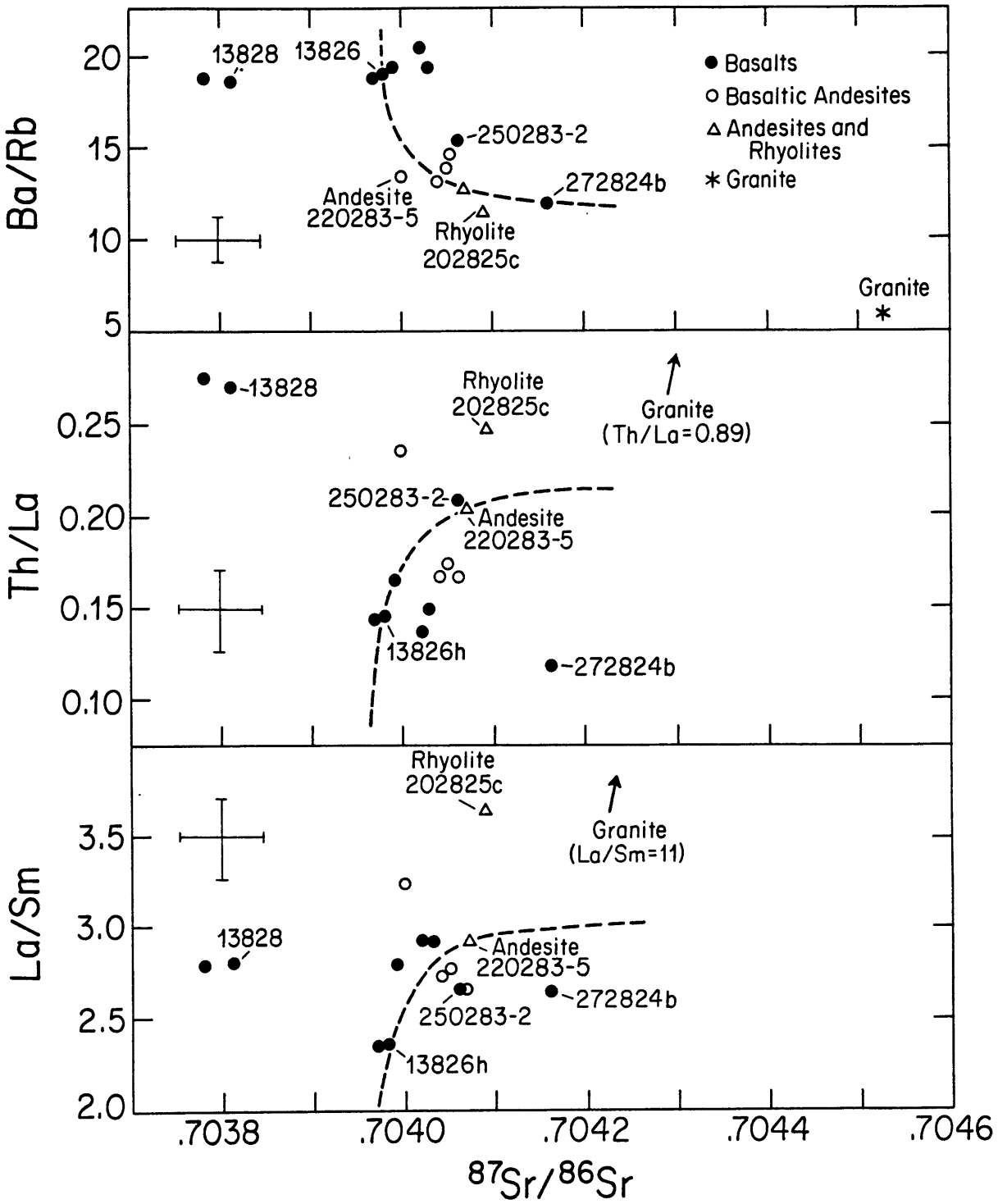
Ba/Rb
20
15
10
5
13828
13826
250283-2
272824b
Andesite
220283-5
Rhyolite
202825c
Granite
Basalts
Basaltic Andesites
Andesites and Rhyolites
Granite
Th/La
0.25
0.20
0.15
0.10
13828
Rhyolite
202825c
Granite
(Th/La=0.89)
250283-2
Andesite
220283-5
13826h
272824b
La/Sm
3.5
3.0
2.5
2.0
Rhyolite
202825c
Granite
(La/Sm=11)
13828
Andesite
220283-5
272824b
250283-2
13826h
.7038
.7040
.7042
.7044
.7046
87Sr/86Sr

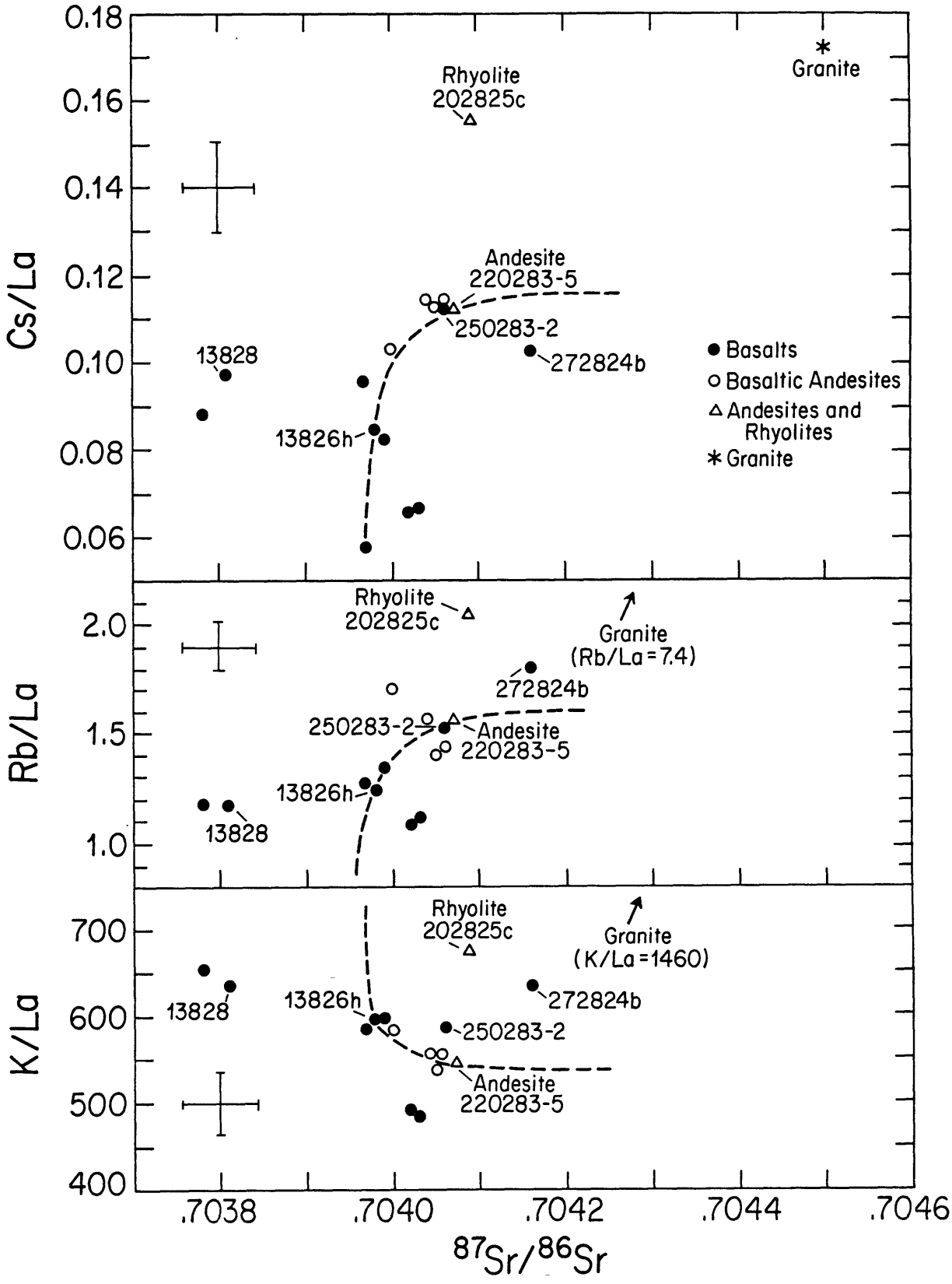
Cs/La
0.18
0.16
0.14
0.12
0.10
0.08
0.06
Rhyolite
202825c
Granite
Andesite
220283-5
250283-2
272824b
13828
13826h
Basalts
Basaltic Andesites
Andesites and
Rhyolites
Granite
Rb/La
2.0
1.5
1.0
Rhyolite
202825c
Granite
(Rb/La=7.4)
272824b
250283-2
Andesite
220283-5
13826h
13828
K/La
700
600
500
400
Rhyolite
202825c
Granite
(K/La=1460)
13828
13826h
272824b
250283-2
Andesite
220283-5
.7038
.7040
.7042
.7044
.7046
87Sr/86Sr

do not appear to be an alternative in Figure 35. For a granite such as the Mirador granite with $^{87}Sr/^{86}Sr$ = .70453 and 195 ppm Sr, bulk assimilation of nearly an equivalent volume of granite by basalt is required to explain the higher $^{87}Sr/^{86}Sr$ in these two basalts. The resulting mixture would not be basaltic in composition and would be characterized by substantially higher La/Sm and Th/La ratios than are observed in the two basalts (Fig. 35). This problem may be alleviated by speculating that the contaminated basalts were produced by contamination of basaltic magma by a small amount of bulk assimilation of mafic wallrock of similar major-element composition and trace element abundances and relatively higher $^{87}Sr/^{86}Sr$. Wallrock of basaltic composition in this situation would have liquidus temperatures approximating that of the basaltic magma, and this scenario would require unreasonably high temperatures in the basaltic magma. Furthermore, it may be an unrealistic requirement that wallrock be similar in major-element composition but have significantly higher Cs/La, Rb/La, and K/La ratios as suggested in Figure 35.

An alternative is that the two basalts 250283-2 and 272824b were produced by contamination of basaltic magma by partial melts of wallrock or solid-liquid diffusional exchange with wallrock. A trademark of either of these mechanisms would be selective contamination, which may be the best explanation of the deviant characteristics of these two basalts relative to the remainder of the basalts. The two basalts have apparently been selectively enriched in Cs, Rb, and possibly K, and have undergone a process which modified their Sr-isotopic composition. Based on results of relevant experimental studies (Watson, 1982; Watson and Jurewicz, 1984), this selective enrichment of alkalis in basaltic magma

may be explained as the result of liquid-liquid diffusion between basaltic magma and a silicic melt derived from wallrock, or solid-liquid diffusion between basaltic magma and granitic wallrock. Watson (1982) has suggested that uptake of SiO_2 by a basaltic magma may also be relatively rapid, however there is no distinct elevation of SiO_2 content in the two contaminated basalts. Other trace elements including Th, REE, and HFSE were apparently unaffected or not mobilized, possibly due to lower diffusivities and/or retention in refractory accessory phases in wallrocks. An alternative mechanism is that basaltic magmas mixed with a vapor or (aqueous?) fluid phase relatively enriched in alkalis and derived from wallrock. In this case, relatively lower solubilities of Th, REE, and HFSE in vapor and fluid phases may account for a lack of noticeable increases or relative enrichments of these elements in the two basalts. These elements are, however, enriched in basalts 250283-2 and 272824b relative to basalts such as 13828 and 13826h. The major-element compositions of basalts 13826h, 272824b, and 250283-2 are similar (MgO = 5.9-6.0 wt.%, FeO*/MgO = 1.37-1.55, CaO/Al_2O_3 = 0.541-0.556) while basalt 13828 is different (MgO = 9.5 wt.%, FeO*/MgO = 0.85, CaO/Al_2O_3 = 0.628). Since TiO_2 and P_2O_5 contents are slightly higher in 250283-2 and 272824b, it is possible that abundances of all incompatible and moderately incompatible trace elements were increased by fractional crystallization, and alkalis increased further by selective contamination. It is likely that selective contamination by vapor/fluid transfer or diffusive interaction occurred during fractional crystallization and this combined process may be considered a form of AFC modification of basaltic magma.

Modification of the Sr-isotopic composition of the two basalts which are apparently contaminated may have been a result of diffusive exchange

with wallrock or addition of relatively more radiogenic Sr in a vapor or fluid phase derived from wallrock. Available data (Misra and Venkatasubramanian, 1977) suggest that diffusion of Sr in solids is slow and the Sr-isotopic composition of basaltic magma will not be significantly modified by solid-liquid diffusion. Partial melts of wallrock may be rich in a feldspar component, but may be low in Sr relative to basaltic magma if there is significant residual feldspar in the wallrock upon formation of equilibrium melts. Mixing of such melts with basaltic magma will be less effective in modifying the Sr-isotopic composition of the basaltic magma than would mixing of wallrock partial melts produced by disequilibrium melting; these would be higher in Sr relative to equilibrium melts. Partial melts, fluid phases, or vapor phases derived from wallrock may contain Rb and Sr derived from the low-temperature breakdown of hydrous minerals characterized by high Rb/Sr and $^{87}Sr/^{86}Sr$ relative to the whole rock values, and addition of this material to a basaltic magma may effectively modify its Sr-isotopic composition (Patchett, 1980), especially if accompanied by fractional crystallization of plagioclase.

The bulk composition of wallrock and of partial melts and vapor/fluid phases may not be constant with time as the wallrock may be continually altered with repeated intrusions and contamination events (cf. Myers, et al., 1984). If the compositions of basalts are constant as well as the thermal regime below a single volcanic center, this may result in an apparent decrease in the amount or extent of crustal contamination with time. For Puyehue basalts, the variability in their primary geochemical characteristics may outweigh any temporal changes in the composition of wallrock or crustally-derived modifying components.

Assuming that the effects of crustal contamination may be consistent with time, it may be possible to identify which basalts may represent uncontaminated precursors to each of the two contaminated basalts. This approach is facilitated by differences between 250283-2 and 272824b in Sr-isotopic composition and in abundances of Th, Sr, Ni, and Cr.

In Figure 36, trace element abundances in 272824b and 250283-2 are normalized to basalts 13828 and 13826h on a diagram similar to that presented in Figure 26. Basalts 13826h and 13828 were selected for consideration as uncontaminated equivalents or parental precursors because of their generally lower abundances of most incomptaible trace elements relative to basalts 250283-2 and 272824b. If crustal contamination occurs by bulk assimilation (bulk melting) of wallrock, mixing with partial melts of wallrock, or some other process, it is likely that abundances of at least a few incompatible trace elements may be increased in contaminated basaltic magma. Abundances of incompatible trace elements will also be increased and those of compatible trace elements will be decreased in basaltic magma undergoing fractional crystallization during an AFC process. For this reason, basalts such as 220283-1, which is higher in many incompatible element abundances than 272824b and 250283-2, is not considered as an uncontaminated equivalent of these two basalts. Other basalts are characterized by lower or equivalent abundances of compatible trace elements such as Ni and Cr and are also less suitable for this purpose.

As seen in Figure 36, bulk assimilation of granite such as the Mirador granite would result in negative P and Ti anomalies and positive Hf anomalies mirrored in the contaminated basalts, but none are apparent. This approach illustrates that trace element enrichment in both

36 Trace element abundances in the Mirador granite xenolith (dot-dashed line), basalt sample 250283-2 (dashed line in upper diagram, solid line in lower) and basalt sample 272824b (solid line in upper diagram, dashed in lower), normalized to trace element abundances in basalts 13826h and 13828 in the upper and lower diagrams, respectively. Solid lines in each of the diagrams relate the more likely pair consisting of contaminated basalt and a complementary, uncontaminated precursor (either basalt 13826h or 13828). Normalized granite abundances are illustrated in connection with discussion of crustal contamination occurring by bulk assimilation vs. selective contamination.

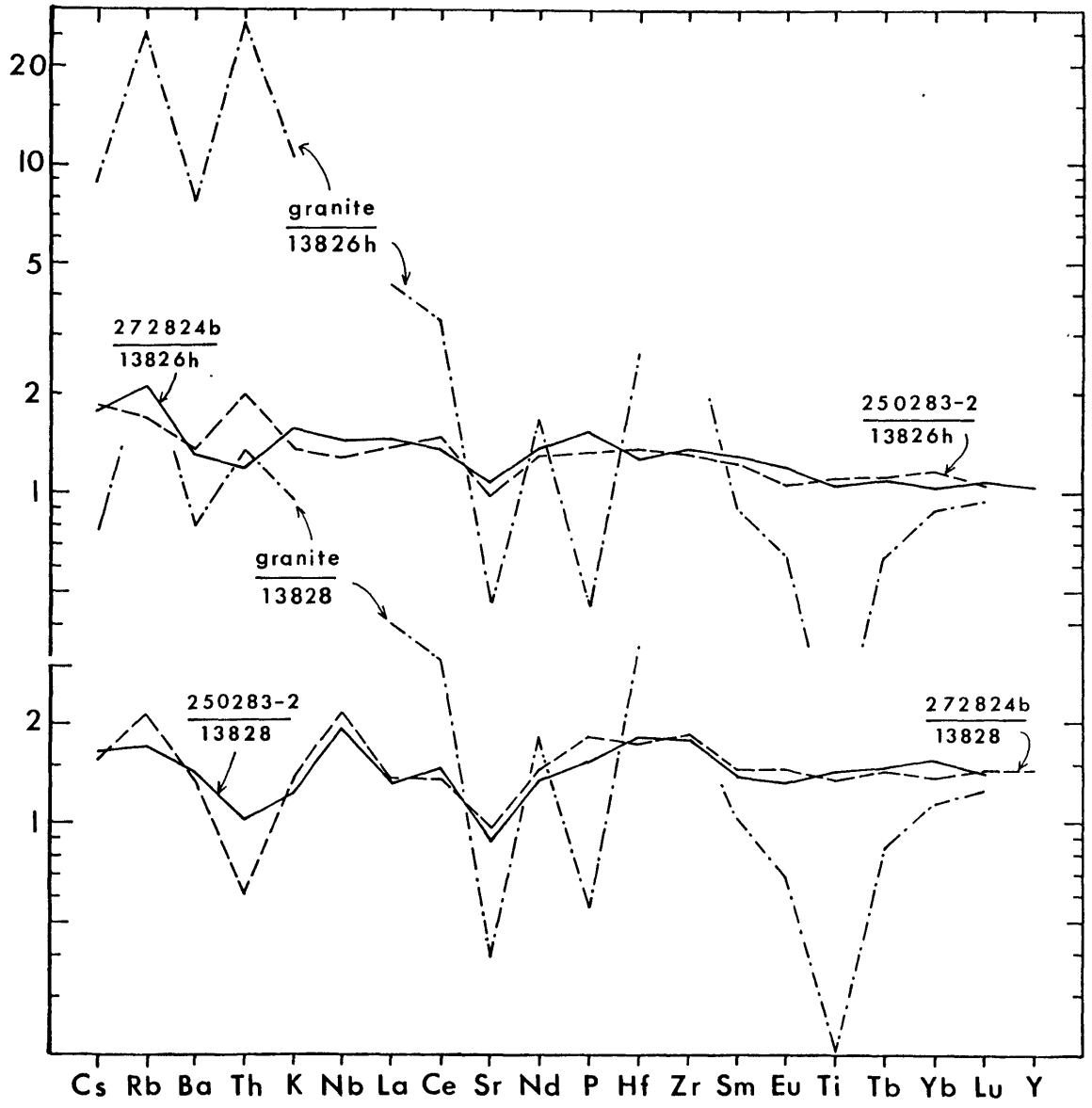
20
10
5
2
1
2
1
granite
13826h
272824b
13826h
250283-2
13826h
granite
13828
250283-2
13828
272824b
13828
Cs Rb Ba Th K Nb La Ce Sr Nd P Hf Zr Sm Eu Ti Tb Yb Lu Y

contaminated basalts which has arisen as a result of AFC processes does not necessarily reflect the composition or trace element pattern of an expected granitic wallrock contaminant and therefore mitigates against bulk assimilation as a contamination mechanism. Based on previous discussion this component may be represented more by alkali element 'spikes' (Cs, Rb, and K), whereas the effect of fractional crystallization is to produce relatively smooth, subparallel increases in most other trace elements and a decrease in Sr abundances.

The 'normalized' patterns of 272824b and 250283-2 are subparallel to either of the basalts with lower abundances (13828 and 13826h) but differences related to Th abundances are apparent. Sample 250283-2 normalized to basalt 13826h (i.e. '250283-2/13826h') results in a positive Th 'spike,' and the curve 272824b/13828 displays a negative Th anomaly. It is unlikely that Th would be greatly enriched relative to K by crustal contamination as suggested if 250283-2 were produced from 13826h, especially if Th-bearing minerals such as zircon behave as refractory phases in partial melting. It is more likely that 272824b was produced by selective contamination of a basaltic magma represented by 13826h, and 250283-2 by contamination of basalt such as 13828. The normalized patterns representing this pairing (Fig. 36) are similar and subparallel, suggesting that an AFC process for these two basalts was similar and that the crustal component was similar at least in the effects produced, but that the basaltic magmas in each case were geochemically distinct. Some mismatch is observed for 250283-2 normalized to 13828 (Fig. 36): HFSE 'spikes' relative to 13828 are apparent, and 250283-2 is relatively less LREE-enriched than 13828. A basalt more intermediate in various characteristics between 13828 and

13826h may be more plausible as an uncontaminated precursor for 250283-2 but is not represented in the sample set. Alternatively, if 250283-2 was produced by selective contamination of a basalt such as 13828, HFSE such as Nb, Zr, and Hf, in addition to HREE such as Yb may have been enriched in the contaminating phases by preferential breakdown of hydrous phases such as mica and amphibole (cf. Fujimaki et al., 1984). Sample 272824b is enriched in LREE relative to 13826h and fractional crystallization of clinopyroxene to produce this result in 272824b is not likely since the two basalts have very similar CaO/Al_2O_3 ratios and Sc abundances.

Crustal contamination as part of an AFC process was probably important in the generation of evolved lavas ranging from andesites to rhyolites, but it is possible that either the exact process or its efficacy, or even the wallrock/contaminant composition differed from that involved in the modification of basalts 250283-2 and 272824b. Ratios such as Cs/La, Rb/La, Th/La, and La/Sm may increase, and K/La and Ba/Rb decrease, during fractional crystallization as illustrated for high-TiO_2, high-P_2O_5 andesite (sample 220283-5, Figure 35) but this was accompanied by increasing $^{87}Sr/^{86}Sr$, suggesting concurrent contamination with relatively more radiogenic Sr. Still higher ratios of Cs/La, Rb/La, and K/La and $^{87}Sr/^{86}Sr$ in rhyolite (Fig. 35) may be evidence of a combination of processes, including volatile transfer of alkalies, late-stage relative fractionation of REE, and crustal contamination.

Basalts such as 250283-2 and 272824b must have been produced by contamination of basaltic magma by crustal material relatively less radiogenic than that which may have been involved in an AFC process leading to the production of evolved lavas. This is illustrated by re-examining mixing relationships on a plot of K/Rb vs. $^{87}Sr/^{86}Sr$

37 Mixing relationships between basalts, basaltic andesites, andesite, and rhyolite in a plot of K/Rb vs. $^{87}Sr/^{86}Sr$ and a complementary diagram of K/Rb vs. $^{87}Sr/Rb$. Arbitrary curves assuming specific basalts as mixtures of unspecified endmembers were calculated using the methods of Langmuir et al. (1978). A single curve cannot be calculated to include all basalts (cf. Figure 32, 34a) and three mixing curves, I, II, and III, are possible as shown. A straight line relating all basalts included on mixing curve III is not possible in the complementary diagram of K/Rb vs. $^{87}Sr/Rb$. Mixing curve IV (dashed) relates basalt and andesite in the specific mixing model of Table 7d, also depicted in Figure 35, and the dashed line on the complementary plot (K/Rb vs. $^{87}Sr/Rb$) is shown to have a different slope than any lines for basalt-basalt mixing. The composition of the Mirador granitic xenolith is shown, in connection with discussion concerning crustal contamination (see text).

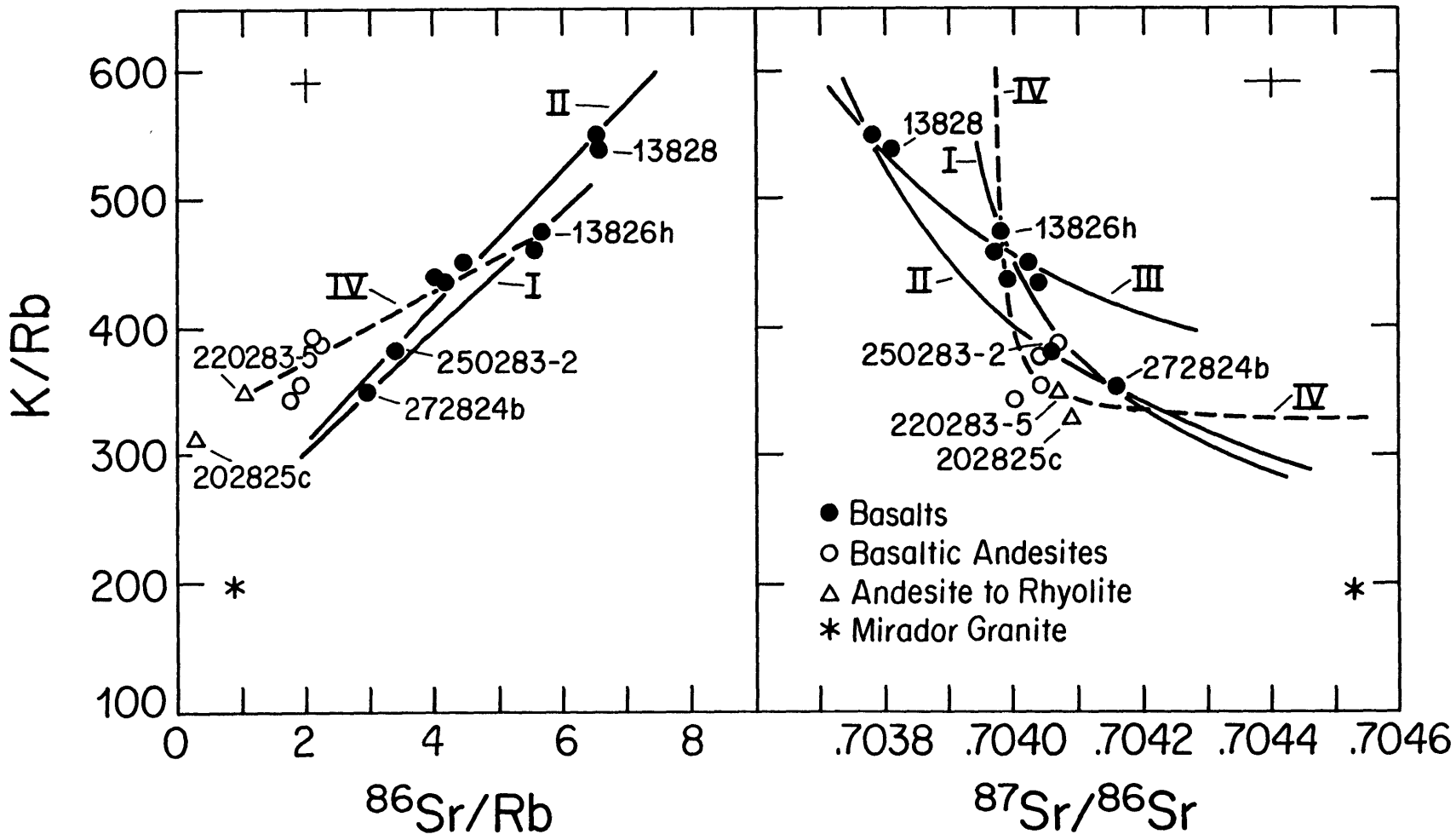
600
500
400
300
200
100
K/Rb
0
2
4
6
8
$^{86}Sr/Rb$
II
13828
13826h
IV
I
220283-5
250283-2
272824b
202825c
.7038
.7040
.7042
.7044
.7046
$^{87}Sr/^{86}Sr$
III
● Basalts
○ Basaltic Andesites
△ Andesite to Rhyolite
* Mirador Granite

(Fig. 37). Mixing curves I and II in Figure 37 relate basalts 13826h and 272824b, and 13828 and 250283-2 respectively, and indicate that 250283-2 and 272824b may have been produced by contamination (or mixing) of basalts 13826h and 13828 with endmember components characterized by similar K/Rb and $^{87}Sr/^{86}Sr$ ratios. Mixing curve III attempts to relate the basalts with low $^{87}Sr/^{86}Sr$ (.70378-.70381) to those with intermediate $^{87}Sr/^{86}Sr$ (.70397-.70403), but this is not well supported by a good linear correlation on the companion plot of K/Rb vs. $^{87}Sr/Rb$ (Fig. 37). Basaltic andesites fall on mixing lines (curve IV) between basalts and andesites or rhyolites (Fig. 37). Mixing curve IV in Figure 37 does not necessarily model the effects of a protracted AFC process, however, since K/Rb and $^{87}Sr/^{86}Sr$ ratios in wallrock may not be constant with time if the contamination is selective and the magma chamber stationary. Otherwise, the difference between mixing curves I and IV, for example, suggests that contaminated basalts were produced by contamination of basaltic magma by wallrock with relatively higher Rb/Sr and lower K/Rb, and an AFC process that produced the stratigraphically younger andesites to rhyolites involved wallrock with lower or equivalent Rb/Sr and relatively higher K/Rb. This is contradictory if all processes were occurring within the same portion of crust or wallrock which, if being progressively 'leached' by extraction of melt, fluid, or vapor phases, would yield relatively more radiogenic Sr at earlier stages as in contamination of the basalts rather than at later stages accompanying the production of late-stage andesites and rhyolites. If contamination of basalts occurred as a relatively short-term, single-stage process, possibly in another magma chamber, then mixing curves I, II, or III in Figure 37 may approximate, at least in a qualitative sense, differences

in K/Rb and $^{87}Sr/^{86}Sr$ in components which modified only the basalts. Basalts lying on mixing curve III may delineate a contamination trend involving crust with relatively higher K/Rb ratios compared to basalts on mixing curve I or II. High K/Rb ratios may be more characteristic of older, metamorphic (lower?) crust while low K/Rb ratios may be typical of younger (upper?) crust. In neither case, can the present data set be used to uniquely constrain the Sr-isotopic composition of wallrock contaminant, nor changes in this parameter with time.

In summary, crustal contamination may have modified the isotopic, and to a certain extent, bulk composition of many lavas at Puyehue Volcano ranging from basalts to more evolved lavas. The most obvious effect seen in two basalts especially is that of selective enrichment of alkalis and an increase in $^{87}Sr/^{86}Sr$ ratios in the basalts. This in turn suggests that the contamination did not occur as bulk assimilation of crustal material, but rather by extraction of alkali-enriched, relatively radiogenic fluid, vapor, or partial melt phases from wallrock lining magma chambers or conduits. These two basalts are disqualified from use in consideration of subcrustal processes or source characteristics. The remainder of the basalts may be used to address these questions. Some of these other basalts may also have experienced crustal contamination but it is less obvious.

10.5 Subcrustal Sources and Processes

Potential sources contributing to parental magmas of basalts from Puyehue Volcano include the upper mantle, consisting of OIB-type to N-MORB type sources, and the subducted slab of oceanic crust, consisting of ultramafic to mafic cumulates, basalts, and sediments. The major

processes in the subcrustal arc environment which produce and modify ascending magmas, include partial melting, fractional crystallization, and magma mixing. All specific processes or mechanisms fall into these three categories, e.g., metasomatism, veining, or hybridization of mantle peridotite by slab-derived materials may be considered a mixing process, while separation of magma from solids in an ascending diapir in the overlying mantle wedge involves melting and possibly crystallization process.

Abundances and abundance ratios of only the most incompatible trace elements may be informative as to source characteristics, or in defining the proportions of geochemically distinct components combined in the source, and helpful in addressing differences in sources or processes that produced Puyehue basalts. Abundances of most trace elements may have been increased in the basalts by fractional crystallization of olivine ± plagioclase. Neither phase incorporates trace elements (except Sr) to any degree, and abundance ratios in the basalts may be representative of their sources. However, Puyehue basalts are characterized by lower CaO/Al_2O_3 ratios than many arc basalts (Table 16), and may represent products of high-pressure fractional crystallization of clinopyroxene in parental or primary magmas. The middle and heavy REE (MREE and HREE), Hf, and Zr are relatively more compatible in clinopyroxene than LREE and alkalies, thus any ratios of elements from these two groups may be affected by clinopyroxene fractionation.

The simplest model addressing variability among the basalts and their respective sources is that the parental magmas of the basalts were produced in discrete single-stage melting events, were separated from the source, experienced negligible interaction with upper mantle or crustal

wallrocks, and finally crystallized only olivine and plagioclase under low pressure conditions at crustal levels. For the moment, the effect of clinopyroxene fractionation at relatively high pressures (>10-12 kb) will be ignored. Selected trace element abundances and abundance ratios can be used, via non-modal batch melting calculations, to evaluate relative implied differences in source abundances, source modal mineralogy, and degree of partial melting.

10.5.1 REE systematics and modelling

Variations in REE abundances and degrees of relative LREE-enrichment among the basalts are apparently decoupled from Th, HFSE, and alkali elements. Therefore, partial melting calculations will be used first to address variations in relative degrees of LREE enrichment. If materials, possibly melts or vapors, derived from the subducted slab of oceanic crust contain mostly alkali elements which are then added to upper mantle peridotite, variations in REE abundances and relative LREE-enrichment in the basalts may allow inferences concerning the bulk composition of the upper mantle peridotite. Assuming a lherzolite source with depleted abundance patterns, and $D_{Oliv}^{La} = D_{Opx}^{La} = D_{Cpx}^{La} = D_{Oliv}^{Sm} = D_{Opx}^{Sm} = 0$, equation (15) of Shaw (1970) for non-modal batch melting may be used to solve for D_{Cpx}^{Sm} using observed La/Sm ratios in basalts:

$$1) \quad \left[\frac{C_L^{La}}{C_L^{Sm}}\right]\left[\frac{C_o^{Sm}}{C_o^{La}}\right] = \frac{D_o^{Sm} + F\,(1-P_o^{Sm})}{D_o^{La} + F\,(1-P_o^{La})}$$

where F = melt fraction, D_o^i = bulk partition coefficient for element i, P_o^i = bulk melting proportion for i, and C_o^i and C_L^i refer to abundances in the source and aggregate liquid produced, respectively. By assuming a depleted abundance pattern in the source (i.e., $C^o_{La}/C^o_{Sm} = 1$) this reduces to:

2) $D_o^{Sm} = F \left(\frac{C_L^{La}}{C_L^{Sm}}\right) - F\,(1-P_o^{Sm})$; $P_o^{La} = D_o^{La} = 0$.

If it is assumed that the mode and melting of clinopyroxene chiefly control the relative LREE-enrichment of melts produced, or at least Sm abundances therein, then it is of interest to express the above relationship as

3) $$X^o_{cpx} = \frac{F}{D_{cpx}^{Sm}} \left[\frac{C_L^{La}}{C_L^{Sm}} + P_{cpx}\, D_{cpx}^{Sm} - 1\right]$$

where X_{cpx} refers to the modal proportion of clinopyroxene in the source. Abundances of Sm in the source may be then solved for:

4) $C_o^{Sm} = C_L^{Sm} \left[X_{cpx}\, D_{cpx}^{Sm} + F\,(1- P_{cpx}\, D_{cpx}^{Sm})\right]$

Since Puyehue basalts vary in both La/Sm ratios and Sm abundances, and neither are linearly correlated (Fig. 30), these variations may be indicative of corresponding differences in the sources from which their respective parental magmas were derived. For a given melt fraction F, different values of X^o_{cpx} and C_o^{Sm} would be suggested in different sources for the basalts. To this end, three diverse Puyehue basalts, samples 13828, 13826h, and 220283-1, were chosen to evaluate this possibility. For various melt fractions, Sm abundances and La/Sm ratios in these three basalts were used to calculate X^o_{cpx} and C_o^{Sm} as above. Values of D_{cpx}^{Sm} (0.3) and P_{cpx} (0.6) were assumed. This results in three different linear trajectories of differing slope (Fig. 38) for the three basalts, respectively. Specific values of X^o_{cpx} and C_o^{Sm} for a given value of F on each trajectory may be connected and the diagram 'contoured' for various F values.

The resulting diagram is useful only for evaluating relative differences in sources for the basalts, and not absolute values of X^o_{cpx} and C_o^{Sm} in the respective sources. This is because La and Sm abundances

in the basalts may have been uniformly enriched above abundances in the parental or primary magmas by fractional crystallization of olivine and plagioclase as mentioned earlier. Abundances in parental magmas may also have been increased during ascent through the upper mantle. Abundances of incompatible elements in magmas may be increased by continuous re-equilibration with upper mantle wallrock, provided that abundances in the wallrock are greater than those in the primary source of the magma and that the volume of the magma is constant. Abundances in the magma may also be increased by the incorporation of partial melts extracted from wallrock provided that the wallrock contains higher abundances than the source of the magma and/or the melts added were generated by smaller degrees of partial melting relative to that which produced the original magma. Either of these processes, in addition to that of low-pressure fractional crystallization of olivine and plagioclase, may increase trace element abundances in such a way as to suggest that the parental magmas were initially produced by lesser degrees of partial melting. Assuming that La/Sm ratios are not significantly affected by any of these processes, the slopes of trajectories for different basalts would not change, nor the curvature of the F contours in Figure 38, however lower (and possibly more reasonable) values of X^{o}_{cpx} and C_o^{Sm} and higher degrees of melting would be indicated.

The topology of the petrogenetic 'grid' in Figure 38 illustrates that if any one of the three variables, X^{o}_{cpx}, C_o^{Sm}, or melt fraction F, is constant in single-stage melting processes, then the other two variables must differ such that three different sources are required to explain the characteristics of the three basalts. For example, if all basalts were derived from sources with similar modal mineralogy, then

38 Calculated modal abundances of clinopyroxene (X_{cpx}) vs. abundances of Sm (C_o^{Sm}) required in sources to generate three diverse basalt-types from Puyehue Volcano. Curved lines are melting degrees (F) required to generate each basalt for a particular value of X_{cpx} and C_o^{Sm} and are calculated for a non-modal batch melting process (see text). A ratio of 1.0 for C_o^{La}/C_o^{Sm} was assumed for the source and is approximately equivalent to N-type MORB sources (cf. Tarney et al., 1980). A chondritic or higher ratio of C_o^{La}/C_o^{Sm} assumed in the source would require lower values of X_{cpx} for a given melt fraction (F) and vice versa.

39 Results of non-modal batch melting models as in Figure 38 except that values of C_L^{La}/C_L^{Sm} and C_L^{Sm} were adjusted in two basalts (13826h and 220283-1) for ~10% clinopyroxene fractionation relative to basalt 13828, based on major-element compositions.

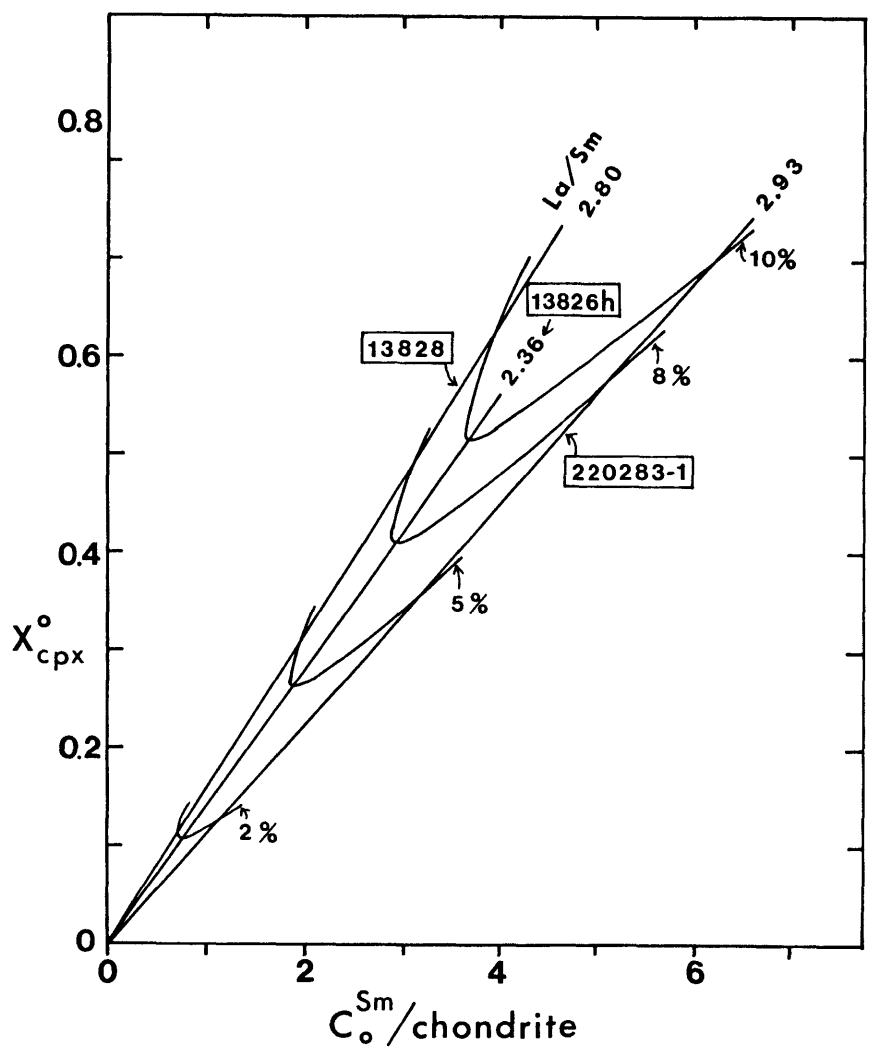
0.8
0.6
0.4
0.2
0
0
2
4
6
X^{o}_{cpx}
C^{Sm}_{o}/chondrite
La/Sm
2.80
2.93
13826h
13828
2.36
10%
8%
220283-1
5%
2%

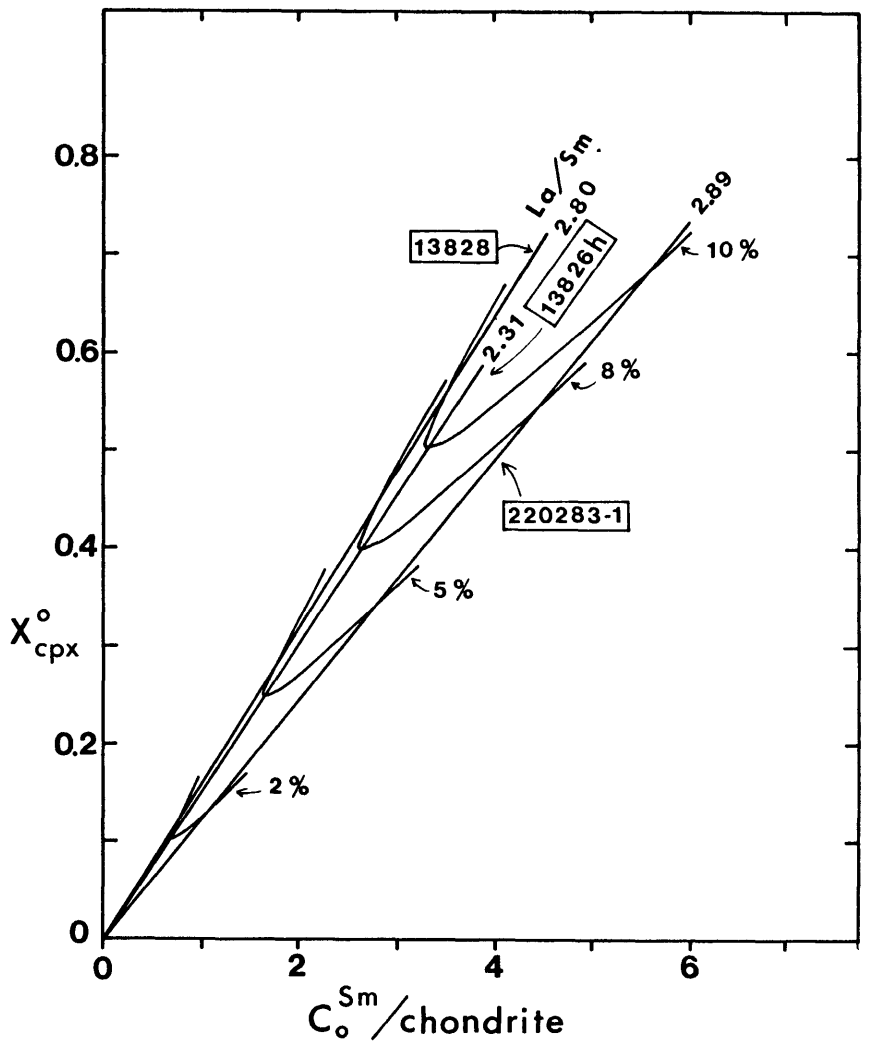
0.8
0.6
0.4
0.2
0
0
2
4
6
X^{o}_{cpx}
C^{Sm}_{o}/chondrite
La/Sm
2.80
2.89
13828
13826h
2.31
10%
8%
220283-1
5%
2%

parental magmas for basalts 13828 and 220283-1 were derived by lower degrees of partial melting relative to that indicated for basalt 13826h, and source abundances (C_o^{Sm}) were progressively higher in sources related to basalts 13828, 13826h, and 220283-1, respectively. If source abundances were similar for all basalts, parental magmas for basalts 13828 and 13826h were produced by roughly similar degrees of partial melting which were high relative to that for basalt 220283-1, and progressively higher modal abundances of clinopyroxene are indicated in sources related to basalts 220283-1, 13826h, and 13828, respectively. If a chondritic or LREE-enriched source ($C_o^{La}/C_o^{Sm} \geq 1.64$) is assumed, the slopes of trajectories for each of the three basalts are steepened such that smaller degrees of melting (F) and lower source abundances (C_o^{Sm}) are required for a given value of X^o_{cpx} compared to the model calculations in Figure 38 based on a relatively LREE-depleted source ($C_o^{La}/C_o^{Sm} = 1.0$).

If parental magmas crystallized clinopyroxene at high pressures during ascent, relative differences (topological relationships) in a diagram such as Figure 38 will be affected, since $D_{cpx}^{Sm} > D_{cpx}^{La}$. This is especially true if various parental magmas underwent different amounts of clinopyroxene fractionation relative to one another. The absolute bulk compositions of initial, primitive magmas for each basalt cannot be constrained, nor can the amount of clinopyroxene fractionation during ascent be estimated with any accuracy. Basalts 13826h and 220283-1 are characterized by lower CaO/Al_2O_3 ratios relative to 13828, suggesting that they are products of fractional crystallization with clinopyroxene as a more dominant phase in these than for 13828. By adjusting the bulk compositions of 13826h and 220283-1 so that they are similar to that of

13828 at least with respect to CaO and Al_2O_3 contents and CaO/Al_2O_3 ratios, a more accurate evaluation of relative source differences may emerge on a diagram such as Figure 38. Compositions of all three basalts were adjusted to account for olivine and plagioclase phenocrysts, and the adjusted compositions of 13826h and 220283-1 were further adjusted by adding clinopyroxene, guided by $KD_{cpx}^{Fe-Mg} = 0.28$ (cf., Grove and Baker, 1984), in an amount (approximately 10%) to match Ca/Al_2O_3 ratios and CaO and Al_2O_3 contents to those of 13828. Abundances of La and Sm in basalts 13826h and 220283-1 were also adjusted assuming $D_{cpx}^{La} = 0$ and $D_{cpx}^{Sm} = 0.3$. Values of X_{cpx} and C_o^{Sm} were calculated as before using the adjusted Sm abundances and La/Sm ratios and results are shown in Figure 39. For any given value of F, this adjustment results in lower X_{cpx} and C_o^{Sm} source values, and steeper slopes of trajectories for the adjusted basalts. Trajectories for basalts 13828 and 13826h are nearly coincident (Fig. 39). However, it is now apparent that parental magmas for these two basalts may have been derived by different degrees of partial melting of sources with similar trace element abundances and different modal mineralogy. A source of parental magma for basalt 220283-1 would also differ by having higher Sm abundances and greater amounts of clinopyroxene relative to a source for 13826h if 220283-1 was produced by similar degree of melting as 13826h.

In general, the total possible range in both X_{cpx} and C_o^{Sm} in sources, as enveloped by trajectories for samples 13828 and 220283-1 is narrowed by the adjustment for hypothetical high-pressure fractionation. The net result is that a relatively narrow range of C_o^{Sm} and X_{cpx} is required in sources if parental magmas for the basalts were produced by variable degrees of melting. A related possibility which is suggested by

the configuration of curves of equivalent melt fraction F (Figures 38, 39) is that parental magma for basalt 13826h, which is relatively less LREE-enriched, may have been produced by melting of a residuum after production of magmas parental to basalt 220283-1. However, simple calculations using equation (1) suggest that for an initially depleted source which is further depleted in producing basalt 220283-1, the degree of melting required to produce basalt 13826h from the residue is at least an order of magnitude less than that which produced basalt 220283-1. Very small degree melt fractions may not be easily separated from the matrix or residue (Maaloe and Scheie, 1982; McKenzie, 1984). Thus, the basalts and their parental magmas are not easily explained as representing repeated melting events of the same source. A more reasonable alternative discussed later is that parental magmas for basalts 13826h and 220283-1 were generated by different degrees of partial melting of separate sources similar in composition.

Differences in source characteristics and/or complex melting histories are also suggested by crossing REE patterns in some basalts (Fig. 26). One basalt, 13828, contains similar La abundances to 13826h but is lower in middle REE and HREE compared to 13826h. This may in turn suggest a role for garnet in controlling HREE abundances in parental magmas, i.e., sources for different basalts may be characterized by different modal abundances of garnet. Relative variations of garnet in respective sources of parental magmas for the different basalts may be evaluated as before, using equations (1) through (4), and La/Yb ratios and Yb abundances in the basalts. A partition coefficient D_{gar}^{Yb} of 4 was assumed for garnet (Frey et al., 1978) and D_{cpx}^{Yb} was considered negligible for a garnet lherzolite source. This assumption is

unrealistic since $0<D_{cpx}^{Yb}<1$, but it must be emphasized that the model calculations are only performed to assess relative differences in source abundances, source modes, or degrees of melting involved in the generation of the basalts. In addition, the effect of high-pressure fractionation in basaltic magmas during ascent was ignored for the moment. A LREE depleted source was assumed for simplicity (C_o^{La}/C_o^{Yb} = 1.0). In addition, D_o^{La} was assumed to be zero and P_{cpx} and P_{gar} equivalent to 0.4. With these assumptions, equations similar to (3) and (4) were used to derive a plot of X_{gar} vs. C_o^{Yb}, 'contoured' for equivalent melt fractions (Fig. 40). Contours of equivalent melting fractions display the same curvature as in Figure 38 and 39, and apparent relationships between source mineralogy (X^o_{gar}), source abundances (C_o^{Yb}), and degrees of melting (F) are similar to those outlined in Figures 38 and 39. In all three figures (38, 39, and 40), the concave shape of curves of equivalent melt fraction is largely because La/Sm and La/Yb ratios are not well correlated with La, Sm, or Yb abundances in these three basalts (Fig. 30).

Relative differences in clinopyroxene/garnet ratios in garnet lherzolite sources may also explain the variability in the basalts. The nature of the variability in Puyehue basalts and the limited data set does not permit evaluation of modal mineralogy and trace element abundances in sources, using inversion methods after the fashion of Minster and Allegre (1978) or Hofmann and Feigenson (1983, 1984). Instead, equations (3) and (4) may be used with La/Sm ratios and Sm abundances in the basalts to calculate relative clinopyroxene/garnet ratios. Melting proportions for garnet (P_{gar}) and clinopyroxene (P_{cpx}) are assumed to be subequal and equivalent to 0.4 as before. D_{cpx}^{Sm} was

40 Calculated modal abundances of garnet (X_{gar}) vs. abundances of Yb (C_o^{Yb}) required in sources to generate the three basalts. As in Figure 38, curved lines are melting degrees (F) required to generate each basalt for a particular value of X_{gar} and C_o^{Yb} for non-modal batch melting (see text). A ratio of 1.0 for C_o^{La}/C_o^{Yb} C_o^{La}/C_o^{Yb} was assumed for the source and approximates an N-type MORB source. A chondritic or more enriched source would require lower values of X_{gar} for a given melt fraction (F) and vice versa.

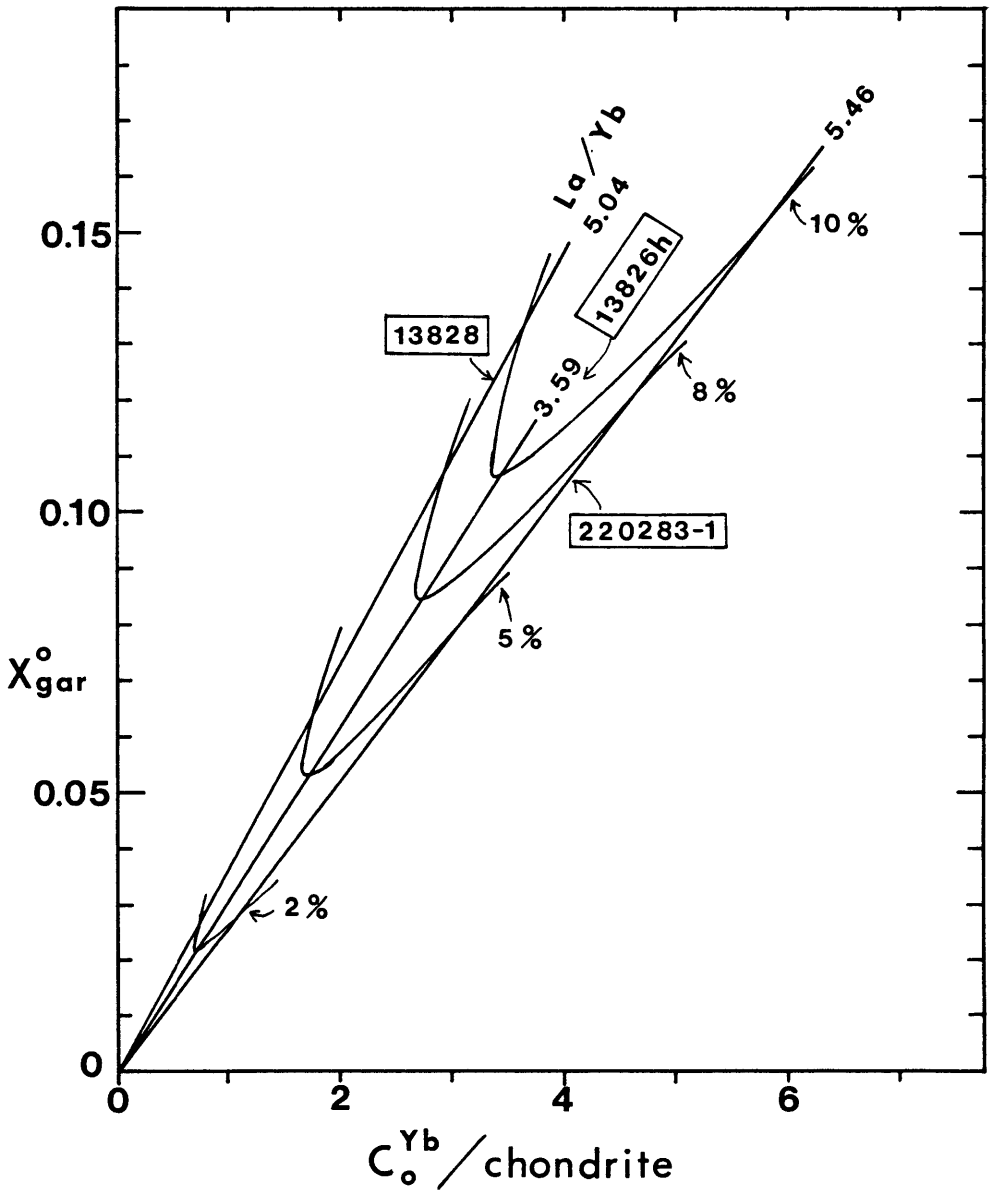
0.15
0.10
0.05
0
X^o_{gar}
0
2
4
6
C^{Yb}_o / chondrite
La/Yb
5.04
5.46
13826h
13828
3.59
10%
8%
220283-1
5%
2%

assumed to equal 0.3, and D_{cpx}^{Sm} was assumed to be twice the value of D_{gar}^{Sm}, a value slightly higher than the mean of a number of natural garnet/clinopyroxene pairs compiled by Frey et al. (1978). Values of X^o_{gar} in sources calculated independently using La/Yb ratios and Yb abundances in the basalts were used with the above simplifying assumptions to solve for X_{cpx} in sources for each basalt at a given melt fraction F. A value of X^o_{gar} was calculated using a version of equation (3):

$$5) \quad X^o_{gar} = \frac{F}{D_{gar}^{Yb}} \left[\frac{C_L^{La}}{C_L^{Yb}} + P_o^{Yb} - 1\right]; \quad P_o^{Yb} = P_{gar}\, D_{gar}^{Yb}$$

Assuming that $D_{gar}^{Sm} = 1/2\ D_{cpx}^{Sm}$ and $P_{cpx} = P_{gar}$

$$6) \quad D_o^{Sm} = D_{cpx}^{Sm} \left(X^o_{cpx} + \frac{1}{2} X^o_{gar}\right) \quad \text{and}$$

$$7) \quad P_o^{Sm} = P_{cpx}\, D_{cpx}^{Sm} + P_{gar}\, D_{gar}^{Sm} = \frac{3}{2} D_{cpx}^{Sm}\, P_{cpx} \cdot$$

With the additional assumptions $P_o^{La} = D_o^{La} = 0$ and $C_o^{La}/C_o^{Sm} = 1.0$, equation (1) simplifies to:

$$8) \quad \frac{C_L^{La}}{C_L^{Sm}} = \frac{D_o^{Sm} + F\,(1-P_o^{Sm})}{F}$$

Substituting equations (6) and (7) into (8), an expression to solve for X^o_{cpx} results:

$$9) \quad X^o_{cpx} = \frac{F}{D_{cpx}^{Sm}} \left[\frac{C_L^{La}}{C_L^{Sm}} + \frac{3}{2} P_{cpx} - 1\right] - \frac{1}{2} X^o_{gar}$$

A plot of X^o_{cpx} vs. X^o_{gar} contoured for constant melt fraction F (Fig. 41) demonstrates that if parental magmas for the three basalts were produced by equivalent degrees of melting, clinopyroxene/garnet ratios are indicated as progressively lower in sources for basalts 13826h,

13828, and 220283-1, respectively. Alternatively, if either X^{o}_{cpx} or X^{o}_{gar} was similar in all sources, parental magmas for 13826h, 13828, and 220283-1 may have been produced by progressively lower degrees of partial melting respectively. Assuming a chondritic or LREE-enriched source ($C_o^{La}/C_o^{Yb} \geq 1.51$) will not change the relative configuration of curves in Figure 41, but will lower slopes, i.e., lower cpx/gar ratios, for each basalt and larger melt fractions are required for given X^{o}_{cpx} and X^{o}_{gar} values, compared to curves in Figure 41 which were calculated assuming a LREE-depleted source.

Parental magmas for various basalts cannot be easily explained as successive melts from a single, progressively depleted source. If parental magmas for 220283-1, 13828, and 13826h were produced by successive melting events, i.e., the first residue serving as a source for the second melting episode, sources would then be characterized by increasing cpx/gar ratios since $X_{cpx} > X_{gar}$ as calculated, and $P_{gar} \geq P_{cpx}$ may be likely. This is suggested by the increasing cpx/gar ratios indicated in sources for 220283-1 to 13826h (Fig. 41), although, as suggested earlier based on results in Figures 38 to 40, abundances of La would be far too depleted in residues to yield other basalts.

All of the above partial melting models illustrate the difficulty in relating parental magmas to a single source and that, instead, three distinct or separate sources are suggested. The concept of three sources presumes that the geochemical criteria supporting this argument are unaffected by processes that may occur during ascent of the magma after separation from a melt residue. Processes on ascent that can affect REE abundances and LREE/HREE abundance ratios in magmas include 1) re-equilibration of magmas with upper mantle wallrock, 2) mixing with

41 Calculated modal abundances of X_{cpx} vs. X_{gar} required in sources to generate the three basalts (13826h, 13828, 220283-1). Straight lines through the origin are lines of constant cpx/gar ratios implied in sources for the three basalts. Curved lines are melting degrees (F) required to generate each basalt for particular values of X_{cpx} and X_{gar}. Values of X_{gar} from Figure 40 were used to solve for Xcpx in non-modal batch melting calculations using values of C_L^{La}/C_L^{Yb} and C_L^{Sm} in the basalts and assumed values for C_o^{La}/C_o^{Yb}, D_{cpx}^{Sm}, D_{gar}^{Sm}, P_{cpx}, and P_{gar} (see text).

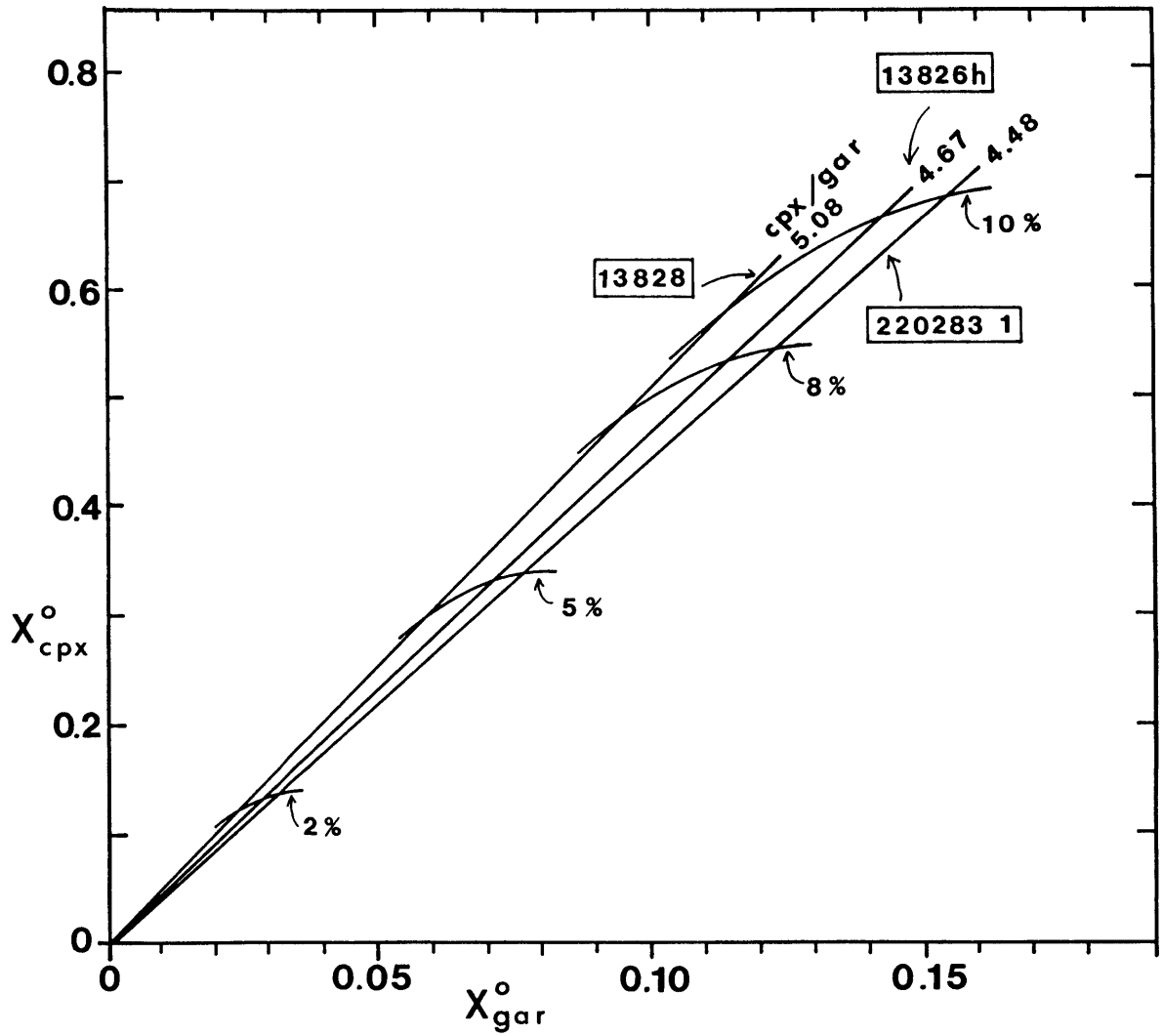
0.8
0.6
0.4
0.2
0
0
0.05
0.10
0.15
X^{o}_{cpx}
X^{o}_{gar}
13826h
4.67
4.48
cpx/gar
5.08
13828
220283 1
10 %
8 %
5 %
2 %

partial melts derived from upper mantle wallrock, and 3) open or closed-system high-pressure fractional crystallization of clinopyroxene or garnet. All of these processes are capable of producing variable LREE/HREE ratios if operating to variable extents in different magmas. However, each of the processes may result in substantial increases in REE abundances accompanying increases in LREE/HREE ratios in the magmas and major-element bulk compositions will be buffered in all processes except closed-system fractional crystallization. Abundances of REE in 13826h (La = 6.1 ppm, La/Sm = 2.36, La/Yb = 3.59) and 13828 (La = 6.3 ppm, La/Sm = 2.80, La/Yb = 5.04) are low and similar despite differing degrees of relative LREE enrichment and abundances in 220283-1 (La/Sm = 2.93, La/Yb = 5.46) are not much higher (Fig. 26). While processes during ascent may have had some effects as described above, these effects may be less significant than controls imposed by source characteristics and degree of partial melting during initial melting.

10.5.2 HFSE anomalies: partial melting models

A similar approach to that behind Figures 38 to 40 may be taken using abundance ratios of other trace elements in the basalts. By choosing trace elements with similar bulk D's in mantle lithologies, or with near-zero bulk D's, it may be possible to calculate differences between sources for basalts with variable abundance ratios. Incompatible trace elements meeting these requirements include Ba, La, Th, and Nb. Other incompatible elements such as Cs, Rb, and K may be modified by minor late stage alteration, and Ta abundances are subject to high analytical uncertainty. The most variable abundance ratios in the basalts involve Ba, La, Th, and Nb, and as mentioned earlier, no ratios

among these elements are linearly correlated with abundances of these elements. Abundance ratios of Ba/Nb, La/Nb, and Th/Nb are variable in the basalts and will be used to address relationships involving sources and degree of melting in simple batch melting models. The results of these calculations are used to (1) discuss the origin of negative HFSE (Nb) anomalies in arc lavas, and (2) to speculate on the nature of hypothetical components derived from a subducted slab of oceanic crust. Specific abundance ratios may yield clues as to whether or not the slab-derived component contains alkalies (Ba/Nb), REE (La/Nb), or Th (Th/Nb).

The same basalt samples (13826h, 220283-1, and 13828) were used to consider relative differences in source characteristics and degree of melting using their Nb abundances and Ba/Nb, La/Nb, and Th/Nb ratios. These basalts display large variations in these abundance ratios and in abundances of Nb. All three ratios in these basalts are significantly higher than chondritic ratios due to the negative HFSE Nb anomaly and Nb is apparently more 'compatible' relative to Ba, La, and Th. The presence of a Nb-containing refractory phase has been suggested to be the cause of this effect (Saunders et al., 1980; Green, 1981; Stern and Ito, 1983; Morris and Hart, 1983). Thus, partial melting model calculations for these abundance ratios are best displayed on plots of D_o^{Nb} vs. C_o^{Nb}. Equations (1) through (4) are easily modified; it is assumed that for a refractory, Nb-retaining phase, P = 0, and $D_o^{Ba} = D_o^{La} = D_o^{Th} = 0$. Equation (3) reduces to:

$$(10)\quad D_o^{Nb} = F\left[\left(\frac{C_o^{Nb}}{C_o^{Ba}}\right)\left(\frac{C_L^{Ba}}{C_L^{Nb}}\right) - 1\right]$$

to solve for D_o^{Nb}. This is proportional to the amount of refractory

phase present and is similar to calculating X_{cpx} or X_{gar} in Figures 38 to 40, except that no mineral/melt partition coefficient specific to the refractory phase need be estimated. Chondritic (C_0^{Ba}/C_0^{Nb} = 9) and enriched (C_0^{Ba}/C_0^{Nb} = 11.0) source abundance ratios were used in calculations. Source abundances (C_0^{Nb}) are calculated by using the melt fraction F which is used in equation (10) to calculate D_0^{Nb}; for the assumed F, the calculated D_0^{Nb} and the abundance of Nb in a specific basalt (C_L^{Nb}), C_0^{Nb} is calculated using the following expression,

(11) $C_0^{Nb} = C_L^{Nb} (D_0^{Nb} + F)$

which is a simplified version of the general equation for batch melting, assuming that $P_0^{Nb} = 0$. Results of the calculations are illustrated in Figure 42. For the three basalts, the relationships between degree of melting F, the partition coefficient D_0^{Nb}, source abundance(s) C_0^{Nb}, and the curvature of contours for constant F are much the same as in previous diagrams (Figures 38-40).

For both chondritic and 'enriched' mantle sources represented by appropriate Ba/Nb (9.0 and 11.0), La/Nb (0.80 and 0.70), and Th/Nb (0.128 and 0.145), high bulk partition coefficients (D_0^{Nb}) are required to explain ratios of Ba/Nb, La/Nb, and Th/Nb in the basalts which are high relative to chondrites or predicted compositions of mantle sources for N-type or E-type MORB (Tarney et al., 1980). This supports the role of a HFSE-rich refractory accessory phase in retaining HFSE during production of arc magmas by partial melting (Saunders et al., 1980; Stern and Ito, 1983; Morris and Hart, 1983). The implications of the curvature of melt fraction contours may be interpreted in a similar manner to those in Figures 38-40. For a constant value of D_0^{Nb}, basalts 13826h and 220283-1 could be generated by equivalent degrees of partial melting of sources

with different abundances, while basalt 13828 may have been produced by a relatively smaller degree of partial melting of a source with lowest Nb abundances (Fig. 42). For a constant source abundance C_0^{Nb}, the degree of partial melting required to generate each basalt decreases from 13826h to 13828 to 220283-1, while required values of D_0^{Nb} decrease from 13828 to 13826h to 220283-1. If all three basalts were generated by an equivalent degree of partial melting, source abundances may be similar for basalts 13828 and 13826h (except on the plot of D_0^{Nb} vs. C_0^{Nb} based on Th/Nb ratios) while a larger D_0^{Nb} is required for 13828. Basalts 13826h and 220283-1, however, require similar D_0^{Nb}, lower than that for 13828, and differing source abundances. Similar ratios of Ba/Th, Ba/Nb, La/Nb, and Th/Nb between basalts 13826h and 220283-1 may suggest that parental magmas for these basalts were derived from sources with similar abundance ratios (Table 17), similar proportions of a hypothetical HFSE-rich accessory mineral, and differing source abundances. Variations in La/Sm and La/Yb ratios between these two basalts may reflect their respective origins by melting of sources differing in REE abundances or in relative proportions of clinopyroxene and/or garnet. The most significant difference, that of relatively higher LIL/HFSE and REE/HFSE ratios, in basalt 13828 compared to the other two basalts may suggest a relatively greater role of a HFSE-retaining phase in the source of this basalt. Variations in such ratios as Ba/La, K/La, Rb/La, and Ba/Rb among all three basalts (Table 17) may be related to varying amounts of an alkali element-enriched slab-derived component added to each mantle source.

42 Calculated values of bulk partition coefficients for Nb (D_o^{Nb}) vs. source abundances of Nb (C_o^{Nb}) required to generate the three basalts. Curved lines indicate the degree of partial melting required to generate the basalts for given values of D_o^{Nb} and C_o^{Nb}. In all three plots, the effect of a refractory Nb-retaining phase was assumed and $P^{Nb} = 0$. The trajectory line labelled 13828 is based on an average Ba/Nb (102), La/Nb (4.7) and Th/Nb (1.26) ratios for basalts 13828 and 272829. The line labelled 13826h is based on average abundance ratios for basalts 272825 and 13826h.

(a) Solid lines for various melting degrees were calculated assuming $C_o^{Ba}/C_o^{Nb} = 9$ for a chondritic source, and dashed lines assuming $C_o^{Ba}/C_o^{Nb} = 11$ for an enriched OIB source.

(b) As above, solid and dashed lines for F were calculated assuming a chondritic ($C_o^{La}/C_o^{Nb} = 0.80$) and an enriched ($C_o^{La}/C_o^{Nb} = 0.70$) source, respectively.

(c) Solid and dashed lines for F values relate to a chondritic ($C_o^{Th}/C_o^{Nb} = 0.13$) and an enriched ($C_o^{Th}/C_o^{Nb} = 0.145$) source, respectively.

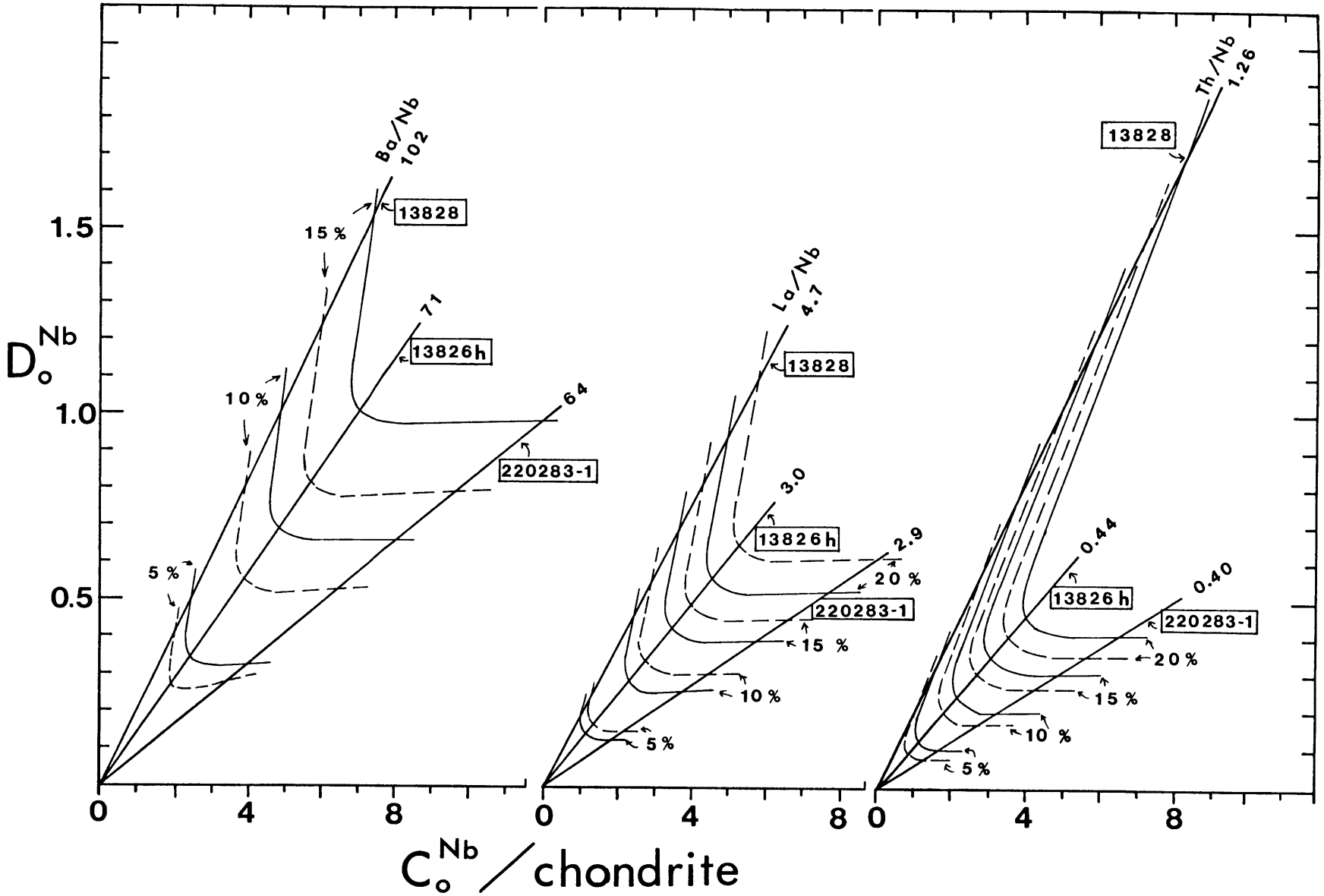
D_o^{Nb}
1.5
1.0
0.5
0
4
8
C_o^{Nb} / chondrite
Ba/Nb
102
71
64
13828
13826h
220283-1
15 %
10 %
5 %
La/Nb
4.7
3.0
2.9
20 %
15 %
10 %
5 %
Th/Nb
1.26
0.44
0.40
20 %
15 %
10 %
5 %

Table 17

Trace element abundance ratios in basalts, mantle sources, and crustal sourcces

	Puyehue basalts (1)			oceanic basalts (2)		oceanic basalt sources (3)		chondritic (4)	crustal sources (5)	
	13828	13826h	220283-1	average N-type MORB	average oceanic island basalt	N-type MORB source	E-type MORB source	values	average upper crust	average lower crust
K	5010	4120	5805	1160	4916	106	216	120	27400	5000
Rb	9.2	8.7	12.9	1.11	14.4	0.1	0.39	0.35	110	8
Cs	0.75	0.59	0.78	0.012	0.115	0.0013	0.007	0.012	3.7	0.7
Ba	173	165	263	10.5	154	1.2	4.77	3.5	700	175
Sr	500	410	459	136	290	13.2	17.9	11	350	425
Nb	1.7	2.4	4.1	4.6	13	0.31	0.72	0.39	25	4
Ta	0.07	0.10	0.19	-	-	0.022	0.062	0.02	-	-
Zr	53	67	100	90	150	11.4	11.3	5.6	240	30
Hf	1.39	1.73	2.42	2.3	4	0.34	0.26	0.18	5.8	1.6
Th	2.14	1.00	1.62	0.21	0.98	0.02	0.06	0.05	10.5	1.95
Pb	7	6	-	0.6	1.2	-	-	-	15	7.5
U	-	-	-	-	-	0.01	0.015	0.013	2.5	0.63
La	7.91	6.92	11.9	2.6	10	0.31	0.66	0.315	30	14
Ce	19.1	17.6	29.9	7.9	26	0.95	1.68	0.813	64	25
Nd	11.5	11.1	17.3	6	12	0.86	1.11	0.597	26	11
Sm	2.82	2.92	4.06	3.3	5.4	0.32	0.42	0.192	4.5	3.3
Yb	1.57	1.93	2.18	-	-	-	-	0.208	-	-
Y	15.0	19.1	-	29.2	-	4.1	2.7	2.2	22	22
La/Sm	2.80	2.37	2.93	0.79	1.85	0.97	1.57	1.64	6.67	4.24
La/Yb	5.05	3.59	5.46	-	-	-	-	1.51	-	-
Rb/Cs	12.9	14.8	16.5	93	125	77	56	29.2	29.7	11.4
K/Rb	538	475	450	1045	341	1060	554	343	249	625
Ba/Rb	18.5	19.0	20.4	9.5	10.7	12	12.2	10	6.36	21.9
Ba/La	21.8	23.8	22.1	4.0	15.4	3.87	7.23	11.1	23.3	12.5
Ba/Th	81	164	162	50	157	60	80	70	66.7	89.7
Ba/Nb	99	68	64	2.3	11.8	3.87	6.63	8.97	28	43.8
La/Nb	4.5	2.9	2.9	0.57	0.77	1.0	0.92	0.81	1.2	3.50
Zr/Sm	19.0	22.8	24.6	27.3	27.8	35.6	26.9	29.2	53.3	9.1
Sr/Nd	44.4	37.0	26.5	22.7	24.2	15.3	16.1	18.4	13.5	38.6
Ba/Zr	3.26	2.46	2.63	0.12	1.03	0.11	0.42	0.63	2.92	5.83
Zr/Nb	31.2	27.9	24.4	19.6	11.5	36.8	15.7	14.4	9.6	7.5
Th/La	0.271	0.145	0.136	0.081	0.098	0.065	0.091	0.159	0.350	0.139

(1) trace element abundaces adjusted for olivine and plagioclase phenocryst content (see text)
(2) Wood et al. (1979)
(3) Tarney et al. (1980)
(4) Sun and Nesbitt (1976); Masuda et al. (1976); Sun et al. (1979)
(5) Taylor and McLennan (1981)

10.5.3 Contributions from subducted oceanic crust

An alternative means for explaining high Ba/Nb, La/Nb, and Th/Nb ratios in arc basalts may be that an agent or component derived from the subducted slab of oceanic crust modifies the mantle above the Wadati-Benioff zone, and primary arc magmas are produced by partial melting of this modified mantle. If the slab-derived component is enriched primarily in alkalies, LREE, Pb (cf., Kay, 1980), and possibly Th, then it is possible that upper mantle modified by the addition of such a component will be characterized by negative HFSE anomalies. This simple model is partly supported by the fact that abundances of HFSE in most arc basalts overlap with those of normal or N-type MORB. If ratios of Ba/Nb, La/Nb, and Th/Nb in the modified mantle source are sufficiently high, then retention of Nb and other HFSE elements in a hypothetical refractory phase may not be necessary to explain the negative HFSE anomalies observed in most arc basalts. In the above model, the characteristics of a slab-derived component do not necessarily depend on the existence of a HFSE-retaining phase in the subducted and transformed slab of oceanic crust nor in the modified mantle. Enrichments of alkalies and LREE in such a component may be due to the greater solubility of these elements relative to the HFSE in this component. This is effectively a partitioning process, requiring that HFSE be retained by some means in the subducted slab residuum after extraction of the component enriched in alkalies and LREE. During metamorphism of the subducted slab, the HFSE and HREE may be redistributed in residual oxide phases, phlogopite, and garnet in the subducted slab which presumably is transformed to eclogite at or prior to its arrival beneath the volcanic arc. A variety of oxide phases, especially titanates, are common in

exposed eclogite terranes (Ernst, 1976, 1977; Ernst and Dal Piaz, 1978). Hydrous fluids or vapors in equilibrium with eclogite, phlogopite-bearing peridotite, or amphibole peridotite will be enriched in LREE, Si, and Al, relative to other elements, especially Ti (Mysen, 1983; Schneider and Eggler, 1984). Thus, a slab-derived melt, fluid, or vapor phase may be characterized by inherent negative HFSE anomalies (Hole et al., 1984). As this material percolates upward in the mantle, it may selectively leach alkalies, LREE, Si, and Al from surrounding mantle, and the inherent negative HFSE anomalies in this component will be further amplified. A process such as this may not necessarily be unique to arcs, but may occur in subcontinental regions as indicated by xenoliths of metasomatized peridotite in alkaline basalts (Menzies and Wass, 1983; Roden et al., 1984), in which there is no apparent relationship with subducted crust, although negative HFSE anomalies are not observed in intraplate basalts. Precipitation, or fractional crystallization of phlogopite during such a mantle-hybridization process may occur (Sekine and Wyllie, 1983), and thus aid in magnifying negative HFSE anomalies in the melt, fluid, or vapor component, since $D^{Zr} \cong D^{Nb} > D^{REE}$ for phlogopite (Fujimaki et al., 1984). The amount of phlogopite formed would be dependent on the amount of Al available and since phlogopite incorporates alkalis to a greater degree than HFSE (i.e., $D_{phlog}^{Ba} > D_{phlog}^{Nb}$), an excess of alkalies over Al in a metasomatic component would be required.

The composition of a slab-derived component is dependent on the bulk composition of the subducted oceanic crust. If only the thin (<2 km), uppermost portion of the subducted slab is subjected to the most dehydration or metamorphism during subduction (Marsh, 1979; DeVore, 1983), this uppermost portion may consist principally of sediments, and

the nature and composition of the sedimentary column oceanward of any given arc may be important in controlling the characteristics of the slab-derived component. Many different types of sediments are found within marine or continental margin depositional environments. The subduction process is complex, and it is not necessarily true that the compositions of forearc or trench sediments are analogous to materials/components which modify or mix with mantle in the zone of magma genesis below the active volcanic front of an arc. Nevertheless, data for sediments may provide several clues as to the nature of the process, compositions of endmember components or materials, and volumes of sedimentary components involved in magma genesis.

Sediments are typically enriched in alkalies and Pb relative to arc basalts but display wide ranges of abundances in most trace elements (Table 18). Detailed analyses of sediments are uncommon, however a recent study of abyssal sediments from the Nazca plate (Hole et al., 1984) demonstrates that these types of sediments may be characterized by extreme alkali element enrichments and dramatic negative HFSE anomalies. High ratios of Ba/La, Sr/Nd, Ba/Th, and Ba/Nb required in slab-derived components to explain the characteristics of arc volcanics are a primary feature of these sediments (Table 18). Fine abyssal sediments such as these are often characterized by negative Ce anomalies, and Hole et al., (1984) suggest that such sediments are retained in the slab to depths of magma genesis and are mixed in bulk with mantle compositions, as suggested by the complementary negative Ce anomalies in Marianas arc lavas. Negative Ce anomalies may be typical of slowly-deposited, deep-sea sediments (Hole et al., 1984; Kay, 1984) and may reflect negative Ce anomalies observed in sea water (DeBaar et al., 1983) and

Table 18

Trace element abundances and abundance ratios in sediments

	(1) pelagic sediments, range	(2) authigenic and metallogenic sediments, range	(3) Aleutian core, range	(4) Nazca core, range	(5) P.A.M.W.S.	(6)	(7)
K	500 - 31000	1000 - 9600				10205	16187
Rb	1 - 150	5 - 205		1 - 25	3.6	32.3	19
Cs	<1 - 11		1 - 4			2.3	
Ba	3 - 12000	160 - 700	780 - 2440	188 - 11937	1338	382	
Sr	<1 - 1400	180 - 1200		604 - 1377	1144	361	334
Nb	<1 - 65			1 - 6	1.25		
Ta	.05 - 0.8	0.2 - 1.2	0.14 - 0.78	<.05 - .13	0.05		
Zr	13 - 374	20 - 400		13 - 152	21.6		
Hf	.07 - 4.3	? - 3.6	1.74 - 4.3	<.04 - .09			
Th	.08 - 20	5 - 30	1.7 - 8.2	.08 - 2.38	0.23		
Pb	9 - 80	45 - 560					
U			0.9 - 2.7				
La	7.0 - 195	19 - 105	7 - 25	8.3 - 195	25.8	28	
Ce	2.1 - 350	7 - 500	14 - 51	2.1 - 54.5	9.6		
Nd	6.2 - 125	15 - 154	7.5 - 21	6.2 - 124.8	19.3	24	
Sm	1.4 - 22	4.9 - 130	2.4 - 5.3	1.4 - 27.6	4.40	5.1	
Yb	1.2 - 27.8	1.9 - 19.7	1.0 - 3.9	1.2 - 27.8	5.55	2.4	
Y	17 - 501	25 - 290		17 - 501	46.3		
La/Sm	3.0 - 7.1	2.9 - 4.0	3.0 - 4.7	5.4 - 6.0	5.86	5.49	
La/Yb	5.4 - 10.4	5.3 - 9.8	5.5 - 7.2	5.9 - 8.5	4.65	11.7	
Rb/Cs	12 - 30	15 - 20				14	
K/Rb	200 - 600	200 - 730				316	
Ba/Rb	2 - 570	12 - 143		264 - 570	372	11.8	
Ba/La	7.5 - 346	18 - 21	32 - 346	32 - 117	52		
Ba/Th	95 - 10310		95 - 1417	1540 - 10310	5817		
Ba/Nb	18 - 2400			320 - 2400	1070		
La/Nb	0.4 - 32.5			10.6 - 32.5	20.6		
Zr/Sm	3 - 10			3 - 10	4.9		
Sr/Nd	5.0 - 186	7 - 18		5.0 - 186	59.3		
Ba/Zr	14 - 147			14.4 - 147	62		
Zr/Nb	3.8 - 36(?)			16.2 - 36	17.3		

(1) Sources of data: Shimokawa et al. (1972), McLennan and Taylor (1981), Papavassiliou and Cosgrove (1982), Barreiro (1983), Morris and Hart (1983), Brigueu and Lancelot (1983), Stern and Ito (1983), Hole et al. (1984), Kay (1984).
(2) Sources of data: Calvert and Price (1977), Elderfield et al. (1981), Barrett and Friedricksen (1982), Stern and Ito (1983), Kay (1984).
(3) Sediments ranging from turbidite to diatomaceous ooze from DSDP hole 183 100 km south of the Aleutian trench from Kay (1984).
(4) Sediments ranging from clays to nannofossil ooze, DSDP holes 319 and 320, Nazca Plate, from Hole et al. (1984).
(5) Pacific Authigenic Weighted Mean Sediment (Hole et al. 1984).
(6) Weighted average of K, Rb, Cs, Ba, and Sr for Western Pacific seafloor (Stern and Ito, 1983). Average REE abundances in pelagic sediments (McLennan and Taylor, 1981).
(7) Weighted average for forearc sediments, DSDP hole 286, New Hebrides arc (Briqueu and Lancelot, 1983).

mirror positive Ce anomalies in Mn nodules. Continentally derived detrital sediments ordinarily do not display negative Ce anomalies, and in combination with Mn nodules, may cancel the effect of negative Ce anomalies in abyssal sediments (Hole et al., 1984). Also, continental, terrigenous, or volcaniclastic sediments may be characterized by relatively lower values of Ba/Nb, Ba/Th ratios, etc., as represented by lower ratios in turbidite sediment in Aleutian forearc sediments (Table 18). Thus, the magnitude of primary negative HFSE anomalies in sediments varies with sediment type. In a given marine sedimentary column oceanward of any arc, the bulk composition, presence or absence of negative Ce anomalies, and magnitude of HFSE anomalies depend on the relative proportions of various sediment types. These relative proportions depend on the tectonic setting of the arc. In theory, oceanic arc volcanics might be characterized by higher Ba/Nb, Ba/Th, Ba/La, and Sr/Nd ratios than continental arc volcanics.

As shown in Table 19, abundance ratios (Ba/Th, Ba/Nb, Ba/La, and Sr/Nd) in basalts and basaltic andesites that may reflect the role of sediments/slab components in any given arc vary widely. Ranges of these abundance ratios in oceanic arcs (Marianas, S. Sandwich, Grenada, New Britain), arcs located in transitional or complex tectonic settings (Bismarck, New Hebrides, Halmahera, Aleutians, Santorini), and continental arcs (Cascades, S. Central Chile, Puyehue Volcano) overlap entirely and display no differences that may be related to tectonic setting or the type of sedimentary material subducted. Although there is much overlap between arcs in ranges of the selected abundance ratios in Table 19, the variability or total range in these ratios appears to be greater in most oceanic arcs. This may be because the oceanic arcs

Table 19

Selected trace element abundance ratios for basalts and basaltic andesites from various arcs

Arc	Ba/Th	Ba/Nb	Ba/La	Sr/Nd
Marianas	177-503	87-220	18-58	28-47
South Sandwich	-	-	29-91	13-54
Grenada	28-127	34-96	15-30	25-71
New Britain	50-600	10-236	4-54	17-108
Bismarck Arc (Manam Volcano)	-	-	29-54	62-130
New Hebrides	96-462	96-310	18-49	31-78
Halmahera	45-125	23-61	15-22	22-51
Aleutians		22-110	20-54	
Semisopochnoi	345-399	233-256	52	30-45
Santorini, Greece	18-58	32-63	14-23	8-25
Hokkaido (East Japan)				
tholeiitic series	91-482			34-101
calcalkaline series	64-110			22-38
alkalic series	92-179			17-36
Cascades, U.S.A.				
Mt. St. Helens	120-144		14-27	
Indian Heaven	66-218		13-22	
S. Central Chile	66-209(287?)	43-136	15-36	26-54
Puyehue Volcano	81-181	63-108	21-26	33-54

Sources of data: Marianas (Dixon and Batiza, 1979; Hole et al., 1984); South Sandwich (Hawkesworth et al., 1979; Barreiro, 1983); Grenada (Shimizu and Arculus, 1975; Hawkesworth et al., 1979; Thirlwall and Graham, 1984); New Britain (DePaolo and Johnson, 1979; Johnson, 1981); Manam Volcano, Bismarck Arc (Johnson, et al., in press); New Hebrides (Gorton, 1977); Halmahera (Morris et al., 1983; Morris, 1984); Aleutians (Kienle et al., 1979; McCulloch and Perfit, 1981; Kay et al., 1982; DeLong et al., in press); Santorini, Greece (Mann, 1983; Barton et al., 1983); Japan (Masuda et al., 1975); Mt. St. Helens and Indian Heaven, Cascades, U.S.A. (Smith, 1984); South Central Chile (Hickey et al., in prep.; Frey, unpub. data); Puyehue Volcano, Chile (this study).

listed are dominated by tholeiitic arc volcanism, as tholeiitic series basalts and basaltic andesites may characteristically display greater ranges in these abundance ratios relative to those of the calcalkaline or alkalic series (Masuda et al., 1975). This may be explained if basalts from tholeiitic arc volcanic centers are relatively lower in trace element abundances and are therefore more susceptible to contamination processes that may occur within the upper mantle or continental crust, as suggested by Hickey et al., (in press). However, Kay et al. (1982) observe that the most primitive basalts from tholeiitic and calcalkaline centers in the Aleutian arc are similar and speculate that the two types of centers share a common parental magma type. This would seem to conflict with the data of Masuda et al. (1975) which suggests that primitive basalts of tholeiitic, calcalkaline, and alkaline centers are geochemically distinct. However, Masuda et al., (1975) were essentially comparing samples from centers that vary in distance from the Japan trench, while Kay et al. ,(1982) compared data for centers which are all approximately the same distance from the trench but which are distinguished by their locations near (large tholeiitc centers) or away from (small calcalkaline centers) fracture zones which crosscut the trench and segment the volcanic arc. In the latter case presented by Kay et al. (1982), it is not surprising that primitive magmas supplied to tholeiitic or calcalkaline centers may be similar. This would suggest, then, that relatively large degrees of geochemical heterogeneity in some centers is not necessarily dependent on relatively lower abundances in basalts that are associated with geochemically heterogeneous centers nor with the type of magma series (tholeiitic vs. calcalkaline). As Kay et al. (1982) point out, the classification of a center as tholeiitic or

calcalkaline is based on the characteristics of relatively more evolved lavas and these characteristics are produced by different near surface processes (fractional crystallization vs. magma mixing) predominant in each center which may ultimately be associated with tectonic setting.

The data of Kay et al. (1982) are inadequate to determine whether or not basalts from tholeiitic centers are geochemically more heterogeneous with regard to trace element abundance ratios and isotopic composition than basalts from calcalkaline centers. Geochemical heterogeneity in individual volcanic centers may decrease with time (Myers et al., 1984). Larger, more mature, or relatively long-lived centers would be geochemically homogeneous relative to smaller, youthful centers, a conclusion made by Myers et al. (in press) based on comparison of two centers, Adak and Atka, in the Aleutian arc; however, there is no strong evidence indicating that Atka is relatively longer-lived than Adak (S. Kay, pers. comm., 1985). This may also be suggested by a lesser range in Ba/Th (120-144) in basalts and basaltic andesites from Mt. St. Helens compared to that observed (Ba/Th = 66-218, Table 18) in the relatively less mature Indian Heaven basalt field (D. Smith, unpub. data), however Mt. St. Helens lavas are isotopically heterogeneous and preliminary data are supportive of ongoing crustal contamination or AFC processes (Kurasawa et al., 1982). On the basis of data for other volcanic centers in the central South Chile segment of the Southern Andes (Frey et al., unpub. data), Puyehue Volcano may be geochemically heterogeneous relative to other centers of similar size and maturity. Geochemical variability in individual centers may therefore be less related to the relative maturity or size of the center than the rates of magma production and variations in sub-arc components and processes occurring beneath each center and throughout the arc.

At some point, the slab-derived component induces partial melting in an amount sufficient to lead to diapirism or possibly separation of primary basaltic melts. The upper mantle above the Wadati-Benioff zone may be characterized by a complete lack of negative HFSE anomalies and mixing of primary melts with upper mantle wallrock melts will reduce the magnitude or 'negativity' of HFSE anomalies in the resulting mixed magmas. If abundances of HFSE in upper mantle wallrock are higher than those in the primary source of a magma in transit, re-equilibration of the magma with upper mantle wallrock will result in an increase of HFSE abundances in the magma, if the volume of the magma is constant. This mechanism will also reduce the magnitude of negative HFSE anomalies in magmas. A slab-derived component may also modify the isotopic composition of sub-arc mantle, although the extent of this effect may depend on the age and degree of alteration of the subducted oceanic crust (cf. DePaolo and Johnson, 1979; Hawkesworth et al., 1977) or the amount of sediment contributed. However, the average isotopic composition of the subducted oceanic crust may not be directly relevant. It is likely that the subducted slab of oceanic crust is isotopically heterogeneous and it may be that the most radiogenic portions, i.e., surficial sediments, tend to breakdown at lower pressure and temperatures relative to other portions or phases. DeVore (1983) estimates that only the uppermost 2 km of subducted oceanic crust may be involved in the dehydration or fluid/vapor extraction process, and therefore slab-derived components inherit the isotopic characteristics of only this uppermost possibly sediment-dominated portion of the subducted crust. Thus, even if isotopic analyses of forearc trench sediments and basalts are available for a given arc, this information cannot be applied

unambiguously in estimating the characteristics of the slab-derived component at the depth of magma genesis below the arc.

A sedimentary Pb-isotopic signature is seen in many arcs (Armstrong and Cooper, 1970; Oversby and Ewart, 1972; Meijer, 1976; Kay et al., 1978; Barreiro, 1983) and many arc lavas display high $^{87}Sr/^{86}Sr$ for a given $^{143}Nd/^{144}Nd$ such that they fall to the 'high' side of the mantle array on a plot of $^{143}Nd/^{144}Nd$ vs. $^{87}Sr/^{86}S$ (cf., Hawkesworth et al., 1977). Many arc lavas fall within the mantle Nd-Sr array but fall outside of the MORB field defined by Pb-Pb plots. This indicates that Pb isotopes may be a sensitive indicator of a slab-derived sedimentary component which probably results from relative abundance contrasts between the slab-derived component and the sub-arc mantle which may decrease from Pb to Sr to Nd, respectively. Therefore, a sedimentary component may persist in a subduction zone to the depth of magma genesis. Sedimentary-derived alkalies, LREE, and Pb may be incorporated in phases such as phlogopite or jadeite which may be stable to these depths (~ 100-110 km),and cooler temperatures in the descending slab and the overall thermal structure may favor the stability and preservation of such sub-arc phases.

Re-equilibration of melt in an ascending diapir with upper mantle wallrock as suggested earlier may result in changes in the abundances of incompatible trace elements and abundance ratios in the melt, but the extent of re-equilibration may be insufficient to significantly change the isotopic composition of the magmas (cf., Hofmann and Hart, 1978). If magmas are not modified by re-equilibration or contamination during ascent through the sub-arc mantle wedge, then one might expect positive correlations between Pb and Sr isotopic compositions and ratios such as Ba/Nb or Sr/Nd if varying proportions of a slab-derived component were

added to relatively less radiogenic upper mantle with relatively lower abundances of trace elements. Abundance ratios such as Ba/La, Ba/Nb, and Sr/Nd should be high in a slab-derived component. Arculus and Johnson (1981) note a negative correlation of $^{87}Sr/^{86}Sr$ with abundance ratios such as these for many arcs, most notably the Lesser Antilles (Shimizu and Arculus, 1975; Hawkesworth et al., 1979; Thirlwall and Graham, 1984) and suggested that the role of slab-derived components is subordinate to that of crustal contamination in producing the characteristics displayed by most arc suites. However, many arcs are not underlain by significant thicknesses of continental crust or even lower crust consisting of high-grade metamorphic rocks. Other arcs display positive correlations of $^{87}Sr/^{86}Sr$ with Ba/La and Sr/Nd, ratios identified with a slab-derived component, as at Manam Volcano in the Bismarck Arc (Johnson et al., in press).

Positive correlations of Ba/Th vs. $^{87}Sr/^{86}Sr$, Ba/Th vs. $^{206}Pb/^{204}Pb$, and Sr/Nd vs. Ba/Nb are observed in basalts from Puyehue Volcano (Fig. 43), and are consistent with a model whereby a slab-derived component with high Ba/Th, high $^{206}Pb/^{204}Pb$, and high $^{87}Sr/^{86}Sr$ has modified, or mixed with sub-arc mantle to varying degrees. Those basalts with relatively higher $^{87}Sr/^{86}Sr$, $^{206}Pb/^{204}Pb$, and Ba/Th may have been derived from sources containing a relatively greater proportion of slab-derived component. However the positive correlation of Sr/Nd vs. Ba/Nb may not be explained by such a simple model because each of these abundance ratios are negatively correlated with $^{87}Sr/^{86}Sr$ and $^{206}Pb/^{204}Pb$ (Fig. 43). Negative correlations of $^{87}Sr/^{86}Sr$ and $^{206}Pb/^{204}Pb$ with slab component-related abundance ratios such as Sr/Nd or Ba/Nb are observed in some arcs (Arculus and Johnson, 1981) and more complex processes are

43 Covariations of Ba/Th, Ba/Nb, and Sr/Nd vs. $^{87}Sr/^{86}Sr$ and $^{206}Pb/^{204}Pb$ in Puyehue basalts. Also shown are plots of Ba/Th vs. Sr/Nd and Sr/Nd vs. Ba/Nb for Puyehue basalts.

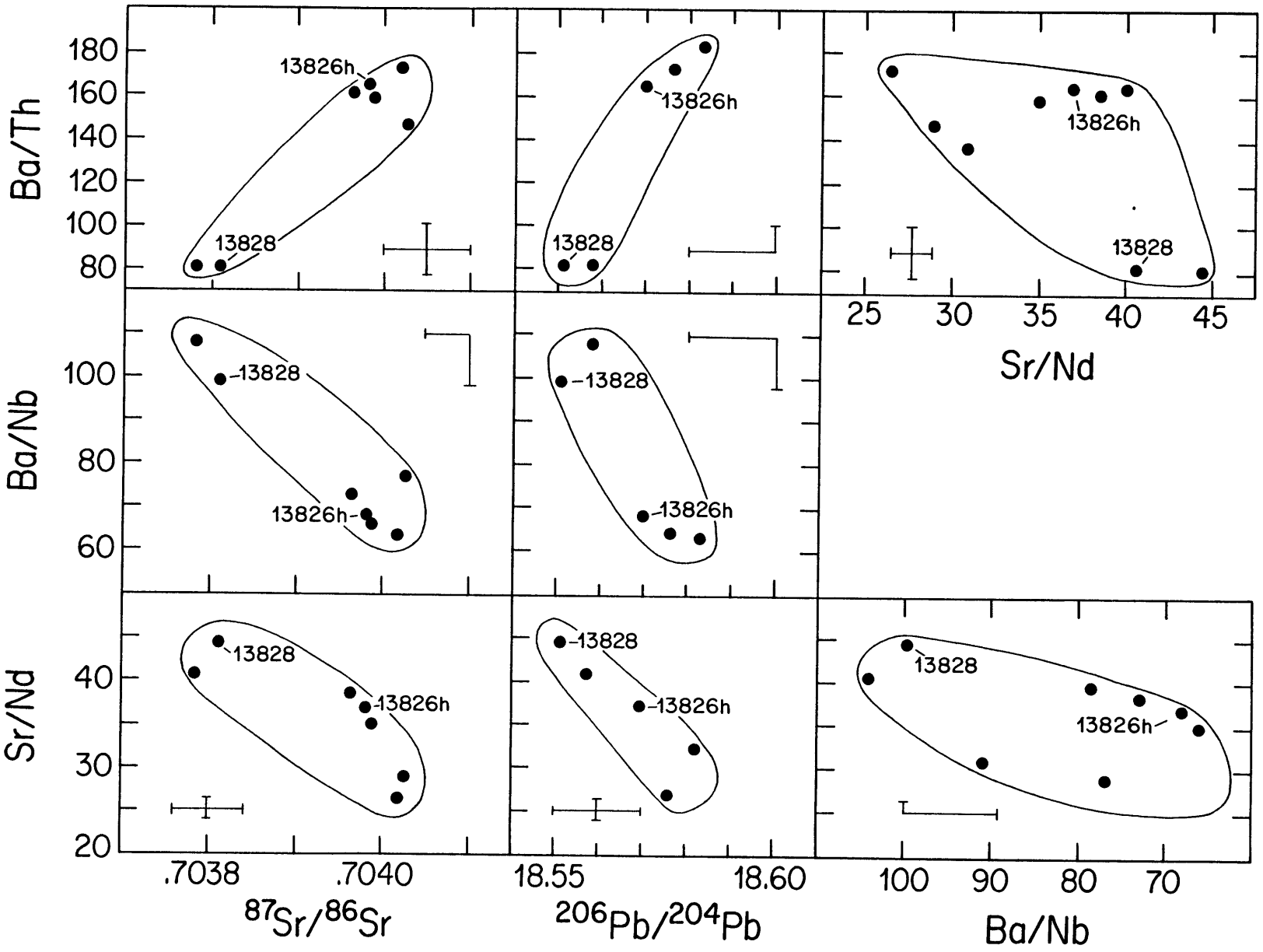
Ba/Th
180
160
140
120
100
80
13826h
13828
13826h
13828
13826h
13828
Ba/Nb
100
80
60
13828
13826h
13828
13826h
25
30
35
40
45
Sr/Nd
Sr/Nd
40
30
20
13828
13826h
13828
13826h
13828
13826h
.7038
.7040
87Sr/86Sr
18.55
18.60
206Pb/204Pb
100
90
80
70
Ba/Nb

required to explain this pheonomenon. Two possible general models will be demonstrated using Ba/Nb, Sr/Nd, and $^{87}Sr/^{86}Sr$ ratios in Puyehue basalts.

Model (1) requires variable mantle compositions and a homogeneous slab component characterized by high Sr/Nd, Ba/Nb, and $^{87}Sr/^{86}Sr$. For purposes of demonstration, two mantle endmembers, N-type and E-type MORB sources (Table 17), were assumed. Ratios of $^{87}Sr/^{86}Sr$ in N-type and E-type sources were assumed to be 0.7025 and 0.7030, respectively. Basalts 13828 and 13826h were chosen as endmembers for modelling because they are characterized by extreme Ba/Nb and $^{87}Sr/^{86}Sr$ ratios. Basalt 220283-1 is characterized by slightly lower Ba/Nb and Sr/Nd, and slightly higher $^{87}Sr/^{86}Sr$ than 13826h, but contains higher abundances of incompatible trace elements than 13826h. To demonstrate the feasibility of the model, basalts 13828 and 13826h were used, and are similar in their trace element abundances; this may introduce less uncertainty in the results. Assuming that Ba/Nb, Sr/Nd, and $^{87}Sr/^{86}Sr$ ratios in these basalts are representative of their respective sources, i.e., these ratios were not modified in parental magma bodies or diapirs on ascent, abundances of Sr, Nd, Ba, and Nb in sources for these two basalts were calculated assuming 25% fractional crystallization en route to the surface for both, and 25% and 10% partial melting respectively for basalt 13826h and basalts 13828 based on qualitative differences in degrees of partial melting indicated earlier (Figures 38 to 40). Assumed and calculated source characteristics for all models are listed in Table 19.

Mixing curves (cf. Langmuir et al., 1978) through N-type mantle and a source for basalt 13828, and E-type mantle and a source for basalt 13826h project towards an indicated slab-derived component with high

Sr/Nd and Ba/Nb, but relatively low $^{87}Sr/^{86}Sr$ (< .704-.705, Figures 44a, 44b). If Sr/Nd ratios in the basalts are partly due to plagioclase accumulation, then parental magmas were characterized by relatively lower Sr/Nd ratios, in turn requiring relatively lower Sr/Nd ratios and higher $^{87}Sr/^{86}Sr$ in a slab-derived component added to E-type and N-type mantle (Fig. 44a). This is illustrated in Figure 44a by assuming 25% plagioclase accumulation in respective parental magmas for basalts 13828 and 13826h and recalculating source trace element abundances as above (Table 20). This is possibly an 'over-correction', since these basalts do not contain 25% accumulated plagioclase phenocrysts, but this measure serves to demonstrate the effect on mixing curves. If high Ba/Nb ratios in the basalts are partly due to differentiation on partial melting, i.e., the influence of a Nb-retaining refractory phase in the source, then relatively lower Ba/Nb and higher $^{87}Sr/^{86}Sr$ ratios are indicated for the slab-derived component. As illustrated in Figure 44b, sources for basalts 13828 and 13826h were calculated assuming bulk partition coefficients for Nb (D_o^{Nb}) of 0, 0.1 and 0.5. Mixing curves calculated through an N-type source and sources for basalt 13828, and an E-type source and a source for basalt 13826h project to hypothetical slab component compositions with higher $^{87}Sr/^{86}$ and lower Ba/Nb ratios as D_o^{Nb} increases. Due to different degrees of partial melting assumed for basalt 13828 (10%) and basalt 13826h (25%), recalculated sources assuming $D_o^{Nb} = 0.5$ display a slight positive correlation in that a recalculated source for 13828 would then have lower Ba/Nb in addition to lower $^{87}Sr/^{86}Sr$ relative to the source for 13826h. Mixing curves for these sources and the respective mantle endmembers assumed project towards quite different compositions in slab-derived components (Figures 38b) and illustrate uncertainties in the model.

44(a) Plot of Sr/Nd vs. $^{87}Sr/^{86}Sr$ illustrating hypothetical source mixing models for two basalts in terms of model (1) (see text). Solid lines are mixing curves through sources for basalts 13828 and 13826h, and N-type (noted as 'N') and E-type ('E') mantle sources (Table 21), respectively. Dashed line is a mixing line between N-type mantle and a source for basalt 13826h. Lower curves in each case are drawn through basalt sources calculated assuming 25% plagioclase accumulation. Note that the dashed line nearly coincides with lower mixing curve through a source for basalt 13828 based on plagioclase accumulation.

(b) Plot of Ba/Nb vs. $^{87}Sr/^{86}Sr$ illustrating source mixing models for two basalts in terms of model (1). Solid lines are mixing curves through sources for basalts 13828 and 13826h, and N-type and E-type mantle sources (Table 20), respectively. Two alternate sources for each basalt were calculated assuming $D_o^{Nb} = 0.1$ and $D_o^{Nb} = 0.5$, and result in lower mixing curves through respective mantle sources. Dashed line is a mixing curve through basalt 13826h source ($D_o^{Nb} = 0$) and N-type mantle as in (a) above.

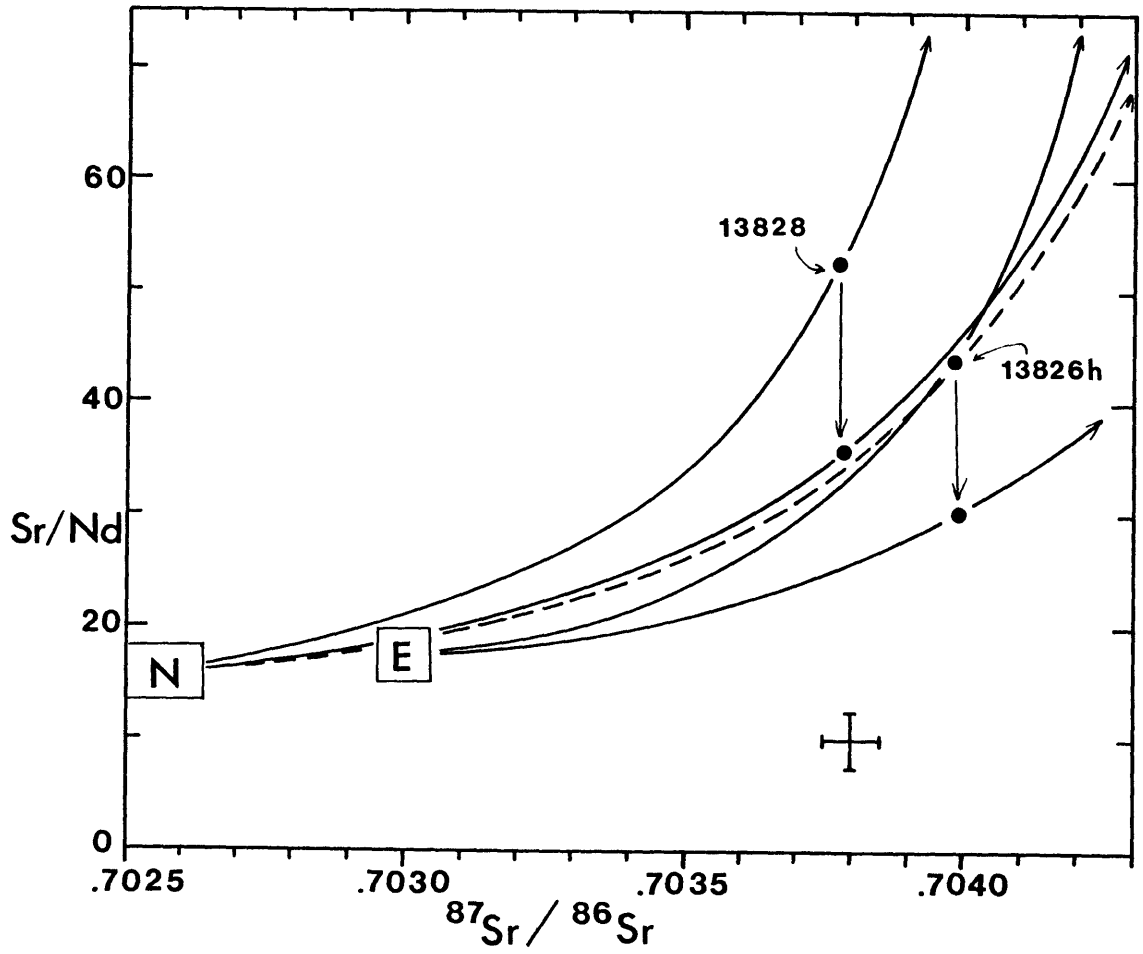
60
40
20
0
Sr/Nd
13828
13826h
N
E
.7025
.7030
.7035
.7040
87Sr / 86Sr

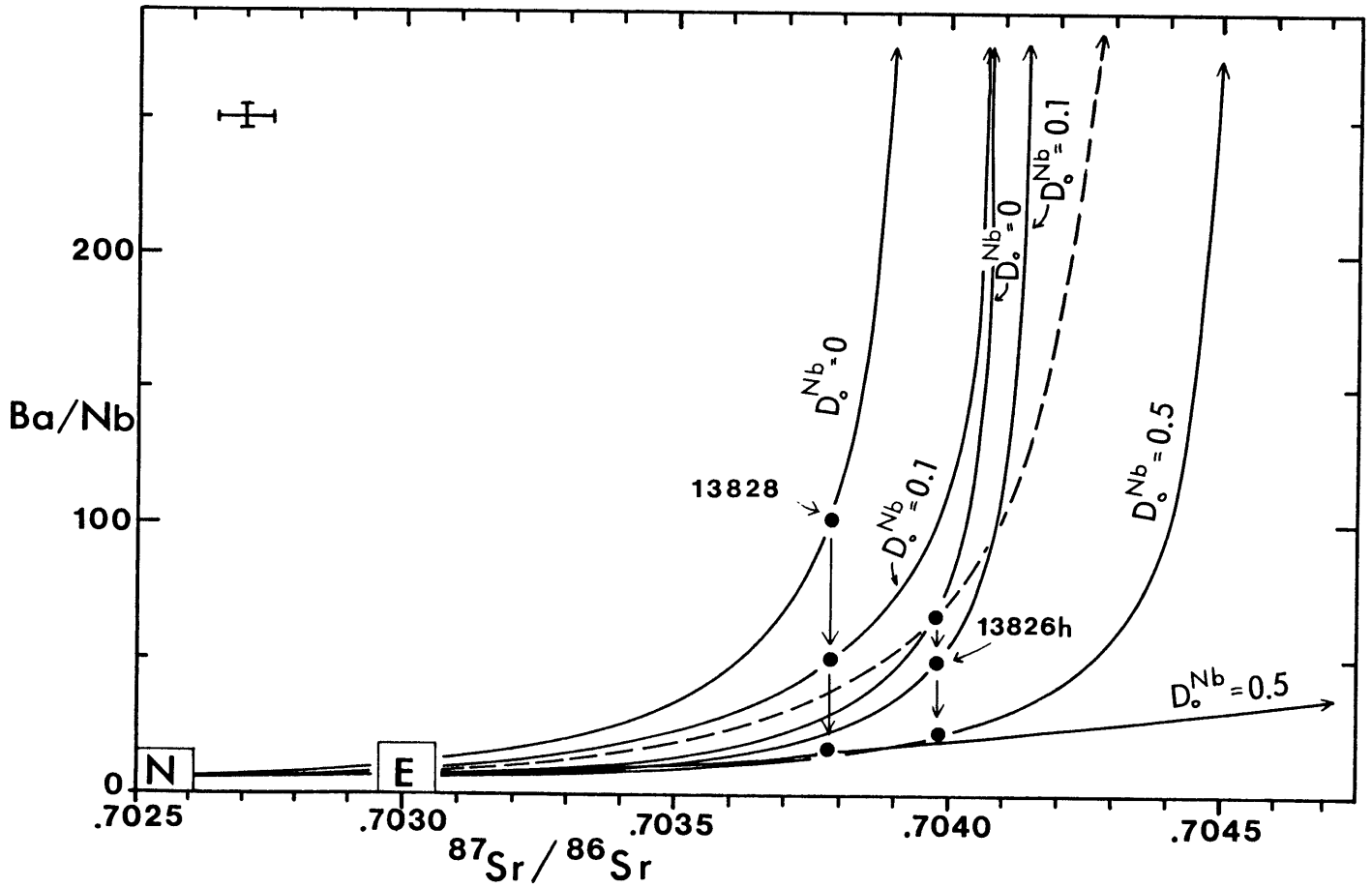
Ba/Nb
200
100
0
.7025
.7030
.7035
.7040
.7045
87Sr/86Sr
N
E
13828
13826h
D°Nb=0
D°Nb=0.1
D°Nb=0
D°Nb=0.1
D°Nb=0.5
D°Nb=0.5

Table 20

Model source characteristics

Model (1)

	Mantle Sources		Basalt Sources	
	N-type	E-type	13826h [1]	13828 [2]
$^{87}Sr/^{86}Sr$	.7025	.7030	.70398	.70378
Ba	1.2	4.77	26.6	10.17
Th	0.02	0.06	0.16	0.128
Nd	0.86	1.11	1.81	0.69
Sr	13.2	17.9	[1] 80 [2] 37	
			[3] 73 [3] 33	
Nb	0.31	0.72	(D_o^{Nb}=0) 0.4	0.11
			(D_o^{Nb}=0.1) 0.55	0.21
			(D_o^{Nb}=0.5) 1.18	.63
Ba/Nb	3.87	6.63	67	98
Ba/Th	60	80	166	82
Sr/Nd	15.3	16.1	44	54

Model (2)

	10% Partial Melt N-type Source	Calculated Sources, Basalt 13826h [4]		
		10%	20%	30%
$^{87}Sr/^{86}Sr$	.7025	.70404	.70410	.70418
Ba	12.0	29.2	32.6	37.8
Th	0.20	0.175	0.192	0.218
Nd	8.6	1.78	1.73	1.67
Sr	132	85	92	100
Nb	3.1	0.35	0.30	0.23
Ba/Nb	3.87	82	107	156
Ba/Th	60	167	170	174
Sr/Nd	15.3	48	53	60

[1] Calculated assuming 25% fractional crystallization (w/o plag), and 25% partial melting (see text)

[2] Calculated assuming 25% fractional crystallization (w/o plag), and 10% partial melting

[3] Calculated assuming 25% plagioclase accumulation with D_{plag}^{Sr} = 1.5, in addition to assumptions in [1] and [2]

[4] Sources calculated assuming that parental magmas for basalt 13826h consisted of 10%, 20%, and 30% (by volume) of melts derived from upper mantle. Calculated sources as listed represent characteristics of sources of the parental magmas prior to mixing with upper mantle melts. Additional assumption in [1] apply with regard to the petrogenesis of the presumed uncontaminated or pristine parental magmas (see text).

The effect of assuming N- or E-type sources is shown in Figure 44 for basalt 13826h. If sources for both basalts were produced by mixing of a slab-derived component with N-type MORB mantle, a relatively more radiogenic slab component mixed with mantle for the source of 13826h (Fig. 44). This variation of model (1) then, is similar in requiring three endmembers, a homogeneous mantle and two compositions of slab-derived components. Both versions of model (1) are consistent with Pb isotopic data. The different Pb isotopic compositions of basalts 13828 ($^{206}Pb/^{204}Pb$ = 18.551) and 13826h ($^{206}Pb/^{204}Pb$ = 18.570) may reflect differences in two assumed mantle endmembers if a slab-derived component is of fixed composition, or differences in the isotopic compositions of two different slab-derived components added to a single mantle endmember.

Model (2) requires only two endmembers, a mantle component and a slab-derived component. The basic premise of model (2) is that a spectrum of modified mantle sources may be produced by the addition of varying amounts of a slab-derived component of fixed composition. The compositions of sources thus produced will lie on a single mixing line between the mantle and slab-derived components. If basalts are representative of their source, positive correlations of Sr/Nd or Ba/Nb vs. $^{87}Sr/^{86}Sr$ or $^{206}Pb/^{204}Pb$ would be observed. Parental melts or diapirs separated from these sources may interact during ascent with upper mantle material. As outlined earlier, Sr/Nd and Ba/Nb ratios will be lowered in ascending magmas by their re-equilibration with upper mantle wallrock only if abundances of Nd and Nb in the wallrock are higher than those in the primary source of the magma. This interaction during ascent is a contamination process whereby ascending melts or

diapirs may incorporate solids or partial melts of surrounding mantle given a sufficient thermal contrast. Bulk assimilation of upper mantle wallrock, which would be characterized by lower Sr/Nd and Ba/Nb ratios relative to the magma, would result in lower Sr/Nd and Ba/Nb ratios in the mixture. Partial melts of upper mantle wallrock would also be characterized by low Sr/Nd and Ba/Nb ratios and mixing of these melts with alkali-enriched magma would also lower Sr/Nd and Ba/Nb in the resulting mixed magma. The simplest way of viewing this process is a two-stage procedure, production of alkali-enriched magmas near the slab-mantle interface and mixing of these magmas with pre-existing mantle melts with low Sr/Nd and Ba/Nb. If low Sr/Nd and Ba/Nb melts are produced from upper mantle wallrock upon contact with ascending magma, these should be formed by batch melting, since disequilibrium melts may be characterized by relatively higher Sr/Nd and Ba/Nb ratios due to greater diffusivities of alkalies relative to REE and HFSE. To produce negative correlations between such ratios as Sr/Nd or Ba/Nb vs. $^{87}Sr/^{86}Sr$, parental magmas derived from mantle sources modified by a relatively larger proportion of a slab-derived component must have undergone greater amounts of contamination or mixing with upper mantle during ascent, however, this may require a number of special conditions as reviewed above.

Model (2) is demonstrated on a plots of Ba/Nb and Sr/Nd vs. $^{87}Sr/^{86}Sr$ (Fig. 45). Compositions of parental magmas for basalts 13828 and 13826h were calculated assuming 25% fractional crystallization. A source for basalt 13828 was calculated assuming 10% partial melting and it was assumed that magmas parental to 13828 were not modified or contaminated during ascent (Table 20). Characteristics of sources prior

45(a) Plot of Ba/Nb vs. $^{87}Sr/^{86}Sr$ illustrating source mixing models for two basalts in terms of model (2). Sources for basalt 13826h were calculated assuming that 10% (labelled SC10), 20% (SC20), and 30% (SC30) of the total volume of magmas parental to basalt 13826h consisted of mantle-derived melts (see text and Table 20). Mixing curves through these three sources, especially SC20 and SC30, and a source for basalt 13828 (Table 20), should presumably project to mantle endmember compositions and those of hypothetical slab-derived components. Approximate values for N-type mantle are designated by 'N'.

(b) Plot of Sr/Nd vs. $^{87}Sr/^{86}Sr$ for mixing models as above. Sources were calculated and noted in figure as above and are listed in Table 20.

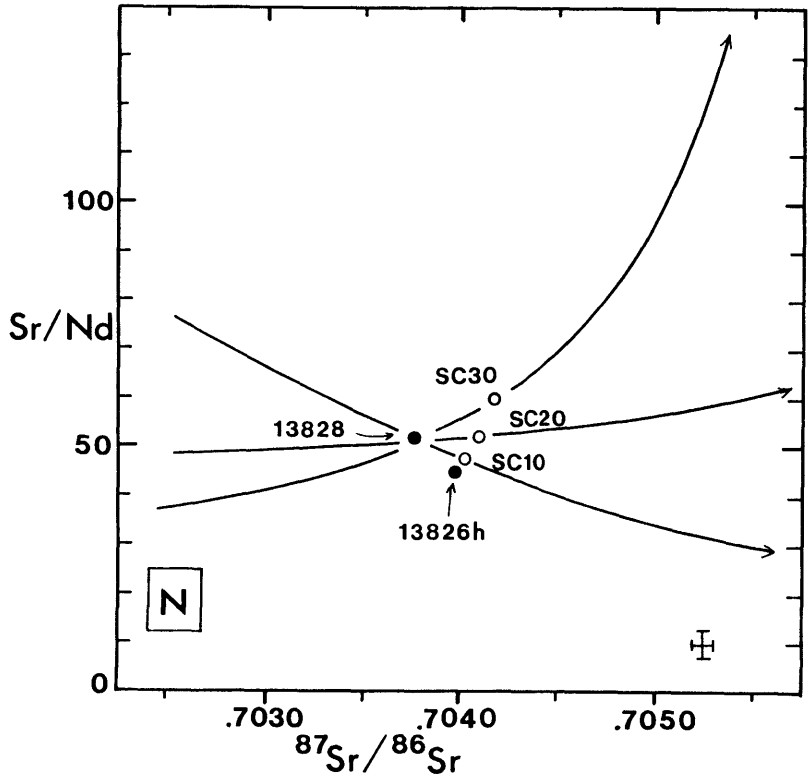
100
50
0
Sr/Nd
SC30
SC20
SC10
13828
13826h
N
.7030
.7040
.7050
87Sr/86Sr

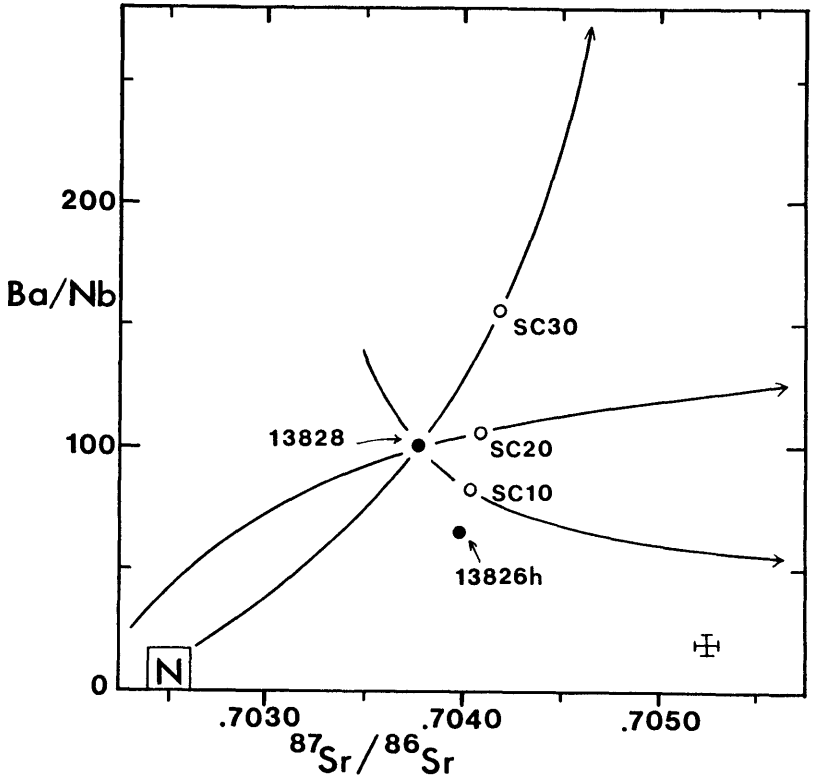
200
100
0
Ba/Nb
SC30
13828
SC20
SC10
13826h
N
.7030
.7040
.7050
87Sr/86Sr

to contamination of parental magmas for basalt 13826h were calculated assuming that pristine parental magmas mixed with melts of N-type upper mantle (Table 20). This is a simpler model to test rather than re-equilibration of magmas with upper mantle wallrock, in which a greater number of assumptions and special conditions are required to change abundance ratios of elements which are equally incompatible in mantle systems.

It was assumed that the average composition of upper mantle melts added to magma parental to basalt 13826h may be approximated by 10% melting of N-type mantle. Three different sources (Table 20) were calculated assuming that 10%, 20%, and 30% of the total volume of magma parental to 13826h was composed of contaminating melts from surrounding N-type MORB mantle. This was done by first calculating abundances in pristine magmas by mass balance knowing the composition of contaminated parental magmas (represented by Ba/Nb, Sr/Nd, and $^{87}Sr/^{86}Sr$ in 13826h), presumed to be mixtures, and that of the assumed mantle melt. The pristine magmas were assumed to be produced by 25% partial melting in order to calculate the three various sources (Table 20). This melting event is presumed to be an initial event that occurs at some depth close to the interface between the subducted slab and the sub-arc upper mantle. Since the contaminating upper mantle melts are characterized by low Ba/Nb, Sr/Nd, and $^{87}Sr/^{86}Sr$ relative to basalt 13826h, sources of pristine uncomtaminated magma components are characterized by high Ba/Nb, Sr/Nd, and $^{87}Sr/^{86}Sr$ relative to 13826h which correspond to assumptions regarding the relative proportions of the contaminating mantle melt endmember. Mixing curves were then calculated between each of the three sources recalculated for 13826h and the source calculated for basalt

13828 (Fig. 45). Mixing curves calculated in this manner should extrapolate to both the composition (Ba/Nb, Sr/Nd, $^{87}Sr/^{86}Sr$) of the sub-arc mantle endmember and that of the slab-derived component.

As seen in Figure 45a, for the given assumptions and chosen parameters, sources calculated assuming that 20% or 30% of magmas parental to 13826h consisted of N-type MORB are characterized by high Ba/Nb and $^{87}Sr/^{86}Sr$ relative to basalt 13826h. Mixing curves between these sources and that for 13828 project to low Ba/Nb and $^{87}Sr/^{86}Sr$ ratios characteristic of N-type mantle, and to high Ba/Nb and high $^{87}Sr/^{86}Sr$ ratios assumed to be characteristic of the slab-derived component. These two mixing curves project to similar mantle compositions but quite different compositions for a slab-derived component (Fig. 45a). The other mixing curve calculated assuming that 10% of the volume of magma parental to 13826h consisted of mantle-derived melt illustrates a less possible model suggesting that either the slab-derived component was characterized by a lower Ba/Nb ratio than basalt 13826h, or magmas parental to 13828 underwent greater differentiation on partial melting (high D_o^{Nb}) relative to magmas parental to 13826h. Mixing curves assuming that 20% and 30% of the total volume of magma parental to 13826h consisted of N-type MORB melts do not project back to low Sr/Nd (15-16, Table 17) ratios at relatively lower values of $^{87}Sr/^{86}Sr$ (< 0.70378). A correction for plagioclase accumulation as in Figure 44a would result in mixing curves which would extrapolate to low Sr/Nd ratios believed to be characteristic of an unmodified mantle endmember (Fig. 45b).

In both model (1) and model (2) variations in any of the processes involved or in endmember compositions will produce scatter along

46(a) Plot of Ba/Th vs. $^{87}Sr/^{86}Sr$ illustrating source mixing models for the two basalts in terms of model (2). Sources SC10, SC20, and SC30 were calculated as described in the text; calculated mixing curves through these three sources, a source for basalt 13826h assuming no upper mantle contamination, and through a source for basalt 13828 are shown. Approximate compositions of N-type and E-type mantle are shown for reference, as are values for Ba/Th in chondrites and a range of Ba/Th in sediments (cf., Tables 17 and 18).

(b) Plot of Ba/Th vs. $^{87}Sr/^{86}Sr$ illustrating source mixing models for the two basalts in terms of model (1). Mixing curves from N-type and E-type mantle endmembers through sources for basalts 13828 and 13826h, respectively, project to hypothetical compositions for slab-derived components.

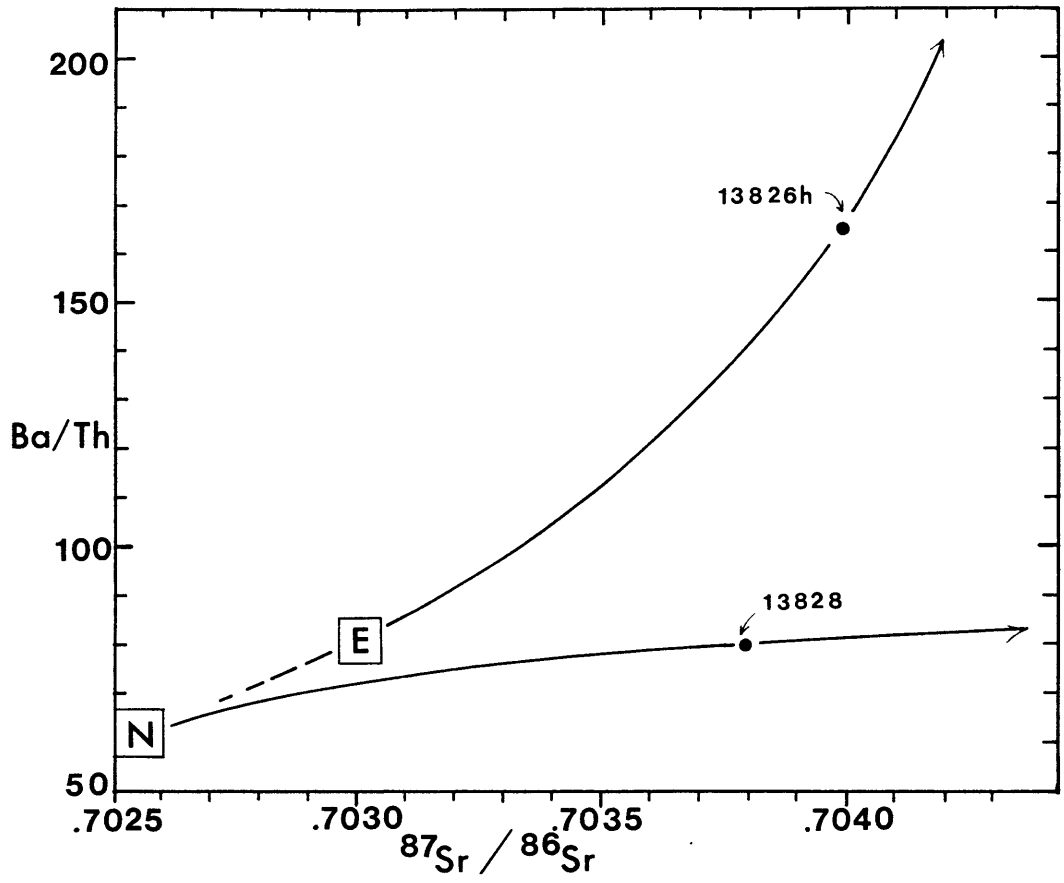
200
150
100
50
Ba/Th
13826h
13828
E
N
.7025
.7030
.7035
.7040
87Sr / 86Sr

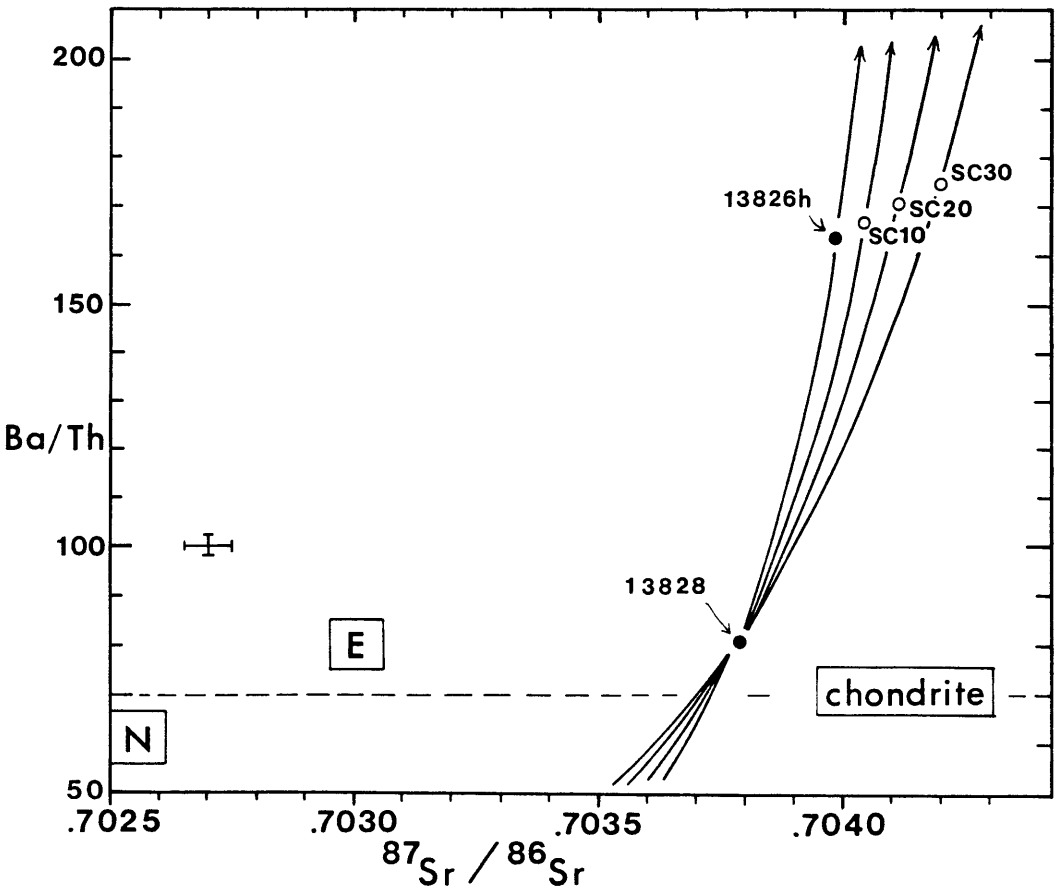
200
150
100
50
Ba/Th
13826h
SC10'
SC20
SC30
13828
E
N
chondrite
.7025
.7030
.7035
.7040
87Sr / 86Sr

theoretical trends between Ba/Nb and $^{87}Sr/^{86}Sr$. These models may explain the characteristics of Puyehue basalts since a smooth continuous trend is not observed (Fig. 43). Continuous trends and negative correlations of the Sr 'spike' vs. $^{87}Sr/^{86}Sr$ observed in some arcs (cf. Arculus and Johnson, 1981) may be explained by either model (1) or model (2) followed by high-level mixing of two geochemically distinct basaltic magmas.

The crude positive correlation of Ba/Th and $^{87}Sr/^{86}Sr$ for Puyehue basalts (Fig. 43) poses problems for the application of model (1) or model (2) in explaining the characteristics of Puyehue basalts. An additional problem arises from the low, near-chondritic Ba/Th (81) ratios in basalts with the lowest $^{87}Sr/^{86}Sr$ ratios. On a plot of Ba/Th vs. $^{87}Sr/^{86}Sr$, sources calculated for basalt 13826h after the method of model (2) are characterized by higher Ba/Th and $^{87}Sr/^{86}Sr$ as expected (Fig. 46a). Mixing curves connecting four possible sources (including a source for 13826h assuming no contamination by upper mantle) with a source for basalt 13828 do not project back to any reasonable mantle Ba/Th ratios (60-80, Table 17) for $^{87}Sr/^{86}Sr$ values assumed to be representative of mantle endmembers in the model (Fig. 46a). Ba/Th ratios as low as 18 have been detected in some arc lavas (Table 19) and may be indicative of a mantle component relatively more depleted than N-type MORB mantle (Table 17). Mixing curves for model (1) on a plot of Ba/Th vs. $^{87}Sr/^{86}Sr$ do not require two different mantle endmembers but do project to slab-derived components with very different compositions (Fig. 46b). However, this is a more complex model in that it requires three components, including N-type MORB mantle, a slab-derived component with high Ba/Th and relatively low $^{87}Sr/^{86}Sr$ for the source of basalt 13826h, and a second, relatively more radiogenic component with relatively low Ba/Th for the source of basalt 13828.

It is possible that basalt 13828 is representative of mantle in this region, as suggested by the low Ba/Th ratio and this may be considered a third model. It may be unlikely that a low Ba/Th ratio is the result of addition of significant amounts of Th to a mantle source, since analyzed sediments or presumed compositions of hypothetical slab-derived components predict that sub-arc mantle is modified at or near the slab-melt interface by a high-Ba/Th component. Addition of such a component to the source of basalt 13828 may have been negligible and the source of basalt 13826h may have resulted from addition of a slab-derived component to the same source as that for basalt 13828. Assuming that basalt 13828 is nearly representative of the mantle source leads to a simpler model related to model (2) and requires a slab-derived component with high Ba/Th and $^{87}Sr/^{86}Sr$ (relative to basalt 13826h, at least) as a modifying agent to produce sources for basalts with higher Ba/Th and $^{87}Sr/^{86}Sr$ relative to basalt 13828.

Basalt 13828 is characterized by a low Ba/Th ratio, but also by Ba/Nb ($\sim$ 100) and Th/La (0.27) ratios higher than mantle or chondritic (Ba/Nb = 3.9-9.0; Th/La = 0.06-0.16) values. The high Ba/Nb and Th/La ratios may be produced by differentiation on partial melting involving HFSE and LREE-retaining refractory phase. Lower ratios of Ba/Nb (66) and Th/La (0.145) in basalt 13826h relative to 13828 may reflect a lesser amount (lower D_o^{Nb} and D_o^{La}) of such a refractory phase, consistent with partial melting model calculations presented earlier (Fig. 42).

The isotopic characteristics of basalt 13828 fall outside a range for MORB but are grossly similar to OIB (cf., Morris and Hart, 1983), suggesting that mantle in this area may be relatively more enriched relative to MORB-type mantle. The only significant isotopic difference

47(a) Plot of $^{208}Pb/^{204}Pb$ vs. $^{207}Pb/^{204}Pb$ illustrating source mixing models for two basalts (13826h, 13828) in terms of model (1). Fields of data for oceanic island basalts (OIB), mid-ocean ridge basalts (MORB), and sediments are taken from Hickey and Frey (1984). Regression lines for a range of Pb-isotopic compositions of MORB glasses (Cohen et al., 1980) and for a range of MORB and OIB in the northern hemisphere (NHRL) compiled by Hart (1984) are shown. Data for oceanic islands (San Felix and the Juan Fernandez Islands) in the Nazca plate are also shown (Hart and Gerlach, unpub. data). A mantle (noted as 'M1') source on the NHRL was assumed to have mixed with 0.6% sediment to generate the source of basalt 13828. The Pb-isotopic composition of a hypothetical sediment endmember(s) was then calculated, and the proportion (2%) of S required in the source of basalt 13826h was also calculated, assuming that the Pb-isotopic composition of a second mantle source ('M2') lies at the intersection of a mixing line through the basalt 13826h source and S with the NHRL.

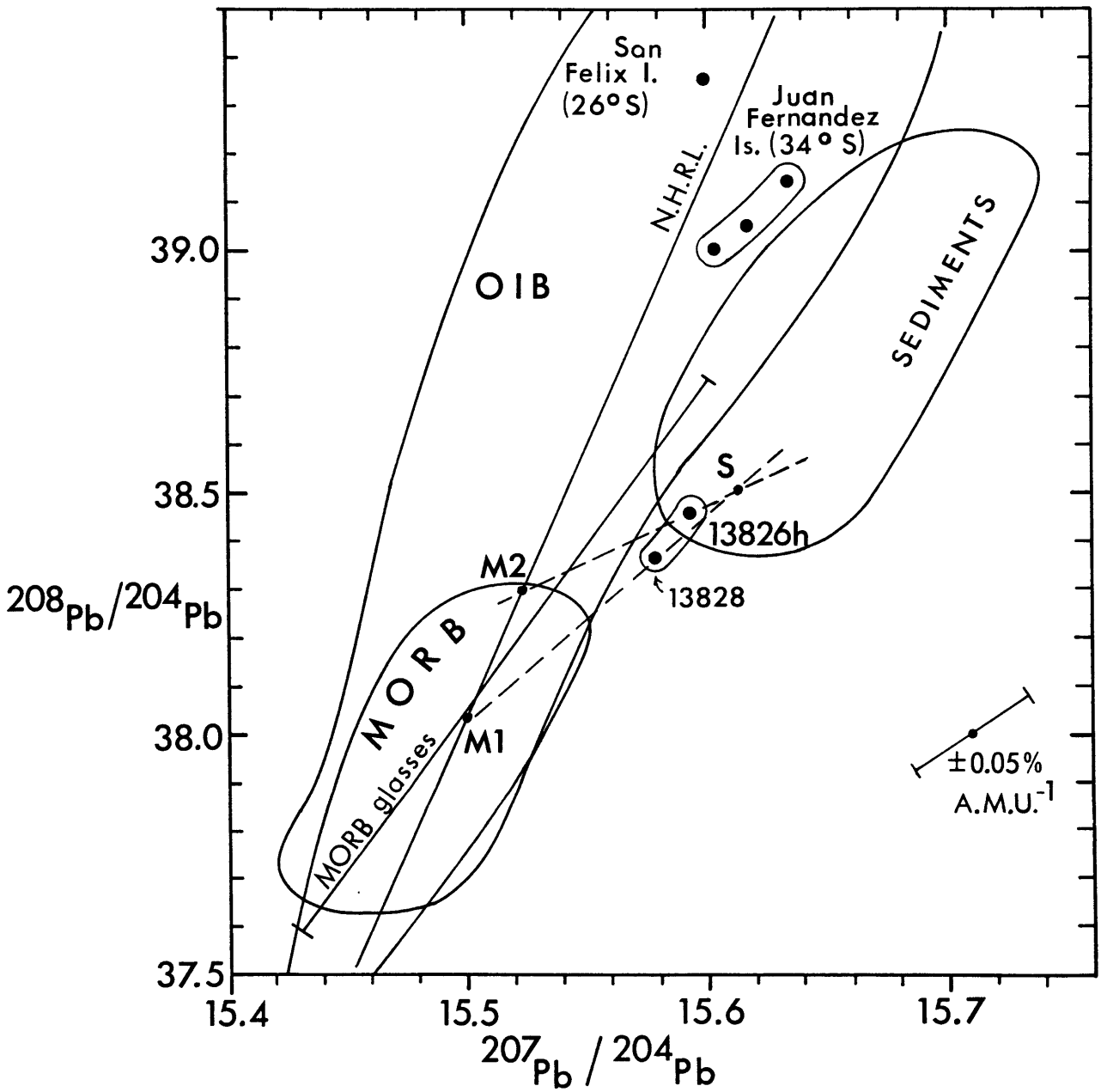
San
Felix I.
(26°S)
Juan
Fernandez
Is. (34° S)
N.H.R.L.
OIB
SEDIMENTS
S
13826h
13828
M2
M1
MORB
MORB glasses
±0.05%
A.M.U.-1
39.0
38.5
38.0
37.5
15.4
15.5
15.6
15.7
208Pb/204Pb
207Pb / 204Pb

47(b) Plot of $^{208}Pb/^{204}Pb$ vs. $^{207}Pb/^{204}Pb$ illustrating a source mixing model for two basalts (13826h, 13828) which is a variant of model (2). All data, reference lines and fields of data are repeated from Figure 47a. The Pb-isotopic composition of a mantle endmember source (M) is assumed to be the intersection of a line through the basalt data with the NHRL. The source of basalt 13828 was assumed to be a mixture of M plus 0.6% sediment endmember (S). The Pb-isotopic composition was then calculated, and then the proportion of S required to generate the source of basalt 13826h was calculated. Although the characteristics of mantle and sediment endmembers cannot be uniquely determined, it is shown that relative proportions of a sediment or slab-derived component may differ in sources for the two basalts.

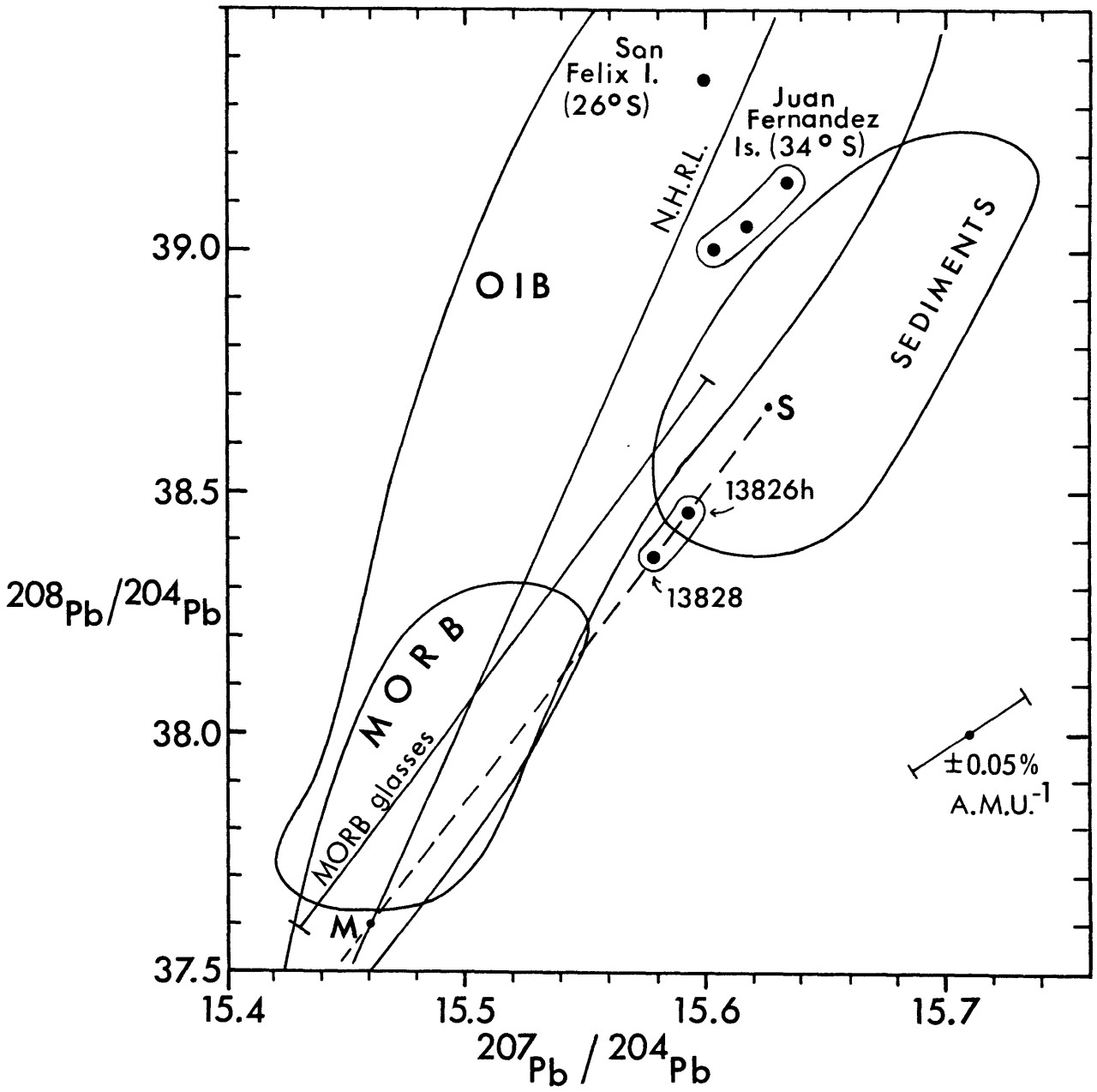
San
Felix I.
(26°S)
Juan
Fernandez
Is. (34° S)
N.H.R.L.
OIB
SEDIMENTS
S
13826h
13828
MORB
MORB glasses
M
±0.05%
A.M.U.-1
39.0
38.5
38.0
37.5
15.4
15.5
15.6
15.7
208Pb/204Pb
207Pb / 204Pb

between Puyehue basalts and OIB is that Puyehue basalts are characterized by higher $^{207}Pb/^{204}Pb$ for a given $^{208}Pb/^{204}Pb$ relative to OIB (Fig. 47), a feature of many arcs that suggests sediment contamination in the source. Since basalt 13828 has higher $^{207}Pb/^{204}Pb$ relative to OIB (Fig. 47), it cannot be strictly representative of unmodifed mantle. It is possible that a source for basalt 13828 may have been produced by mixing of MORB-type mantle, or OIB-type mantle and relatively radiogenic sediment (Pd and Sr) with relatively low Ba/Th. A source for basalt 13826h, by comparison, may have been produced by mixing of relatively more enriched mantle and a relatively less radiogenic sedimentary or slab-derived component with a high Ba/Th ratio. This suggests a still more complex model requiring a total of four components. For this scenario to be an explanation of geochemical heterogeneity of basalts in a single volcanic center, small-scale mantle heterogeneity (cf. Morris and Hart, 1983), or at least vertical mantle heterogeneity, coupled with localized compositional variations in the slab-derived component at the slab-mantle interface, is required. Unfortunately, available data for sediments are inadequate to evaluate the accompanying implication that sediments which are relatively more radiogenic with respect to Sr may also be characterized by more radiogenic Pb-isotopic compositions, or at least higher $^{207}Pb/^{204}Pb$ ratios.

Mixing curves consistent with model (1) are displayed in Figure 47a. A mantle endmember (M1) for the source of basalt 13828 was arbitrarily chosen to lie on the Northern Hemisphere Reference Line determined by Hart (1984) and was assumed to contain 0.05 ppm Pb. This assumption may be reasonable since oceanic islands in the Nazca Plate (San Felix, Juan Fernandez) plot to both sides of this line (Fig. 47a). Assuming that

approximately 0.6% sediment containing 20 ppm Pb (Cohen and O'Nions, 1982) mixed with the mantle source M1, the Pb-isotopic ratios of a sediment (or slab-derived component) may be determined. A mixing line from the sediment Pb-isotopic composition through that of basalt 13826h intersects the NHRL at a second, presumed mantle Pb-isotopic composition M2 (Fig. 47a). Assuming this point to represent a mantle endmember for the source of basalt 13826h, approximately 2.1% of the sediment endmember is required. Just how reasonable this demonstrative calculation may be, can be checked by another approach. Assuming a Ba/Th ratio of 60 (Table 17) for the mantle endmember and the proportion of sediment (0.6%) assumed for the source of basalt 13828, a sediment endmember must have a Ba/Th ratio of approximately 3500. Assuming that a proportion of 2.1% of the same sediment endmember constitutes the source of basalt 13826h, the mantle endmember M2 must have a Ba/Th ratio of approximately 90, which is reasonable. Although these calculations are neither unique nor do they yield accurate characteristics or proportions of endmembers, but they may demonstrate that more than three times the amount of slab-derived component of fixed composition added to the mantle endmember for 13828 may be added or mixed with a second mantle source for the source of 13826h.

Model (1) as outlined in Figure 47a assumes a sedimentary or slab-derived component of fixed composition (Ba/Th ratio). This is not consistent with model (1) source mixing curves in Figure 46b where slab-derived components with different Ba/Th and $^{87}Sr/^{86}Sr$ ratios are required given the assumed characteristics of the mantle endmembers. Higher $^{87}Sr/^{86}Sr$ ratios (to 0.7036 or 0.7037) in the mantle endmembers would result in convergence of mixing curves in Figure 46b to similar

Ba/Th and $^{87}Sr/^{86}Sr$ ratios in a slab component, especially if it is speculated that the mantle endmember source for basalt 13828 has higher $^{87}Sr/^{86}Sr$ relative to that for 13826h.

The possibility that sources for basalts 13828 and 13826h are various mixtures of a single mantle source and a specific slab-derived or sedimentary component is further addressed in Figure 47b. A line through the two basalts projects back to Pb-isotopic values of a mantle endmember relatively less radiogenic than those assumed in Figure 47a. A mantle source M (Fig. 47b) at the intersection of the NHRL line was assumed to have ~ 0.05 ppm Pb. Assuming 0.6 wt.% sediment was added to produce the source of basalt 13828, the Pb-isotopic composition of the sedimentary component may be calculated, as well as the proportion of the component (~ 1 wt.%) required to produce the source for basalt 13826h. With the same assumptions given earlier for mantle Ba/Th ratios this sedimentary component has a Ba/Th ratio of ~ 3500 to produce the source for basalt 13828, but only ~ 1100 to produce the source for 13826h with the calculated sediment proportions based on Pb isotopes in the basalts. Better agreement is possible with the assumption that Ba/Th ratios in addition to Sr and Pb-isotopic ratios in magmas parental to basalt 13826h were lowered by contamination processes during transit in the upper mantle as modelled in Figures 45 and 46a. This model (Fig. 47b) is essentially an additional consideration of model (2).

10.5.4 Summary

In summary, a choice between any of the three models is not easily made. Model (1) requires two different upper mantle endmembers and a component of fixed composition derived from the subducted slab of oceanic

crust, and assumes that characteristics of the parental magmas related to either basalt (13826h or 13828) were not modified after separation from sources consisting of these components. High LIL/REE or LIL/HFSE abundance ratios in the basalts are produced simply by addition of the slab-derived component to a mantle source (Figs. 44, 47a) rather than by refractory HFSE and REE-rich accessory phases. Variations in these abundance ratios correspond to varying proportions of the slab component added to each mantle endmember. Depending on the isotopic composition of the sedimentary slab-derived component, the two mantle endmembers may differ greatly in isotopic composition (Fig. 47a). Thus, model (1) requires geochemical heterogeneity, possibly on a small scale, within the sub-arc mantle wedge.

Model (2) requires only two endmembers, a mantle component and a slab-derived component, and as in model (1), high LIL/HFSE and LIL/REE ratios are caused by addition of an LIL-enriched slab-derived component to the mantle source. A spectrum of source compositions may be created by the addition of various amounts of a slab-derived component to mantle endmembers, and basalts produced from these sources would be expected to display positive correlations of LIL/REE and LIL/HFSE abundance ratios with isotopic composition (Sr and Pb). A few arcs do display these trends, but in other arcs and in Puyehue Volcano, negative correlations between LIL/REE and LIL/HFSE and $^{87}Sr/^{86}Sr$ are suggested by the data. It is a tenet of model (2) that magmas may be contaminated during ascent through the upper mantle, and the simplest way to consider this contamination process is by the addition of partial melts derived from the upper mantle. Contamination in the upper mantle may reduce LIL/REE, LIL/HFSE and Sr and Pb isotopic ratios in ascending magmas, and at the

very least will produce scattered correlations between any of these ratios. Negative correlations of LIL/REE or LIL/HFSE vs. $^{87}Sr/^{86}Sr$ may result by magma mixing if a magma derived from a source containing a relatively greater amount of slab-derived component has experienced a relatively greater amount of contamination by upper mantle melts. This model does not require any geochemical heterogeneity in the sub-arc upper mantle region.

A third model is suggested by low Ba/Th (80) ratios in Puyehue basalts with low $^{87}Sr/^{86}Sr$ (0.70378 to 0.70381). If estimates of Ba/Th ratios (60-80) in the upper mantle are accurate, these basalts may be nearly representative of the upper mantle in this region, and other basalts with higher Ba/Th and $^{87}Sr/^{86}Sr$ were derived from sources consisting of a mantle endmember represented by the low-Ba/Th, low-$^{87}Sr/^{86}Sr$ basalts and a high-Ba/Th, high-$^{87}Sr/^{86}Sr$ slab-derived component. However, the Pb-isotopic compositions of the low-Ba/Th, low-$^{87}Sr/^{86}Sr$ basalts indicate that the source of these basalts was also modified by a sedimentary slab-derived component, though to a lesser degree than the sources of basalts with higher Ba/Th and $^{87}Sr/^{86}Sr$. High ratios of Ba/Nb and Sr/Nd in the low-Ba/Th, less radiogenic basalts indicate the role of HFSE- and LREE-beraring refractory phases in their generation.

A few generalized conclusions may be made regarding the respective sources of basalts 13826h and 13828 based on modelling in Figures 44 through 47. It is not possible to choose between models which require geochemical heterogeneity in the upper mantle such as model (1), and those which do not, such as models (2) and (3). The initial mantle source of basalt 13826h may have been modified by a slab-derived

component characterized by high Ba/Th, Sr/Nd, and Ba/Nb ratios and a relatively less radiogenic Sr-isotopic composition. Primary melts were produced by higher degrees of partial melting relative to 13828 and were contaminated by upper mantle during ascent, which lowered Ba/Nb, Sr/Nd, and $^{87}Sr/^{86}Sr$ ratios in the magmas. The initial mantle source of basalt 13828 may have been less radiogenic relative to that for 13826h and may have been modified by a slab-derived component characterized by a relatively lower Ba/Th ratio and a relatively more radiogenic Sr-isotopic composition. Ratios of Ba/Nb, Sr/Nd, and Th/La in primary magmas parental to 13828 that are high relative to basalt 13826h or mantle values were created during partial melting, and were not changed significantly by upper mantle contamination during ascent.

11. Evolution of recent volcanism in the Puyehue Volcano-Cordon Caulle Area

11.1 Preglacial Volcanics

With regard to major-element compositions, preglacial volcanics are similar to postglacial volcanics (Table 4) with a few exceptions. Preglacial basaltic andesites and andesites are characterized by higher FeO*/MgO ratios relative to postglacial samples. This may be an artifact of the fewer samples ranging from 54-60 wt.% SiO_2 represented among the postglacial volcanics compared to the preglacial samples suite. In many variation diagrams (cf. Figures 6-9) preglacial basaltic andesites and andesites bridge a gap or 'flesh' out a trend suggestive of low-pressure fractional crystallization. This is because the majority of postglacial volcanics sampled within this compositional range are best explained as products of fractional crystallization/AFC at relatively higher pressures

or magma mixing. Magma mixing may have been a less important process relative to that of fractional crystallization in generating the characteristics of the preglacial volcanics.

In the oliv-cpx-qtz pseudoternary diagram, projected compositions of preglacial basaltic andesites apparently coincide with the 1-atm oliv-pig-plag reaction curve, whereas those of postglacial basaltic andesites may define a oliv-cpx-plag high-pressure cotectic as discussed earlier (Fig. 12). Sample 162826 may be considered a basalt due to its SiO_2 content (51.61 wt.%), but in all other respects, it is very similar in composition to low-SiO_2 postglacial basaltic andesites (Table 4). The composition of 162826 as projected in the oliv-cpx-qtz pseudoternary also coincides with the projected compositions of low-SiO_2 postglacial basaltic andesites (cf., Figs. 18b and 48). Without samples of other preglacial basalts, or at least samples relatively more primitive than 162826, the liquid line of descent that produced the composition of 162826 cannot be constrained, i.e., whether this sample is a product of magma mixing, or fractional crystallization at low or high pressures. The liquid line of descent beyond sample 162826 can be qualitatively constrained, however, and displays significant differences in comparison to that defined by postglacial volcanics. Moderate to low-pressure fractional crystallization of olivine + plagioclase ± clinopyroxene from magma represented by 162826 would drive compositions of residual liquids towards the oliv-pig-plag reaction curve. Depending on the proportion of clinopyroxene in the fractionating assemblage, resulting residual liquids may fall on either side of the 1-atm thermal divide on the oliv-pig-plag reaction curve. Most preglacial basaltic andesites plot on the portion of this reaction curve opposite SiO_2 and this suggests that they define a

liquid line of descent produced by subsequent reaction of olivine and crystallization of pigeonite and plagioclase which may have driven compositions of residual liquids to reaction point A (Fig. 48). Preglacial volcanics ranging in composition from andesite to rhyolite that appear to plot along the 1-atm opx-pig-plag reaction curve (Fig. 48) may have been produced by fractional crystallization of basaltic andesite as outlined earlier (section 7) for postglacial volcanics of Puyehue Volcano.

Samples of preglacial volcanics were collected over a fairly large area, including the areas around Puyehue Volcano and Cordon Caulle. It is possible that these samples are associated with more than one vent or magma chamber, and this may explain the variable geochemical characteristics of the preglacial volcanics and preclude the use of compositional data towards reconstructing unique liquid lines of descent that integrate both major-element and trace element data.

The preglacial basaltic andesites are variable in that major-element compositions do not vary in a smooth manner with increasing SiO_2 content or Th abundances. Samples with 54-55 wt.% SiO_2 vary in FeO*/MgO ratios (2.2 to 3.1) and CaO/Al_2O_3 ratios (0.49-0.54), and display greater than twofold variations in TiO_2 (1.26-2.56 wt.%) and P_2O_5 (0.21-0.54 wt.%) contents, and abundances of Nb, Th, and La (Fig. 9, Table 4). The relative degree of LREE-enrichment varies (La/Yb = 3.4-5.0) more than expected for such a narrow compositional range if these basaltic andesites are related by fractional crystallization of reasonable assemblages (olivine, plagioclase, clinopyroxene) at low to moderate pressures. One sample (82825) contains less SiO_2 (53.7 wt.%) than other basaltic andesites but is characterized by relatively higher FeO*/MgO

48 Compositions of preglacial volcanics from the Puyehue Volcano-Cordon Caulle area projected on the oliv-cpx-qtz pseudoternary with 1-atm phase equilibria after Grove et al. (1982, 1983) as in Figure 12a.

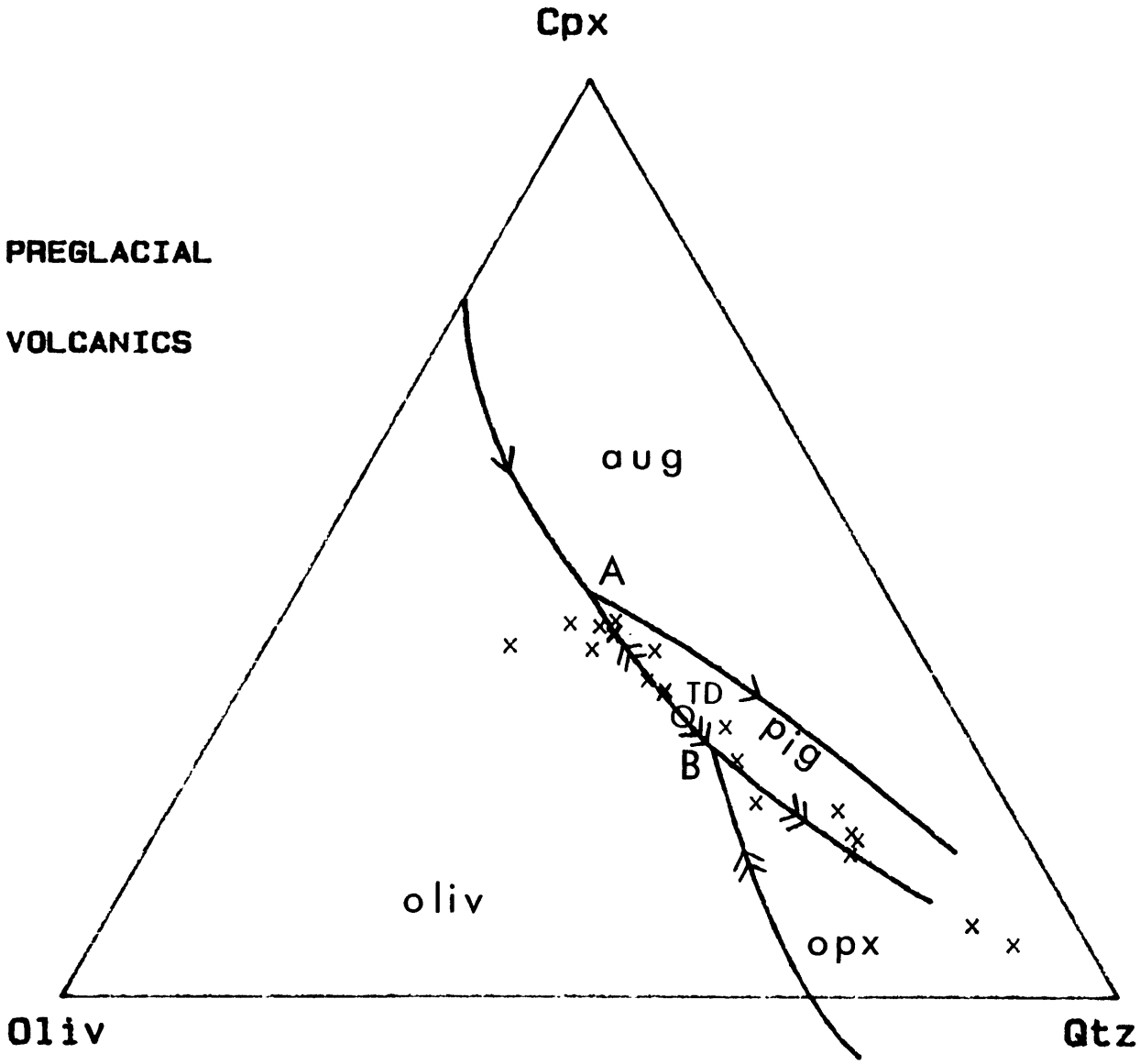
Cpx
PREGLACIAL
VOLCANICS
aug
A
TD
Qtz
pig
B
oliv
opx
Oliv
Qtz

ratios, TiO_2 and P_2O_5 contents, and higher abundances of incompatible trace elements relative to other basaltic andesites with 54-55 wt.% SiO_2 (Figures 6-8, Table 4). Sample 82825 may have resulted from crystallization of basaltic andesitic liquids at reaction point A (Fig. 48), which involves reaction of olivine and liquid to produce dramatic Fe-enrichment with a decrease or buffering of SiO_2 contents such as that generally seen in tholeiitic evolved lavas (Grove and Baker, 1984). Other basaltic andesites are discounted as representing intermediate parental precursors to 82825 on the basis of relatively higher abundances of incompatible trace elements (e.g., Ba and Th abundances in sample 172829c), or abundances which are too low (e.g., Th and REE in 162828a) and would require > 50% fractional crystallization.

Among these preglacial basaltic andesites (53.7-55 wt.% SiO_2), incompatible trace elements such as La, Th, and Nb vary more than a factor of two, while other incompatible elements such as Rb are less variable. Selected abundance ratios such as La/Yb (3.4-5.0), Ba/La (19.4-36.2), Zr/Sm (24.5-44.8), and Ba/Th (97-197) are also variable in these samples, while other ratios such as Zr/Hf (38.9-43.1) and K/Rb (360-370) are fairly constant. Thus, basaltic magmas parental to these basaltic andesites may have been equally diverse in their geochemical characteristics. Decoupling of major-element compositions and trace element abundances is also observed in more evolved preglacial volcanics by comparing dacite samples 23825 and 182823a. The major-element compositions of these two samples differ only in their FeO*/MgO ratios (4.5 vs. 5.3), though sample 23825 contains relatively higher abundances of REE, Sr, and Y, while 182823a contains relatively higher abundances of Rb, Ba, Zr, Nb, Hf, and Th (Table 4).

Preglacial volcanics are mostly aphyric and do not display any evidence of magma mixing in the form of disequilibrium phenocryst assemblages or phenocryst textural characteristics that are evident in the postglacial mixed andesites. Anomalously high abundances of compatible trace elements such as Cr and Ni, seen in postglacial mixed andesites, are not observed in any of the preglacial volcanics (Fig. 9). The trend of preglacial basaltic andesites and andesites defined by their projected compositions on the oliv-cpx-SiO_2 pseudoternary (Fig. 48), if a mixing trend, requires a basaltic endmember which would plot on or near the oliv-cpx-plag cotectic, and none is represented in the sample set. In the postglacial volcanics, Ba/Rb ratios in basaltic andesites (13.4-14.9) which were low relative to those of the basalts (18.1-20.4) served as one indication of their origin by magma mixing, i.e., basaltic magmas mixed with andesitic (Ba/Rb = 12.7) or rhyolitic (Ba/Rb = 10.-11.4) magmas. Ba/Rb ratios are low (11.2-14.9) in preglacial basaltic andesites and in a similar manner may be suggestive of magma mixing. However, Ba/Rb ratios (14.9-8.1) in preglacial volcanics ranging from basaltic andesite to rhyolite extend to lower values relative to those of the postglacial volcanic suite (Ba/Rb = 20.4-10.0). It is possible that preglacial basaltic magmas may have been characterized by relatively low Ba/Rb ratios similar to those observed in the basaltic andesites and this would be consistent with a fractional crystallization origin rather than a magma mixing origin for the preglacial basaltic andesites. In the postglacial volcanics of Puyehue Volcano, it is as much the availability of basaltic and evolved lavas with appropriate geochemical characteristics as the characteristics of those intermediate lavas themselves which supported the likelihood of magma mixing. A more

thorough and representative sampling of preglacial volcanics would aid in evaluating the relative importance of fractional crystallization and magma mixing processes in their genesis, however, this effort would still be inhibited by the uncertainty that not all samples were comagmatic or were erupted from the same magma chamber or volcano.

Preglacial volcanics are slightly isotopically variable; the six samples analyzed display ranges of $^{87}Sr/^{86}Sr$ (0.70402-0.70414) and $^{143}Nd/^{144}Nd$ (0.512820-0.512892) which are less than or equal to ranges observed in postglacial volcanics ($^{87}Sr/^{86}Sr$ = 0.70378 to 0.70416, $^{143}Nd/^{144}Nd$ = 0.512818 to 0.512900) Although the data set for preglacial volcanics may not be representative of the total variability possible, there is no indication that the older preglacial volcanics are drastically different or more isotopically heterogeneous, in opposition to an idea proposed by Myers et al. (1984; in press). Myers et al. (1984a, 1984b, and in press) suggest that the earliest, or immature volcanic centers, in an arc setting should be characterized by a greater degree of geochemical heterogeneity relative to later, larger, or more mature volcanic centers as the crustal conduits are progressively conditioned, or 'flushed' by repeated extraction of volatiles or eutectic melts. One major result of such a process would be that later volcanics or more mature volcanic centers would be less likely to display geochemical signatures of crustal contamination. There is no variation of $^{87}Sr/^{86}Sr$ or $^{143}Nd/^{144}Nd$ with bulk composition in the preglacial volcanics analyzed, and thus no clear evidence of crustal contamination in these samples. As suggested earlier (section 9.4), two samples of postglacial basalt from Puyehue Volcano were probably affected by selective crustal contamination, while postglacial evolved lavas ranging

from basaltic andesites to rhyolites may have experienced a small degree of crustal contamination during an AFC process. The only indication that the older, preglacial volcanics may be relatively more variable is suggested by the larger ranges of Ba/Th (66-197) and Ba/La (17.4-36.2) ratios in these samples relative to postglacial volcanics. However, the relatively larger ranges of these abundance ratios in the preglacial volcanics are defined by single aberrant samples such as basaltic andesite 162828a with low Th and REE abundances, and dacite 182823a with a high Th abundance.

Thus, there are no major differences in the degrees of geochemical heterogeneity in the preglacial volcanics compared to the postglacial volcanics. Preglacial basaltic andesites may have been produced by fractional crystallization at low pressure which resulted in a mild Fe-enrichment, followed by Si-enrichment accompanying further fractional crystallization that produced more evolved preglacial volcanics. If magma mixing processes generated the observed compositions of preglacial volcanics, an appropriate basaltic endmember is not represented in the data set. By contrast, evidence of magma mixing is more clearly seen in postglacial volcanics.

11.2 Magma mixing: general comments and inferred evolution of the volcano

The textural characteristics of lavas thought to be a result of magma mixing are useful in identifying mixing endmembers. The thermal curvature of cotectics from 1-atm experiments as projected from the olivine-diopside-silica subprojection on to the olivine-silica pseudo-binary and plotted as a function of temperature enabled Gerlach and Grove (1982) to interpret the origin of textures of mixed lavas in a calcalkaline volcanic suite at Medicine Lake Highlands, California. Porphyritic intergranular basaltic andesites were interpreted as mixtures of basaltic and rhyolitic magmas resulting in supercooled liquids. Trachytic, aphyric andesites were interpreted as mixtures of basaltic magma with a relatively greater proportion of rhyolitic magma resulting in superheated liquids. The latter effect is suggested, since the compositions of the aphyric andesites as represented by the ratio oliv/oliv.+qtz correspond to a portion of a mixing curve between basalt and rhyolite that lies above a thermal minimum on a 1-atm cotectic (Figure 6, Gerlach and Grove, 1982). In a similar manner, compositions of the porphyritic intergranular basaltic andesites correspond to a portion of a mixing curve between basalt and rhyolite that lies below a thermal maximum.

Textural characteristics in mixed lavas of Puyehue Volcano are different than those reported by Gerlach and Grove (1982). Basaltic andesites at Puyehue display aphyric trachytic textures, while the mixed andesites with disequilibrium phenocryst assemblages are characterized by porphyritic intergranular textures. In this case, the basaltic andesites may represent superheated liquids. Since the composition of the

postulated Fe-rich, TiO_2-rich andesite endmember would appear to lie on a thermal maximum (Fig. 49), the resulting mixing line between this andesite and basalt lies above a thermal trough and defines a possible compositional range for superheated liquids produced by mixing. The textural characteristics of the aphyric basaltic andesites from Puyehue, previously postulated as representing mixing of basaltic and andesitic magmas on the basis of geochemical data, may be explained if they were superheated liquids, and indeed, their bulk compositions appear to plot on a mixing line above this thermal 'trough.' Thus, a different choice of relatively more evolved, silicic endmember, given the thermal curvature of the 1-atm cotectics, may result in either aphyric, trachytic basaltic andesites at Puyehue in this study, or in porphyritic, intergranular basaltic andesites with disequilibrium phenocrysts assemblages as described by Gerlach and Grove (1982).

The mixed andesites at Puyehue (samples 242824, 272822) are characterized by porphyritic intergranular textures and are compositionally similar to aphyric trachytic andesites at Medicine Lake Highland (Gerlach and Grove, 1982). By postulating a very silicic rhyolitic mixing endmember (as suggested by the Fe-rich olivine phenocrysts in samples 242824), a mixing curve on a plot of temperature vs. composition (oliv/oliv + qtz) has steeper slope (Fig. 49). Compositions corresponding to the mixed andesites appear to lie on a portion of this mixing line somewhat below a thermal maximum and would be erupted as supercooled liquids. A mixing curve between an average basalt and rhyolite falls below the projected thermal maxima (Fig. 49) and this explains why mixtures resulting in andesitic bulk compositions at Puyehue are characterized by intergranular porphyritic textures. This situation

49 Cotectics from 1-atm experiments after Grove et al. (1982, 1983) vs. temperature on an oliv-qtz pseudo-binary (cf., Fig. 6, Gerlach and Grove, 1982). Compositional ranges of postglacial basalts, basaltic andesites, and dacites to rhyolites from Puyehue Volcano are shown as open-sided boxes, since actual temperatures of crystallization are unknown. Compositions of a high-TiO_2, high-P_2O_5 andesite (220283-5) and two mixed andesites (242824, 272822) are plotted on mixing lines (dashed). A mixing line between andesite 220283-5 and basalts refers to mixing models discussed earlier (section 5.2.1, Table 7d) for basaltic andesites, which may be erupted as superheated liquids as an explanation of their aphyric textures. A mixing line between basalt and rhyolite illustrates that mixed andesites such as 242824 and 272822 may be erupted as supercooled liquids whereby phenocrysts from each endmember may be preserved as a disequilibrium phenocryst assemblage.

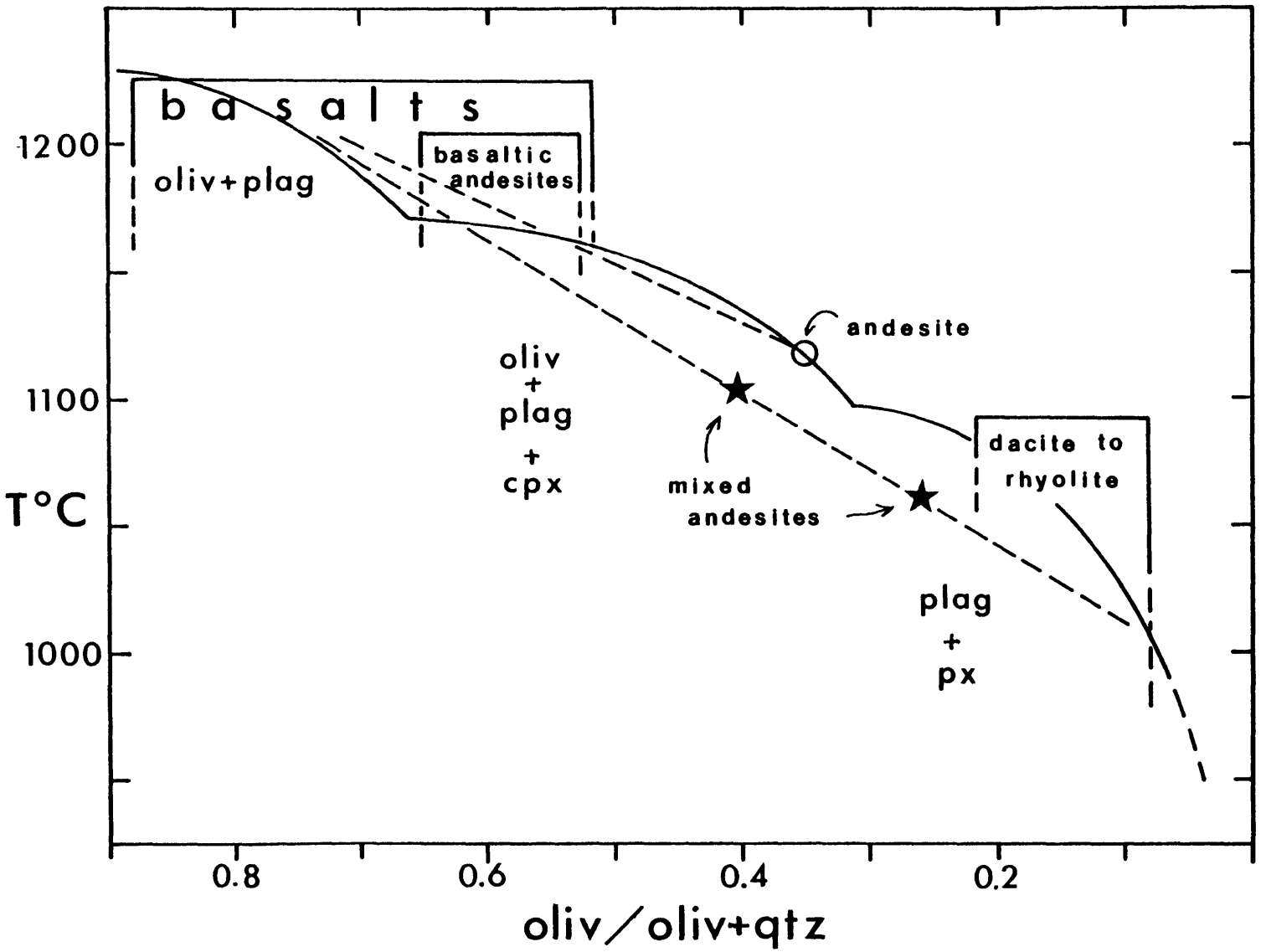
basalts
basaltic andesites
oliv+plag
andesite
oliv + plag + cpx
mixed andesites
dacite to rhyolite
plag + px
1200
1100
1000
T°C
0.8
0.6
0.4
0.2
oliv/oliv+qtz

(a lack of heat available for resorption) serves to preserve the assemblage of phenocrysts incorporated from both mixing endmembers, even though they are out of equilibrium with the resulting bulk composition. Eruption shortly after mixing and relatively rapid cooling after eruption would also preserve disequilibrium phenocryst assemblages. In the specific case of the basaltic andesites, the amount of heat available was sufficient to cause virtually complete resorption of phenocrysts that may have been contributed from either mixing endmember, if one or both of the magma mixing endmembers contained crystals.

The hypothetical mixing relationships in Figure 49 suggest a viable cause of the various textures in mixed Puyehue lavas, however these arguments are based on 1-atm anhydrous phase relationships after Grove et al. (1982). As discussed earlier, it is likely that most Puyehue lavas crystallized under conditions of relatively higher pressure and possibly higher P_{H_2O}, and 1-atm phase equilibria are not strictly relevant in shedding light on the causes of various textures in Puyehue mixed lavas.

Geochemical and petrographic data for the lavas representing mixed magmas may be used to make inferences concerning the compositional evolution of the volcano and the characteristics of magma chamber(s) that existed, or presently exist below the volcano. Most aphyric basaltic andesites postulated as products of magma mixing processes are contemporaneous with the basalts sampled (unit PII) and are older than the late-stage (unit PIV) mixed andesites. Those basaltic andesites produced by mixing of basaltic and andesitic magmas are relatively older than the basaltic andesite (272826b) produced by mixing of basalt and rhyolite. Basaltic mixing endmembers for all basaltic andesites as a

group may have been relatively homogeneous with respect to their Sr-isotopic composition and characterized by intermediate values of $^{87}Sr/^{86}Sr$ (.7039-.7040), e.g., see Figure 17. The basaltic endmember for basaltic andesite 272826b must have been relatively more LREE enriched, as suggested earlier (Fig. 17). Basaltic endmembers for the late-stage mixed andesites were also relatively more LREE-enriched but more variable in Sr-isotopic composition (Fig. 17). These observations do not imply a change in basalt chemistry or degree of variability with time, since these variations are observed in contemporaneous basalts in the PII unit alone, with no apparent correlation of relative stratigraphic position and basalt geochemistry within this unit. The major implication is that, although basaltic magmas are not represented as eruptive products in the later units PIII and PIV, evidence indicates that basaltic magmas were available as mixing endmembers and were variable in their geochemical composition, especially with regard to trace element abudances, abundance ratios, and isotopic composition.

Assuming that the basaltic andesites and late-stage mixed andesites analyzed are a thorough and representative sampling of mixed lavas produced at particular times during the evolution of the volcano, and that in addition, these lavas reflect the compositional range of magmas available at any time for mixing, then further inferences may be made about the magma chamber(s) at any given stage. The earliest basaltic andesites, presumed to be products of mixing of basaltic and andesitic magma, could be interpreted to indicate that processes of fractional crystallization in any magma reservoirs at this stage had only proceeded so far as to produce andesitic residual liquids. This is not true however, since minor amounts of dacite flows interbedded with PII basalts

indicate that dacitic magma was also created and available during the production of these earlier basaltic andesites, although as argued earlier, dacite would not be a suitable magma mixing endmember in this case. Rhyolitic to rhyodacitic magma is present as discrete flows and pyroclastics in unit PIII and is also indicated as a magma mixing endmember for the later mixed lavas, such as basaltic andesite 272826b and mixed andesites 242824 and 272822. This may signify an increasing general tendency towards production of silicic magmas with time throughout the evolution of the volcano. In the simplest (possibly naive) case, a single magma chamber below the volcano may have experienced a gradual decrease in frequency or volume of eruption while input of new magma decreased or remained constant. This may have permitted increasing degrees of fractional crystallization and establishment of a reservoir or layer of highly siicic magma.

Establishment of a magma chamber possibly zoned with respect to composition, temperature, density, and viscosity is supported by petrographic and field observations of late stage PIV lavas. All samples collected from this volumetrically minor unit can be considered virtually contemporaneous. Andesites such as samples 43821 and 220283-5 were apparently produced by fractional crystallization (section 7.1) and were erupted on the lower flank of the volcano, particularly the SW flank (Fig. 2). Dacites (samples 212826 and 23823a) and mixed andesites (samples 242824 and 272822) were erupted from near the summit. These spatial relationships suggest that the summit lavas were drawn through a central vent from an upper, more silicic portion of a zoned magma chamber, and that andesitic lavas were drawn from a lower portion through a peripheral or secondary vent. Furthermore, the magma chamber was

subjected to periodic intrusion of basaltic magma varying in geochemical character that mixed with the silicic 'roof' magma and resulting mixtures were subsequently erupted as supercooled liquids in the form of porphyritic intergranular mixed andesites.

The basaltic component in the mixed andesite lavas is often manifest as diffuse vesicular inclusions with large olivine and plagioclase phenocrysts. The basal portion of the preceding, largely pyroclastic unit PIII contains scoriaceous inclusions of porphyritic basalt as described earlier (section 3). Both observations suggest that the basaltic magma was vesicular upon, or prior to mixing with rhyolitic magma. Vesiculation of basaltic magma may be the principal means by which mixing between basaltic and (overlying) rhyolitic magmas can occur, due to large differences in viscosity and density (Eichelberger, 1980; Huppert et al., 1982). Explosive eruptions that produced the pyroclastics of unit PIII may have been triggered by intrusion of basaltic magma into the lower portion of a large silicic magma chamber, and heat transfer between the two magmas led to crystallization and exsolution of volatiles from the basaltic magma (Huppert et al., 1982). The basaltic magma may then have eventually achieved an equivalent bulk density by this proces and extensive, possibly rapid, convective overturning of the basaltic and silicic layers induced mixing and subsequent explosive eruptions (Huppert and Sparks, 1980; Sparks et al., 1977).

An alternative mechanism by which the PIII pyroclastics and PIV mixed andesites may have been produced is by the forceful injection and 'fountaining' of basaltic magma into a silicic magma chamber (Campbell and Turner, 1984). Vesiculation of the basaltic magma, forceful

entrainment of silicic magma, and possible explosive eruption would also be part of this scenario. Eruption and relatively rapid cooling shortly after mixing is required for preservation of the disequilibrium phenocrysts in the PIV mixed andesites as noted earlier.

Olivine (Fo_{74} to Fo_{85}) and plagioclase (An_{80} to An_{88}) phenocrysts in the PIV mixed andesites may be too large (up to 2-3 mm) in size to have nucleated upon contact with relatively cooler silicic magma (cf., Huppert et al., 1982) and to have grown to such dimensions in the postulated relatively short time prior to eruption. It may be more likely that the phenocrysts grew in basaltic magma in another (lower) reservoir, were entrained by the host basaltic magma, and were thus present in the basalt when intruded into a silicic magma chamber. Textural and compositional relationships in the olivine and plagioclase phenocrysts both in the basalts and mixed andesites support this proposed sequence of events. Relatively calcic (An_{80} to An_{88}) plagioclase phenocrysts in mixed andesite 242824 display sodic overgrowths and relatively sodic (An_{29} to An_{37}) phenocrysts may display a few relatively more calcic overgrowths. Overgrowths on the plagioclase phenocrysts probably formed after mixing and represent compositions of plagioclase in equilibrium with the resulting mixed andesitic composition. The more sodic plagioclase phenocrysts and very Fe-rich mafic phenocryst phases in the mixed andesites probably crystallized in equilibrium with a silicic magma, dacitic to rhyolitic in composition, along a boundary layer or wall contact in the top portion of a silicic magma chamber. If the magma chamber was zoned from andesitic to rhyolitic compositions as suggested by the late stage flank eruptions of high-TiO_2 andesite, then side-wall boundary layer crystallization could have produced phenocrysts in

equilibrium with andesitic magma, however large phenocrysts of intermediate composition are not observed in the PIV mixed andesites. The bimodal compositional distribution of large phenocrysts in the mixed andesites (Figs. 3a and 4) may indicate that (1) little or no crystallization of phases in andesitic magma was occurring at the time, (2) that andesitic magma per se was not present in the magma chamber at the time, or (3) that a forceful intrusion of porphyritic basaltic magma straight up into a relatively large magma chamber only passed through central crystal-poor layers of andesitic to dacitic magma and incorporated only phenocrysts from the crystallizing rhyodacitic or rhyolitic 'roof' magma before eruption. Thus, at the time of production and eruption of all PIV lavas including dacites and mixed andesites, and possibly during eruptions of PIII pyroclastics, the situation may have been that of a shallow compositionally zoned magma chamber containing magmas ranging in composition from andesitic to rhyolitic, which was periodically invaded by intrusions of basaltic magma.

A contrasting situation may have prevailed in earlier stages when the mixed PII basaltic andesites were produced. No lavas with the characteristics of the late PIV mixed andesites have been sampled from unit PII. There is no evidence of explosive eruptions during this period, and fractional crystallization may have proceeded to a point to produce dacitic residual liquids at various times. Alternatively, the dacites may simply be products of boundary layer or 'sidewall' fractional crystallization of andesitic magma. Although not strictly represented among PII samples collected, the existence, at this stage, of high-TiO_2, high-P_2O_5 andesitic magma is implied since it may be the best mixing endmember to explain the characteristics of the mixed basaltic andesites

(section 5.2.1). If a magma chamber during this period contained mostly Fe-rich, TiO_2-rich andesitic magma with minor dacitic magma, then andesitic magma of this type would be relatively more dense, on the basis of composition (Grove and Baker, 1983) and temperature (Sparks et al., 1980), than basaltic magma intruded from below, and turbulent mixing between basaltic and andesitic magmas would occur. This type of mixing, and the superheated state of this mixture would result in very thorough mixing and resorption of any phenocrysts derived from either mixing endmember. This process, however, did not appear to result in explosive eruptions, suggesting that volatile contents of newly input basaltic magma and evolved magmas in residence were similar (Huppert et al., 1982). The aspect ratio (width/depth) of the magma chamber to bring about efficient and thorough mixing to produce the early basaltic andesites may have been low relative to that inferred for the magma chamber(s) at later stages, which may have been characterized by stronger composition zonation and less thorough mixing as represented by the PIV mixed andesites (Sparks et al., 1980; Sparks et al., 1984).

In a crude sense, the compositional gap between magma mixing endmembers may broaden with time, as suggested by evidence that early basaltic andesites were produced by mixing of basaltic + andesitic magmas, and later basaltic andesites and mixed andesites were produced by mixing of basaltic and rhyolitic magmas. This trend is also observed in other calcalkaline volcanic centers (Sakuyama, 1981), and may be a function of an increasing aspect ratio of a magma chamber with time, with accompanying increasing degrees of compositional zonation and differences in types of magma mixing.

The isotopic composition of various lavas in Puyehue Volcano may also be correlated with changes in the magma chamber and mixing processes or mechanisms. As stated earlier, basalts are variable throughout the section. It may be that since the early mixed basaltic andesites in unit PII are characterized by intermediate values of $^{87}Sr/^{86}Sr$, the similarly intermediate values of $^{87}Sr/^{86}Sr$ required in the basaltic endmembers reflect mixing of basaltic magmas with one another prior to the mixing event(s) that produced the basaltic andesites. Since basalts with intermediate values of $^{87}Sr/^{86}Sr$ (.70396-.70403) are also characterized by the maximum observed extremes in their relative degrees of LREE-enrichment (La/Sm = 2.36-2.92), this does not appear to be the case, or else La/Sm ratios in these basalts might also be intermediate in value. Thus, it may only be a coincidence that the early basaltic andesites do not reflect evidence of a high $^{87}Sr/^{86}Sr$ or low $^{87}Sr/^{86}Sr$ relatively LREE-enriched basaltic mixing endmember, or that basalts with extreme Sr-isotopic compositions were not involved in mixing although they are contemporaneous (interbedded) with the early mixed basaltic andesites. The opposite is observed in late stage mixed andesites which reflect derivation by mixing of basaltic magmas extreme in isotopic composition (Fig. 17) with rhyolitic magmas. From these latter lavas, pulses of isotopically distinct basaltic magma may have been small in volume relative to the size of the magma chamber, entrained silicic magma prior to eruption as mixed andesites, and thereby caused no change in the isotopic composition of the remaining magma in the magma chamber.

Inherent in this proposed evolution of the volcano is the implication that static magma chambers present at any stage contained volumes of magma large in size relative to amounts withdrawn by eruption

or amounts of new magma input, and that the magma residing in the chamber was intermediate with respect to (Sr) isotopic composition. This does not imply that the magma residing in any chamber was well-mixed with respect to major- and trace element composition. Since Sr-isotopic compositions appear to 'converge' to intermediate values with increasing SiO_2, and since the majority of the basalts also feature intermediate $^{87}Sr/^{86}Sr$ values, the extreme low and high values seen in some basalts may be exceptional, and these basalts may be minor in volume. This may also imply that a magma chamber present at any one time contained magmas with intermediate $^{87}Sr/^{86}Sr$. Such a long-term buffered effect may have been brought about by several conditions. As suggested previously, the magma chamber might have been large in size relative to pulses of basaltic magma, which at various times may have been isotopically distinct. It is likely that the average abundance of Sr throughout the magma chamber was lower than Sr abundances in intruding basaltic magmas, another reason for speculating that volumes of isotopically variable intruding basalt may have been negligible relative to the volume of the magma chamber, and also that at least in earlier stages, mixing was sufficiently thorough to 'average out' the effects of intruding or replenishing basalts with different isotopic compositions. If the mixed andesites were produced by the entrainment of silicic magma in 'fountains' of intruding basaltic magma with relatively higher Sr abundances and variable $^{87}Sr/^{86}Sr$, the Sr-isotopic composition of the mixture may end up being relatively closer to that of the basaltic magma. Again, this is implied by the variable Sr-isotopic compositions of the mixed andesites (Fig. 17).

Isotopic evidence for wallrock assimilation in any form may be difficult to detect, since near-surface country rock in the area may not be drastically different in isotopic character. This may be especially true for shallow magma chambers or shallow portions of magma chamber where older volcanics, such as may be represented by the preglacial volcanics analyzed in this study, are likely sources of wallrock contaminant material. Assimilation either by stoping (bulk assimilation or incorporation of partial melts of wallrock material are two processes that would accompany expansion of a magma chamber, and in this case, these processes may have also aided in 'buffering' the overall isotopic composition of magma(s) residing in a magma chamber.

Lack of significant contamination by assimilation of wallrock may also be explained if the magma chamber was shallow and largely silicic in composition (as suggested by late stage activity). In this situation, it would follow that magma temperature may have been low, and wallrock relatively cool, and the resulting thermal conditions may have been inadequate for melting of significant amounts of wallrock.

Temperatures and oxygen fugacities were estimated for oxide pairs in PIV lavas (sample 242824, 272822, and 212826) after the method of Spencer and Lindsley (1981). Estimates of log $^{f}O_2$ and temperature for oxide pairs in mixed andesite 242824 (log $^{f}O_2$ = -7.6, temp. = 1185°C), mixed andesite 272822 (-10.3, 990°C), and dacite 212826 (-10.9, 975°C) vary widely and correspond closely to the Ni-NiO buffer, as may be expected in a shallow, relatively O_2-rich magma chamber. Temperatures calculated for oxide pairs in the dacite lava 212826 and those in the mixed andesite 272822 are similar, thus, the oxides in 272822 are derived from a dacitic or rhyolitic mixing endmember. In either case, these temperatures

indicate that some portion of the magma chamber was at a temperature which may be low relative to solidus temperatures for wallrock, in support of the preceding suggestion for lack of evidence of wallrock assimilation. A temperature estimate for the mixed dacite andesite 242824 is based on analyses of a phenocryst of Ti-magnetite with exsolution lamellae of ilmenite. This textural relationship may represent beginning subsolidus exsolution in the oxide which was effectively quenched on eruption of the host mixed andesite. The calculated temperature of 1185°C is significantly higher than those for the other two samples. If this temperature is in fact a 'quench' temperature, then this phenocryst must have been derived from a basaltic mixing endmember for 242824, and the calculated temperature is a minimum for this basaltic magma endmember. For this sample, the basaltic component contained olivine and plagioclase phenocrysts, and this temperature is within the range observed for 2-phase saturated basalts in 1-atm experiments by Grove et al. (1982).

If the above temperature estimates are accurate, then water contents in the magmas, especially silicic magmas, may be estimated based on recent experimental studies of Mt. St. Helens dacites by Merzbacher and Eggler (1984). The lack of any hydrous phenocryst phases even in rhyolites in this study suggests relatively low H_2O contents in all magmas throughout the evolution of the volcano. Phase relations for dacites under high pressure and H_2O-saturated or undersaturated conditions (Merzbacher and Eggler, 1984) may be used to estimate H_2O contents in dacites to rhyolites of Puyehue Volcano. All dacites, rhyodacites, and rhyolites contain small amounts of plagioclase, augite, orthopyroxene, and oxide phenocrysts and compositions of the phenocrysts

indicate that the phenocrysts are in equilibrium with the host liquid for the most part. Plagioclase phenocrysts are the most numerous and are probably the primary liquidus phase, suggesting H_2O contents of less than 4.5 wt.% at the liquidus, since orthopyroxene is the stable primary liquidus phase at greater H_2O contents (Figure 2, Merzbacher and Eggler, 1984). Since Puyehue dacites, rhyodacites, and rhyolites are apparently multiply saturated (with amphibole conspicuously absent), for the temperatures calculated above (975°-990°C), H_2O contents in these silicic lavas were a maximum of 2 wt.% at low pressures (0.5-1 kb) and a maximum of 2.5 wt.% at total pressures up to 4 kb (Merzbacher and Eggler, 1984). Merzbacher and Eggler (1984) were able to contour the plag-opx-qtz + or plane for H_2O contents in experimental melts, and plotted andesitic to dacitic glass compositions from other volcanic suites. Results indicate that silicic volcanics from island arcs apparently contain no more than 1-2 wt.% H_2O, while continental margin calcalkaline silicic volcanics may contain higher H_2O contents adequate for crystallization of amphibole in some examples (Ritchey, 1980). Higher total pressure in addition to higher H_2O contents may favor amphibole crystallization (Eggler, 1972; Merzbacher and Eggler, 1984). The maximum upper temperature stability limit of amphibole at low pressure (< 5 kb) and H_2O-undersaturated conditions may be about 950°C (Eggler, 1972; Merzbacher and Eggler, 1984). Temperatures estimated for Puyehue dacite 212826 are higher than this, so that it is possible that silicic lavas at Puyehue never reach low temperatures sufficient to crystallize amphibole for their given H_2O content (2.5 wt.% max.). Frequent dewatering or outgassing of magma may have occurred in association with pyroclastic eruptive events and prevented achievement of H_2O contents high enough to stabilize amphibole.

Many silicic volcanics in the northern part of the Southern Andes between latitude 33°-36°S contain amphibole and even biotite. It is likely that parental magmas were relatively more hydrous initially, or incorporated H_2O by crustal contamination, and that crystallization often proceeds to low temperatures sufficient to stabilize hydrous phases. This may occur in magma chambers at greater depth below these volcanos compared to volcanos south of 36°S, because higher pressures generally enhance the solubility of H_2O in magmas (Hamilton et al., 1964; Burnham and Davis, 1971, 1974; Burnham, 1975). For volcanos such as Puyehue, parental magmas are probably relatively less hydrous and highly evolved silicic magmas are consequently less hydrous and are erupted at higher temperatures relative to their amphibole- and biotite-bearing counterparts in volcanos to the north. The possible occurrence of dewatering or volatile transfer processes within the magma chamber and the demonstrated likelihood of open system magmatism at Puyehue inhibits estimation of H_2O contents in basaltic and andesitic magmas from estimates of H_2O contents in dacites based on preliminary experimental data (Merzbacher and Eggler, 1984), assuming the latter were produced by fractional crystallization of basaltic or andesitic magma. Plagioclase is apparently the primary liquidus phase in all samples from Puyehue, based on petrographic observations. Eggler (1972) determined that in a Paricutin andesite, plagioclase was the liquidus phase at pressures to 6 kb ($P_{H_2O} < P_{total}$) and at water contents less than 2 wt.%, and this may be considered a maximum content for basaltic to andesitic magmas at Puyehue Volcano.

12. Summary

1. Recent volcanism in the Puyehue-Cordon Caulle area in the Southern Andes (34°-42°S) of South Central Chile may be separated into two groups by an erosional hiatus related to Pleistocene glaciation. Preglacial volcanics range widely in character and record a period of extensive explosive activity from centers represented by prominent erosional remnants. Based on sampling efforts in this study, preglacial volcanism may have been more intermediate in composition relative to the postglacial Puyehue Volcano, which is predominantly basaltic in its overall composition. This apparent compositional distinction between older and younger volcanics has been recognized on a preliminary basis at other predominantly basaltic volcanos in the Southern Andes.

2. The types of phenocrysts and phenocryst assemblages in lavas at Puyehue Volcano suggest that crystallization occurred in magmas at low (from 1 atm) to moderate (to 5 Kb) pressures at low P_{H_2O}, based on results of published and on-going experimental studies. Compositions of phenocrysts in basalts are similar to those in basalts from other calcalkaline centers, but phenocrysts may have accumulated to varying degrees such that the generally porphyritic basalts are not strictly representative of liquids. A sequence of crystallization throughout the suite is difficult to estimate, since basaltic andesites and andesites are aphyric or nearly aphyric. An exception is represented by porphyritic mixed andesites which contain disequilibrium phenocryst assemblages, including olivine and plagioclase phenocrysts which are bimodally distributed with respect to composition. Compositions of pyroxene phenocrysts in evolved lavas ranging from dacite to rhyolite are exceptionally Fe-rich, and these compositions have been only rarely

reported in calcalkaline suites. Fe-rich pyroxene and olivine phenocrysts (Fo_{25} to Fo_{27}) occur in rhyolite and in the mixed andesites.

3. The major-element compositions of lavas from Puyehue Volcano indicate that they constitute a medium-K suite of tholeiitic affinity. Puyehue lavas display enrichments in LIL elements (Cs, Rb, Ba, K) and relative depletions in HFSE (Ta, Nb, Hf, Zr, Ti) which are characteristic of volcanics in subduction-related tectonic settings.

4. Isotopic compositions of Puyehue lavas vary over restricted ranges and are not simply correlated with any bulk compositional parameters. Samples analyzed for Pb-isotopic composition are characterized by elevated $^{207}Pb/^{204}Pb$ ratios relative to MORB and OIB as featured in many other suites of arc volcanics. The Sr-isotopic compositions of Puyehue basalts are variable ($^{87}Sr/^{86}Sr$ = 0.70378-0.70416) and display extreme values, while those of evolved lavas are more intermediate (0.70388-0.70414), and Sr-isotopic compositions appear to converge to intermediate values of $^{87}Sr/^{86}Sr$ (~ 0.70407-0.70409) with increasing SiO_2. This apparent feature, however, is an artifact in that the intermediate range of $^{87}Sr/^{86}Sr$ (0.70388-0.70414) is displayed by two samples of mixed andesites produced by mixing of isotopically extreme basaltic magmas with dacitic to rhyolitic magmas. The remainder of the samples ranging from basaltic andesite to rhyolite display an intermediate and relatively restricted range in $^{87}Sr/^{86}Sr$ (0.70400 to 0.70409).

5. Basalts of Puyehue Volcano are geochemically heterogeneous and display wide ranges in abundances of many incompatible trace elements. The basalts display variable degrees of relative LREE enrichment (La/Sm = 2.36-2.93, La/Yb = 3.6-5.4), and display variations in other trace

element abundance ratios. For these reasons, care was taken in selecting particular basalts to model liquid lines of descent leading to compositionally more evolved lavas. In modelling the petrogenesis of evolved lavas, restricted compositional ranges were discussed separately.

6. Basaltic andesites of Puyehue Volcano are variable in their major-element and isotopic compositions, and in trace element abundances and abundance ratios. The major-element compositions of the basaltic andesites suggested that they may be derived by approximately 10-30% fractional crystallization of oliv+plag or oliv+plag+cpx±magnetite from basaltic magma as represented by samples of Puyehue basalts. A clinopyroxene-bearing assemblage suggests crystallization at moderate pressure, and projected compositions of basaltic andesites in the oliv-cpx-qtz pseudoternary (Grove et al., 1982) may be subparallel to a hypothetical oliv-aug-plag cotectic at moderate pressure (Grove and Baker, 1984). However, clinopyroxene and magnetite phenocrysts are not observed in the basalts. Furthermore, fractional crystallization models are inadequate in explaining the incompatible element abundance ratios and elevated (> two-fold increases) trace element abundances in the basaltic andesites. Models of simultaneous fractional crystallization and crystal assimilation (AFC) are possible, but cannot be tested to any degree of accuracy given the variability in the basalts and unknown wallrock contaminants. Magma mixing models are relatively more successful in explaining the bulk compositions of the basaltic andesites, especially those with elevated TiO_2 and P_2O_5 contents.

7. Mixed andesites with disequilibrium phenocryst assemblages are clearly produced by magma mixing and may be linked to specific basaltic

and silicic endmembers within the data set on the basis of major-element compositions, trace element abundances, phenocryst compositions, and Sr-isotopic compositions.

8. Evolved lavas ranging from andesites to rhyolites may be explained as products of fractional crystallization of basaltic andesite. A specific group of andesites relatively high in TiO_2 and P_2O_5 contents may have been produced by approximately 50% fractional crystallization of basaltic andesitic magma, and this is consistent with the approximate two-fold enrichment in most incompatible trace elements in these andesites relative to the basaltic andesites. The four- to five-fold enrichment in incompatible elements in the andesites relative to most basalts inhibits a direct linkage of the andesites to the basalts via closed-system fractional crystallization. Fractional crystallization of oliv+plag+aug+magnetite from basaltic andesite at moderate pressures can produce residual liquids with major-element compositions, trace element abundances, and abundance ratios similar to those of the high-TiO_2, high-P_2O_5 andesites. This is supported by geochemical data, since the basaltic andesites and andesites lack phenocrysts.

9. Silicic lavas from Puyehue Volcano ranging from dacites to rhyolites were probably produced by fractional crystallization of andesitic magma. Crystallizing assemblages consisted of plagioclase, augite, orthopyroxene, pigeonite, magnetite, ilmenite, and apatite, and this is consistent with petrographic observations and geochemical data for dacites, rhyodacites, and rhyolites. Within this compositional range, trace element abundances, especially of REE, and certain abundance ratios (e.g., Zr/Sm) were affected by the proportion of apatite removed by fractional crystallization. Although the silicic lavas may form a

geochemically coherent series related by fractional crystallization, differences in pyroxene phenocrysts between dacites (augite+ orthopyroxene) and rhyolites (augite+pigeonite or augite = pigeonite) imply that crystallization occurred under varying total pressures and P_{H_2O}.

10. Cordon Caulle rhyodacites and rhyolites are petrographically and geochemically similar to rhyodacites and rhyolites of Puyehue Volcano. Being the youngest eruptives in the area, they also may represent final, late-stage volcanism related to Puyehue Volcano and eruptive vents shifted due to structural controls. The three distinct prehistoric and historic eruptive units of Cordon Caulle may be related by fractional crystallization, however, as in some Puyehue lavas, different pyroxene phenocryst assemblages also indicate that different magmas were crystallizing at different total pressures and P_{H_2O}. One eruptive unit is isotopically distinct, although all three units are closely related in space and time. Thus, the Cordon Caulle lavas may be comagmatic, but this suggests that silicic magmas may have been zoned with respect to composition and possibly underwent crystallization under varying conditions in different levels of a complex magma chamber or volcanic plumbing system.

11. Basalts from Puyehue Volcano are geochemically heterogeneous. Aside from differences in major-element compositions of the basalts which might be explained by varying proportions of accumulated olivine and plagioclase phenocrysts, noticeable differences in CaO/Al_2O_3, FeO^*/MgO, and Na_2O/K_2O ratios are observed. Abundances of several trace elements vary more than two-fold among the basalts, and observed ranges of the most incompatible elements decrease in the order Rb>Nb>Th>Zr>Cs>La>Ba>K.

This order is different from a general order of incompatibility suggested for MORB. Intercorrelations of abundances and abundance ratios are not observed within LIL and REE element groups nor between these groups in the basalts, while better trends are seen for HFSE. Abundance ratios of LIL/REE, LIL/HFSE, and REE/HFSE are variable in the basalts (e.g., Ba/Nb = 36-108, Rb/La = 1.1-1.8, La/Nb = 2.4-4.9, Ba/Th = 80-188) and display few correlations which would support simple two-component mixing. The basalts are most variable in $^{87}Sr/^{86}Sr$ (0.70378-0.70416) and less variable in Nd ($^{143}Nd/^{144}Nd$ = 0.51282-0.51288) and Pb ($^{206}Pb/^{204}Pb$ = 18.551-18.583 isotopic compositions. Only Sr-isotopic compositions of the basalts display any correlations with abundances and abundance ratios of LIL and HFSE, while variations in REE abundances and degrees of relative LREE enrichment are decoupled from isotopic variations in the basalts.

12. The geochemical compositions of many lavas of Puyehue Volcano may have been affected by crustal contamination, however, among the evolved lavas, this is difficult to demonstrate unambiguously with regard to specific samples; it can only be speculated that crustal contamination may have accompanied fractional crystallization. The only obvious crustal contamination is seen in two basalts which are characterized by higher $^{87}Sr/^{86}Sr$ and higher alkali abundances (Cs, Rb) relative to other basalts, and this may be explained as a result of selective contamination rather than bulk assimilation of crustal materials.

13. Simple batch melting models demonstrated that variations in source trace element abundances, source modal mineralogy, and degree of partial melting are required to explain the varying degrees of relative LREE enrichment in the basalts. Variations in these three parameters are also

required to explain ranges in the magnitudes of HFSE anomalies in the basalts indicated by variable LIL/HFSE and REE/HFSE ratios. Differing amounts of fractional crystallization of clinopyroxene at high pressures will also contribute to variability in degrees of relative LREE enrichment.

14. Correlations or groupings of LIL/HFSE or LIL/REE ratios vs. Sr- and Pb-isotopic compositions in the basalts allow the testing of various models concerning subcrustal processes of magma genesis. High LIL/REE or LIL/HFSE abundance ratios in the basalts may have been produced by addition of an alkali-enriched component derived from subducted oceanic crust to a mantle source rather than differentiation on partial melting by HFSE- and REE-rich refractory phases. Addition of varying amounts of a subducted slab-derived component to a mantle source may produce basalts which display positive correlations of LIL/HFSE and LIL/REE abundances with radiogenic isotopic composition as observed in some arcs. However, Puyehue basalts instead display negative correlations or groupings between these geochemical parameters linked to subducted crust (e.g., Ba/Nb vs. $^{87}Sr/^{86}Sr$, Sr/Nd vs. $^{87}Sr/^{86}Sr$), also observed in some arcs. Two types of models may explain such trends:

(a) A model of heterogeneous sub-arc mantle, whereby different mantle endmembers are affected by different amounts of slab-derived component.

(b) A two-stage model whereby homogeneous mantle sources are affected by different amounts of slab-derived component; basalts derived from a mixed source consisting of a greater proportion of slab-derived component subsequently mix with partial melts of upper mantle which may lower LIL/HFSE and LIL/REE ratios in ascending magmas.

Model (a) or (b) may also explain the lack of correlation between LIL 'spikes' and radiogenic isotopes observed in many arcs. A clear negative correlation between these parameters may be observed if mixing of geochemically distinct magmas occurs after separation from two endmember sources in either model (a) or (b).

15. A third model is suggested by Puyehue basalts which are characterized by low $^{87}Sr/^{86}Sr$, $^{206}Pb/^{204}Pb$, and ratios of LIL/Th and REE/Th which approach estimated values for the upper mantle. However, these basalts cannot represent an unmodified mantle source or endmember in this region since they are also characterized by higher $^{207}Pb/^{204}Pb$ ratios than MORB or OIB. This suggests a variation of model (b) calling on mixing of homogeneous mantle with varying amounts of a slab-derived component. Since the basalts with low LIL/Th and REE/Th ratios are also characterized by the highest LIL/REE and LIL/HFSE ratios, a role for a refractory HFSE and REE-retaining phase is suggested in their genesis.

16. Andesitic compositions are represented more among the preglacial volcanics than in postglacial volcanics of Puyehue Volcano. Major-element compositions of preglacial volcanics suggest that they define a different liquid line of descent or crystallized under different total pressures relative to postglacial volcanics. The relative importance of either of these alternatives in addition to that of magma mixing cannot be addressed since the preglacial volcanics are aphyric and, aside from one basalt, samples of preglacial basic rocks for consideration as parental magmas are not represented in the sample set. There is no evidence for a greater degree of geochemical and isotopic heterogeneity in the preglacial volcanics relative to postglacial volcanics in support of recent ideas that the relative degree of crustal

contamination and geochemical heterogeneity should decrease with time as magma conduits or magma chamber walls are 'conditioned.'

17. Puyehue Volcano displays an overall compositional evolution with time. Increasingly silicic lavas were produced (or at least, erupted) in greater proportions with time. The main constructional phase of the volcano consisted of basalt, with minor basaltic andesite and dacite. This was followed by a period of relatively more explosive activity, featuring eruption of dacitic to rhyolitic pyroclastics and minor flows. Basaltic magma in late stages is represented only in minor horizons of basaltic scoria, and as inclusions in pyroclastic and mixed andesites. This evolution of the volcano may be consistent with a decrease in the frequency of both magma replenishment and eruptions with time. In early stages dominated by eruption of basaltic lavas, fractional crystallization may have proceeded so far as to produce dacitic liquids. In later stages, fractional crystallization proceeded further and produced rhyolitic magmas in magma chambers which may have been compositionally zoned, or at least were infrequently intruded by batches of basaltic magma. This sequence is indirectly supported by samples of lava produced by magma mixing. Basaltic andesites produced by mixing of basaltic and andesitic magmas precede late-stage mixed andesites produced by mixing of basaltic, dacitic and rhyolitic magmas, i.e., mixed lavas may incorporate the most compositionally evolved magmas available at any particular stage in the evolution of the volcano. Furthermore, geochemically distinct basaltic components in the late-stage mixed andesites are evidence that the degree of heterogeneity in replenishing basaltic magmas was maintained and crustal contamination of basaltic magmas continued throughout the evolution of the volcano.

18. A variety of high-level crustal processes, including fractional crystallization, magma mixing, and crustal contamination were involved in the generation of the various lavas sampled from Puyehue Volcano. The compositions of several of the most basic lavas sampled were affected by these processes with the result that these lavas cannot be considered to represent subcrustal sources or be used to make inferences concerning subcrustal processes. Data for other basic lavas were used to demonstrate models of sub-arc magma genesis with varying proportions of two major components, an upper mantle component and a component derived from subducted oceanic crust. However, geochemical characteristics of primary magmas may even be modified during transit in the upper mantle and this further limits attempts in characterizing primary sources and mechanisms of magma genesis. Puyehue Volcano is not necessarily an atypical volcano relative to other predominantly basaltic volcanos in the Southern Andes of Chile (34°-42°S). It is possible that all or some of the same crustal and subcrustal processes have operated to varying extents in other volcanos in this region. The implication is that detailed studies similar to the present study are necessary before inferences can be made with regard to geographical and temporal variations in compositions of recent volcanics, and the relative importance of crustal contamination, subducted oceanic crust, and heterogeneous upper mantle may be assessed. Further detailed studies of major centers or small areas may lead to major re-assessment in current models of magma genesis in the Southern Andes and in continental arcs in general.

References Cited

Albee, A.L., Ray, L., 1970, Correction factors for electron microprobe microanalysis of silicates, oxides, carbonates, phosphates and sulfates. Anal. Chem. 42, 1408-1414.

Arculus, R.J., Johnson, R.W., 1981, Island-arc magma sources: a geochemical assessment of the roles of slab-derived components and crustal contamination. Geochem. J. 15, 109-133.

Armstrong, R.L., Cooper, J.A., 1971, Lead isotopes in island arcs. Bull. Volcanol. 35, 27-63.

Baitis, H.W., Lindstrom, M.M., 1980, Geology, petrography, and petrology of Pinzon Island, Galapagos Archipelago. Contrib. Mineral. Petrol. 72, 367-386.

Barazangi, M., Isacks, B.L., 1976, Spatial distribution of earthquakes and subduction of the NAZCA plate beneath South America. Geology 4, 686-692.

Barreiro, B., 1983, Lead isotopic compositions of South Sandwich Island volcanic rocks and their bearing on magmagenesis in intra-oceanic island arcs. Geochim. Cosmochim. Acta 47, 817-822.

Barrett, T.J., Friedrichsen, H., 1982, Elemental and isotopic compositions of some metalliferous and pelagic sediments from the Galapagos Mounds area, D.S.D.P. Leg 70. Chem. Geol. 36, 275-298.

Barton, M., Salters, V.J.M., Huijsmans, J.P.P., 1983, Sr isotope and trace element evidence for the role of continental crust in calcalkaline volcanism on Santorini and Milos, Aegean Sea, Greece. Earth Planet. Sci. Lett. 63, 273-291.

Bence, A.E., Albee, A.L., 1968, Empirical correction factors for the electron microanalysis of silicates and oxides. J. Geol. 76, 382-403.

Benjamin, T., Heuser, W.R., Burnett, D.S., Seitz, M.G., 1980, Actinide crystal-liquid partitioning for clinopyroxene and $Ca_3(PO_4)_2$. Geochim. Cosmochim. Acta 44, No. 9, 1251-1264.

Briqueu, L., Lancelot, J.R., 1979, Rb-Sr systematics and crustal contamination models for calc-alkaline igneous rocks. Earth Planet. Sci. Lett. 43, 385-396.

Briqueu, L., Lancelot, J.R., 1983, Sr isotopes and K, Rb, Sr balance in sediments and igneous rocks from the subducted plate of the Vanuatu (New Hebrides) active margin. Geochim. Cosmochim. Acta 47, 191-200.

Burnham, C.W., 1975, Water and magmas: a mixing model. Geochim. Cosmochim. Acta 39, 1077-1084.

Burnham, C.W., Davis, N.F., 1971, The role of H_2O in silicate melts: I. P-V-T relations in the system $NaAlSi_3O_8$-H_2O to 10 kb and 1000°C. Amer. J. Sci. 270, 54-79.

Burnham, C.W., Davis, N.F., 1974, The role of H_2O in silicate melts: II. Thermodynamic and phase relations in the system $NaAlSi_3O_8$-H_2O to 10 kb, 700°C to 1100°C. Amer. J. Sci. 274, 902-940.

Byers, F.M., Jr., 1961, Petrology of three volcanic suites, Umnak and Bogoslof Islands, Aleutian Islands, Alaska. Geol. Soc. Amer. Bull. 72, 93-128.

Calvert, S.R., Price, N.B., 1977, Geochemical variation in ferro-manganese nodules and associated sediments from the Pacific Ocean. Marine Chem. 5, 43-74.

Campbell, I.H., Turner, J.S., 1984, The fluid dynamics of fountains in magma chambers. Proc. Conf. Open Magma Systems (Dungan, M.A., Grove, T.L., Hildreth, W., eds.) Southern Methodist University, Dallas, 23-25.

Casertano, L., 1963, General characteristics of active Andean volcanoes and a summary of their activities during recent centuries. Bull. Seis. Soc. Amer. 53, No. 6, 1415-1433.

Cerrai, E., Testa, C., 1963, Separation of rare earths by means of small columns of Kel-F supporting di (2-ethylhexyl) orthophosphoric acid. J. Inorg. Nucl. Chem. 25, 1045-1050.

Clague, D.A., Frey, F.A., 1982, Petrology and trace element geochemistry of the Honolulu Volcanics, Oahu: Implications of the oceanic mantle beneath Hawaii. J. Petrol. 23, 447-504.

Cohen, R.S., Evensen, N.M., Hamilton, P.J., O'Nions, R.K., 1980, U-Pb, Sm-Nd, and Rb-Sr systematics of mid-ocean ridge basalt glasses. Nature 283, 149-153.

DeBaar, H.J.W., Bacon, M.P., Brewer, P.G., 1983, Rare earth distributions with a positive Ce anomaly in the Western North Atlantic Ocean. Nature 301, 324-327.

DeLong, S.E., Perfit, M.R., McCulloch, M.T., Ach, J., Magmatic evolution of Semisopochnoi Island, Alaska: trace element and isotopic constraints. J. Geol, in press.

DePaolo, D.J., 1981, Trace element and isotopic effects of combined wallrock assimilation and fractional crystallization. Earth & Plan. Sci. Lett. 53, 189-202.

DePaolo, D.J., Johnson, R.W., 1979, Magma genesis in the New Britain island-arc: constraints from Nd and Sr isotopes and trace-element patterns. Contrib. Mineral. Petrol. 70, 367-379.

Deruelle, B., 1982, Petrology of the Plio-Quaternary volcanism of the south-central and meridional Andes. J. of Volc. and Geoth. Res. 14, 77-124.

Deruelle, B., Harmon, R.S., Moorbath, S., 1983, Combined Sr-O isotope relationships and petrogenesis of Andean volcanics of South America. Nature 302, 814-816.

DeVore, G.W., 1983, Relations between subduction, slab heating, slab dehydration and continental growth. Lithos 16, 255-263.

Dixon, T.H., Batiza, R., 1979, Petrology and chemistry of Recent lavas in the northern Marianas: implications for the origin of island arc basalts. Contrib. Mineral. Petrol. 70, 167-181.

Drake, M.J., 1975, The oxidation state of europium as an indicator of oxygen fugacity. Geochim. Cosmochim. Acta 39, 55-64.

Drake, M.J., Weill, D.F., 1975, The partition of Sr, Ba, Ca, Y, Eu^{2+}, Eu^{3+} and other REE between plagioclase feldspar and magmatic silicate liquid: an experimental study. Geochim. Cosmochim. Acta 39, 689-712.

Drake, R.E., 1976, Chronology of Cenozoic igneous and tectonic events in tne Central Chilean Andes - Latitudes 35°30' to 36°S. J. Volc. Geotherm. Res. 1, 285-295.

Dunn, T., McCallum, I. S., 1982, The partitioning of Zr and Nb between diopside and melts in the system diopside-albite-anorthite. Geochim. Cosmochim. Acta 46, 623-629.

Dupuy, C., Dostal, J., Marcelot, G., Bougault, H., Joron, J.L., Treuil, M., 1982, Geochemistry of basalts from central and southern New Hebrides arc: implications for their source rock composition. Earth Planet. Sci. Lett. 60, 207-225.

Eggler, D.H., 1972, Water-saturated and undersaturated melting relations in a Paricutin andesite and an estimate of water content in the natural magma. Contrib. Mineral. Petrol. 34, 261-271.

Eichelberger, J.C., 1980, Vesiculation of mafic magma during replenishment of silicic magma reservoirs. Nature 288, 446-450.

Elderfield, H., Hawkesworth, C.J., Greaves, M.J., Calvert, S.E., 1981, Rare earth element geochemistry of oceanic ferro-manganese nodules and associated sediments. Geochim. Cosmochim. Acta 45, 513-528.

Ernst, W.G., 1976, Mineral chemistry of eclogites and related rocks from the Voltri Group, Western Liguria, Italy. Schweizerische mineralogische und petrographische Mitteilungen 56, 293-343.

Ernst, W.G., 1977, Mineralogic study of eclogitic rocks from Alpe Arami, Lepontine Alps, southern Switzerland. J. of Petrol. 18, 371-398.

Ernst, W.G., Dal Piaz, G.V., 1978, Mineral parageneses of eclogitic rocks and related mafic schists of the Piemonte ophiolite nappe, Breuil-St. Jacques area, Italian Western Alps. Amer. Mineral. 63, 621-640.

Ewart, A., 1976, A petrological study of the younger Tongan andesites and dacites, and the olivine tholeiites of Nina Fo'ou Island, S.W. Pacific. Contrib. Mineral. Petrol. 58, 1-21.

Fairbrothers, G.E., Carr, M.J., Mayfield, D.G., 1978, Temporal magmatic variations at Boqueron Volcano, El Salvador. Contrib. Mineral. Petrol. 67, 1-9.

Feigenson, M.D., Hofmann, A.W., Spera, F.J., 1983, Case studies on the origin of basalt II. The transition from tholeiitic to alkalic volcanism on Kohala volcano. Hawaii. Contrib. Mineral. Petrol. 84, 390-405.

Flanagan, F.J., 1978, Reference samples for the earth sciences. Geochim. Cosmochim. Acta 38, 1731-1744.

Ford, C.E., Russel, D.G., Craven, J.A., Fisk, M.R., 1983, Olivine-liquid equilibria: temperature, pressure, and composition dependence of the crystal/liquid cation partition coefficients for Mg, Fe^{2+}, Ca, and Mn. J. Petrol. 24, 256-265.

Francis, P.W., Roobal, M.J., Coward, M.P., Cobbold, D.R., Walker, G.P.L., 1974, The San Pedro and San Pablo volcanoes of northern Chile and their hot avalanche deposits. Geol. Rundsch. 63, 357-388.

Francis, P.W., Thorpe, R.S., Moorbath, S., Kretzschmar, G.A., Hammill, M., 1980, Strontium isotope evidence for crustal contamination of calc-alkaline volcanic rocks from Cerro Galan, northwest Argentina. Earth Planet. Sci. Lett. 48, 257-267.

Frey, F.A., Gerlach, D.C., Hickey, R.L., Lopez-Escobar, L., Munizaga-Villavicencio, F., 1984, Petrogenesis of the Laguna del Maule volcanic complex, Chile (36°S). Contrib. Mineral. Petrol. 88, 133-149.

Frey, F.A., Green, D.H., Roy, S.D., 1978, Integrated models of basalt petrogenesis: a study of quartz tholeiites to olivine melilitites from southeastern Australia utilizing geochemical and experimental petrological data. J. Petrol. 19, 463-513.

Fujimaki, H., Tatsumoto, M., Aoki, K., 1984, Partition coefficients of Hf, Zr, and REE between phenocrysts and groundmasses. J. Geophys. Res. 89, B662-672.

Gerlach, D.C., Grove, T.L., 1982, Petrology of Medicine Lake Highland Volcanics: characterization of endmembers of magma mixing. Contrib. Mineral. Petrol. 80, 147-159.

Gerlach, D.C., Frey, F.A., Hickey, R., Moreno-Roa, H., Hildreth, W., 1983, Geochemistry of Puyehue Volcano and Cordon Caulle, Southern Andes (40.5°S). Trans. Amer. Geophys. Union EOS 64, 326.

Gill, J., 1981, Orogenic Andesites and Plate Tectonics, Springer-Verlag.

Gladney, E.S., Goode, W.E., 1981, Elemental concentrations in eight new United States Geological Survey rock standards: a review. Geostandards Newsletter 5, 31-64.

Gladney, E.S., Burns, C.E., 1983, 1982 compilation of elemental concentrations in eleven United States Geological Survey rock standards. Geostandards Newsletter 7, 3-60.

Gonzalez-Ferran, O., 1970, Evolucion del volcanismo y tectonica de los Andes Centrales de Sudamerica durante el Cenozoico superior. Perfil de Arica a Potosi. IX Asamblea General del I.P.P.H., Washington, D.C., 97-101.

Gorton, M.P., 1977, The geochemistry and origin of Quaternary volcanism in the New Hebrides. Geochim. Cosmochim. Acta 41, 1257-1270.

Green, T.H., 1981, Experimental evidence for the role of accessory phases in magma genesis. J. Volc. Geotherm. Res. 10, 405-422.

Grove, T.L., Baker, M.B., 1983, Effects of melt density on magma mixing in calcalkaline series lavas. Nature 305, 416-418.

Grove T.L., Baker M.B., 1984, Phase equilibrium controls on the tholeiitic vs calc-alkaline differentiation trends. J. Geophys. Res. 89, No. B5, 3253-3274.

Grove, T.L., Bryan, W.B., 1983, Fractionation of pyroxene-phyric MORB at low pressure: an experimental study. Contrib. Mineral. Petrol. 84, 293-309.

Grove, T.L., Gerlach, D.C., Sando, T.W., 1982, Origin of calc-alkaline series lavas at Medicine Lake volcano by fractionation, assimilation, and mixing. Contrib. Mineral. Petrol. 80, 160-182.

Grove, T.L., Gerlach, D.C., Sando, T.W., Baker, M.B., 1983, Origin of calcalkaline series lavas at Medicine Lake Volcano by fractionation, assimilation, and mixing: corrections and clarifications. Contrib. Mineral. Petrol. 82, 407-408.

Grunder, A.L., 1983, The Calabozos volcanic system: a major Quaternary silicic center in the Central Chilean Andes, Trans. Amer. Geophys. Union, EOS 64, 326.

Grunder, A.L., 1984, The evolution of a zoned intermediate to silicic magma system at the Calabozos caldera in the Andes of Central Chile. Prof. Conf. Open Magma Systems (Dungan, M.A., Grove, T.L., Hildreth, W., eds.) Southern Methodist University, Dallas, 63-65.

Grutzeck, M., Kridelbaugh, S., Weill, D., 1974, The distribution of Sr and REE between diopside and silicate melt. Geophys. Res. Letts. 1, 273-275.

Guest, J.E., 1969, Upper Tertiary ignimbrites in the Andean Cordillera of part of the Antofagasta Province, northern Chile. Geol. Soc. Amer. Bull. 80, 337-362.

Hamilton, D.L., Burnham, C.W., Osborn, E.F., 1964, The solubility of water and effects of oxygen fugacity and water content on crystallization in mafic magmas. J. Petrol. 5, 21-39.

Hanus, V., Vanek, J., 1978, Morphology of the Andean Wadati-Benioff Zone, andesitic volcanism, and tectonic features of the NAZCA plate. Tectonophysics 44, 65-77.

Harmon, R.S., Moorbath, S., McHugh, J.M., 1983, O-, Sr-, and Pb-isotope relationships in Recent Andean volcanics. EOS 64, 325.

Harrington, R., Amini, H., Stern, C.R., Charrier, R., 1984, The Maipo stratovolcano-caldera complex in the southern Andes of central Chile. Trans. Amer. Geophys. Union 65, 1136.

Harrison, T.M., Watson, E.B., 1984, The behaviour of apatite during crustal anatexis: equilibrium and kinetic considerations. Geochim. Cosmochim. Acta 48, 1467-1477.

Hart, S.R., 1976, LIL-element geochemistry, Leg 34 basalts, D.S.D.P. Leg 34, in Initial Reports of the Deep Sea Drilling Project, v. 34, 763-768 (U.S. Government Printing Office).

Hart, S.R., 1984, A large-scale isotopic anomaly in the Southern Hemisphere mantle. Nature 309, 753-757.

Hart, S.R., Brooks, C., 1977, The geochemistry and evolution of the early Precambrian mantle. Contrib. Mineral. Petrol. 61, 109-128.

Hart, S.R., Davis K.E., 1978, Nickel partitioning between olivine and silicate melt. Earth Planet. Sci. Letts. 40, 203-219.

Hawkesworth, C.J., Norry, M.J., Roddick, J.C., Baker, P.E., 1979, $^{143}Nd/^{144}Nd$, $^{87}Sr/^{86}Sr$, and incompatible element variations in calc-alkaline andesites and plateau lavas from South America. Earth. Planet. Sci. Lett. 42, 45-57.

Hawkesworth, C. J., Hammill, M., Gledhill, A.R., Van Calsteren, P., Rogers, G., 1982, Isotope and trace element evidence for late-stage intra-crustal melting in the High Andes. Earth. Planet. Sci. Lett. 58, 240-254.

Hawkesworth, C.J., O'Nions, R.K., Pankhurst, R.J., Hamilton, P.J., Evensen, N.M., 1977, A geochemical study of island arc and back arc tholeiites from the Scotia Sea. Earth Planet. Sci. Lett. 36, 253-262.

Hawkesworth, C.J., O'Nions, R.K., Arculus, R.J., 1979 $^{143}Nd/^{144}Nd$ and $^{87}Sr/^{86}Sr$ geochemistry of the alkalic rock suite, Grenada, Lesser Antilles. Earth Planet. Sci. Lett. 45, 237-248.

Herron, E.M., 1981, Chile margin near lat. 38°S: evidence for a genetic relationship between continental and marine geologic features or a case of curious coincidences? Mem. Geol. Soc. Amer. 154, 755-760.

Herron, E.M., Cande, S.C., Hall, B.R., 1981, An active spreading center collides with a subduction zone: A geophysical survey of the Chile margin triple junction. Mem. Geol. Soc. Amer. 154, 683-702.

Herve, F., Moreno, H., Parada, M.A., 1974, Granitoids of the Andean range of Valdivia Province, Chile. Pacific Geology 8, 39-45.

Hickey, R.L., Frey, F.A., 1984, Sources for arc volcanics: evidence from Central South Chilean Basalts. Proc. Conf. Open Magma Systems (Dungan, M.A., Grove, T.L., Hildreth, W., eds.) Southern Methodist University, Dallas, 76-78.

Hickey, R.L., Frey, F., Gerlach, D., Lopez-Escobar, L. 1983, Isotopic and trace element data bearing on the origin of volcanic rocks from Central South Chile. Trans. Amer. Geophys. Union EOS 64, 326.

Hickey, R.L., Gerlach, D.C., Frey, F.A., 1984, Geochemical variations in volcanic rocks from central south Chile (33°-42°S): implications for their petrogenesis, in, Andean Magmatism: chemical and isotopic constraints (R.S. Harmon, B. Barreiro, eds.), Shiva Publ. Ltd., England, 72-95.

Hickey, R.L., Frey, F.A., Gerlach, D.C., Multiple sources for basaltic arc rocks from central south Chile: trace element and isotopic evidence for contributions from subducted oceanic crust, mantle and continental crust. J. Geophys. Res., in press.

Hildreth, W., 1979, The Bishop Tuff: evidence for the origin of compositional zonation in silicic magma chambers. Geol. Soc. Amer. Spec. Paper 180, 43-75.

Hildreth, W., 1981, Gradients in silicic magma chambers: implications for lithospheric magmatism. J. Geophys. Res. 86, 10153-10193.

Hildreth, W., Drake, R.E., 1983, 1932 eruption of Quizapu, central Chilean Andes. Geol. Soc. Amer. Abstracts with Progs. 15, 390.

Hildreth, W., Grunder, A.L., Drake, R.E., 1984, The Loma Seca Tuff and the Calabozos Caldera: a major ash-flow and caldera complex in the Southern Andes of Central Chile. Geol. Soc. Amer. Bull. 95, 45-54.

Hofmann, A.W., Feigenson, M.D., 1983, Case studies on the origin of basalt I. Theory and reassessment of Grenada lavas. Contrib. Mineral. Petrol. 84, 382-389.

Hofmann, A.W., Feigenson, M.D., Raczek, I., 1984, Case studies on the origin of basalt: III. Petrogenesis of the Mauna Ulu eruption, Kilauea, 1969-1971. Contrib. Mineral. Petrol. 84, 24-35.

Hofmann, A.W., Hart, S.R., 1978, An assessment of local and regional isotopic equilibrium in the mantle. Earth Planet. Sci. Lett. 38, 44-62.

Hofmann, A.W., Jochum, K.P., Seufert, H.M., White, W.M., 1983, The compatibility sequence of trace elements in MORB and the properties of two-stage melting models. Terra Cognita 3, 123.

Hole, M.J., Saunders, A.D., Marriner, G.F., Tarney, J., 1984, Subduction of pelagic sediments: implications for the origin of Ce-anomalous basalts from the Mariana Islands. J. Geol. Soc. London 141, 453-472.

Huppert, H.E., Sparks, R.S.J., 1980, The fluid dynamics of a basaltic magma chamber replenished by influx of hot dense ultrabasic magma. Contrib. Mineral. Petrol. 75, 279-289.

Huppert, H.E., Sparks, R.S.J., Turner, J.S., 1982, Effects of volatiles on mixing in calcalkaline magma systems. Nature 297, 554-557.

Ila, P., Frey, F.A., Utilization of neutron activation analysis in the study of geologic materials, Atomkernenergie Kerntectnik, in press.

Irving, A.J., 1978, A review of experimental studies of crystal/liquid trace element partitioning. Geochim. Cosmochim. Acta 42, 743-770.

James, D.E., 1981, Role of subducted continental material in the genesis of calcalkaline volcanics of the Central Andes. Mem. Geol. Soc. Amer. 154, 769-790.

James, D.E., 1982, A combined O, Sr, Nd, and Pb isotopic and trace element study of crustal contamination in central Andean lavas: I. Local geochemical variations. Earth Planet. Sci. Lett. 57, 47-62.

James, D.E., Murcia, L.A., 1984, Crustal contamination in northern Andean volcanics. J. Geol. Soc. London 141, 823-830.

Johannes, W., 1978, Melting of plagioclase in the system Ab-An-H_2O and Qz-Ab-An-H_2O at P_{H_2O} = 5 kb, an equilibrium problem. Contrib. Mineral. Petrol. 66, 295-303.

Johnson, R.W., 1981, Island arc basalts. In: Basaltic Volcanism on the Terrestrial Planets, Basaltic Volcanism Study Project, Pergamon Press, New York, 193-213.

Johnson, R.W., Arculus, R.J., 1978, Volcanic rocks of the Witu Islands, Papua, New Guinea: the origin of magmas above the deepest part of the New Britain Benioff zone. Bull. Volcanol. 41, 609-655.

Johnson, R.W., Jaques, L., Hickey, R.L., McKee, C.O., Chappell, B.W., Manam Island, Papua New Guinea: petrology and geochemistry of a low-TiO_2 basaltic island-arc volcano. J. Petrol., in press.

Jordan, T.E., Isacks, B.I., Allmendinger, R.W., Brewer, J.A., Ramos, V.A. Ando, C.J., 1983, Andean tectonics related to geometry of subducted Nazca plate. Geol. Soc. Amer. Bull. 94, 341-361.

Katsui, Y., 1972, Late Cenozoic volcanism and petrographic provinces in the Andes and Antarctica. J. Fac. Sci. Hokkaido Univ. Series IV, 25, 27-41.

Katsui, Y., Katz, H.R., 1967, Lateral fissure eruptions in the southern Andes of Chile. J. Fac. Sci. Hokkaido Univ. Series IV, 13, 433-448.

Kay, R.W., 1980, Volcanic arc magmas: implications of a melting-mixing model for element recycling in the crust-upper mantle system. J. Geol. 88, 497-522.

Kay, R.W., 1984, Elemental abundances relevant to identification of magma sources. Phil. Trans. Roy. Soc. London A310, 535-547.

Kay, R.W., Sun, S.S., Lee-Ha, C.-N., 1978, Pb and Sr isotopes in volcanic rocks from the Aleutian Islands and the Pribilof Islands, Alaska. Geochim. Cosmochim. Acta 42, 263-273.

Kay, S.M., Kay, R.W., Citron, G.P., 1982, Tectonic controls on tholeiitic and calc-alkaline magmatism in the Aleutian arc. J. Geophys. Res. 87, 4051-4072.

Kienle, J., Kyle, P.R., Self, S., Motyka, R.J., Lorenz, V., 1980, Ukinrek Maars, Alaska, I. April 1977 eruption sequence, petrology and tectonic setting. J. Volc. Geotherm. Res. 7, 11-37.

Kilinc, A., Carmichael, I.S.E., Rivers, M.L., Sack, R.O., 1983, The ferric-ferrous ratio of natural silicate liquids equilibrated in air. Contrib. Mineral. Petrol. 83, 136-140.

Klerkx, J., Deutsch, S., Pichler, H., Zeil, W., 1977, Strontium isotopic composition and trace element data bearing on the origin of Cenozoic volcanic rocks of the central and southern Andes. J. Volc. Geoth. Res. 2, 49-71.

Kuno, H., 1968, Differentiation of basalt magmas, in, Basalt: The Poldervaart treatise on rocks of basaltic composition, v. 2 (H.H. Hess, A. Poldervaart, eds.), John Wiley & Sons, Inc., New York, 623-688.

Kuno, 1969, Pigeonite-bearing andesite and associated dacite from Asio, Japan. Amer. J. Sci. 267-A, 257-268.

Kurasawa, H., Leeman, W.P., Smith;, D.R., 1982, Strontium isotopic studies of Mt. St. Helens volcano. Trans. Amer. Geophys. Union EOS 63, 457.

Langmuir, C.H., Vocke, R.D., Jr., Hanson, G.N., Hart, S.R., 1978, A general mixing equation with applications to Icelandic basalts. Earth Planet. Sci. Lett. 37, 380-392.

Leeman, W.P., 1976, Petrogenesis of McKinney (Snake River) olivine tholeiite in light of rare earth element and Cr/Ni distributions. Geol. Soc. Amer. Bull. 87, 1582-1586.

Leeman, W.P., Lindstrom, D.J., 1978, Partitioning of Ni^{2+} between basaltic and synthetic melts and olivines - an experimental study. Geochim. Cosmochim. Acta 42, 801-816.

Leeman, W.P., Scheidegger, K.F., 1977, Olivine-liquid distribution coefficients and a test for crystal-liquid equilibrium. Earth Planet. Sci. Lett. 35, 247-257.

Leeman, W.P., Ma, M.-S., Murali, A.V., Schmitt, R.A., 1978, Empirical estimation of magnetite/liquid distribution coefficients for some transition elements. Contrib. Mineral. Petrol. 65, 269-272.

Lindstrom, D.L., Korotev, R.L., 1982, TEABAGS: Computer programs for instrumental neutron activation analysis. Jour. Radioanal. Chem. 70, 439-458.

Lindstrom, D.J., Weill, D.F., 1978, Partitioning of transition metals between diopside and coexisting silicate liquids. Geochim. Cosmochim. Acta 42, 817-831.

Lomnitz, C., 1962, On Andean structure. J. Geophys. Res. 76, 351-363.

Lopez-Escobar, L., Frey, F.A., Vergara, M., 1977, Andesites and high-alumina basalts from the central-south Chilean high Andes: Geochemical evidence bearing on their petrogenesis. Contrib. Mineral Petrol. 63, 199-228.

Lopez-Escobar, L., Moreno, H., Tagiri, M., Notsu, K., Onuma, N., Geochemistry and petrology of lavas from San Jose Volcano, Southern Andes (33°45'S), in prep.

Lowrie, A., Hey, R., 1981, Geological and geophysical variations along the western margin of Chile near lat. 33° to 36°S and their reaction to Nazca plate subduction. Mem. Geol. Soc. Amer. 154, 741-754.

Maaloe, S., Scheie, A., 1982, The permeability controlled accumulation of primary magma. Contrib. Mineral. Petrol. 81, 350-357.

Mahood, G., Hildreth, W., 1983, Large partition coefficients for trace elements in high-silica rhyolites. Geochim. Cosmochim. Acta 47, 11-30.

Manhes, G., Minster, J.-F., Allegre, C.J., 1978, Comparative uranium-thorium-lead and rubidium strontium of St. Severin amphoterite: consequences for early solar system chronology. Earth Planet. Sci. Lett. 39, 14-24.

Mann, A.C., 1983, Trace element geochemistry of high alumina basalt-andeite-dacite-rhyodacite lavas of the Main Volcanic Series of Santorini Volcano, Greece. Contrib. Mineral. Petrol. 84, 43-57.

Masuda, Y., Nishimura, S., Ikeda, T., Katsui, Y., 1975, Rare-earth and trace elements in the Quaternary volcanic rocks of Hokkaido, Japan. Chem. Geol. 15, 251-271.

Masuda, A., Nakamura, N., Tanaka, T., 1973, Fine structures of mutually normalized rare-earth patterns of chondrites. Geochim. Cosmochim. Acta 37, 239-248.

Marsh, B., 1979, Island arc development: some observations, experiments, and speculation. J. Geol. 87, 687-714.

Marsh, B., 1982, On the mechanics of igneous diapirism, stoping, and zone melting. Amer. J. Sci. 282, 808-855.

McCallum, I.S., Charette, M.P., 1978, Zr and Nb partition coefficients: implications for the genesis of mare basalts, KREEP, and sea-floor basalts. Geochim. Cosmochim. Acta 42, 859-869.

McCulloch, M.T., Perfit, M.R., 1981, $^{143}Nd/^{144}Nd$, $^{87}Sr/^{86}Sr$, and trace element constraints on the petrogenesis of Aleutian island arc magmas. Earth Planet. Sci. Lett. 56, 167-179.

McKay, G.A., Weill, D.F., 1976, Petrogenesis of KREEP. Proc. Lunar Sci. Conf. VII, 2426-2447.

McKay, G.A., Weill, D.F., 1977, KREEP petrogenesis revisited. Proc. Lunar Sci. Conf. VIII, 2339-2355.

McKenzie, D., 1984, The generation and compaction of partially molten rocks. J. Petrol. 25, 713-765.

Meijer, A., 1976, Pb and Sr isotopic data bearing on the origin of lavas from the Mariana arc system. Geol. Soc. Amer. Bull. 87, 1358-1369.

Menzies, M.A., Wass, S.Y., 1983, CO_2 and LREE-rich mantle below eastern Australia: a REE and isotopic study of alkaline magmas and apatite-rich mantle xenoliths from the Southern Highlands Province, Australia. Earth Planet. Sci. Lett. 65, 287-302.

Merzbacher, C., Eggler, D.H., 1984, A magmatic geohygrometer: Application to Mt. St. Helens and other dacitic magmas. Geology 12, 587-590.

Minster, J.F., Allegre, C.J., 1978, Systematic use of trace elements in igneous processes. Part III: Inverse problem of batch partial melting in volcanic suites. Contrib. Mineral. Petrol. 68, 37-52.

Misra, N.K., Venkatasubramanian, V.S., 1977, Strontium diffusion in feldspars; a laboratory study. Geochim. Cosmochim. Acta 41, 837-838.

Miyashiro, A., 1974, Volcanic rock series in island arcs and active continental margins. Amer. J. Sci. 274, 321-355.

Moreno-Roa, H., 1974, Airplane flight over active volcanoes of central-south Chile. IAVCEI Guide book excursion D-3, Int. Symposium Volcanology Andean and Antarctic Volcanology Problems, Santiago, Chile, 56 pp.

Moreno-Roa, H., Parada, M.A., 1976, Esquema geologico de la Cordillera de los Andes entre los paralelos 39°00' y 41°30'S. I. Congreso Geol. Chileno (Universidad de Chile) V. I, A213-A226.

Moreno-Roa, H.A., 1976, The upper Cenozoic volcanism in the Andes of southern Chile (from 40°00' to 41°30' S.L.). Proc. Symposium Andean and Antarctic Volcanology Problems (Gonzalez-Ferra, O., ed.), IAVCEI Special Series, Rome, 143-171.

Moreno-Roa, H.A., Geologia del area volcanica Puyehue Carran en Los Andes del sur de Chile, Thesis, Univ. de Chile, Santiago, 170 pp.

Morris, J.D., 1984, Enriched geochemical signatures in Aleutian and Indonesian arc lavas: an isotopic and trace element investigation. Ph.D. thesis, Mass. Inst. of Technology.

Morris, J.D., Hart, S.R., 1983, Isotopic and incompatible element constraints on the genesis of island arc volcanics, Cold Bay and Amak Island, Aleutians, and implications for mantle structure. Geochim. Cosmochim. Acta, 47, 2015-2030.

Morris, J.D., Jezek, P.A., Hart, S.R., Gill, J.B., 1983, The Halmahera island arc, Molucca sea collision zone, Indonesia: a geochemical survey. In: The Tectonic and Geologic Evolution of Southeast Asian seas and islands, Part 2 (Hayes, D.E., ed.) Amer. Geophys. Union Monograph 27, 373-387.

Myers, J.D., Marsh, B.D., Sinha, A.K., 1984, Pb-isotopic data from two Aleutian volcanic centers: additional evidence for the evolution of lithospheric plumbing systems. Trans. Amer. Geophys. Union EOS 65, 1135.

Myers, J.D., Sinha, A.K., Marsh, B.D., 1984, Assimilation of crustal material by basaltic magma: strontium isotopic and trace element data from the Edgecumbe volcanic field, SE Alaska. J. Petrol. 25, 1-26.

Myers, J.D., Marsh, B.D., Sinha, A.K., Strontium isotopic and selected trace element variations between two Aleutian volcanic centers (Adak and Atka): implications for the development of arc volcanic plumbing systems. J. Geol., in press.

Mysen, B.O., 1983, Rare earth element partitioning between (H_2O+CO_2) vapor and upper mantle minerals: exprimental data bearing on the conditions of formation of alkali basalt and kimberlite. Neues Jahrbuch Miner. Abh. 146, 41-65.

Nakamura, Y., Kushiro, I., 1970, Compositional relations of coexisting orthopyroxene, pigeonite and augite in a tholeiitic andesite from Hakone Volcano. Contrib. Mineral. Petrol. 26, 265-275.

Nicholls, I.A., Harris, K.L., 1980, Experimental rare earth element partition coefficients for garnet, clinopyroxene, and amphibole coexisting with andesitic and basaltic liquids. Geochim. Cosmochim. Acta 44, 287-308.

Noble, D.C., 1970, Loss of sodium from crystallized comendite welded tuffs of the Miocene Grouse Canyon member of the Belted Range Tuff, Nevada. Geol. Soc. Amer. Bull. 81, 2677-2688.

O'Hara, M.J., 1984, Evolution of very highly incompatible (VHI) element concentrations and ratios in refilled, tapped, and fractionated (RTF) magma chambers: effects of varying the magnitude of the parameters, x, y, and the simulation of effects of small mass fractions of perfect fractional (PFPM) and continuous partial (CPM) melting. Proc. Conf. Open Magma Systems (Dungan, M.A., Grove, T.L., Hildreth, W., eds.) Southern Methodist University, Dallas, 122-124.

O'Hara, M.J., Mathews, R.E., 1981, Geochemical evolution in an advancing, periodically replenished, periodically tapped, continuously fractionated magma chamber. J. Geol. Soc. London 138, 237-277.

Oversby, V.M., Ewart, A., 1972, Lead isotopic compositions of Tonga-Kermadec volcanics and their petrogenetic significance. Contrib. Mineral. Petrol. 37, 181-210.

Papavassiliou, C.T., Cosgrove, M.E., 1982, The geochemistry of D.S.D.P. sediments from site 223, Indian Ocean. Chem. Geol. 37, 299-315.

Patchett, P.J., 1980, Thermal effects of basalt on continental crust and crustal contamination of magmas. Nature 283, 559-561.

Peccerillo, A., Taylor, S.R., 1976, Geochemistry of Eocene calcalkaline volcanic rocks from the Kastamonu area, northern Turkey. Contrib. Mineral. Petrol. 58, 63-81.

Pegram, B.J., 1985, The isotope, trace-element, and major-element geochemistry of the Mesozoic Appalachian tholeiite province. Ph.D. thesis, Mass. Inst. of Technology.

Perfit, M.R., Gust, D.A., Bence, A.E., Arculus, R.J., Taylor, S.R., 1980, Chemical characteristics of island-arc basalts: Implications for mantle sources. Chem. Geol. 30, 227-256.

Perfit, M.R., Gust, C.A., 1981, Petrochemistry and experimental crystallization of basalts from the Aleutian Islands, Alaska. IAVCEI Symposium Arc Volcanism, Tokyo-Hakone, 288-289.

Pichler, H., Zeil, W., 1972, The Cenozoic rhyolite-andesite association of the Chilean Andes. Bull. Volcanol. 35, 424-452.

Pichler, H., Hormann, P.K., Braun, A.F., 1976, First petrologic data on lavas of the volcano El Reventador (eastern Ecuador). Munster. Forsch. Geol. Palaont. 38/39, 129-141.

Ramirez, J.E., 1968, Los Volcans de Colombia. Rev. Acad. Colomb. Ciencos Exactos 13, 227-235.

Rhodes, J.M., Blanchard, D.P., Rodgers, K.V., Jacobs, J.W., Brannon, J.C., 1976, Petrology and chemistry of basalts from the Nazca plate. Part 2. Major-and trace element geochemistry. In, Initial Reports of the Deep Sea Drilling Project 34, 239-244 (U.S. Government Printing Office).

Richard, P., Shimizu, N., Allegre, C.J., 1976, $^{143}Nd/^{146}Nd$, a natural tracer: an application to natural basalts. Earth Planet. Sci. Lett. 31, 269-278.

Richardson, S.H., 1984, Evolution of enriched mantle from derivative basalt, peridotite, and diamond inclusion geochemistry. Ph.D. thesis, Mass. Inst. of Technology.

Ritchey, J.L., 1980, Divergent magmas at Crater Lake, Oregon: products of fractional crystallization and vertical zoning in a shallow, water-undersaturated chamber. J. Volc. Geotherm. Res. 7, 373-386.

Roden, M.F., Frey, F.A., Francis, D.M., 1984, An example of consequent mantle metasomatism in peridotite inclusions from Nunivak Island, Alaska. J. Petrol. 25, 546-577.

Roobol, M.J., Francis, P.W., Ridley, W.I., Rhodes, M., Walker, G.P.L., 1976, Physico-chemical characteristics of the Andean volcanic chain between 21° and 22° south. Proc. Symposium Andean and Antarctic Volcanology Problems (Gonzalez-Ferran, O., ed.), IAVCEI Special Series, Rome, 450-464.

Saint Amand, P., 1961, Observaciones y interpretacion de los Terremotos Chilenos de 1960. Com. Esc. Geol., Universidad de Chile, 1.

Sakuyama, M., 1981, Petrological study of the Myoko and Kurohime volcanoes, Japan: crystallization sequence and evidence for magma mixing. J. of Petrology 22, 553-583.

Saunders, A.D., Tarney, J., Weaver, S.D., 1980, Transverse geochemical variations across the Antarctic Peninsula: implications for the genesis of calcalkaline magmas. Earth Planet. Sci. Lett. 46, 344-360.

Schneider, M.E., Eggler, D.H., 1983, Compositions of fluids in equilibrium with peridotite: implications for alkaline magmatism-metasomatism. Proc. Int. Kimberlite Conf. III, in press.

Sekine, T., Wyllie, P.J., 1983, Experimental simulation of mantle hybridization in subduction zones. J. Geol. 91, 511-528.

Shackleton, R.M., Ries, A.C., Coward, M.P., Cobbold, P.R., 1979, Structure, metamorphism and geochronology of the Arequipa Massif of coastal Peru. J. Geol. Soc. London 136, 195-214.

Shaw, D.M., 1970, Trace element fractionation during anatexis. Geochim. Cosmochim. Acta 34, 237-243.

Shimizu, N., Arculus, R.J., 1975, Rare earth element concentrations in a suite of basanitoids and alkali olivine basalts from Grenada, Lesser Antilles. Contrib. Mineral. Petrol. 50, 231-240.

Shimokawa, T., Masuda, A., Izawa, K., 1972, Rare-earth elements in the top samples of the cores from the Pacific ocean floor. Geochem. J. 6, 75-81.

Smith, D.R., 1984, The petrology and geochemistry of High Cascade volcanics in southern Washington: Mt. St. Helens Volcano and the Indian Heaven basalt field. Ph.D. thesis, Rice University.

Sparks, R.S.J., Huppert, H.E., Kerr, R., Tait, S.R., Turner, J.S., 1984, The fluid dynamic behaviour of open system magma chambers. Proc. Conf. Open Magma System (Dungan, M.A., Grove, T.L., Hildreth, W., eds.) Southern Methodist University, Dallas, 146-148.

Spencer, K.J., Lindsley, D.H., 1981, A solution model for coexisting iron-titanium oxides. Amer. Mineral. 66, 1189-1201.

Spulber, S.D., Rutherford, M.J., 1983, The origin of rhyolite and plagiogranite in oceanic crust: an experimental study. J. Petrol. 24, 1-25.

Stauder, W., 1973, Mechanism and spatial distribution of Chilean earthquakes with relation to subduction of the oceanic plates. J. Geophys. Res. 78, 5033-5061.

Stauder, W., 1975, Subduction of the Nazca plate under Peru as evidenced by focal mechanisms and by seismicity. J. Geophys. Res. 80, 1053-1064.

Stern, C.R., Skewes, M.A., Duran, M., 1976, Volcanismo calcalkaline en Chile austral. Actas Primero Congreso Geologico Chileno 2, 195-212.

Stern, C.R., Futa, K., Muehlenbachs, K., 1983, Trace element and isotopic constraints on the origin of Recent calc-alkaline andesites of southernmost Chile. Trans. Amer. Geophys. Union EOS 64, 326.

Stern, R.J., Ito, E., 1983, Trace-element and isotopic constraints on the source of magmas in the active Volcano and Mariana island arcs, Western Pacific. J. Volc. Geotherm. Res. 18, 461-482.

Strelow, F.W.E., Toerien, F. von S., 1966, Separation of lead (II) from bismuth (III), thalium (III), cadmium (II), mercury (II), gold (III), platinum (IV), palladium (II), and other elements by anion exchange chromatography. Anal. Chem. 38, 545-548.

Sun, S.-S., 1980, Lead isotopic study of young volcanic rocks from mid-ocean ridges, ocean islands and island arcs. Phil. Trans. R. Soc. Lond. A297, 409-445.

Sun, S.S., Nesbitt, R.W., Sharaskin, A.Y., 1979, Geochemical characteristics of mid-ocean ridge basalts. Earth Planet. Sci. Lett. 44, 119-138.

Sun, C.O., Williams, R.J., Sun, S.-S., 1974, Distribution coefficients of Eu and Sr for plagioclase-liquid and clinopyroxene-liquid in oceanic ridge basalt: an experimental study. Geochim. Cosmochim. Acta, 38, 1415-1433.

Swift, S.A., Carr, M.J., 1974, The segmented nature of the Chilean seismic zone. Phys. of Earth & Plan. Int. 9, 183-191.

Takahashi, E., Kushiro, I., 1983, Melting of a dry peridotite at high pressures and basalt magma genesis. Amer. Mineral. 68, 859-879.

Tarney, J., Wood, D.A., Saunders, A.D., Cann, J.R., Varet, J., 1980, Nature of mantle heterogeneity in the North Atlantic: evidence from deep-sea drilling. Phil. Trans. Roy. Soc. London A297, 179-202.

Taylor, S.R., McLennan, S.M., 1981, The composition and evolution of the continental crust: rare earth evidence from sedimentary rocks. Phil. Trans. Roy. Soc. London A301, 381-399.

Thirlwall, M.F., Graham, A.M., 1984, Evolution of high-Ca, high-Sr C-series basalts from Grenada, Lesser Antilles: the effects of intra-crustal contamination. J. Geol. Soc. London 141, 427-445.

Thompson, G., Bryan, W.B., Frey, F.A., Dickey, J.S., Suen, C.J., 1976, Petrology and geochemistry of basalts from D.S.D.P. Leg 34, Nazca plate. In, Initial Reports of the Deep Sea Drilling Project 34, 215-226 (U.S. Government Printing Office).

Thorpe, R.S., 1984, The tectonic setting of active Andean volcanism. In: Andean Magmatism: chemical and isotopic constraints (R.S. Harmon, B. Barreiro, eds.), Shiva Publ. Ltd., England, 4-8.

Thorpe, R.S., Potts, P.J., Francis, P.W., 1976, Rare earth data and petrogenesis of andesite from the North Chilean Andes. Contrib. Mineral. Petrol. 54, 65-78.

Thompson, G., W.B. Bryan, F.A. Frey, J.S. Dickey, J. Suen, 1976, Petrology and geochemistry of basalts from DSDP Leg 34 NAZCA Plate In, Initial Reports of the Deep Sea Drilling Project, Volume 34, Washington, D.C. (U.S. Government Printing Office), 215-226.

Thorpe, R.S., ed., 1982, Andesites: Orogenic Andesites and Related Rocks, J. Wiley & Sons, 724 pp.

Thorpe, R.S., Francis, P.W., 1979, Variations in Andean andesite compositions and their petrogenetic significance. Tectonophysics 57, 53-70.

Thorpe, R.S., Francis, P.W., Moorbath, S., 1979, Rare earth and strontium isotope evidence concerning the petrogenesis of North Chilean ignimbrites. Earth Planet. Sci. Letts. 42, 359-367.

Veyl, C., 1960, Los fenomenos volcanicos y sismicos de fines de Mayo de 1960 en el Sur de Chile. Inst. Cent. Quim., Depto. Geol. Min., Universidad de Concepcion, Chile.

Walker, D., Shibata, T., DeLong, S.F., 1979, Abyssal tholeiites from the Oceanographer Fracture Zone II: Phase equilibrium and mixing. Contrib. Mineral. Petrol. 70, 111-125.

Watson, E.B., 1980, Apatite and phosphorus in mantle source regions: an experimental study of apatite/melt equilibria at pressures to 25 Kb. Earth Planet. Sci. Lett. 51, 322-335.

Watson, E.B., 1982, Basalt contamination by continental crust: some experiments and models. Contrib. Mineral. Petrol. 80, 73-87.

Watson, E.B. Capobianco, C.J., 1981, Phosphorus and the REE elements in felsic magmas: an assessment of the role of apatite. Geochim. Cosmmochim. Acta 45, 2349-2358.

Watson, E.B., Green, T.H., 1981, Apatite/liquid partition coefficients for the rare earth elemeents and strontium. Earth Planet. Sci. Lett. 56, 405-421.

Watson, E.B., Harrison, T. M., 1983, Zircon saturation revisited; temperature and composition effects in a variety of crustal magma types. In press.

Watson, E.B., Jurewicz, S.R., Behavior of alkalies during diffusive interaction of granitic xenoliths with basaltic magma. J. Geol., in press.

Weill, D.F., Drake, M.J., 1973, Europium anomaly in plagioclase feldspar: experimental results and semiquantitative model. Science 180, 1059-1060.

Wood, D.A., Gibson, I.L., Thompson, R.N., 1976, Elemental mobility during zeolite facies metamorphism of the Tertiary basalts of E. Iceland. Contrib. Mineral. Petrol. 55, 241-254.

Wood, D.A., Joron, J.-L., Treuil, M., Norry, M., Tarney, J., 1979, Elemental and Sr-isotope variation in basic lavas from Iceland and the surrounding ocean floor. Contrib. Mineral. Petrol. 70, 319-339.

Wortel, M.J.R., Vlaar, N.J., 1978, Age-dependent subduction of oceanic lithosphere beneath western South America. Phys. of Earth & Plan. Int. 17, 201-208.

Zindler, A., 1980, Geochemical processes in the Earth's mantle and the nature of crust-mantle interactions: evidence from studies of Nd and Sr isotope ratios in mantle-derived igneous rocks and lherzolite nodules. Ph.D. Thesis, Mass. Inst. of Technology.

Zindler, A., Hart, S.R., Frey, F.A., Jakobsson, S.P., 1979, Nd and Sr isotope ratios and rare earth element abundances in Reykjanes Peninsula basalts: evidence for mantle heterogeneity beneath Iceland. Earth Planet. Sci. Lett. 45, 249-262.

Appendix 1: Analytical methods

A.1: Mineral compositions

Compositions of phenocrysts were obtained with an automated 3-spectrometer MAC-5 electron microprobe with on-line data reduction employing the matrix correction procedures of Bence and Albee (1968) with modifications of Albee and Ray (1970). Appropriate natural and synthetic mineral compositions were used as standards.

A.2: Sample preparation

The majority of samples were sawn in slabs, altered portions and saw marks were removed, and the slabs crushed by a hammer after wrapping in plastic. Other samples were crushed in a steel jaw crusher. All chips were cleaned in weak HCl and double-distilled H_2O and powdered in an agate shatterbox. Portions of chips prepared by this method were reserved for later powdering in a tungsten carbide shatterbox to investigate possible Pb contamination from the the jaw crusher and the agate shatterbox (see section A.5).

A.3: Major elements

Bulk rock major-element compositions were obtained by XRF analysis with the automated Siemens XRF analyzer with on-line data reduction in the University of Massachusetts, Amherst, Department of Geology and Geography. Analyses of standard rocks BCR-1 and GSP-1 are presented in Table A-1. Splits of powders for samples analyzed in this study were ignited, mixed with Johnson and Matthey Spectroflux 105, quickly fused at 1020°C in Pt(95%) + Au(5%) crucibles, and pressed into discs for analysis. Duplicate glass disc were prepared for each sample.

Table A-1 Analyses of standard rocks

	BHVO-1		BCR-1		GSP-1	
	this[1] study	consensus[2] values	this study (avg. of 26)	consensus values	this study (avg. of 5)	consensus values
SiO_2		49.9	54.31±33	54.35	67.7±17	67.37
Al_2O_3		13.8	13.41±5	13.63	15.01±7	15.16
$^3Fe_2O_3$		12.18	13.40±8	13.46	4.27±2	4.32
FeO		-		-	-	
MnO		0.17	0.18±1	0.18	0.04±1	0.04
MgO		7.14	3.32±3	3.45	0.67±3	0.99
CaO		11.4	6.95±3	6.95	2.00±1	2.04
Na_2O	2.24±1	2.21	3.37±19	3.27	2.61±13	2.80
K_2O		0.55	1.71±2	1.69	5.50±6	5.50
TiO_2		2.65	2.25±1	2.22	0.67±1	0.66
P_2O_5		0.29	0.38±1	0.37	0.28±1	0.28
Sc	31.5±1	30.2				
V	285.1±5.2	314				
Cr	284.±1.1	300				
Co	44.7±3	45				
Ni	116.9±2.4	117				
Zn	128.±11	102				
Ga	21.2±5	22				
Rb	9.0±3	10				
Sr	390.2±2.9	440				
Ba	129.±11	142				
Y	24.7±4	28				
Zr	181.9±2.4	180				
Nb	19.5±5	19				
Hf	4.24±10	4.2				
Ta	1.12±4	1.1				
Pb	4.6±1.1	4				
Th	1.15±8	1.1				
La	15.4±1	16.7				
Ce	39.9±2.4	41				
Nd	23.8±1.2	24				
Sm	5.93±24	6.1				
Eu	2.11±3	2.0				
Tb	0.95±7	1.0				
Yb	1.95±7	2.1				
Lu	0.28±1	0.32				

[1]analysis of BHVO-1 consists of average of 25 XRF analyses for V, Ni, Zn, Ga, Rb, Sr, Ba, Y, Zr, Nb, and Pb, and an average of 3 INAA analyses for Na_2O, Sc, Cr, Co, Hf, Ta, Th, and REE. $1\sigma_{mean}$ errors correspond to least significant digits.

[2]consensus values for BCR-1 and GSP-1 from Gladney and Burns (1983) and for BHVO-1 from Gladney and Goode (1981).

[3]total iron as Fe_2O_3.

Analyses were considered acceptable if deviations between the duplicate glass discs were approximately 0.5% or less for SiO_2, TiO_2, Al_2O_3, Fe_2O_3, MgO, CaO, and K_2O. Larger deviations (up to ~5%) were accepted for 1) Na_2O measurements due to low counting rates and the potential for sample contamination, 2) MnO and P_2O_5 measurements due to low contents in all samples, and 3) TiO_2, Fe_2O_3, MgO, MnO, and P_2O_5 measurements in rhyodacites and rhyolites due to low contents in these samples. Water and CO_2 contents were measured with an automated Perkin-Elmer CHN analyzer in the Department of Chemistry, Woods Hole Oceanographic Institution.

A.4: Trace elements

Abundances of selected trace elements were determined by XRF analysis of duplicate pressed powder discs with boric acid backing at the University of Massachusetts, Amherst, Department of Geology and Geography. Abundances of Rb, Sr, Y, Pb, and Ga were measured using a Mo tube and those of Nb, Zr, Zn, Ni, Cr, V, Ba, and also Sr were measured using a Au tube. Standard rock BHVO-1 was analyzed as a monitor in each run accompanying four sample unknowns in duplicate, and results are presented in Table A-1. The deviation in a particular trace element abundance measurement for duplicate discs is inversely correlated with abundance for most elements. This is shown in Table A-2 by average relative deviations for each element between discs as determined in basalts, basaltic andesites, andesites, and dacites to rhyolites. For example, the precision for Zr abundance measurements as monitored by duplicate discs increases from basalts to rhyolites (Table A-2). Examples of deviations between discs for individual samples are also listed in Table A-2.

Table A-2

Quality assessment of XRF trace element analyses of samples

	basalts (< 52% SiO_2)		basaltic andesites (52-56% SiO_2)	
	[1]mean relative deviation (%) [3](n=9,16)	[2]sample deviation (%) (13828)	mean relative deviation (%) (n=9,10)	sample deviation (%) (272827)
V	1.62	1.90	2.77	1.49
Cr	2.60	0.92	2.78	0.39
Ni	4.66	2.00	2.17	0.69
Zn	1.98	0.70	2.21	0.40
Ga	2.41	1.34	1.88	3.2
Rb	4.28	8.51	1.56	1.67
[4]Sr	0.37	0.43	0.26	0.20
Ba	4.24	-	-	-
[5]Sr	0.49	0.19	0.55	0.64
Y	1.63	1.10	0.98	0.44
Zr	2.0	4.78	0.83	0.55
Nb	9.5	5.7	5.6	12.0
Pb	18	39	11	25.5
Th	32	5.4	27	9.4

	andesites (56-63% SiO_2)		dacites to rhyolites (63-72% SiO_2)	
	mean relative deviation (%) [3](n=9,12)	sample deviation (%) (43821)	mean relative deviation (%) (n=26,32)	sample deviation (%) (42824a)
V	1.62	5.4	20	29.5
Cr	40	16	>100	>100
Ni	20	34	22	34.5
Zn	2.57	0.48	1.50	0.37
Ga	1.62	3.78	2.44	2.6
Rb	0.68	0.42	0.67	1.63
[4]Sr	0.20	0.37	0.38	0.97
Ba	1.1	3.0	0.81	-
[5]Sr	0.34	0.5	0.55	0.41
Y	0.39	0.11	0.24	0.55
Zr	0.67	1.30	0.41	0.59
Nb	7.8	6.0	3.2	8.1
Pb	9	5.6	3.5	5.0
Th	15	10.6	5.5	5.4

1 (standard deviation ÷ mean) x 100

2 for two duplicate pellets of one sample

3 n = # of XRF analyses. first number is total number of Mo-tube analyses for Ga, Rb, Sr, Y, Pb, Th, and second is number of Au-tube analyses for V, Cr, Ni, Zn, Sr, Ba Zr, and Nb.

4 Mo-tube analysis of Sr

5 Au-tube analysis of Sr

Abundances of Sr, Rb, and Ba for many samples were determined by both XRF analysis and isotope dilution methods, and comparisons are presented in Table A-3. Sr values determined by Mo-tube XRF analysis, considered more precise than Au-tube XRF analysis, agree well with abundances determined by isotope dilution (ID). Those determined by Au-tube XRF analysis are consistently higher than ID and Mo-tube XRF values (Table A-3) and this can be attributed to relative differences in mass absorption coefficients for Au tubes and Mo tubes. Mo-tube XRF determinations of Rb and Au-tube XRF analyses of Ba abundances agree reasonably well with isotope dilution values with a few exceptions, and the % difference between the two methods for specific samples in Table A-3 is approximately equivalent to 1σ uncertainties for multiple XRF analyses of BHVO-1 reported in Table A-1.

Instrumental neutron activation analysis (INAA) of selected samples was performed at M.I.T. using methods described by Ila and Frey (1984) and a data reduction algorithm (TEABAGS) of Lindstrom and Korotev (1983). Three splits of standard rock BHVO-1 were analyzed by INAA during this study and results with $1\sigma_{mean}$ uncertainties are presented in Table A-1. To monitor precision, eight sample splits of a basalt (13826h) and eleven splits of a rhyodacite (281822bh) were analyzed at various times during this study. From the results for these two samples, estimated uncertainties indicated by replicate analyses vary inversely with abundance. Mean abundances of replicate analyses of the basalt and the rhyodacite are listed in Table 4 with 1σ mean values. Maximum (1σ) uncertainties are observed for most elements in the basalt. These are: La(3%), Ce(5%), Nd(5%), Sm(6%), Eu(1%), Tb(8%), Yb(5%), Lu(3%), Hf(4%), Th (10%), and Ta25%). These figures are greater than typical counting

Table A-3. Comparison of Sr, Rb, and Ba abundances determined by XRF analysis and isotope dilution (ID) methods

Sample number	Sr				Rb			Ba		
	XRF(Mo)	XRF(Au)	ID	$\frac{XRF(Mo)-ID}{ID} \times 100$	XRF(Mo)	ID	$\frac{XRF(Mo)-ID}{ID} \times 100$	XRF(Au)	ID	$\frac{XRF(Mo)-ID}{ID} \times 100$
82826b	392.1	403.7	394.3	-0.56	28.0	27.8	+0.72			
82825	416.7	432.9	423.3	-1.56	21.0	23.2	-9.48			
82821	344.5	355.2	347.6	-0.89	34.0	33.9	+0.29			
222821b	355.4	360.4	353.6	+0.51	41.4	40.9	+1.22			
1428212	403.4	408.0	401.0	+0.60	17.0	17.3	-1.73			
162828a	387.6	398.2	391.7	-1.01	20.6	20.6	0			
272825	437.1	454.6	436.6	+0.11	7.7	7.76	-0.77			
138212	401.3	413.9	397.2	+1.03	18.1	18.3	-1.09			
13828	499.7	512.3	496.3	+0.69	7.3	7.46	-2.14			
272827	394.6	412.3	397.0	-0.60	19.1	20.2	-5.45			
13826h	439.2	453.4	434.5	+1.08	7.3	7.52	-2.93			
272826b	351.2	363.4	349.5	+0.49	19.7	19.8	-0.51			
272824b	475.9	497.5	476.5	-0.13	16.1	15.8	+1.90			
272829	497.1	504.8	494.8	+0.46	7.8	7.49	+4.14			
230283-2		474.2	455.2					223.2	209.0	+6.79
230283-5		475.3	463.0					223.5	218.1	+2.48
250283-2		451.2	435.0					189.4	195.4	-3.07
220283-3		402.1	398.0					271.9	273.5	-0.59
272822	376.9	392.3	374.7	+0.59	39.0	38.8	+0.52			
242824	290.1	294.3	288.8	+0.45	54.3	54.0	+0.56			
212826	235.2	235.5	230.4	+2.08	57.2	56.5	+1.24			
212824	184.4	184.6	182.6	+0.99	66.1	66.5	-0.60			
202825c	164.9	167.6	161.2	+2.30	70.3	68.3	+2.93			
220283-1		478.0	462.2					222.0	209.6	+5.92
12679-2		486.0	474.9					179.2	185.6	-3.45
170283-1		501.2	486.9					185.1	174.1	+6.32
170283-7		506.5	490.3					229.7	228.4	+0.57
211282-7		462.0	446.9					179.3	176.0	+1.88
72822	190.8	193.1	188.0	+1.49	66.7	65.2	+2.30			
42821	189.5	188.0	185.9	+1.94	66.9	65.2	+2.61	664.0	687.4	-3.40
42824a	172.0	171.4	168.7	+1.96	70.6	68.9	+2.47			
281822bh	161.4	163.0	160.9	+0.31	70.5	70.5	0			
212823a	168.3	166.4	162.8	+3.38	72.1	69.7	+3.44			
182821b	144.0	146.0	141.6	+1.69	73.8	71.2	+3.65			
301821b	144.8	149.2	143.1	+1.19	72.8	70.4	+3.41	771.7	779.6	-1.01
9282-3	469.2	475.0	472.3	-0.66	14.2	14.4	-1.39	230.5	231.9	-0.60
10282-1	456.3	469.1	451.4	+1.09	11.6	11.8	-1.69	206.9	207.0	-0.05
28281-4	451.0	468.3	446.2	+1.08	11.6	11.4	+1.75	168.7	163.3	+3.31
28281-5	448.0	457.8	443.6	+0.99	21.5	21.2	+1.42	323.5	307.7	+5.13
120183-2		460.2	453.6					246.0	249.0	-1.21
242811		418.3	406.3			11.8				
252811		343.0	335.0			22.4				
201282-1		627.7	612.2					215.1	204.0	+5.44
32822b	342.0	347.0	342.3	-0.09	16.0	16.3	-1.84	156.0	155.9	+0.06
32824	346.1	346.2	340.4	+1.67	18.2	17.7	+2.82	196.2	184.2	+6.51
32825	349.9	351.0	346.6	+0.95	12.1	11.5	+5.22	156.1	156.1	0
200283-1		456.0	444.0					570.7	574.5	-0.66
200283-2		492.0	485.7					623.6	642.2	-2.90
200283-3		627.6	628.4					341.8	360.0	-5.06
200283-4		530.0	521.6					515.6	518.0	-0.46

Table A-4 Comparison of Sm and Nd abundances determined by instrumental neutron activation analysis (INAA) and isotope dilution methods

	Sm						Nd			
	5D[1]	TEABAGS			% diff. in ID[2] relative to TEABAGS:		calc.[1]	TEABAGS		diff.
Sample number	calc.	5D	8D	ID	(5D)	(8D)	Nd	Nd	ID	w/TEABAGS[2]
[4]13826h[3]	2.49±13	2.52±14	2.46±4	2.54	-0.79	-3.15	9.22±20	9.32±42	9.66	+3.52
281822bh[3]	8.20±19	8.22±18	8.51±56	8.45	-2.72	+0.71	34.7±2.0	36.7±1.9	37.1	+1.08
212823a	8.52	8.51	9.27	8.44	-0.83	-9.83	41.1	38.2	37.0	-3.24
42824a	8.42	8.40	9.36	8.44	+0.47	-10.9	36.5	38.5	37.1	-3.77
72822	8.28	8.19	9.27	8.41	+2.62	-10.2	38.7	36.4	36.8	+1.09
212826	8.41	8.26	9.45	8.67	+4.73	-9.00	36.3	37.2	37.3	+0.27
202825c	8.92	8.90	9.52	9.17	+2.94	-3.82	42.5	43.8	40.2	-8.95
182821b	8.77	8.95	9.65	9.28	+3.56	-3.99	42.1	43.4	40.8	-6.37
301821b	9.04	9.12	9.69	9.34	+2.36	-3.75	44.2	44.6	41.1	-8.51
[5]82826b	6.16	6.19	6.36	6.45	+4.03	+1.40	24.4	25.2	26.2	+3.82
272824b	3.06	3.15	3.28	3.32	+5.12	+1.20	11.6	12.1	13.2	+8.33
1428212	3.99	3.98	4.18	4.22	+5.69	+0.95	15.1	16.0	16.6	+3.61
138212	4.40	4.46	4.62	4.66	+4.29	+0.86	17.1	18.1	18.7	+3.21
13828	2.07	2.08	2.28	2.27	+8.37	-0.44	9.13	8.7	9.25	+5.95
272825	2.36	2.36	2.56	2.56	+7.87	0	9.53	9.3	9.76	+4.71
162828a	2.86	2.90	3.05	3.05	+4.92	0	12.2	11.5	11.5	0
222821b	8.25	8.32	8.44	8.32	0	-1.44	37.4	36.5	35.6	-2.52
272827	4.51	4.55	4.76	4.70	+3.19	-1.28	19.6	19.5	19.1	-2.09
212824	7.94	8.02	8.37	8.30	+3.37	-0.84	38.4	37.0	36.2	-2.21
242824	6.91	7.05	7.27	7.19	+1.95	-1.11	28.6	29.2	31.2	+6.41
42821	8.45	8.39	8.52	8.40	+0.12	-1.43	37.4	37.8	36.7	-3.00
272822	5.44	5.49	5.75	5.68	+3.35	-1.23	24.9	24.6	24.2	-1.65
272826b	3.48	3.49	3.62	3.62	+3.59	0	15.1	15.3	15.1	-1.32
[5]272829	2.25	2.27	2.13	2.27	0	+6.17	9.56	9.8	9.23	-6.18
220283-1	3.21	3.29	3.08	3.23	-1.86	+4.64	13.6	13.8	13.4	-2.99
250283-2	3.10	3.14	2.97	3.14	0	+5.41	12.5	13.1	12.5	-4.80
2112827	2.78	2.81	2.64	2.81	0	+6.05	10.6	10.7	10.5	-1.91
170283-1	1.15	1.17	1.11	1.17	0	+5.12	3.55	3.61	3.85	+6.23
170283-7	3.63	3.67	3.45	3.64	-0.82	+5.22	13.7	14.0	13.7	-2.19
12679-2	3.38	3.41	3.19	3.29	-3.65	+3.04	10.9	10.8	11.95	+9.62
120183-2	3.58	3.61	3.31	3.48	-3.74	+4.89	14.2	14.1	14.1	0
28281-4	2.66	2.69	2.62	2.63	-2.28	+0.38	9.92	10.0	10.2	+1.96
28281-5	3.68	3.69	3.56	3.69	0	+3.52	14.3	14.2	15.5	+8.39
10282-1	2.92	2.92	2.82	3.03	+3.63	+6.93	11.7	11.5	12.5	+8.00
9282-3	2.80	2.82	2.74	2.87	+1.74	4.53	11.6	11.6	12.1	+4.13
32822b	3.10	3.13	2.91	3.00	-4.33	+3.00	11.7	11.6	11.0	-5.45
32824	3.40	3.44	3.11	3.22	-6.83	+3.42	12.3	12.5	12.4	-0.81
32825	3.29	3.33	3.06	3.19	-4.39	+4.08	12.1	12.0	12.0	0
220283-5	8.03	8.07	7.46	7.93	-1.77	+5.93	34.6	35.6	33.2	-7.22
201282-1	3.53	3.58	3.38	3.51	-1.99	+3.70	14.3	14.4	14.8	+2.70
200283-1	7.97	7.98	7.62	7.98	0	+4.51	36.1	36.8	36.3	-1.38
200283-2	6.74	6.70	6.52	6.68	-0.30	+2.40	33.2	33.0	33.2	+0.60
200283-3	3.44	3.46	3.38	3.48	+0.60	+2.87	15.4	15.5	15.9	+2.52

1 Calculations done manually from printed spectra
2 ID-TEABAGS/ID x 100
3 1σ uncertainties for replicate analyses (n = 8 for 13826h; n = 12 for 281822bh) taken from Table 4.
4 irradiated with NG synthetic standard
5 irradiated with NB synthetic standard

uncertainties and are probably more realistic estimates of precision, at least for samples in this study with relatively lower abundances.

Abundances of K, Rb, Cs, Sr, and Ba were determined in some samples by isotope dilution methods described in Hart and Brooks (1977). Concentrations of Nd and Sm were measured in sample splits spiked with enriched isotopes of ^{150}Nd and ^{149}Sm as described by Zindler et al. (1979). Spike solutions of combined Nd and Sm were prepared and calibrated by S. H. Richardson, and procedures are described in detail in Richardson (1984). Uncertainties in isotope dilution (ID) measurements of K(1%), Cs(2%), Ba(1%), Rb(1%), Sr(0.5%), Sm(0.5%), and Nd(0.1%) are estimated from duplicate measurements (Table 5) of different sample split + spike dissolutions in each case. Total chemistry blanks during this study for K(0.2 ng/g), Rb (0.01-0.01 ng/g), Cs (12 pg/g), Ba (1.5 ng/g), Sr (0.2 ng/g), Sm (<0.1 ng/g), Nd (<0.1 ng/g), and Pb (500-800 pg/g) were considered negligible.

Abundances of Sm and Nd were determined in a number of samples by both INAA and ID methods and results are compared in Table A-4. Values for Nd by INAA and ID agree reasonably well, approximately within the uncertainty estimated for Nd by replicate INAA analyses (see above discussion). Significant photopeaks for Sm appear in the first two counts (approximately 5 and 8-9 days after irradiation) on two different detectors which also have different sample-detector geometries. The Sm abundances determined for the 5-day (5D) and 8-day (8D) counts usually differ (see Table A-4). Samples in Table A-4 are listed in approximate chronological order from top to bottom, according to when they were analyzed by INAA. Prior to sample 272829, 8D Sm values were consistently higher than 5D determinations, and the opposite true thereafter. It is

desirable to determine which count, 5D or 8D, yields the best Sm abundance estimate by comparison with Sm ID determinations. For samples prior to 272829, there is no consistent indication as to which count is better and this may be attributed to two causes: (1) samples prior to 272829 were analyzed against either in-house synthetic standard NG or NB, and (2), samples 13828 to 272829 were prepared with more stringent geometry controls i.e., the volumes of samples and standards were carefully adjusted to be identical. All samples after 272829 were prepared in this manner and were analyzed against the in-house NB standard. For samples after, and including 272829, there is a crude indication that Sm ID values agree better with those determined during the INAA 5-day count.

A.5: Isotopic analyses

For Sr and Nd isotopic composition (IC) analyses, sample powders were dissolved in open beakers with a HF-$HClO_4$ mixture and K, Rb, Cs, Sr, Ba, and REE were separated on standard cation exchange columns (Hart and Brooks, 1977) described in detail in Zindler (1980). The REE fraction is processed in a second column as described by Richard et al. (1976) based on the technique of Cerrae and Testa (1963). Sr isotopic data are normalized to $^{86}Sr/^{88}Sr$ = 0.1194 and $^{87}Sr/^{86}Sr$ values reported in Table 5 are relative to an accepted value of 0.70800 for the Eimer and Amend $SrCO_3$ standard. All Sr and Nd IC analyses were performed on a 9"60° radius mass spectrometer (NIMA-B). $^{143}Nd/^{144}Nd$ values in Table 5 are normalized to $^{144}Nd/^{146}Nd$ = 0.7219, and $^{143}Nd/^{144}Nd$ = 0.51264 in standard rock BCR-1. In-run precision for $^{87}Sr/^{86}Sr$ and $^{143}Nd/^{144}Nd$ as represented by $2\sigma_{mean}$ is typically 0.005% or better. Duplicate analyses

of $^{87}Sr/^{86}Sr$ and $^{143}Nd/^{144}Nd$ of selected samples were determined on different spike + sample mixtures or on spiked versus unspiked samples as noted in Table 5, and agree within the range of uncertainty as estimated from in-run precision.

For Pb IC determinations, separate splits of sample powders were dissolved in a HBr-HF mixture, and Pb was separated on anion exchange columns in a manner described by Manhes et al. (1978) based on the technique of Strelow and Toerien (1966) adapted for use in this laboratory (see Pegram, 1985). Total chemistry Pb blanks range from 500-800 pg/g, and were considered negligible. Pb isotope ratios are normalized for mass discrimination based on in-house replicate measurements of the NBS SRM 981 Pb standard performed during the time covered by this study.

Analytical uncertainty due to mass fractionation is estimated to be 0.05% per a.m.u. based on the multiple analyses of NBS SRM 981. From duplicate measurements of selected samples reported in Table A-5, this uncertainty is on the order of 0.03% per a.m.u. Most analyses were run on the 12" radius mass spectrometer (TIMER). In-run precision for all Pb-isotopic analyses is typically 0.012% to 0.015%, and 0.003% to 0.006% for $^{207/206}Pb$ and $^{208/206}Pb$.

As seen in Table A-5, especially data for basalt 13826h, no differences outside of analytical uncertainty are observed for samples prepared and powdered in different ways, i.e., using the jaw crusher or not, and powdering in either an agate or tungsten carbide shatterbox. Listings for other samples in Table A-5 (272824b, 272822, 32822b, 242811, 32822f) illustrate differences which may be attributed to in-run fractionation, however, Pb-isotopic composition runs were generally

Table A-5. Replicate analyses of Pb isotopic ratios

Sample number	Method of Sample Preparation	Mass spectrometer	$^{206}Pb/^{204}Pb$	$^{207}Pb/^{204}Pb$	$^{208}Pb/^{204}Pb$
18326h	jaw crusher, agate shatterbox	TIMER	18.568	15.589	38.440
	hammer/plastic, WC shatterbox	TIMER	18.566	15.583	38.425
	hammer/plastic, agate shatterbox	TIMER	18.565	15.589	38.436
	hammer/plastic, agate shatterbox	TIMER	18.567	15.592	38.452
13828	hammer/plastic, agate shatterbox	TIMER	18.551	15.580	38.366
	hammer/plastic, agate shatterbox	NIMA-B	18.550	15.576	38.363
	hammer/plastic, WC shatterbox	TIMER	18.551	15.577	38.361
272824b	hammer/plastic, agate shatterbox	NIMA-B	18.587	15.596	38.487
	hammer/plastic, agate shatterbox	TIMER	18.579	15.591	38.458
272822	hammer/plastic, agate shatterbox	TIMER	18.587	15.600	38.496
	hammer/plastic, agate shatterbox	TIMER	18.575	15.586	38.442
32822B	hammer/plastic, agate shatterbox	TIMER	18.637	15.608	38.529
	hammer/plastic, agate shatterbox	TIMER	18.636	15.608	38.528
	prepared at Universidad de Chile	NIMA-B[1]	18.559	15.609	38.496
242811	jaw crusher, WC shatterbox	TIMER	18.595	15.596	38.480
	jaw crusher, WC shatterbox	TIMER	18.603	15.608	38.525
201282-1	prepared at Universidad de Chile	NIMA-B	18.499	15.588	38.359
	prepared at Universidad de Chile	TIMER	18.486	15.582	38.331
	hammer/plastic, WC shatterbox	TIMER	18.542	15.577	38.354
200283-3	prepared at Universidad de Chile	TIMER	18.475	15.609	38.465
	hammer/plastic, WC shatterbox	TIMER	18.524	15.595	38.462
12679-2	prepared at Universidad de Chile	TIMER	18.391	15.600	38.312
	hammer/plastic, WC shatterbox	TIMER	18.591	15.591	38.463
32822f	hammer/plastic, WC shatterbox	TIMER	18.463	15.561	38.243
	hammer/plastic, WC shatterbox	TIMER	18.462	15.564	38.251

[1] analyst R. Hickey

considered acceptable if $^{208/206}Pb$ ratios increased less than 0.03%. Analysis of some sample powders prepared at the Univ. de Chile were noticeably lower in $^{206}Pb/^{204}Pb$ and $^{208}Pb/^{204}Pb$ ratios. Different analyses were obtained on new powders prepared from portions of the same samples on hand at M.I.T., and the resulting differences were outside of analytical error for all four samples (Table A-5). This suggests that sample powders prepared at the Univ. de Chile experienced variable environment contamination.

PLATE I

GEOLOGIC MAP OF THE PUYEHUE-CARRAN VOLCANIC COMPLEX

after H. Moreno Roa (1977)

92822 sample locality
geologic contact
fault (dashed where inferred)
volcanic neck
crater
caldera

Qc colluvium
Qda alluvium
Qdf fluvial deposits
Qdfa alluvial and fluvial deposits
Qm glacial deposits
DPp / DPeb undifferentiated pumice/basaltic scoria

Lago Ranco
CORDILLERA NEVADA
LOS VENADOS
CORDON CAULLE
ANTICURA
VOLCAN PUYEHUE
Caulle Grande
Caulle Chico
El Azufral
Gris
Macizo de Mencheca
Pichi-Golgol
Río Golgol
VN. Pocura
VN. Carran
VN. Riñinahue
VN. Media Luna
Detail shown in figure 2

		Carran-Los Venados Volcanic Group	Mencheca Volcanic Group	Cordillera Nevada Volcano	Puyehue Volcano	Cordon Caulle	Other Volcanic Centers
Holocene - Recent (post-glacial)		Media Luna: MLIIc/MLIIi pyroclastic cone; lava flows; MLI lava flows. Riñinahue: RIIIcp/RIIIp pyroclastic cone; pyroclastic ring (maar); lava flows, 1907; RII pyroclastic ring (maar); RI pyroclastics and lavas. Carran: CV pyroclastic cone (V. Mirador), 1979; CIV pyroclastic deposits, 1955; CIIIp/CIII pyroclastic cones; lava flows; CIIp/CII pyroclastic rings (maars); lava flows. Los Venados: LVIIp/LVIIi pyroclastic cones, maars; lava flows; LVI lava flows. Pichi: PCHp/PCHi pyroclastic cones; lava flows	LN Los Nirres pyroclastic rings (maars); MIII pyroclastic cones			CCVIp/CCVIi pyroclastic cones; lava flows, 1960; CCVp/CCVi pyroclastic cones; lava flows, 1921-1922; CCIVp/CCIVi pyroclastic cones; lava flows	CVAp/CVAi Anticura volcanic centers lava flows, pyroclastics; cp/fl pyroclastic cone and lava flow
Pleistocene	late glacial	CI lava flows	PG Pichi-Golgol pyroclastic rings (maars), lava flows	CNIII pyroclastic cone and lava flows	PIIIi/PIII laharrs; lava flows and pyroclastics; PII lava flows and pyroclastics	CCIIIL/CCIIIi laharrs; ignimbrite; CCIII lava flows, domes, and pyroclastics	
	glacial		MII lavas and pyroclastics; MI pyroclastics, lava flows, agglomerates	CNII lava flows; CNI lava flows, ignimbrites, and agglomerates	PI lavas, pyroclastics, and agglomerates	CCII pyroclastics, lava flows, agglomerates; CCI pyroclastics, lava flows, agglomerates	
Pliocene (pre-glacial)							

PZim Paleozoic granitoids